



# Fracture Mechanics Applied to the Design of Adhesively Bonded Joints

Filipe José Palhares Chaves PRODEM 2013

#### THESIS FOR THE DEGREE OF DOCTOR OF PHILOSOPHY

### Fracture Mechanics Applied to the Design of Adhesively Bonded Joints

by

# Filipe José Palhares Chaves



#### Supervisor:

#### Lucas Filipe Martins da Silva

DEMec, Faculdade de Engenharia da Universidade do Porto, Rua Dr. Roberto Frias, 4200-465 Porto, Portugal

Co-Supervisors:

#### Marcelo Francisco de Sousa Ferreira de Moura

DEMec, Faculdade de Engenharia da Universidade do Porto, Rua Dr. Roberto Frias, 4200-465 Porto, Portugal

#### **David Dillard**

Engineering Science and Mechanics Department, Virginia Tech, Blacksburg, VA 24061

# © Filipe José Palhares Chaves

Departamento de Engenharia Mecânica

Faculdade de Engenharia da Universidade do Porto

Rua Dr. Roberto Frias

4200-465 Porto

Portugal

• • • •

#### **ABSTRACT**

The design of adhesively bonded joints is an important task to guarantee structural integrity. Fracture mechanics characterization tests for adhesive joints provide relevant mechanical properties to determine the adhesive toughness. Toughness is usually expressed in terms of the critical value for the strain release rate ( $G_c$ ) which is the energy dissipated during fracture when the crack grows. It is the energy needed for a crack tip to propagate and must also take into account the fracture process zone (FPZ) ahead of the crack tip. Mode I opening, mode II and mode III shearing loadings are the working loads operating at service of an adhesive joint. The combination of mode I with mode II and III is likely to occur and represents the most critical loading.

Performing fracture mechanics tests is essential in order to validate the joint design. Mode I fracture mechanics tests are well characterized and are included in ASTM and ISO standards. Mixed mode bending (MMB) is a mixed-mode I+II fracture mechanics test included in ASTM, however it was developed for delamination purposes using composite specimens and it is not appropriate for aluminum or steel adhesively bonded specimens. These tests use the crack length (a) measurement during its growth as a variable to compute the strain energy release rate, G. This measurement is not easy to perform, mostly when an abrupt and sudden fracture occurs.

There are other tests that can be performed to evaluate the adhesive joint toughness, but there is no consensus regarding its adequacy not even a generalized acceptability within the adhesion science community. Different specimen geometries, such as end loaded-split (ELS), single leg bending (SLB), asymmetric tapered double cantilever beam (ATDCB) or special apparatus, like MMB or even dedicated machines as the dual actuator loading (DAL) frame are used to perform these tests. The objective was to develop a new mixed mode I + II apparatus that could use conventional DCB specimens and that would not need the crack length measurement for computing the toughness. This apparatus would allow to have the fracture envelope in a graph Gi vs. GII for design purposes.

This work tries to achieve this goal, firstly by performing different tests, using several conventional specimen geometries - double cantilever beam (DCB), end notch flexure (ENF), asymmetric double cantilever beam (ADCB), asymmetric tapered double cantilever beam (ATDCB) and single leg bending (SLB) - to obtain the strain energy release rate for pure mode I, pure mode II and a small range of mixed-mode I + II. The bondline thickness effect was also evaluated for pure mode I and pure mode II.

In a second phase, a DAL frame was used to obtain a wider range of mixed mode loading and a data reduction technique was developed to overcome the inherent difficulty of measuring the crack length and improving the results considering the compliance based beam method (CBBM). Despite the fact that this equipment can perform mixed mode tests by applying different displacements rates to each specimen beam, DAL is a sophisticated and expensive solution.

A universal test that can easily be performed and give accurate results is essential to optimize the expensive testing at the design stage.

Complying with the previous statement, a third phase of this work regards the development of a new test that provides expedite and accurate results with a low budget. An apparatus was designed to perform pure mode I, pure mode II and a combination of mode I with mode II loading, using a DCB specimen. A test methodology comprising a data reduction technique was proposed to overcome the troublesome crack length measurement and to take into consideration the compliance based beam method (CBBM).

Numerical modeling using cohesive elements was also carried out to develop the data reduction scheme and to optimize the new mixed mode apparatus. The numerical results were validated with experimental results.

**Keywords:** Adhesively bonded joints, fracture mechanics, mixed-mode I+II testing, mode I testing, mode II testing, apparatus design.

#### **RESUMO**

Projetar juntas adesivas é uma tarefa importante para garantir a integridade estrutural. A caracterização de juntas adesivas através de ensaios de mecânica da fractura fornece propriedades mecânicas relevantes para determinar a tenacidade da junta. A tenacidade é geralmente expressa em termos da taxa crítica de libertação de energia ( $G_c$ ) que representa a energia dissipada durante a fractura quando a fenda propaga. É a energia necessária para que a ponta da fenda se propague e deve contemplar a zona de processo na frente da fenda. Solicitações de abertura em Modo I, de corte em Modo II e modo III são as que ocorrem durante o serviço da junta adesiva. É muito provável que ocorram as combinações de modos I com modo II e III, sendo estas as solicitações mais críticas.

Para validar o projeto de uma junta torna-se essencial a realização de ensaios de mecânica da fratura. Os ensaios de mecânica da fratura para modo I encontram-se bem caracterizados, constituindo mesmo o objeto de normas ASTM e ISO. O ensaio MMB é um ensaio de mecânica da fratura em modo misto I +II incluído na norma ASTM, todavia foi desenvolvido para responder testar a delaminação utilizando provetes de material compósito, não sendo adequado para provetes de alumínio ou aço unidos com adesivo. Estes ensaios recorrem à medição do comprimento de fenda (a) durante a propagação como variável para cálculo da taxa de libertação de energia, G. Contudo esta medição não é fácil de executar, sobretudo quando a fratura ocorre de forma abrupta e repentina.

Existem mais ensaios que podem ser levados a cabo para avaliar a tenacidade de juntas coladas, todavia não existe um consenso acerca da sua adequabilidade nem tão pouco uma aceitação generalizada por parte da comunidade científica de adesão. Provetes com diferentes geometrias, tais como o *end-load split* (ELS), o single leg bending (SLB), *asymmetric tapered double cantilever beam* (ATDCB), ou mecanismos especiais, tais como o MMB, ou então equipamentos dedicados tais como a estrutura *dual actuator loading* (DAL) são utilizados para realizar estes ensaios. O objetivo é determinar um dado número de taxas críticas de libertação de energia para modo I  $G_{Ic}$ , modo II,  $G_{IIc}$ , e o espectro desde o modo I até ao modo II  $G_{Ic,IIc}$  para obter um envelope de fratura que caracterize a junta adesiva, orientado para o projeto.

Este trabalho procura atingir este objetivo, numa primeira fase através da realização de vários ensaios, utilizando provetes convencionais com diferentes geometrias – *double cantilever beam* (DCB), *end notch flexure* (ENF), *asymetric double cantilever beam* (ADCB), *asymetric tapered double cantilever beam* (ARDCB) e *single leg bending* (SLB) – para obter as taxas críticas de libertação de energia para puro modo I, puro modo II e um reduzido intervalo de modo misto I + II. O efeito da espessura do adesivo também foi avaliado para puro modo I e puro modo II.

Numa segunda fase, foi utilizada uma estrutura DAL com o intuito de obter um rácio de carga mais amplo e uma técnica para tratamento dos dados foi desenvolvida para ultrapassar as dificuldades inerentes na medição do comprimento da fenda e melhorando os resultados obtidos contemplando a correção baseada na rigidez da viga (CBBM) — compliance based beam method . Apesar deste equipamento permitir a aplicação de diferentes taxas de deslocamento em cada um dos braços do provete, o DAL é um solução sofisticada e onerosa.

Um ensaio universal que seja de fácil execução e permita obter resultados fidedignos é essencial para otimizar os ensaios ao nível do projeto.

Respondendo ao requisito expresso na frase anterior, uma terceira fase é realizada neste trabalho dedicada ao desenvolvimento de um ensaio que forneça resultados precisos de uma forma expedita e a baixo custo. É projetado um mecanismo que permite realizar puro modo I, puro modo II e combinações de modo I com modo II, para carregamento de um provete DCB. Também é desenvolvida uma metodologia para o ensaio que compreende uma técnica para tratamento de dados para ultrapassar a difícil medição do comprimento da fenda e considerando a correção baseada na rigidez da viga (CBBM).

É realizada modelação numérica, recorrendo a elementos coesivos com o objetivo de validar a técnica para tratamento de dados, para comparação com os resultados experimentais ou para otimizar o projeto do mecanismo proposto.

#### **ACKNOWLEDGEMENTS**

I would like to express my sincere gratitude to my supervisor Prof. Lucas F.M. da Silva for his intellectual and academic support, for believing in my work and being patient throughout all these years. I express also my gratitude to my supervisor Prof. Marcelo F.S.F. de Moura for his support throughout my work and for our interesting discussions about fracture mechanics and constant search for excellent results with numerical analysis. I extend my gratitude to my supervisor Prof. David Dillard at the other side of the Atlantic Ocean for a warm welcoming at Virginia Tech, for sharing his knowledge in adhesive science and for sharing his huge wisdom with me. I will never forget a fracture mechanics lecture, for almost five hours, while traveling from Savannah, Ga. to Blacksburg, Va..

A special thanks to Prof. Paulo Tavares de Castro for being an inspiration in fracture mechanics since my early days as an engineering student.

I would also like to thank Edoardo Nicoli and Leo Youliang Leo Guan for their support while using the test equipment at Virginia Tech's adhesives laboratory and for the helpful discussions. I express my gratitude to Hitendra Singh, Chakraborty, D.J. Pohlit and D. Ohanehi for welcoming me in Virginia Tech's adhesives group.

Special thanks to all my colleagues at FEUP's adhesive group, Eduardo Marques, Ricardo Carbas and Ana Queirós who supported me in any respect during the last years.

A very special thanks to Dr. Mariana Banea for her friendship and support to my thesis and for bringing interesting discussions to my work.

I would also like to thank Prof. Raul Campilho for sharing his knowledge in the adhesive science field, for teaching me how to use ABAQUS<sup>®</sup> and for supporting my work.

I would like to thank the contributions made to this work by master students Ruben Cardoso, Vitor Esteves and Filipe Magalhaes.

During my years at FEUP, I had the support of many people that I would also like to extend my gratitude, especially to Prof. Miguel Figueiredo, Prof. Joaquim Oliveira Fonseca, Rui Silva, Emilia Soares, Mr. José, Mr. Albino and Francisco Moreira for their valuable support throughout the phase of experimental work.

I would like to thank my colleagues and students at IPCA for supporting my PhD work, especially Dr. Paula Tavares and Maria João Félix for giving me the opportunity to teach, learn and sustain my PhD thesis. Thanks to Dr. Álvaro Sampaio, Demétrio Matos, Miguel Terroso and Paulo Simões for their interesting discussions and Professors Ricardo Simões and Gilberto Santos for sharing their experience in materials science.

I would like to thank the "Fundação Luso-Americana para o Desenvolvimento" (FLAD) for the support through project 314/06, 2007 and *Instituto de Engenharia Mecânica* (IDMEC).

Finally, I would like to thank my family, Ana Almeida, Laura Madureira and my good friend Ricardo Alves for their enormous support without which this work would not have been finished.

This thesis is dedicated to the memory of my father.

fracture mechanics applied to the design of adhesively bonded joints **DEMec** L.F.M. da Silva FEUP Faculdade de Engenharia M.F.S.F. de Moura **UVirginiaTech** D. Dillard (idmec filipe chaves

# **CONTENTS**

ABSTRACT	i
ACKNOWLEDGEMENTS	v
LIST OF PUBLICATIONS	ix
SUMMARY OF THESIS	1
1. Introduction	1
1.1 Background and motivation	1
1.2 Problem definition	2
1.3 Objectives	3
1.4 Research methodology	4
1.5 Outline of the thesis	4
2. Adhesives tested	9
3. Test methods	9
4. Apparatus Design	10
5. Numerical modeling	11
6. Conclusion	11
7. Future Work	12
APPENDED PAPERS	
Paper 1	14
Paper 2	52
Paper 3	80
Paper 4	100
Paper 5	120
Paper 6	136
Paper 7	154
Paper 8	172
DRAWINGS (APPENDIX)	198

• • • •

#### LIST OF PUBLICATIONS

- [1] Chaves F.J.P, da Silva L.F.M., de Moura M.F.S.F., Dillard D.A., Fracture mechanics tests in adhesively bonded joints: a literature review, 2013 to be submitted
- [2] Chaves F.J.P ,de Moura M.F.S.F., da Silva L.F.M., Dillard D.A., Fracture characterization of bonded joints using the Dual Actuator Load apparatus, 2013, submitted
- [3] Chaves F.J.P ,de Moura M.F.S.F., da Silva L.F.M., Dillard D.A., Numerical validation of a crack equivalent method for mixed-mode I+II fracture characterization of bonded joints, 2013, submitted to Engineering Fracture Mechanics
- [4] Chaves F.J.P, da Silva L.F.M., de Moura M.F.S.F., Dillard D.A., Fonseca, J.O., Apparatus and method for characterization of bonded joints mixed-mode I+II fracture, 2013, submitted patent
- [5] Chaves F.J.P, de Moura M.F.S.F., da Silva L.F.M., Dillard D.A., Mixed-mode I+II fracture characterization of bonded joints using a multi-mode apparatus, 2013, submitted
- [6] Chaves F.J.P ,de Moura M.F.S.F., da Silva L.F.M., Dillard D.A., Numerical analysis of the dual actuator load test applied to fracture characterization of bonded joints, International Journal of Solids and Structures 48 ,2011, 1572–1578
- [7] da Silva L.F.M., Esteves V.H.C., Chaves F.J.P., Fracture toughness of a structural adhesive under mixed mode loadings, Mat.-wiss. u.Werkstofftech. 2011, 42, 5: 460-470
- [8] V. Richter-Trummer, E.A. Marques, F.J.P. Chaves, J.M.R.S. Tavares, L.F.M. da Silva, P.M.S.T. de Castro, Analysis of crack growth behavior in a double cantilever beam adhesive fracture test by different digital image processing techniques ,Materialwissenschaft und Werkstofftechnik, 42, 2011, 452-459.
- [9] da Silva L. F. M., de Magalhães, F. A. C. R. G., Chaves, F. J. P. and de Moura, M. F. S. F., Mode II Fracture Toughness of a Brittle and a Ductile Adhesive as a Function of the Adhesive Thickness, The Journal of Adhesion. 2010, 86: 9, 889 903

• • • •

#### . . . .

#### **SUMMARY OF THESIS**

#### 1. Introduction

#### 1.1 Background and motivation

Joining two or more parts is an ancient problem since early times for mankind. Bonding with primitive and basic adhesives was proved to be one of the first techniques to solve this problem [1]. Natural glues, obtained from organic products like animals, vegetables or inorganics as tar, were used as joining and sealing elements since then, providing to be valuable solutions for several applications. However, it was only from the early twentieth century that a huge evolution occurred in adhesion science, mostly after the first synthetic adhesives produced with epoxy resins circa the 1940s, used as structural adhesives [2]. Considering the advantages of bonded joints, the use of adhesive as a structural bonding component was spread into a wide range of industrial applications such as aeronautical, automotive and construction building among others. This growth was supported by a considerable effort in research and knowledge of the adhesion science, improving the design of joints and formulating better adhesives. In this context, the characterization of adhesively bonded joints assumes a recognizable relevancy. Fracture mechanics provides excellent tools to obtain the adhesive joint properties and derive failure parameters to be considered for design purposes [3].

Adhesive joints are subjected to opening loads (mode I), shear loads (mode II or mode III) and the various combinations of opening with shear as mixed-mode I + II, I+III and II+III [4]. Mode I loading is well characterized and there is included in ASTM [5] and ISO [6] standards. Mixed-mode I+II is also included in ASTM [7], however it was developed for delamination purposes using composite specimens [8, 9] and it is not appropriate for aluminum or steel adhesively bonded specimens because it would require a too big apparatus due to the loads involved.

Therefore, an improved mixed mode apparatus for testing adhesive joints with the standard geometry and dimensions described in the ASTM or ISO standards is required. Another aspect that makes difficult the determination of the adhesive toughness, especially when loaded in mode II is the correct measurement of the crack length. Even with highly accurate devices such as cameras or travelling microscopes, it is always difficult to tell where the crack tip is exactly. Bearing these two limitations in mind, the aim of this research is to investigate fracture mechanics tests and data reduction scheme methodologies to develop a mechanism suited for

the fracture mechanics evaluation of bonded joints with mixed-mode (I+II) loading. Two epoxy adhesives were used to understand the adequacy of the solutions for brittle and ductile adhesives.

Determining the toughness of adhesive joints requires fracture mechanics tests. A review of the investigations that have been made on fracture mechanics of adhesively bonded joints is presented in **Paper 1**.

In **Paper 2** different tests were carried out, using several conventional specimen geometries - double cantilever beam (DCB), end notch flexure (ENF), asymmetric double cantilever beam (ADCB), asymmetric tapered double cantilever beam (ATDCB) and single leg bending (SLB) - to obtain the strain energy release rate for pure mode I, pure mode II and a small range of mixed-mode I + II. The bondline thickness effect for these two adhesives was also evaluated for pure mode I and pure mode II in **Paper 3**.

Obtaining a wider range of mixed-mode I + II was possible using a dual actuator loading (DAL) frame developed by Dillard et al. [10] at Virginia Tech. This study developed a new data reduction technique based on the compliance based beam method (CBBM), avoiding to measure the crack length. This data reduction technique was numerically validated using ABAQUS® with cohesive zone model using interface elements developed by Gonçalves et al. [11] in **Paper** 4. The methodology was validated with experimental results in **Paper** 5.

This work evolved to the development of a mixed-mode test apparatus, based on the jig proposed by Fernlund and Spelt [12]. The jig was optimized in terms of the space required, inverting the relative specimen position. A CBBM data reduction technique was also developed for this test, avoiding monitoring the crack growth during the test presented in **Paper 6** where this data reduction technique was numerically validated using ABAQUS® with cohesive zone model recurring to interface elements. This new apparatus and test methodology were drawn into a patent in **Paper 7**.

Finally, the proposed new mixed mode apparatus was tested experimentally and the results are presented in **Paper 8.** The experimental results were compared to numerically ones obtained from ABAQUS<sup>®</sup> with cohesive zone model recurring to interface elements.

#### 1.2 Problem definition

As stated previously, obtaining the strain energy release rate is a fundamental task in order to characterize adhesive joints, using fracture mechanics tests as described in **Paper 1**.

Pure mode I testing is well defined, included in ASTM [5] and ISO [6] standards. Although mixed-mode I+II is included in ASTM [7] standard it was developed for delamination testing rather for adhesive joint fracture characterization. Furthermore there is not a wide consensus for mixed-mode I + II testing and methodologies to obtain the strain energy release rate.

Traditional test methodologies rely on the crack length measurement as a variable to include in the strain energy release rate calculation. In some cases, measuring the crack length can be a difficult task. In any case, the crack length does not take into account the fracture process zone (FPZ) ahead of the crack tip. This is a problem, because it neglects an important damaged zone representing some energy amount.

The main goal of this PhD research is to develop a test methodology for pure mode I, pure mode II and mixed-mode I + II fracture mechanics characterization of adhesively bonded joints, allowing to obtain a full fracture envelop without the need to measure the crack length. The fracture envelop represents an important information to design adhesive joints.

#### 1.3 Objectives

The aim of this research is to develop a fracture mechanics test methodology to support the design of adhesive joints.

#### Specific objectives are:

- to review the major fracture mechanic tests for adhesive joints characterization and evaluate the present state of the art;
- perform the adequate tests to obtain the strain energy release rate for pure mode I, pure mode II and some mixed-mode I+II combinations in order to obtain a fracture envelop;
- develop a test apparatus, from the analysis of the data collected from testing and the information about the reviewed fracture mechanics tests;
- develop a test methodology, recurring to a data reduction techniques that does not require crack length monitoring and take into account the FPZ and proposed corrections;
- validate the developed methodologies and test apparatus by comparing the experimental results with CZM numerical models;
- obtain a fracture envelope using the developed methods and apparatus.

#### 1.4 Research methodology

The following methodology was adopted to achieve the goals of this PhD research. Numerical modeling with cohesive elements was the main tool of analysis always supported by experimental results for validation purposes:

- there are several tests used to characterize the fracture behavior of adhesively bonded joints and methodologies to obtain the strain energy release rate. A literature review, comprising these tests and methodologies is done in Paper 1;
- taking into account the literature review, some fracture tests were performed in Paper
   2, Paper 3 and Paper 5 in order to obtain the toughness values for pure mode I, pure mode II and mixed-mode I + II of adhesively bonded joints using tests well described in the literature;
- overcoming some difficulties inherent to test procedure, a data reduction technique based in CBBM was developed for the DAL test in **Paper 4** and also for the novel test based in the SPELT jig presented in **Paper 6**. Both methods (DAL and the novel mixed mode test) were numerical validated using interface elements implemented with ABAQUS<sup>®</sup>;
- experimental results obtained with the novel mixed mode apparatus, which was drawn into a patent by **Paper 7**, were compared with an ABAQUS® numerical model using interface elements in **Paper 8**.

#### 1.5 Outline of the thesis

This thesis consists of seven appended papers, a patent and a summary.

Paper 1	Chaves F.J.P, da Silva L.F.M., de Moura M.F.S.F., Dillard D.A.,
_	Fracture mechanics tests in adhesively bonded joints: a literature
	review, to be submitted

Abstract of paper 1 - Fracture mechanics tests in adhesively bonded joints: a literature review: Fracture mechanics characterization tests for adhesive joints are analyzed and reviewed in order to understand their advantages and disadvantages. Data reduction techniques for analytical methods are summarized to understand the improvements implemented in each test. Numerical approaches are also used complementing tests mode-mixity information. Both linear and non linear methods to obtain the fracture energy release rate are presented. Pure mode I and mode II tests are considered and simple mixed-mode tests, varying only the specimen geometry, with limited mode-mixity are evaluated. Performing a wider mode-mixity range requires

sophisticated apparatus that are studied in detail. There is no general agreement about the test suitability for mixed-mode fracture assessment of adhesive joints. A universal test that can easily be performed and give accurate results is essential to optimize the expensive testing at the design stage.

Paper 2 da Silva L.F.M., Esteves V.H.C., Chaves F.J.P., Fracture toughness of a structural adhesive under mixed mode loadings, Mat.-wiss. u.Werkstofftech. 2011, 42, No. 5, : 460-470

**Abstract of paper 2** - Fracture toughness of a structural adhesive under mixed mode loadings: This aim of this research was to determine the fracture toughness of steel/adhesive/steel joints under mixed mode loadings. A structural and ductile epoxy adhesive was selected in this research. The experimental tests, i. e. Asymmetric Tapered Double Cantilever Beam (ATDCB), Single Leg Bending (SLB) and Asymmetric Double Cantilever Beam (ADCB), were realized to assess the fracture toughness in mixed mode. Experimental tests in pure mode I and II were also realized to complete the fracture envelope. In order to obtain the mode I critical energy release rates, GIc, the standard Double Cantilever Beam test was used, whilst the critical strain energy release rate in mode II, GIIc, was evaluated with the End Notched Flexure test. For various mixed mode tests, the critical strain energy release rate values were partitioned into mode I and mode II components. One of the main conclusions of the present work is that the introduction of a small amount of mode II loading (shear) in the joint results in a decrease of the total fracture energy, GT = GI + GII, when compared to the pure mode I fracture energy.

Paper 3	da Silva L. F. M., de Magalhães, F. A. C. R. G., Chaves, F. J. P.
	and de Moura, M. F. S. F., Mode II Fracture Toughness of a
	Brittle and a Ductile Adhesive as a Function of the Adhesive
	Thickness, The Journal of Adhesion. 2010, 86: 9, 889 — 903

**Abstract of paper 3** - Mode II Fracture Toughness of a Brittle and a Ductile Adhesive as a Function of the Adhesive Thickness: The main goal of this study was to evaluate the effect of the thickness and type of adhesive on the Mode II toughness of an adhesive joint. Two different adhesives were used, Araldite<sup>®</sup> AV138/HV998 which is brittle and Araldite<sup>®</sup> 2015 which is ductile. The end notched flexure (ENF) test was used to determine the Mode II fracture toughness because it is commonly known to be the easiest and widely used to characterize Mode II fracture. The ENF test consists of a

three-point bending test on a notched specimen which induces a shear crack propagation through the bondline. The main conclusion is that the energy release rate for AV138 does not vary with the adhesive thickness whereas for Araldite<sup>®</sup> 2015, the fracture toughness in Mode II increases with the adhesive thickness. This can be explained by the adhesive plasticity at the end of the crack tip.

Paper 4	Chaves F.J.P, de Moura M.F.S.F., da Silva L.F.M., Dillard D.A.,
_	Numerical analysis of the dual actuator load test applied to
	fracture characterization of bonded joints, International Journal of
	Solids and Structures 48 (2011) 1572–1578

Abstract of paper 4 - Numerical analysis of the dual actuator load test applied to fracture characterization of bonded joints: The dual actuator load test was numerically analyzed in order to assess its adequacy for fracture characterization of bonded joints under different mixed-mode loading conditions. This test enables asymmetric loading of double cantilever beam specimens, thus providing a large range of mixed-mode combinations. A new data reduction scheme based on specimen compliance, beam theory and crack equivalent concept was proposed to overcome several difficulties inherent to the test. The method assumes that the dual actuator test can be viewed as a combination of the double cantilever beam and end loaded split tests, which are used for pure modes I and II fracture characterization, respectively. A numerical analysis including a cohesive mixed-mode damage model was performed considering different mixed-mode loading conditions to evaluate the test performance. Some conclusions were drawn about the advantages and drawbacks of the test.

Paper 5	Chaves F.J.P ,de Moura M.F.S.F., da Silva L.F.M., Dillard D.A.,
	Fracture characterization of bonded joints using the Dual Actuator
	Load apparatus, 2013, submitted

**Abstract of paper 5** - Fracture characterization of bonded joints using the Dual Actuator Load apparatus: Mixed-mode I+II fracture characterization tests of steel- bonded joints were carried out with the Dual Actuator Load (DAL) apparatus using a previously developed data reduction scheme in order to obtain the fracture envelop. This test consists on an independent loading of the specimen arms of a clamped double cantilever beam which allows an easy variation of the I+II mode mixity in fracture

characterization altering the applied displacement rates. Difficulties inherent to crack monitoring during its propagation and imperfections of initial crack manufacture are well managed with the proposed method. Three different cases corresponding to different mode mixities were tested. The experimental results revealed that the linear energetic criterion performs well in describing the fracture envelop of these bonded joints. A crack equivalent concept was proposed to overcome several difficulties inherent to the test. The method assumes that the dual actuator test can be viewed as a combination of the double cantilever beam and end loaded split tests, which are used for pure modes I and II fracture characterization, respectively. A numerical analysis including a cohesive mixed-mode damage model was performed considering different mixed-mode loading conditions to evaluate the test performance. Some conclusions were drawn about the advantages and drawbacks of the test.

Paper 6 Chaves F.J.P ,de Moura M.F.S.F., da Silva L.F.M., Dillard D.A., Numerical validation of a crack equivalent method for mixed-mode I+II fracture characterization of bonded joints, 2013, submitted to Engineering Fracture Mechanics

**Abstract of paper 6 -** Numerical validation of a crack equivalent method for mixed-mode I+II fracture characterization of bonded joints: The present work is dedicated to development of a crack equivalent data reduction scheme applied to the load jig previously developed by Fernlund and Spelt in order to characterize fracture of bonded joints under mixed-mode I+II loading. The jig allows for easy alteration of the modemixity and permits covering the full range of mixed-mode I+II combinations. A data reduction scheme based on specimen compliance, beam theory and crack equivalent concept is proposed to overcome several difficulties inherent to the test analysis. The method assumes that the performed test can be viewed as a combination of the double cantilever beam and asymmetrically loaded end-notched flexure tests, which provide modes I and II fracture characterization, respectively. A numerical analysis including a cohesive mixed-mode I+II damage model was performed considering different mixedmode loading conditions to validate the proposed data reduction scheme. Issues regarding self-similar crack growth and fracture process zone development are discussed. It was verified that the considered in-plane mix mode fracture criterion is well captured using the proposed data reduction scheme.

Paper 7 Chaves F.J.P, da Silva L.F.M., de Moura M.F.S.F., Dillard D.A., Fonseca, J.O., Apparatus and method for characterization of bonded joints mixed-mode I+II fracture, 2013, submitted patent

Abstract of paper 7 - Apparatus and method for characterization of bonded joints mixedmode I+II fracture: The present invention relates to an apparatus for measuring the toughness of adhesive joints in various fracture modes from mode I (opening) to mode II (shear) relying exclusively on the load-displacement curve obtained from an universal testing machine and the displacement information from two linear variable differential transformer – LVDT - connected to the specimen beams. This apparatus is an evolution from the jig presented by Spelt and its operation is different from those existing on the market, mostly because it does not use the crack length measurement, instead it uses the displacement obtained from the LVDTs. It presents also another great advantage when compared to the existing solutions that places the specimen in the opposite side of the loading jig, because this invention place the specimen inside its structure, thus reducing the overall dimensions and facilitating the required test operations, improving the usability. Relying exclusively on three machine outputs, the load-displacement data and the displacement data from the two LVDTs, it allows an automated data reduction scheme and, therefore, renders an easier analysis that is accurate, not depending on human observation.

Paper 8 Chaves F.J.P, de Moura M.F.S.F., da Silva L.F.M., Dillard D.A., Mixed-mode I+II fracture characterization of bonded joints using a multi-mode apparatus, submitted

**Abstract of paper 8** - *Mixed-mode I+II fracture characterization of bonded joints using a multi-mode apparatus:* The present work presents the experimental test results to assess the toughness of an adhesive joint, using a previously defined crack equivalent data reduction scheme applied to a new multi-mode apparatus, inspired in a load jig previously developed by Fernlund and Spelt. The jig allows for easy alteration of the mode-mixity and permits covering the full range of mixed-mode I+II combinations. A data reduction scheme based on specimen compliance, beam theory and crack equivalent concept is used to overcome several difficulties inherent to the test analysis. The method assumes that the performed test can be viewed as a combination of the double cantilever beam and asymmetrically loaded end-notched flexure tests, which provide modes I and II fracture characterization, respectively. A numerical analysis

including a cohesive mixed-mode I+II damage model was performed considering different mixed-mode loading conditions to validate the proposed data reduction scheme. Issues regarding self-similar crack growth and fracture process zone development are discussed. It was verified that the considered in-plane mix mode fracture criterion is well captured using the proposed data reduction scheme.

#### 2. Adhesives tested

This thesis studied two types of epoxy adhesives: a ductile adhesive Araldite<sup>®</sup> 2015 and a brittle adhesive Araldite<sup>®</sup> AV 138M with the HV 998 hardener, both from Huntsman.

In **Paper 2**, Araldite<sup>®</sup> 2015 was used to bond different geometry specimens, DCB, ADCB, ATDCB, SLB and ENF, obtaining various points to plot a fracture envelop.

Both Araldite<sup>®</sup> AV 138M with the HV 998 hardener and Araldite<sup>®</sup> 2015 were used in **Paper 3** for the study of the adhesive bondline thickness impact in pure mode II loading.

**Paper 5** uses Araldite<sup>®</sup> AV 138M with the HV 998 hardener to bond DAL specimens tested in mixed-mode loading and used to obtain a fracture envelop.

Araldite<sup>®</sup> 2015 was characterized in pure mode I and two other mixed modes I+II combinations using the proposed apparatus in **Paper 8**. A fracture envelop was also obtained from the results.

#### 3. Test methods

More than the adhesive and adherends properties, adhesive joint design requires the knowledge about the joint behavior. The same adhesive, bonding two ductile adherends, behaves differently when it bonds two brittle and stiffer adherends. This is explained by the ability to dissipate energy ahead of the crack tip, where the adhesive is already damaged at the fracture process zone (FPZ). Stiffer adherends limit energy dissipation in the adhesive layer. The thickness of the adhesive layer is another important parameter to consider and has a big impact in the FPZ size [13].

Properties of adhesives can vary greatly and an appropriate selection is essential for a proper joint design. Thus, it is very important to determine the stresses and strains in adhesive joints for a variety of configurations or loading modes.

**Paper 2** uses different conventional specimen geometries to obtain the pure mode I, pure mode II and mixed-mode I +II energy release rate with DCB, ENF, ADCB, ATDCB and SLB tests.

The adhesive layer thickness impact with a ductile and a brittle adhesive was assessed with mode II, ENF tests in **Paper 3**.

A new test, allowing to apply different displacement ratios for each specimen beam was experimented in **Paper 5**. However, it is an expensive and sophisticated equipment that ready available in most laboratories.

Finally, in **Paper 7** and **Paper 8** a new test methodology is proposed, allowing to apply different mode combinations, using an apparatus designed to fit with an universal testing machine.

Detailed explanation of each test method is the object of this investigation.

#### 4. Apparatus Design

Considering product development methodologies defined by Ulrich and Eppinger [14] and inspired in the problem to solution path proposed by Bruno Munari [15], a methodology was defined to guide the apparatus design. This methodology was based in simulation of the apparatus loading scheme matching the experimental data previously obtained using various software. The different parts were modelled and assembled using Solidworks® that provided a first simulation approach using springs and connectors to emulate the adhesive. This simulation approach was compared with the results obtained using cohesive elements within ABAQUS® and the combined results were compared with the experimental results obtained as shown in Figure 1.

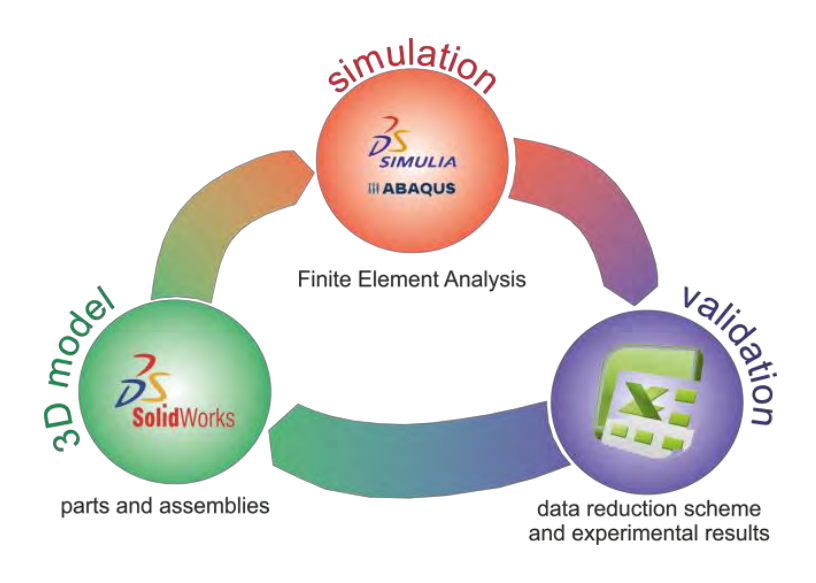


Figure 1. Design methodology scheme.

This design methodology was implemented to optimize the structural strength for the loading apparatus and the iterative process gave good results, optimizing also the resources in terms of time and computational effort.

**Paper 7** presents the final result for the loading apparatus obtained with this product development and design methodology.

#### 5. Numerical modeling

Forecasting the adhesive joint behavior is an important tool for the design of adhesively bonded joints. Furthermore, validating the proposed data reduction techniques is a very important task for any investigation. Numerical modeling provides the solution for forecasting the joint behavior and validating the data reduction techniques prior to experimental testing.

**Paper 4** and **Paper 6** rely on sophisticated numerical models implemented in ABAQUS<sup>®</sup>, using cohesive elements defined in user subroutines [13] to validate the proposed data reduction techniques. Cohesive parameters were determined using an inverse method as defined by Campilho et al. [3, 16]. This method uses iterative comparison between experimental data and numerical predictions using a precise geometry and boundary conditions to obtain the best fit for a defined cohesive law, and ultimately obtaining the cohesive parameters.

Numerical modeling is also used in **Paper 8** providing a comparison with the experimental results obtained.

These models are explained in detail in each paper.

#### 6. Conclusion

The objective of this research was to develop a fracture mechanics test methodology having in mind the adhesively bonded joints design using fracture mechanics concepts. Various fracture mechanics tests were experimented, from the basic pure mode I DCB test up to the sophisticated DAL frame, allowing a better understanding of the phenomena, and to collect valuable experimental data to support the design of the proposed test apparatus. Data reduction techniques were developed to overcome some inherent test difficulties such as the crack length measurement and providing more reliable results. A suitable test methodology, using a new mixed mode test apparatus was obtained and was subsequently used to determine fracture envelop for an adhesive joint.

#### 7. Future Work

This thesis provided a test methodology with an apparatus allowing to perform fracture mechanic tests with adhesively bonded joints. Steel adherend specimens were used in this work bonded with two distinct epoxy adhesives. The logical step forward should be to use different materials for the adherends, such as aluminum, wood and reinforced polymers (RP) and also other adhesives in order to obtain the fracture envelop.

This apparatus is capable of performing pure mode I, pure mode II and mixed-mode I+II combination loading for a DCB specimen. Developing a test apparatus and methodology that could also implement mode III would be an interesting future improvement.

#### References

- [1] J. Koller, U. Baumer, D. Mania, European Journal of Archaeology, 4 (2001) 385-397.
- [2] R.D. Adams, P.A. Fay in: 34th Annual Meeting of the Adhesion Society 2011, The Adhesion Society Savannah, Georgia, USA, 2011, pp. 26.
- [3] L.F.M. Da Silva, R.D.S.G. Campilho, Advances In Numerical Modeling Of Adhesive Joints, SPRINGER-VERLAG BERLIN AND HEIDELBERG GMBH & CO. KG, 2012.
- [4] L.F.M. da Silva, D.A. Dillard, B. Blackman, R.D.e. Adams, Testing Adhesive Joints, Best Practices, Wiley, Weinheim, 2012.
- [5] ASTM D3433 99, in: Annual book of ASTM standards, West Conshohocken, ASTM 15.06, 2012, pp. 225-231.
- [6] ISO 25217:2009, in, ISO, 2009, pp. 24.
- [7] ASTM D6671 / D6671M 06, in: Annual book of ASTM standards, West Conshohocken, ASTM 15.03, 2012.
- [8] J.H. Crews, J.R. Reeder, in, NASA TECHNICAL MEMORANDUM 100662, 1988.
- [9] J.R. Reeder, J.H. Crews, AIAA Journal, 28 (1990) 1270-1276.
- [10] D.A. Dillard, H.K. Singh, S. Park, D. Ohanehi, M.A. McGaw, in: SEM Annual Conference & Exposition on Experimental and Applied Mechanics, Society for Experimental Mechanics, Inc., St. Louis, 2006.
- [11] J.P.M. Gonçalves, M.F.S.F. de Moura, P.M.S.T. de Castro, A.T. Marques, Engineering Computations, 17 (2000) 28 47.
- [12] G. Fernlund, J.K. Spelt, Composites Science and Technology, 50 (1994) 441-449.
- [13] M.F.S.F. De Moura, J.P.M. Gonçalves, J.A.G. Chousal, R.D.S.G. Campilho, International Journal of Adhesion and Adhesives, 28 (2008) 419-426.

 $[14]\ K.$  Ulrich, S. Eppinger, Product Design and Development 3 edition ed., McGraw-Hill/Irwin, 2003.

[15] B. Munari, Da cosa nasce cosa. Appunti per una metodologia progettuale, 16 ed., Laterza, 2010.

[16] R.D.S.G. Campilho, M.F.S.F.d. Moura, D.A. Ramantani, J.P.M. Gonçalves, Ciência & Tecnologia dos Materiais, 20 (2008) 81-86.

• • PAPER 1

LITERATURE REVIEW

Fracture mechanics tests in adhesively bonded joints: a literature review

Filipe J.P. Chaves <sup>1</sup>, L.F.M. da Silva <sup>2</sup>, M.F.S.F. de Moura <sup>2</sup>, D.A. Dillard <sup>3</sup>

<sup>1</sup> IDMEC – Pólo FEUP, Faculdade de Engenharia da Universidade do Porto, Rua Dr. Roberto Frias, 4200-465 Porto, Portugal

<sup>2</sup> DEMec, Faculdade de Engenharia da Universidade do Porto, Rua Dr. Roberto Frias, 4200-465 Porto, Portugal

<sup>3</sup> Engineering Science and Mechanics Department, Virginia Tech, Blacksburg, VA 24061, United States

#### **Abstract**

Fracture mechanics characterization tests for adhesive joints are analyzed and reviewed in order to understand their advantages and disadvantages. Data reduction techniques for analytical methods are summarized to understand the improvements implemented in each test. Numerical approaches are also used complementing tests mode-mixity information. Both linear and non linear methods to obtain the fracture energy release rate are presented. Pure mode I and mode II tests are considered and simple mixed-mode tests, varying only the specimen geometry, with limited mode-mixity are evaluated. Performing a wider mode-mixity range requires sophisticated apparatus that are studied in detail. There is no general agreement about the test suitability for mixed-mode fracture assessment of adhesive joints. A universal test that can easily be performed and give accurate results is essential to optimize the expensive testing at the design stage.

**Keywords:** Adhesively bonded joints, fracture mechanics, mixed-mode I+II testing, mode I testing, mode II testing.

#### 1. Introduction

The growth in structural applications for adhesive joints requires the development of theories and models with a higher sophistication level, allowing to improve the mechanical and structural performance of adhesive joints [1]. Some tools resulting from this development are helping engineers to design better joints. Fracture mechanics applied to the adhesive joint is one

of the best tools to improve the joint design and guarantee its performance, optimizing the behavior and costs.

There are three basic approaches in order to characterize adhesive joints fracture: continuum mechanics; fracture mechanics; and the combination of the previous ones, damage mechanics.

#### 1.1 Continuum Mechanics

Several researchers used continuum mechanics to forecast the strength of adhesive joints. Adhesive and adherends are modeled using continuous elements, assuming a perfect connection between adhesive and adherend. This theory is based in the fact that there is a perfect joining between adhesive and adherend not taking into account the interface properties of adhesion between adhesive and adherend. Continuum mechanics relies on the characterization of stresses and deformations in the bonded parts and in the definition of the maximal force that can be applied to the joint in the four common loading cases: stress, shear, peeling and cleavage. Here we have the maximal stress, strain criteria and maximal deformation criterion that was used by Harris and Adams [2] to characterize the fracture of aluminum single lap joints bonded with epoxy. However these criteria are difficult to apply due to singularities of the joint tip geometry as shown in Figure 1. According with the linear elastic analysis, singularity refers to a point where stress will attain an infinite value, thus presenting a major disadvantage because the stress at those points are mesh dependent [3].

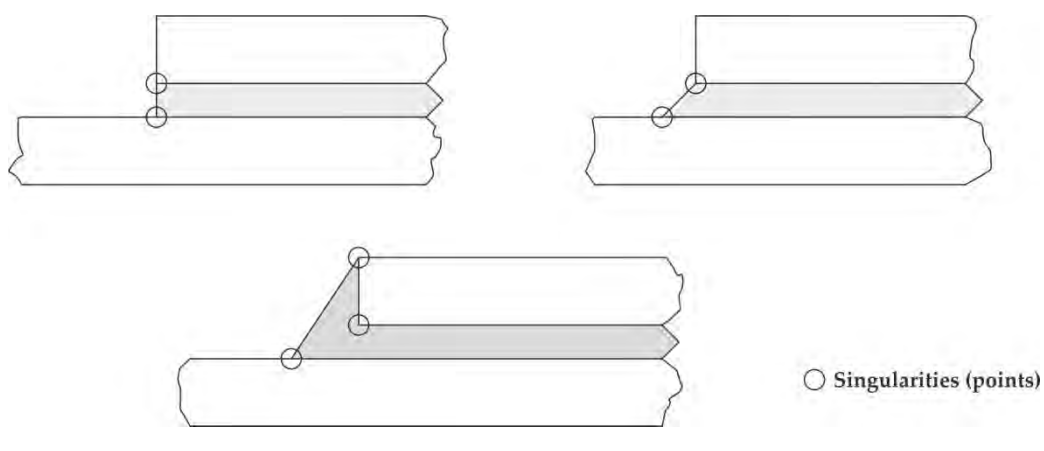


Figure 1. Adhesive joint singularities

Finite element analysis has pointed out this phenomenon, where the stress value increases with the mesh refinement, inhibiting the convergence towards the solution. This method is highly mesh dependent because of the singularities present at the adhesive joints. To overcome this problem, Adams and Harris [4] suggested a fillet of the adhesive or the adherend, to remove the singularity, however they also showed that the stress maximal value is dependent on the fillet

radius. The fillet radius effect on the adherends round corners of single lap joints was studied by Zhao et al. [5] for a ductile and a fragile adhesive. Joints bonded with the fragile adhesive presented a higher impact of the corner round in the stress value than joints bonded with ductile adhesive. When compared with the joint with sharp corners the effect of a round corner, with a considerable radius, improved the fragile adhesive joint strength by 40%. Opposite to this result, the joints bonded with the ductile adhesive reported a better strength for sharp corners joints, when compared with medium round corner. This study shows that different behaviors should be expected for fragile and ductile adhesives presenting different fracture mechanisms.

The problem now is to decide which is the best fillet radius for the joint corner to avoid losing strength. Exact knowledge of the corner rounding at the adherends and adhesive is essential for the correct evaluation of the joint strength. Crocombe [6] studied the failure of specimens under various modes of loading and used a critical peel stress at a distance from the singularity with some success. An alternative method was also proposed to use an effective stress, matched to the uniaxial bulk strength, at a distance. However, it was found for the latter criterion that the critical distance at which it should be applied varied with different modes of loading because of the change in the plastic zone size. Zhao et al. [7] and Chen et al. [8] applied a criterion whereby if the average plastic energy density over a certain distance within the single lap joint reached a critical value, then the joint was deemed to have failed. The integration region is usually chosen as a whole element for numerical convenience. In Zhao et al. [7], the value of  $t_A$  was used for integration and the predictions compared very well with the experimental results for a ductile adhesive. It should be realized that all the above criteria are applicable to continuous structures only. They run into difficulty when defects occur or more than one material is present, since stresses or strains are not well defined at the singular points. As a result, new criteria or modified versions of the above criteria need to be developed.

#### 1.2 Fracture Mechanics

Fracture criteria based on continuum mechanics assumes that the material does not have defects, and therefore the structure and material behave as a continuous body. The presence of defects or two materials with protuberances infringes the continuum mechanics principles. In the other hand, fracture mechanics assumes the structure not to be continuous, allowing manufacture defects or any other damage caused during its life at work [9]. Delamination, debonding, cracks and others imperfections present within materials, often are points of stress concentration and therefore initiation points for fracture to occur and propagate and cause the failure of the component. This method evaluates if the size of each defect does not overcome the critical fracture size leading to structural failure. Fracture Mechanics relies on two basic criteria, both implemented for the study of materials with cracks [10]: A stress intensity factor criterion and

another based on energetic concepts. The stress intensity factor K, represents a scale parameter that defines the changes in the stress state in the neighborhood near the crack tip, originated by the infinite stress in those areas.

Figure 2 shows the three different loading modes leading fracture to occur. Mode I is the opening mode, and mode II and III are the shearing modes. The crack surfaces move perpendicularly to the crack tip, whereas in mode II the movement is parallel to the crack tip. Considering a mode I loading, becomes:

$$K_{\rm I} = Y \sigma_r \sqrt{\pi a}$$
 (Eq. 1)

where Y is an non dimensional function depending on the geometry, load distribution and is given, graphically for a large number of practical cases. The stress intensity factor characterizes the stress at the crack tip and measures the propagation capability. Crack will occur when:

$$K_{\rm I} = K_{\rm Ic}$$
 (Eq. 2)

where  $K_{\rm Ic}$  is a new material property that measures the ability to prevent the crack growth in mode I, named mode I fracture toughness. As long as  $K_{\rm I}$  value computed at the crack tip remains under the value of the material mode I toughness  $K_{\rm Ic}$ , is safe to say that the crack does not propagates. It is important to attain that  $K_{\rm I}$  is a variable exclusively dependent on the part geometry, the crack geometry and the loading type while  $K_{\rm Ic}$  is a parameter characteristic of each material, thus a material mechanical property.

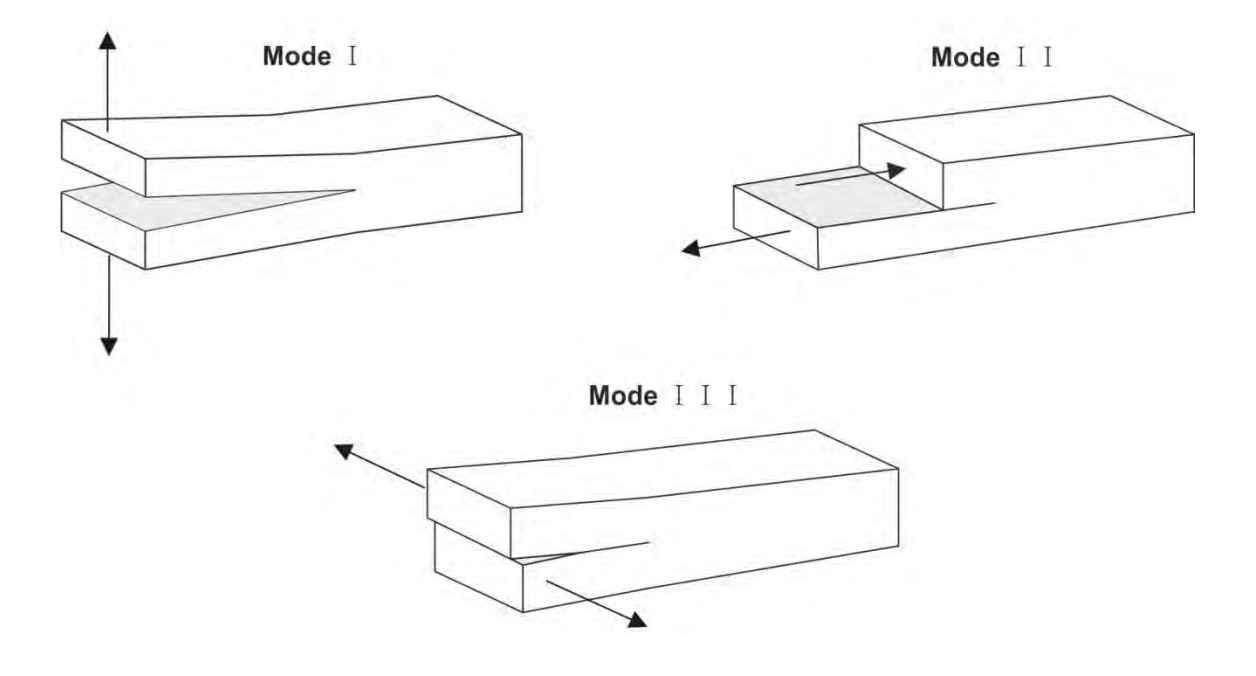


Figure 2. Adhesive joint fracture modes

The energetic criteria relies on the hypothesis that the propagation of an internal defect will occur when the available energy at that defect tip (G - energy release rate) equals the energy needed for the crack to propagate ( $G_c$  - critical energy release rate) for the applied loading [11]. Energy release rate is a material energy, thus the critical condition to avoid crack propagation, is:

$$G \le G_{\rm c}$$
 (Eq. 3)

The presented approaches (stress intensity factor, K, and energy release rate, G) are the same for homogeneous materials, and are related by [12]:

$$G = \frac{K^2}{\overline{F}} \tag{Eq. 4}$$

where  $\overline{E}=E$ , is the Young's modulus for the plane stress or  $\overline{E}=E/(1-v^2)$  for the plane strain state and v is the material Poisson's ratio. These same formulas are true for their critical values  $(G_c \text{ and } K_c)$ .

In most of the daily situations, the applied loading originates a combination of peeling and shear stresses, as a combination of modes occurring simultaneously at the crack tip, requiring a mixed mode criterion allowing a better simulation for damage propagation. Several authors have applied fracture mechanics concepts in forecasting the toughness of adhesive joints. Most of these works relied on the strain energy release rate (SERR) concept. Kinloch [13] states that energetic criterion is better than the stress intensity factor, firstly because, G, has an important physical meaning related with the crack energy absorption process, and secondly because it is very difficult to obtain the stress intensity factor values, K, mostly when the crack grows near the interface. For bulk materials the crack tends to grow in mode I, regardless of the original orientation. However, when a crack propagates within an adhesive joint, the adherends will constrain the crack growth in pure mode I, forcing the crack to propagate in mixed-mode (I+II) crack propagation:

$$\left(\frac{G_{\rm I}}{G_{\rm Ic}}\right)^{\alpha} + \left(\frac{G_{\rm II}}{G_{\rm IIc}}\right)^{\beta} = 1 \tag{Eq. 5}$$

where  $G_{\rm lc}$  and  $G_{\rm llc}$  are the critical Energy release rate for both pure modes (I and II), and  $\alpha$  and  $\beta$  are the exponents. Linear ( $\alpha = \beta = 1$ ) and quadratic ( $\alpha = \beta = 2$ ) criteria are the most common.

In order to characterize the mixed mode (I + II) fracture, a property must be defined, known as ratio mode, very helpful to characterize fracture in planar problems, given by:

$$\varphi = \tan^{-1} \left\lceil \frac{K_{\text{II}}}{K_{\text{I}}} \right\rceil = \tan^{-1} \sqrt{\frac{G_{\text{II}}}{G_{\text{I}}}}$$
 (Eq. 6)

Fracture mechanics criteria are based in the presence of defects that are usually modeled as precracks which are artificially placed to simulate damage initiation. However, these fracture mechanics criteria are best suited for damage propagation instead of initiation [3, 14].

#### 2.3 Damage Mechanics

Cohesive and continuum damage models try to overcome the drawbacks, and explore some advantages of the previously described methods [15]. Both of them are suited for adhesive joint fracture analysis and combine continuum mechanics tools to model damage initiation and fracture mechanics tools to deal with the crack propagation [3]. When a stress criterion is satisfied at an integration point, a relaxation process takes place, ruled by an established fracture energy criterion, simulating the material degradation and originating a stress reduction at the referred integration point and consequently a redistribution of the neighboring stresses. This process avoids the numerical stress peaks at the singularities. Generally, CZM models are based on interface elements [16], connecting planes or three dimensional solids. These elements are characterized for having no thickness and promoting the connection between two solid elements. The ability to simulate both the crack initiation and the crack propagation represents a major advantage for cohesive elements. There is no need for a pre crack and the propagation occurs without any user intervention. Nevertheless the user must know the critical areas promoting the damage initiation and place the cohesive elements accordingly. Adhesive science has used extensively cohesive elements in order to simulate damage [3, 16-19]. Gonçalves et al [20], considered a mixed-mode (I + II) model to simulate the fracture process of aluminum single lap adhesive joints. A triangular traction-separation law was used and load displacement (  $P-\delta$  ) graphs were precisely forecasted when the material plastic behavior was considered for all the studied overlap lengths. Blackman et al. [18] used a CZM including the parameters,  $G_{\rm c}$  and  $\sigma_{\rm max}$  to study adhesive joints fracture. Continuum damage models are also appropriated when adhesive thickness must be considered [21]. Although adhesive thickness is

small when compared to the others joint dimensions, it will have implications in the joint mechanical properties [22]. Continuum damage models are an excellent tool to evaluate the thickness effect on the fracture of adhesive joints. Figure 3 shows the variation of the FPZ according with the adhesive thickness causing the adhesive joint fracture to behave differently. FPZ is a region near the crack tip where inelastic processes occur, such as micro cracking, plastic micro straining, etc. Continuum elements were used by de Moura et al. [3] in order to study the FPZ shape as a function of adhesive thickness (Figure 3) and its influence in the R-curve behavior. These R-curves are graphical representations of the Energy Release Rate variation, G, as a function of the crack length, a. These curves present a well-defined stabilization plateau throughout the crack length, which will be considered the critical energy release rate,  $G_{\rm c}$ , known as the adhesive fracture toughness. The authors understood that thinner adhesive bondlines lead to a stretched thin FPZ originating an initial lower slope in the R – curve, delaying the crack propagation.

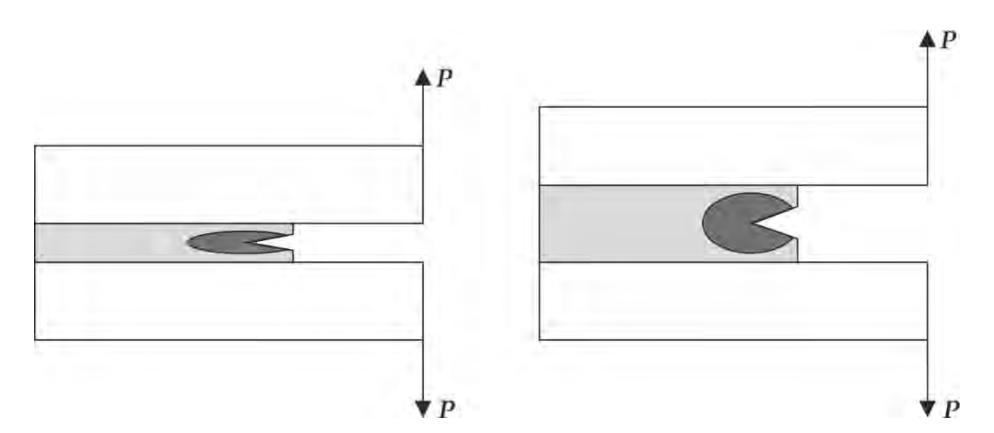


Figure 3. Fracture Process Zone (FPZ) shape as function of adhesive thickness.

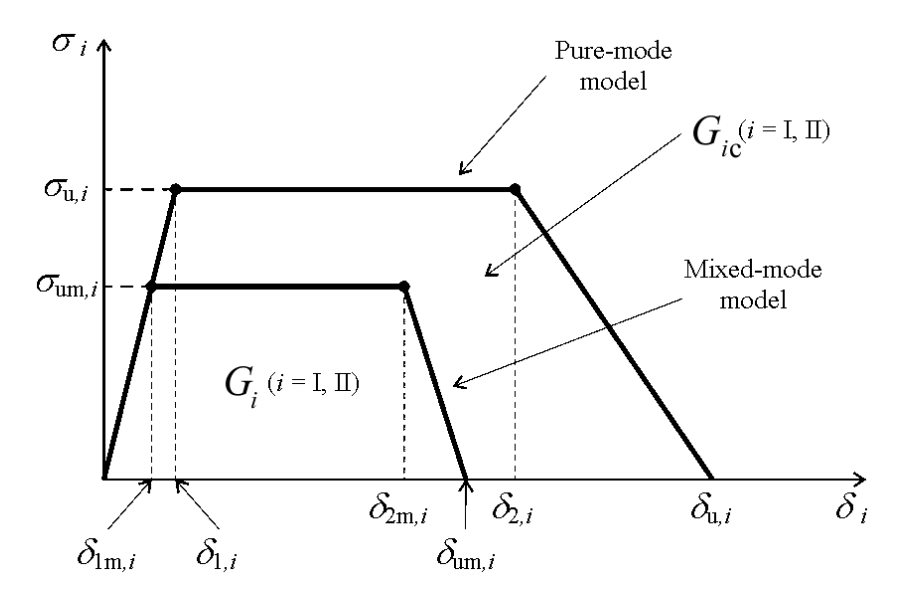


Figure 4. The trapezoidal softening law for pure and mixed-mode cohesive damage model.

Triangular cohesive law is a particular case of the trapezoidal softening law (Figure 4) best suited for brittle adhesives because it does not take into account the plasticity and therefore there is no plateau and the displacements become  $\delta_{1m,i} = \delta_{2m,i}$  and  $\delta_{1,i} = \delta_{2,i}$ .

Fracture mechanics and cohesive damage models are becoming preferential methods to evaluate adhesive joints strength. Fracture toughness,  $G_{\rm c}$ , is the most relevant property to evaluate. Fracture varies with the mode of loading, mode I, mode II and mode III (Figure 2) [23-25] and most working condition loadings are combinations of these modes [26-28].

The next sections describe the best known tests used to characterize adhesive joints fracture mechanics for each mode and the different methods for data reduction.

#### 2 Mode I fracture tests

The most common tests to obtain  $G_{lc}$  are the Double Cantilever Beam (DCB) and the Tapered Double Cantilever Beam (TDCB) [29], described in the American standard ASTM D 3433-99 [30] and recently updated in the ISO 25217:2009 [31].

#### 2.1 Double Cantilever Beam - DCB

The DCB specimen is comprised of two beams with the same length and constant thickness, as shown in Figure 5. An initial region without adhesive is considered to be the pre crack,  $a_0$ , and h is the adherends thickness and t the adhesive thickness.

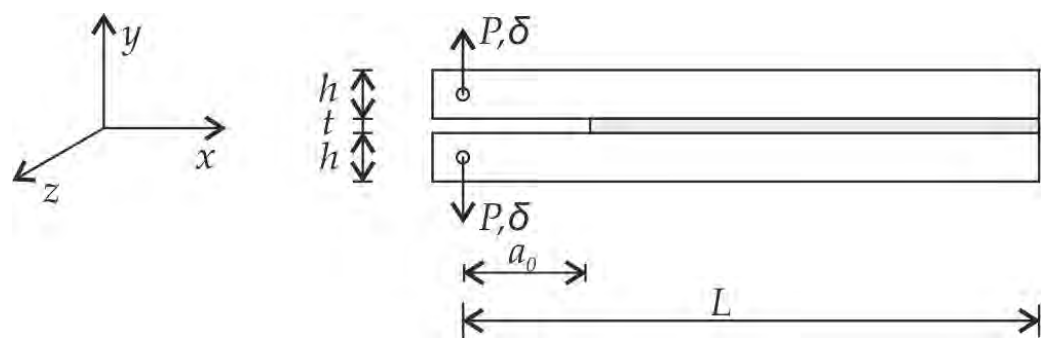


Figure 5. DCB specimen schematics.

The specimen is loaded by opening the beams with test speeds between 0.5 and 3 mm/min, depending on the geometry and material characteristics. During the test, the load P and displacements  $\delta$  are registered for each crack length, a.

 $\bullet$   $\bullet$   $\bullet$ 

For specimens with pre crack and a linear relationship between the load and the displacement, the fracture energy G, is obtained from Irwin-Keyes equation [32]:

$$G = \frac{P^2}{2b} + \frac{dC}{da} \tag{Eq. 7}$$

where P is the applied load, b the specimen width, C is the adherends compliance and a the crack length.

Then, DCB specimen's fracture energy is given by:

$$G_{\rm lc} = \frac{6P^2}{b^2h^3} \left(\frac{2a^2}{E} + \frac{h^2}{5G}\right)$$
 (Eq. 8)

This equation is based in the elementary beam theory, and this method is best known as direct beam theory (DBT) [33]. Nevertheless this equation does not take into account root rotation at the crack tip and has stress concentration issues, which will affect the  $P-\delta$  curve. To overcome these problems, de Moura et al. [3] propose an equivalent flexural module,  $E_{\rm f}$ , instead of E in (Eq. 8). The equivalent modulus is obtained from using an initial flexibility  $C_0$ :

$$E_{\rm f} = \left(C_0 - \frac{12(a_0 + |\Delta|)}{5bhG}\right)^{-1} \frac{8(a_0 + |\Delta|)^3}{bh^3}$$
 (Eq. 9)

where  $\Delta$  is a correction factor for the crack length, determined from the linear regression of  $C^{1/3} = f(a_0)$ . This linear regression can be obtained after testing three specimens with different initial crack length as shown in Figure 6 [3].

 $C^{1/3} (mm/N)^{1/3}$   $A_{01}$   $A_{02}$   $A_{03}$   $A_{03}$   $A_{04}$   $A_{05}$   $A_{06}$   $A_{07}$   $A_{08}$   $A_{09}$   $A_{09}$ 

Figure 6. Method for crack length correction,  $\Delta$ .

Another way to obtain the root rotation effects was proposed by Wang and Williams [34], using the variable  $\Delta_1$ , defined by:

$$\Delta_{\rm I} = h \sqrt{\frac{E}{11G} \left[ 3 - 2 \left( \frac{\Gamma}{1 + \Gamma} \right)^2 \right]} \text{ and } \Gamma = 1.18 \frac{E}{G}$$
 (Eq. 10)

This variable,  $\Delta_I$ , can be used in (Eq. 9) instead of  $\Delta$ .

Also, an equivalent crack length  $a_{\rm e}$  must be considered during the crack propagation accounting for the FPZ effect. Previous studies characterizing mode II fracture revealed that this effect could not be ignored during the crack growth [35]. For ductile adhesives, this effect is even bigger. The equivalent crack length can be obtained from considering  $a_{\rm e}$  instead of a, as function of the specimen compliance registered during the test. Note that  $a_{\rm e} = a + |\Delta| + \Delta a_{\rm FPZ}$ , considering both the root rotation effects at the crack tip and the FPZ. Using these improvements, the mode I fracture energy can be obtained with:

$$G_{\rm lc} = \frac{6P^2}{b^2 h^3} \left( \frac{2a_{\rm e}^2}{E} + \frac{h^2}{5G} \right)$$
 (Eq. 11)

With this method, the fracture energy,  $G_{\rm lc}$ , is obtained exclusively from the  $P-\delta$  curve, and is known as Compliance Based Beam Method (CBBM). This method does not require measuring the crack length during the test, because an equivalent crack length is used, instead of the real crack length.

When ductility exceeds elasticity, LEFM cannot be used. As explained by Suo et al.[36], LEFM solutions for stress intensity factors or energy release rates generally differ from the *J*-integral solution in the case of large-scale plasticity [37]. For most specimens, closed-form analytical solutions for *J*-integral cannot be obtained, since the *J*-integral solution depends on the details of the stress-separation law [38]. Nevertheless, analytical solutions for the *J*-integral are available for a few fracture test specimens [36]. Some solutions were presented for DCB specimen loaded under pure bending moments (for pure mode I stress-separation laws) [36, 39] However, the standard DCB test does not provide a pure bending moment in the specimen arms. It becomes necessary to include the contribution of the rotation of the beams near the crack front for the *J*-integral calculation [40].

#### 2.2 Tapered Double Cantilever Beam – TDCB

ASTM D3433 – 99 [30] standard suggests another specimen geometry to obtain the energy release rate for mode I. Similar to DCB, it is a symmetrical specimen, in this case with a wedge shape. The specimens are manufactured with two sections of constant height at both ends and a middle section where the height changes with the crack length, h = f(a), as shown in Figure 7.

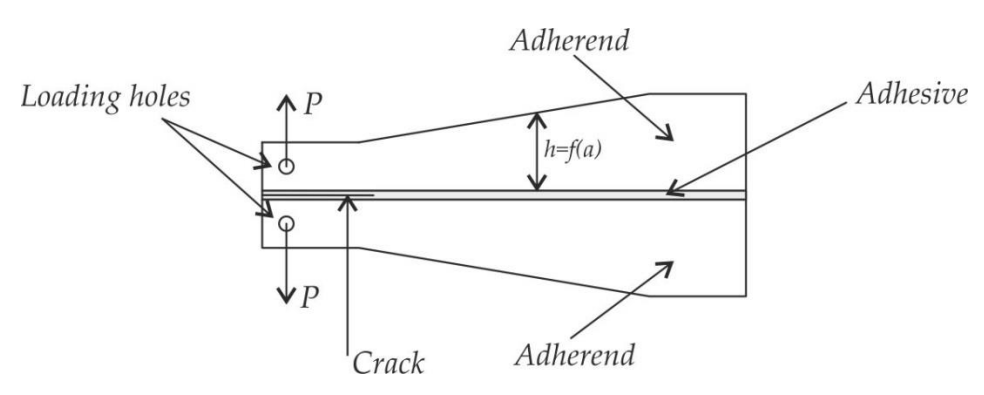


Figure 7. Adhesive joint TDCB specimen.

Beam compliance is obtained considering the flexural moment and shear contributions to the deformation, by:

 $\frac{dC}{da} = \frac{8}{Eb} \left( \frac{3a^2}{h^3} + \frac{1}{h} \right) \tag{Eq. 12}$ 

where E and h are the adherend's Young's modulus and thickness. Ripling at al. [23] suggested that with an adequate profile for the height of each beam, dC/da could remain constant if  $\left(\frac{3a^2}{h^3} + \frac{1}{h}\right)$  from (Eq. 12) was also constant. If the beam is manufactured with a geometric factor, m, defined by:

$$m = \frac{3a^2}{h^3} + \frac{1}{h} = \text{constant}$$
 (Eq. 13)

the value for dC/da must be constant, meaning that compliance must have a linear variation regarding to the crack length, and replacing in Irwin-Keyes equation, (Eq. 7), the critical energy rate becomes:

$$G_{\rm lc} = \frac{4P^2}{Eb^2} \left( \frac{3a^2}{h^3} + \frac{1}{h} \right) = \frac{4P^2}{Eb^2} m$$
 (Eq. 14)

TDCB tests have become popular and are used for static and fatigue tests, and also to describe the adhesive joints ageing when subjected to weather degradation. The great advantage is to obtain the critical energy release rate,  $G_{\rm lc}$ , regardless of the crack length a. The only disadvantage is the higher manufacturing complexity when compared with common DCB, mostly for composite adherends [9, 41]

#### 3 Mode II fracture tests

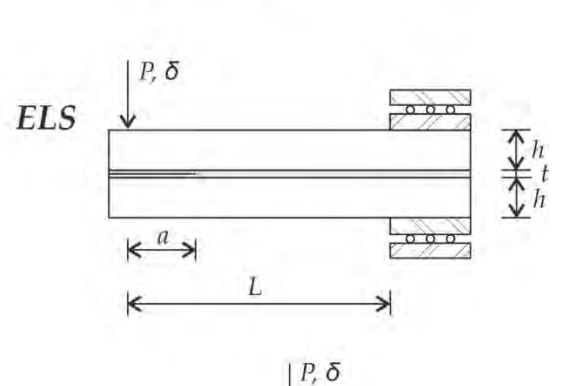
Until the present day, there are no standards for testing mode II fracture of adhesive joints, however there are tests based on interlaminar fracture of composites in mode II adapted to the adhesive joint study. In this context, several tests allowing the determination of mode II fracture toughness of adhesive joints can be used (Figure 8), such as: End Notched Flexure (ENF); End Loaded Split (ELS); and the Four – Point End Notched Flexure (4ENF). There are some advantages and disadvantages associated with each one of these tests. ELS test have some problems with the correct determination of  $G_{\rm IIc}$  due to the presence of big displacements and

some sensitivity to the clamping where the specimen gets prevented from vertical sliding while guided in the horizontal movement. By the other side, ELS promotes a stable crack initiation has been the preferable test for ESIS – European Structural Integrity Society [42]. 4 ENF is a most sophisticated test, which has some friction problems at the pre crack zone, resulting from the loading [22]. The simplest and therefore the most commonly used to characterize mode II adhesive joint fracture is the ENF test.

#### 3.1 End notch flexure (ENF)

Specimens for ENF testing consist of two beams with constant thickness bonded together and simply supported at the extremities. A mid span load is applied causing shear in the adhesive, as shown in the first case of Figure 8. Applying the beam theory, and using the Irwin-Keyes equation, (Eq. 7) mode II energy release rate becomes:

$$G_{\text{IIc}} = \frac{9P^2a^2}{16b^2Eh^3}$$
(Eq. 15)
$$ENF \qquad \qquad \downarrow P, \delta \qquad \qquad \downarrow h$$



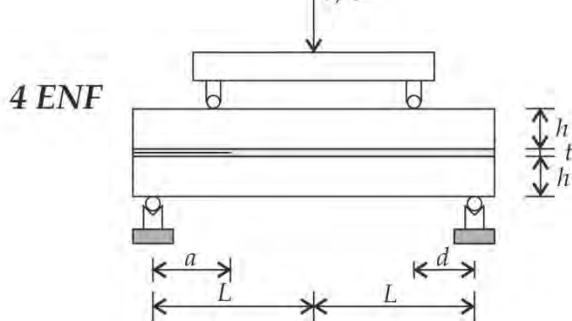


Figure 8. Best known mode II tests for characterization of adhesive joints.

The described method is known as Direct Beam Theory (DBT), however, this simple beam theory does not take into account the transverse shear effect at the crack tip. Fixing this, Wang and Williams [34] proposed the Corrected Beam Theory (CBT) using the following equation:

$$G_{\text{IIc}} = \frac{9P^2 \left( a + |\Delta_{\text{II}}| \right)^2}{16b^2 Eh^3}$$
 (Eq. 16)

where  $\Delta_{\rm II}$  is the crack length correction considering the root rotation at the crack tip,

$$\Delta_{II} = 0.42\Delta_{I} \tag{Eq. 17}$$

and  $\Delta_{\rm I}$  is the crack length correction for mode I with the DCB test, defined by (Eq. 10). The previous methods rely on the crack length measure during the test, which can be very difficult because of the propagation that occurs by shear with adherends friction. Furthermore, the previous methods do not take into account the FPZ at the crack tip, where the damage takes place by plasticization and microstraining, absorbing part of the available energy.

To include the FPZ effect, a correction to the real crack length should be considered during the propagation. The equivalent crack length is [3]:

$$a_{\rm e} = a + \Delta a_{FPZ} = \left[ \frac{C_{\rm corr}}{C_{\rm 0corr}} a_0^3 + \frac{2}{3} \left( \frac{C_{\rm corr}}{C_{\rm 0corr}} - 1 \right) L^3 \right]^{1/3}$$
 (Eq. 18)

where  $C_{\text{corr}}$  and  $C_{0\text{corr}}$  are given by:

$$C_{\text{corr}} = C - \frac{3L}{10Ghh}$$
 and  $C_{\text{0corr}} = C_0 - \frac{3L}{10Ghh}$ 

The energy released rate for mode II,  $G_{\rm II}$ , becomes:

$$G_{\text{IIc}} = \frac{9P^2}{16b^2Eh^3}a_e^3 = \frac{9P^2}{16b^2Eh^3} \left[ \frac{C_{\text{corr}}}{C_{\text{0corr}}}a_0^3 + \frac{2}{3} \left( \frac{C_{\text{corr}}}{C_{\text{0corr}}} - 1 \right) L^3 \right]^{1/3}$$
 (Eq. 19)

This method does not require the crack length measure during the test. Instead, the equivalent crack length  $a_{\rm e}$  considering the FPZ effect is used. This method is based in the material compliance, as is known as Compliance Based Beam Method (CBBM), allowing obtaining the fracture energy  $G_{\rm II}$  using exclusively the  $P-\delta$  curve. It is also possible to obtain the R curve as function of the equivalent crack length and the fracture energy as done by da Silva et al. [22, 43].

3.2 End loaded split (ELS)

The end-loaded split (ELS) test provides a stable crack propagation allowing the measurement of the mode II *R*-curve, thus being favored by the ESIS TC4 committee [44, 45]. However, it requires a more elaborate fixture and data reduction scheme, including the measurement of a clamp correction factor [45] and the specimen is susceptible to large displacements [46].

Using the beam theory, the strain energy release may be defined by [47, 48]:

$$G_{\text{IIc}} = \frac{P^2}{2h} \frac{dC}{da} = \frac{9P^2a^2}{4b^2h^3E}$$
 (Eq. 20)

Blackman et al. [47] proposes a CBT recurring to a correction factor F accounting for large deflections, that gives an energy release rate for mode II as follows:

$$G_{\text{IIc}} = \frac{9P^2 (a + \Delta_{II})^2}{4b^2 h^3 E} \cdot F$$
 (Eq. 21)

where  $\Delta_{II} = 0.42\Delta_{I}$  as defined by Wang and Williams [34] and  $\Delta_{I}$  is the value of the mode I correction measured in a DCB test.

A CBBM approach to ELS was also proposed by de Moura et al. [49], recurring to the compliance:

$$C = \frac{\delta}{P} = \frac{3a^3 + L^3}{2bh^3 E} + \frac{3L}{5bhG}$$
 (Eq. 22)

and defining an effective length,  $E_L$  for a perfect clamping, during propagation an equivalent crack length becomes:

$$a_e = \left[ \left( C - C_0 \right) \frac{2Bh^3 E_L}{3} + a_0^3 \right]^{1/3}$$
 (Eq. 23)

where 
$$C_0 - \frac{3a_0^3}{2bh^3E} = \frac{L_{\text{ef}}^3}{2bh^3E} + \frac{3L_{\text{ef}}}{5bhG}$$
 and  $C_0 - \frac{3a^3}{2bh^3E} = \frac{L_{\text{ef}}^3}{2bh^3E} + \frac{3L_{\text{ef}}}{5bhG}$ 

Combining with (Eq. 20) an energy release rate for mode II is given by:

$$G_{\rm IIc} = \frac{9P^2 a_e^2}{4b^2 h^3 E}$$
 (Eq. 24)

#### 4 Mixed Mode (I + II) fracture tests

There are several tests proposed in literature to characterize the behavior of adhesive joints in mixed mode, however most of them are not standardized. Single Leg Bending (SLB) test [50, 51] is based on the ENF test, but this specimen lower beam has a smaller length, resulting in an unsupported extremity which will lead to an opening mode (mode I) and a shear mode (mode II) simultaneously. Another test is the Asymmetric Tapered Double Cantilever Beam (ATDCB) [52], by varying the beam thickness introduces some degree of mixity (Table 1). Varying the adherends thickness or relative stiffness, using different materials it is also possible to obtain a mixed mode test known as Asymmetric Double Cantilever Beam (ADCB) [53]. Another relatively recent test is the Crack Lap Shear (CLS) [54]. This specimen has mode ratio degree near 49°, varying with the relative stiffness of the adherends. Mixed Mode Bending (MMB) [55, 56] and Spelt [35] tests have variable mode ratio degrees,  $\varphi$ , depending on the loading imposed to the specimen. Table 1 shows some of these different tests, used to characterize adhesive joints fracture under mixed mode loading and the corresponding mode ratio,  $\varphi$ .

Global Mixity, Test name Test scheme Asymmetric Double ≈ - U - 34° Cantilever Beam (ADCB a 41 00 Crack Lap Shear (CLS) Asymmetric Tapered ≈ 20° (ATDCB) Mixed Mode Bending  $\Psi = f(c)$ (MMB)  $\Psi = f(S_1, S_2, S_3, S_4)$ Spell Loading Jig (SPELT) 0000000000000

Table 1. Different mode mixity tests and corresponding mode ratio  $\varphi$ 

• • • •

#### 4.1 Mixed Mode Bending – MMB

The standard [57] "Test method for mixed mode I - mode II interlaminar fracture toughness of unidirectional fiber reinforced polymer matrix composites" suggests the mixed mode bending (MMB) test to determine the fracture toughness, G, of composites and it is the only standard test available to evaluate the mixed mode toughness [58]. MMB test is a combination of two of the most relevant tests for adhesive joints characterization in mode I and mode II, DCB and ENF respectively. This test works by adding an opening mode loading to an ENF test, loading at mid span, as seen in schematic a) of Figure 9. This additional loading promotes the beams separation, such as in the DCB test. The relative value of the two applied forces, establishes the mode mixity degree at the crack tip [55]. Applying these two forces through a loading beam and a hinge, the test can be performed with only one loading P as shown in Figure 9.

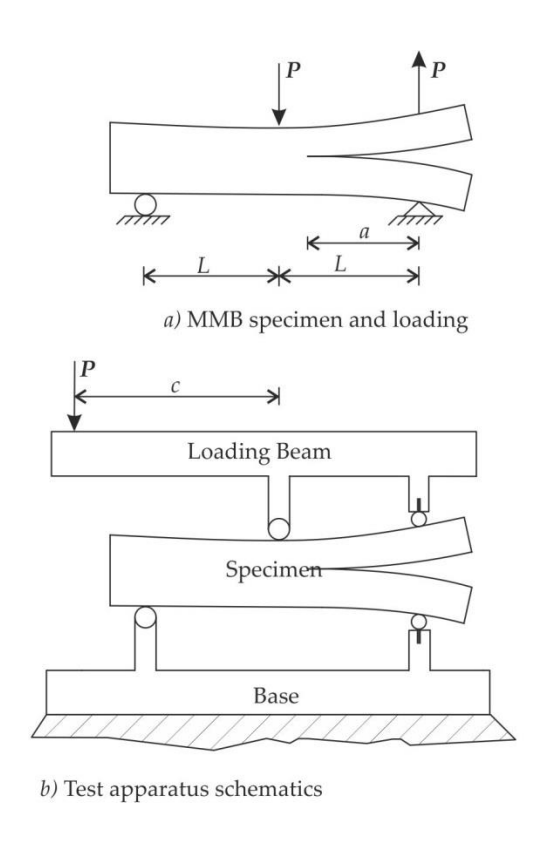


Figure 9. MMB specimen and test shematics.

The loading distance c defines the relative value of these two loads applied to the specimen, and therefore the mode ratio degree,  $\phi$ , for each test. The MMB test loading corresponds to an overlap of the mode I and II loadings, equivalents to the ones used with DCB and ENF tests respectively. Therefore the energy release rate equations found in literature for these tests can be

combined in order to obtain the desired equations for this test. Figure 10 shows the loading mode for the MMB test as function of the applied loading, P, the length of the loading beam,  $^{\mathcal{C}}$ , and half the specimen length, L. As shown in the scheme b) of the same Figure, the mode I loading component is given by:

$$P_{\rm I} = \left(\frac{3c - L}{4L}\right)P\tag{Eq. 25}$$

replacing  $P_{\rm I}$  in (Eq. 8) based in the beam theory and ignoring the transverse shear effects, results in:

$$G_{\rm I} = \frac{3a^2 P^2}{4b^2 E h^3 L^2} (3c - L)^2$$
 (Eq. 26)

The same orientation is applied for mode II loading, (Figure 10 scheme c), equivalent to ENF test and the flexural loading is given by:

$$P_{\rm II} = \left(\frac{c+L}{L}\right)P \tag{Eq. 27}$$

Replacing  $P_{\text{II}}$  in the mode II energy release rate  $G_{\text{II}}$  equation established for ENF test mode II component for MMB test becomes:

$$G_{\rm II} = \frac{9a^2P^2}{16h^2Eh^3L^2} (c+L)^2$$
 (Eq. 28)

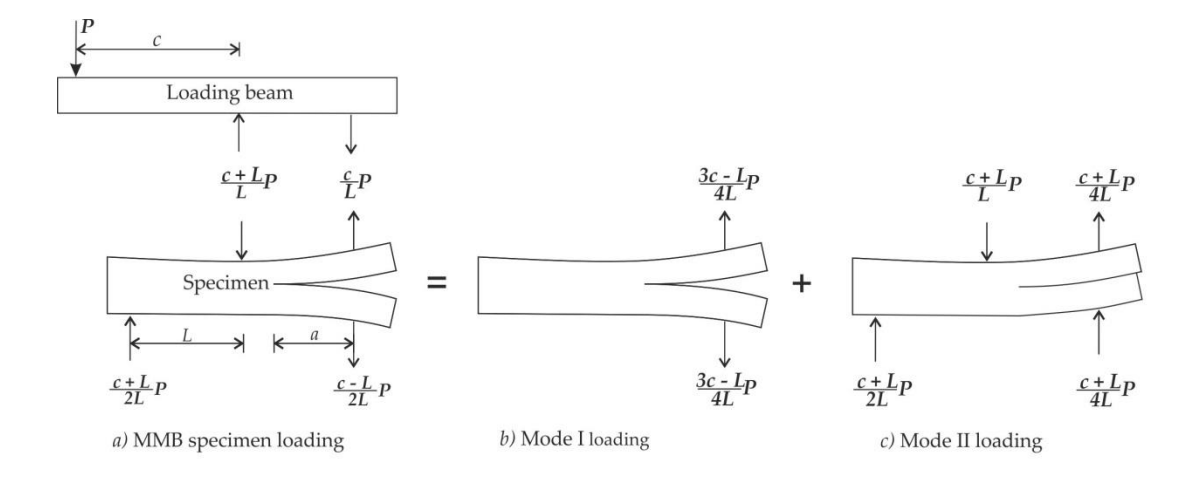


Figure 10. MMB free body diagram

Dividing (Eq. 26) by (Eq. 28), the  $G_{\rm I}/G_{\rm II}$  ratio is obtained for the MMB test:

$$\frac{G_{\rm I}}{G_{\rm II}} = \frac{4}{3} \left( \frac{3c - L}{c + L} \right)^2 \qquad c \ge \frac{L}{3}$$
 (Eq. 29)

(Eq. 29) shows that the ratio  $G_{\rm I}/G_{\rm II}$  is only function of the loading distance, c, and the half length, L.  $G_{\rm I}/G_{\rm II}$  is null when c=L/3, and (Eq. 29) is not valid for small values of c, because this model does not take into account the contact between the two specimen beams. The total energy release rate for MMB test is obtained adding (Eq. 26) and (Eq. 28), becoming:

$$G_{\rm T} = \frac{3a^2P^2}{16b^2Eh^3L^2} \left[ 4(3c-L)^2 + 3(c+L)^2 \right]$$
 (Eq. 30)

However (Eq. 26) and (Eq. 28) underestimate the values for  $G_{\rm I}$  and  $G_{\rm II}$  when applied to composites interlaminar fracture. To overcome this setback and improve the results, Kanninen [59] recommends including the cantilever rotation at the crack tip with the mode I component and also taking into account the shear effects in both the contributions, originating the following equations:

$$G_{\rm I} = \frac{3P^2 (3c - L)^2}{4b^2 E h^3 L^2} \left( a^2 + \frac{2a}{\lambda} + \frac{1}{\lambda^2} + \frac{h^2 E}{10G} \right)$$
 (Eq. 31)

$$G_{II} = \frac{9a^2P^2(c+L)^2}{16b^2Eh^3L^2} \left(a^2 + \frac{0.2h^2E}{G}\right)$$
 (Eq. 32)

where

$$\lambda = \left(\frac{6E_2}{h^4 E}\right)^{1/4} \tag{Eq. 33}$$

and  $E_{\rm 2}$  is the transversal Young modulus (for isotropic materials,  $E_{\rm 2}=E$  ).

An interesting study [60] compared the modified beam theory MBT with the CBT providing good results for experimental data using the MBT as data reduction technique [61].

Using these corrections, and implementing the CBBM, some improvements were done by Oliveira et al. [27] taking into account the compliance and FPZ. The implementation of CBBM brought another advantage, avoiding the crack length monitoring.

The possibility to change the mode-mixity and easy test implementation are advantages for this test, however it was originally designed for delamination with composites, making it inappropriate to use with stiffer aluminum or steel adherends.

#### 4.2 Asymmetric Double Cantilever Beam – ADCB

Asymmetric Double Cantilever Beam (ADCB) is a generalization of the standard DCB test which is altered for mixed mode testing by using different beam thickness or different materials for the adherends. The specimens are manufactured and tested in the same exact manner as the standard DCB test, as shown in Figure 11. The specimen's asymmetry assures a constant mode mixity degree, which is defined by the thickness ratio of the adherends.

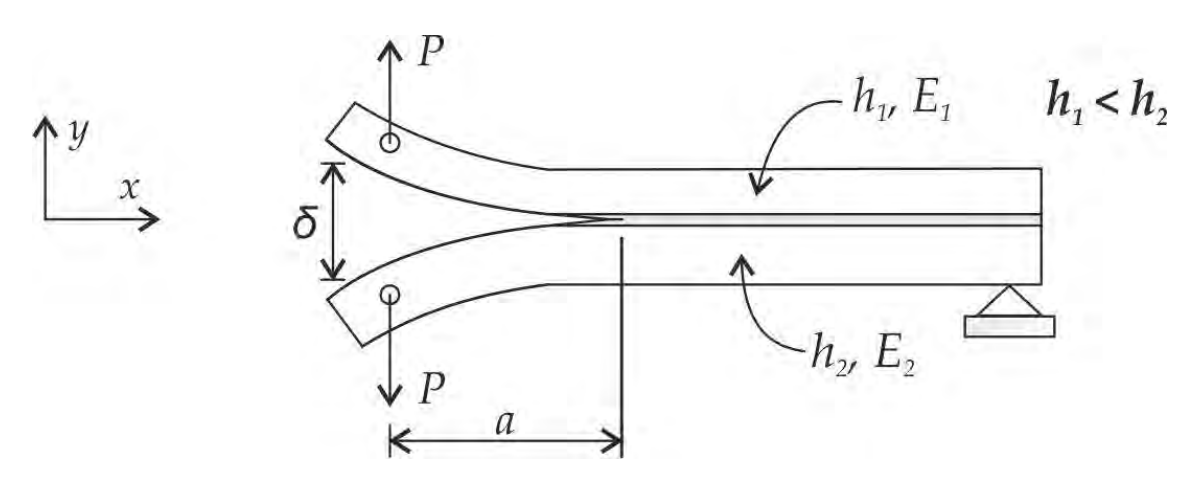


Figure 11. ADCB schematic test representation.

To determine the mixed mode fracture toughness, Xiao et al. [53] propose a model considering the ADCB specimen to be divided in two elastic cantilevers. This model assumes that the entire elastic energy released during the fracture results solely from the flexure of the two specimen beams. Deriving the elastic deformation energy, U, which is stored in the adherends (beams) relatively to the crack length, a, the Energy Release Rate results from the beam theory [53] as:

$$G_{\rm T} = \frac{3\delta^2 E_1 E_2 h_1^3 h_2^3}{8a^4 \left( E_1 h_1^3 + E_2 h_2^3 \right)}$$
 (Eq. 34)

where  $\delta$  is the opening displacement (between the two beams),  $E_1$  and  $E_2$ ,  $h_1$  and  $h_2$  are the stiffnesses and the thicknesses of the thinner and thicker adherends respectively, and a is the crack length. This equation gives a reasonable approximation when the crack length is much bigger when compared with the specimen's adherends thicknesses ( $a \gg h_1, h_2$ ), however, this simple beam model overestimates the energy release rate, G, for smaller crack length, typical of stronger interfaces. A better description for the ADCB mixed mode fracture behavior was proposed by Creton et al. [62] applying the elastic foundation beam model suggested by Kanninen [59] to the simple beam model. This model considers the beam to be free at the fractured zone and supported in by an elastic foundation from the crack tip, thus the energy release rate is given by:

$$G_{\rm T} = \frac{3\delta^2 E_1 E_2 h_1^3 h_2^3}{8a^4} \left| \frac{E_1 h_1^3 C_2^2 + E_2 h_2^3 C_1^2}{\left(E_1 h_1^3 C_2^3 + E_2 h_2^3 C_1^3\right)^2} \right|$$
 (Eq. 35)

where 
$$C_1 = 1 + 0.64(h_1/a)$$
 and  $C_2 = 1 + 0.64(h_2/a)$ .

Simultaneously with the models previously presented, some alternatives were also developed. One of these alternatives, named "Global Method", was proposed by Williams [63], assuming that the pure mode II loading is obtained when the curvature for both adherends of the ADCB specimen is the same. Despite Ducept el al. [64] have shown that the global method is able to compute mode I for DCB asymmetric test it is not adequate to characterize mixed mode fracture for the ADCB test. Alternatively, a "local method" based on the stress intensity factor is used to determine the contribution of each mode to the total Energy Release Rate [65]. Assuming an isotropic and homogeneous material, the general solution for the mode partition given by Ducept et al. [64]:

$$G_{\rm I} = \frac{1}{2b^2 E} \left[ \frac{F}{\sqrt{Ah_{\rm I}}} \cos \omega + \frac{M}{\sqrt{{\rm I}h_{\rm I}^3}} sen(\omega + \gamma) \right]$$
(Eq. 36)
$$G_{\rm II} = \frac{1}{2b^2 E} \left[ \frac{F}{\sqrt{Ah_{\rm I}}} sen\omega + \frac{M}{\sqrt{{\rm I}h_{\rm I}^3}} \cos(\omega + \gamma) \right]$$

variables F and M are given by the following equations (Figure 12):

 $F = -\frac{6h_1h_2}{(h_1 + h_2)^3}M^3$  (Eq. 37)

$$M = M_1 - F \frac{h_1^3}{(h_1 + h_2)^3} M_3$$
 (Eq. 38)

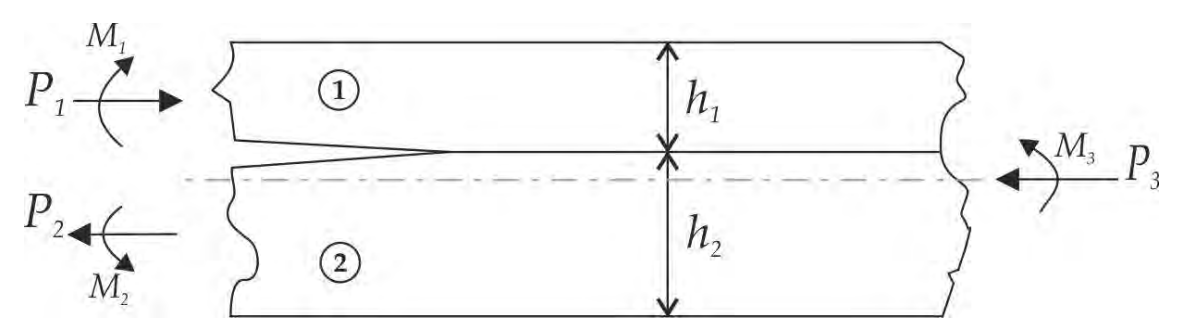


Figure 12. Moments and forces present at a section of an ADCB specimen [65].

After comparing the numerical results with the experimental ones obtained with the "local method", these same authors verified that this method returned a good approximation for the total fracture energy of the ADCB test. The previously analytical formulation present some problems to determine the contribution of each mode separately for the total fracture energy,  $G_{\rm T}$ , because it is difficult to determine the variables F and M. By solving the following system of two equations with two variables:

(Eq. 39) 
$$G_{\rm T} = G_{\rm I} + G_{\rm II}$$

it was possible to determine  $G_{I}$  and  $G_{II}$  for ADCB test.

A numerical analysis using ABAQUS<sup>®</sup>, was done [43] to confirm the mixed mode degree for the ADCB specimen geometry. A two dimensional (2D) numerical model allowed to determine the mixed mode degree for this specimen. The adherends were modeled with 8064 eight node isoparametric finite elements (CPS8R), assuming the plane stress state. The adhesive layer was modeled with cohesive elements with a trapezoidal damage criterion for this joint (ARALDITE<sup>®</sup> 2015) and a 0.2 mm thickness. The Virtual Crack Closure Technique (VCCT) proposed by Agrawal and Karlsson [66] was implemented to determine the Energy Release Rate

at the crack tip. Several simulations were done for different initial crack lengths from  $a_0=30~mm$  until  $a_0=100~mm$  with a 10~mm incrementation. The ratio  $G_{\rm I}/G_{\rm II}$  obtained for all the simulations returned a value of  $G_{\rm I}/G_{\rm II}\approx 81$ , resulting in a constant mixed mode degree of  $\varphi=6^{\rm o}$ .

The mixed mode degree  $\varphi$  obtained for this thicknesses ratio of  $h_2/h_1 = 0.72$  is in accordance with the published work by Chen et al. [67] and Ducept et al. [64] confirming that this test is near to pure mode I.

This method was used with success in the work done by da Silva et al. [43] allowing to plot a fracture envelope for mode I and mode II considering this mixed-mode (I+II) test. Bennati et al. [68] have also proposed a mechanical model, using FEA which proved to be in accordance with the da Silva et al. [43].

This test requires a different beam in height, and has a limited mode mixity as major disadvantages, but is a simple solution to obtain a mode mixity.

#### 4.3 Asymmetric Tapered Double Cantilever Beam – ATDCB

This is a recent test, proposed by Park and Dillard [52], consisting of an hybrid configuration, were one adherend has a constant section and the other adherend has wedge configuration typical of a TDCB as shown in Figure 13.

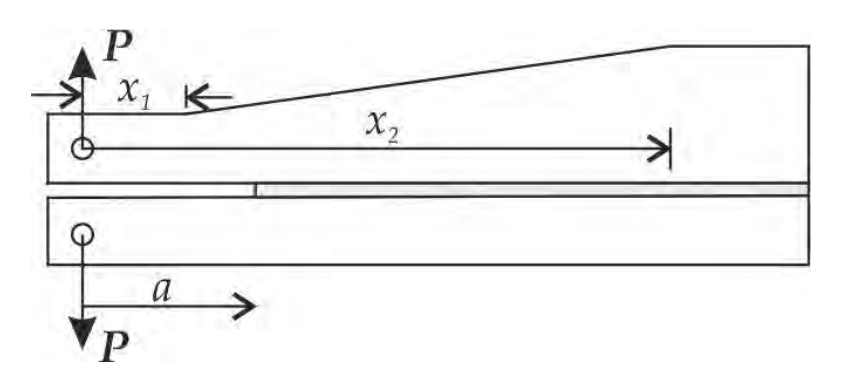


Figure 13. ATDCB test schematic representation.

The energy release rate, G, is obtained recurring to the *Euler Bernoulli* beam theory considering an equivalent system as shown in Figure 14. Once the Energy Release Rate, G, is proportional to dC/da (Eq. 7), the equivalent system flexibility, C is obtained and used to determine the formula for G. The flexibility of these two systems can be considered to be the

same, the flexibility of the system shown in Figure 14 b) is the first one to be determined and then attributed to the system shown in Figure 14 a).

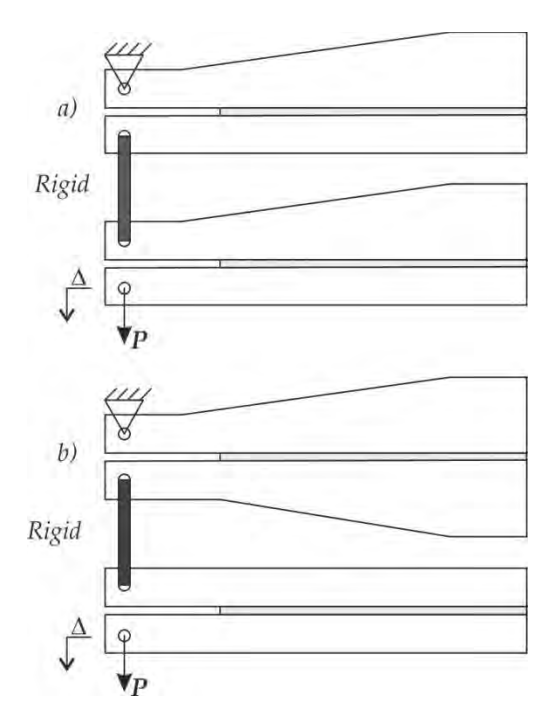


Figure 14. Equivalent systems for ATDCB test analysis.

This means that the system flexibility shown in Figure 14 b) can be expressed as:

$$C_{\text{total}} = C_{\text{const}} + C_{\text{taper}}$$
 (Eq. 40) .

where  $C_{\rm const}$  and  $C_{\rm taper}$  are the specimen flexibilities for DCB and TDCB respectively [52].

The energy release rate for ATDCB specimen is given by half  $G_{
m total}$  , meaning:

$$G_{\mathrm{T}} = \frac{1}{2} \left[ \frac{P^2}{2b} \frac{d\left(C_{\mathrm{const}}\right)}{da} + \frac{P^2}{2b} \frac{d\left(C_{\mathrm{taper}}\right)}{da} \right] = \frac{1}{2} \left(G_{\mathrm{const}} + G_{\mathrm{taper}}\right)$$
(Eq. 41)

This is reasonable if the adhesive layer remains perpendicular to the loading direction during the test, as shown in Figure 14, due to material symmetry for both specimens.

The energy release rate,  $G_{\rm T}$  , for ATDCB is then obtained through (Eq. 41), with  $G_{\rm const}$  and  $G_{\rm taper}$  given by the corresponding formulas for the DCB and TDCB tests respectively [30]:

$$G_{\text{const}} = \frac{4P^2 \left(3a^2 + h^2\right)}{Eh^2 h^3}$$
 (Eq. 42)

$$G_{\text{taper}} = \frac{4P^2}{Eh^2}m\tag{Eq. 43}$$

and m is the geometric factor that will be used to machine the wedge in the adherends, typical of the TDCB specimen (Eq. 13). Numerical analysis done with ABAQUS® was done by da Silva et al. [43] to compute the mode mixity degree  $\varphi$  for ATDCB test. Adherends were modeled with 8879 eight node isoparametric elements (CPS8R), assuming the plane stress state. The adhesive layer was modeled with cohesive elements with the trapezoidal damage criterion for this joint (ARALDITE® 2015) with a 0.2 mm thickness. Several simulations were done by varying the initial crack lengths from 20 to 130 mm with a 10 mm incrementation. The mode mixity degree  $\varphi$  varies slightly with the initial crack length  $a_0$ . This can be explained by the wedge geometry of the upper beam, which makes the relative stiffness of the two adherends to change with the crack propagation. The ratio  $G_{\rm I}/G_{\rm II}$  obtained was 5.2, resulting in a mixed mode ratio degree for the ATDCB test of  $24^{\circ}$ .

Da Silva et al. [43] obtained the mode partition by solving the following system of two equations with two variables:

$$\begin{cases}
\varphi = \tan^{-1} \sqrt{\left(\frac{G_{\text{II}}}{G_{\text{I}}}\right)} = 24^{\circ} \\
G_{\text{T}} = G_{\text{I}} + G_{\text{II}}
\end{cases}$$
(Eq. 44)

and therefore  $G_{\rm I}$  and  $G_{\rm II}$  are given by:

$$G_{\rm I} = \frac{G_{\rm T}}{1 + \tan^2 24^{\rm o}} \label{eq:GI}$$
 (Eq. 45) 
$$G_{\rm II} = G_{\rm T} - G_{\rm I} \label{eq:GI}$$

Park and Dillard [52] and Da Silva et al. [43] have studied this test, obtaining consistent results that were included in the fracture envelop (mode I vs. mode II).

This test requires a special geometry for the tapered beam, and has a limited mode mixity as major disadvantages, but is a clever solution to obtain a mode mixity.

#### 4.4 Single Leg Bending – SLB

Another test for mixed mode (I + II) characterization is the Single Leg Bending (SLB) proposed by Yoon and Hong [69] as an ENF modified specimen. This test has a limited mode mixity range when compared with the MMB, however SLB test requires less equipment and easier experimental procedures [50]. As previously shown, the MMB test requires a complex support equipment and loading hinges. The SLB test is done with a three point bending apparatus as shown in Figure 15. The specimen lower beam is smaller in length relatively to the upper beam, making that one extremity will be supported only by the specimen upper beam. The specimen is loaded at its mid span between the two support points.

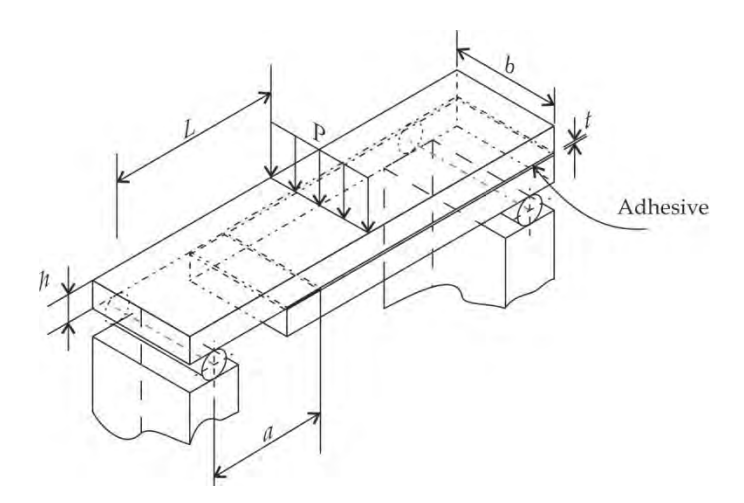


Figure 15. Three dimensional schematic for SLB test.

The formulation takes into account the *Saint Venant* effect, the transverse shear effect, the *Winkler's* beam elastic foundation and the shear deformation at the crack tip. The individual components for each mode are:

$$G_{1} = \frac{12P^{2}a^{2}}{16b^{2}h^{3}E} \begin{bmatrix} 1 + 0.55\left(\frac{h}{a}\right) + 0.31\left(\frac{h}{a}\right)^{2} + 0.32\left(\frac{h}{a}\right)\left(\frac{E}{G}\right)^{1/2} + \\ 0.1\left(\frac{h}{a}\right)^{2}\left(\frac{E}{G}\right) \end{bmatrix}$$
(Eq. 46)

and

$$G_{II} = \frac{9P^2a^2}{16b^2h^3E} \left[ 1 + 0.218 \left( \frac{h}{a} \right) \left( \frac{E}{G} \right)^{1/2} + 0.048 \left( \frac{h}{a} \right)^2 \left( \frac{E}{G} \right) \right]$$
 (Eq. 47) .

where b is the specimen width, a is the crack length, h is the specimen half thickness, L is half the length between supports and k = 5/6 is the shear correction factor.

Total fracture energy  $(G_T = G_I + G_{II})$  is obtained by adding (Eq. 46) with (Eq. 47). However, Szekrenyes e Uj [50] suggested a simplified formulation to determine the SLB Energy Release Rate. Fracture toughness considering both modes (I+II) can be obtained with:

$$G_{\rm T} = \frac{21P^2a^2}{16b^2h^3E} + \frac{P^2}{16b^2hkG} + \frac{P^2a^2}{16b^2h^3E} \left[ 5.42\left(\frac{h}{a}\right) + 2.45\left(\frac{h}{a}\right)^2 \right]$$
 (Eq. 48) .

The same authors presented also a formulation for mode partition based on the beam theory. Taking into account only the shear effect and the beam elastic foundation, the Energy Release Rate components are given by:

$$G_{\rm I} = \frac{12P^2a^2}{16b^2h^3E} + \frac{P^2}{16b^2hkG} + \frac{P^2a^2}{16b^2h^3E} \left[ 5.42 \left(\frac{h}{a}\right) + 2.45 \left(\frac{h}{a}\right)^2 \right]$$
 (Eq. 49) .

$$G_{\rm II} = \frac{9P^2a^2}{16b^2h^3E}$$
 (Eq. 50)

Then, the mode ratio  $(G_{\rm I}/G_{\rm II})$  is given by:

$$\left(\frac{G_{\rm I}}{G_{\rm II}}\right) = \frac{4}{3} + \frac{1}{9} \left[ \frac{1}{k} \frac{E}{G} \left(\frac{h}{a}\right)^2 + 5.42 \left(\frac{h}{a}\right) + 2.45 \left(\frac{h}{a}\right)^2 \right]$$
 (Eq. 51)

Accordingly with (Eq. 51), if the crack length, a, tends to infinite, the ratio  $G_{\rm I}/G_{\rm II}$  tends to 4/3, resulting in a constant mode ratio degree  $\varphi = \tan^{-1} \sqrt{3/4} = 41^{\circ}$ .

The authors [43] have studied this test, obtaining consistent results that were included in the fracture envelop (mode I vs. mode II).

Recently, Oliveira et al. [51] have developed a CBBM method for the SLB test, improving the quality of the results and avoiding the crack length measurement.

This test requires a different specimen, not included in any standard, and some cylindrical adaptors, and has a limited mixity range, that can be disadvantages.

#### 4.5 SPELT test

The loading jig developed by Fernlund and Spelt [35] consists primarily of two rigid beams linked to each other, to the specimen, and to a base plate (Figure 16). Different jig geometries can be achieved by altering the four distances,  $s_1$  -  $s_4$ , thereby varying the mode-mixity of the induced loading. Changing the above referred distances leads to different loads,  $F_1$  and  $F_2$ , applied to the upper and lower adherends, respectively, of the tested specimens. The jig also permits the realization of pure mode tests, namely the Double Cantilever Beam (DCB) for mode I and the End-Notched Flexure (ENF) for mode II, thus being versatile in the context of fracture characterization [70, 71].

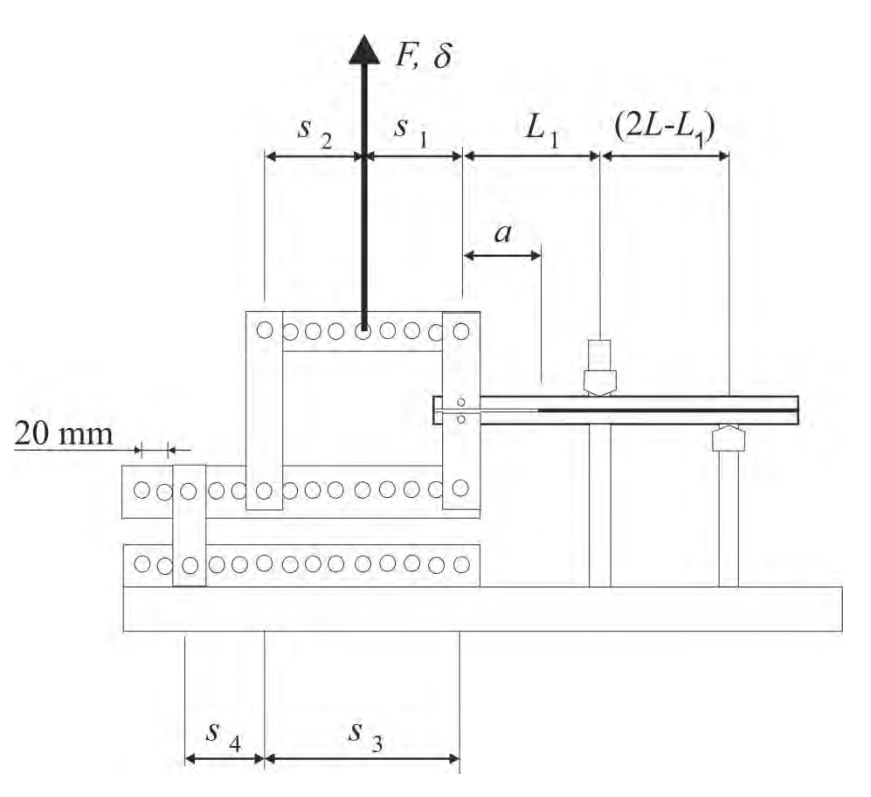


Figure 16. Spelt test schematics.

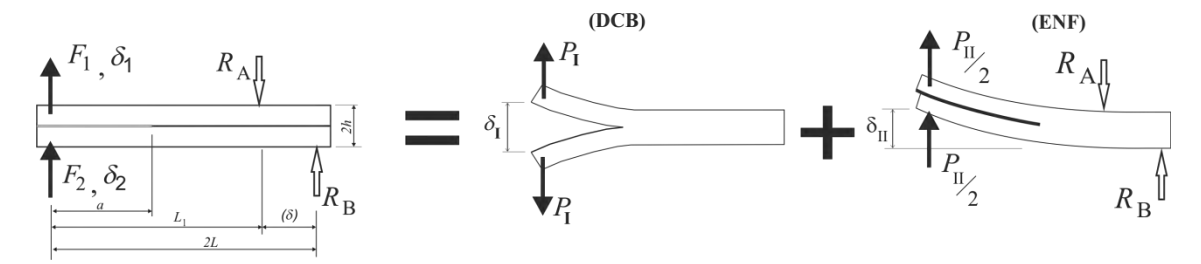


Figure 17. Spelt jig loading scheme.

This test induces a combination of opening and shear loading applied to the specimen that can be partitioned in order to get the components corresponding to mode I and mode II solicitations. The mode I component is induced by an opening loading and mode II will result from longitudinal sliding at the crack tip. Consequently, the partitioning method complies with those objectives (Figure 17). The mode I loading reflects the DCB specimen and the mode II can be viewed as the ENF loaded asymmetrically – it should be remembered that the ENF is a three-point bending test loaded at the mid-span [72]. From Figure 17the following relations can be obtained

$$F_1 = P_1 + \frac{P_{II}}{2}; \quad F_2 = -P_1 + \frac{P_{II}}{2}$$
 (Eq. 52)

$$\delta_{1} = \frac{\delta_{I}}{2} + \delta_{II}; \quad \delta_{2} = -\frac{\delta_{I}}{2} + \delta_{II}$$

The corresponding pure modes (I and II) loading and displacement components become

$$P_{\rm I} = \frac{F_1 - F_2}{2}; \quad \delta_{\rm I} = \delta_1 - \delta_2$$
 (Eq. 53) 
$$P_{\rm II} = F_1 + F_2; \quad \delta_{\rm II} = \frac{\delta_1 + \delta_2}{2}$$

The test can be viewed as a combination of DCB [73] and ENF specimen [74] when  $L_1$ =L, i.e., where the specimen is loaded at its mid-span. This achievement is quite interesting, as it allows the use of simple equations to obtain the strain energy components.

Using the previous concept of an equivalent crack length In mode II the equivalent crack length  $(a_{ell})$  can be directly obtained from:

$$a_{\text{eII}} = \left[ \left( C_{\text{II}} - \frac{6LL_{\text{I}}}{5BhG(2L - L_{\text{I}})} \right) \frac{2Bh^{3}E}{3} - \frac{2LL_{\text{I}}^{2}}{3} \right]^{1/3}$$
 (Eq. 54)

The components of the strain energy release rate can be determined by means of the Irwin-Kies equation

For mode I:

$$G_{\rm I} = \frac{6P_{\rm I}^2}{B^2 h} \left( \frac{2a_{\rm eI}^2}{h^2 E} + \frac{1}{5G} \right)$$
 (Eq. 55)

The strain energy release rate in mode II is obtained as:

$$G_{\rm II} = \frac{9P_{\rm II}^2 a_{\rm eII}^2}{4B^2 h^3 E}$$
 (Eq. 56)

(Eq. 55) and (Eq. 56) represent the evolution of the strain energy release rates components during the test (*R*-curves), thus providing the identification of the mode-mixity as well as the

total fracture energy of the test. The proposed method only requires recording the load F and the displacement components applied to each arm of the specimen  $(\delta_1, \delta_2)$  during the test (Figure 17).

This methodology was applied to an improved spelt testing device [75] and the experimental results are presented as R-curves and summarized in a fracture envelop [76].

Promoting a constant mode-mixity during the test, allowing to easily change the mode-mixity, allowing to perform almost all the fracture envelope range (from mode I to near mode II) and using a simple geometry specimen (DCB), even with stiff steel adherend, are the most relevant advantages.

#### 4.6 Dual Actuator Loading Frame - DAL

All previously presented tests use a universal testing machine to load the specimens or to transfer the load recurring to a loading apparatus connected to the machine grips. There is another equipment that is a testing machine itself, with two actuators working horizontally allowing to apply different displacement or load rates directly to each specimen beam. This machine is known as Dual Actuator Loading (DAL) frame developed by Dillard et al. [77, 78].

The DAL test is based on a DCB specimen loaded asymmetrically by means of two independent hydraulic actuators (Figure 18). The specimen bonded end is clamped (20 to 25 mm) and loaded at the debonded end by means of the independent hydraulic actuators that are attached to the specimen arms with pins. Each hydraulic actuator pivots in order to allow some rotation to accommodate the small vertical displacements of each beam due to foreshortening. Each actuator is equipped with a load cell and a linear variable displacement transducer (LVDT), with the purpose of registering the two load–displacement curves during the test. Different combinations of applied displacement rates provide different levels of mode mixities, thus allowing an easy definition of the fracture envelope in the  $G_I$  versus  $G_{II}$  space.

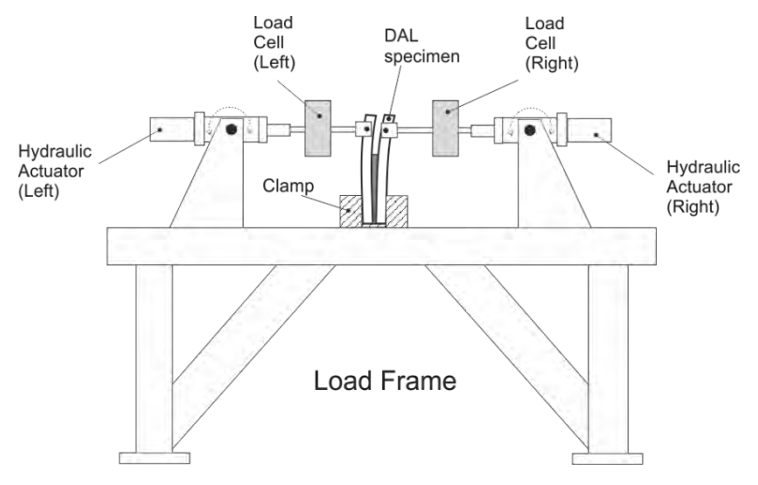


Figure 18. Dual Actuator Load Frame schematics.

Adapted from Grifith's fracture theory [11] the expression for strain energy release rate, G, for a crack at the interface of a specimen with two different adherends bonded together, and subjected to different loads, is given by:

$$G = \frac{M_1^2}{2BE_1I_1} \left[ 1 + \left( \frac{M_2}{M_1} \right)^2 \sum \eta^3 - \left( 1 - \frac{M_2}{M_1} \right)^2 \frac{\sum}{4m} \right]$$
 (Eq. 57)

where  $M_1=P_1a$ ,  $M_2=P_2a$ ,  $\sum_{}=\frac{E_1}{E_2}$ ,  $\eta=\frac{h}{H}$ ,  $E_1$ ,  $I_1$ , h is the elastic modulus, second moment of area, and thickness of substrate 1 and  $E_2$ ,  $I_2$ , H is the elastic modulus, second moment of area, and thickness of substrate and a is the crack length,  $\Lambda=\frac{1+2\sum\eta+\sum\eta^2}{2\eta\left(1+\sum\eta\right)}$ 

and 
$$m = \sum \left[ \left( \Delta - \frac{1}{\eta} \right)^2 - \left( \Delta - \frac{1}{\eta} \right) + \frac{1}{3} \right] + \frac{\Delta}{\eta} \left[ \Delta - \frac{1}{\eta} \right] + \frac{1}{3\eta^3}$$
.

To obtain the contribution of the opening mode I and the sliding or shear mode II, (Eq. 57) can be partitioned as follows:

$$G_{I} = \frac{\left(M_{1} + \Sigma \eta^{3} M_{2}\right)^{2}}{2BE_{1}I_{1}\left(1 + \Sigma \eta^{3}\right)}$$
 (Eq. 58)

$$G_{II} = \frac{\sum \left[12m\eta^{3} - (1 + \Sigma\eta^{3})\right] (M_{1} - M_{2})^{2}}{24BmE_{1}I_{1}(1 + \Sigma\eta^{3})}$$
(Eq. 59)

This formulation requires measuring the crack length and does not take into account the FPZ effect, or the root rotation correction.

Hitendra et al. [77] performed the first tests with this machine, that was also used by Nicoli et al. [79] in the mixed-mode fracture characterization of adhesive joints.

Trying to improve the quality of the results and overcoming the difficult task of crack length measuring Chaves et al. [80] proposed a data reduction technique recurring to CBBM applied to DAL tests that was used to characterize an adhesively bonded joint [81].

DAL test has the advantage of varying the mode-mixity during the test with only one specimen, but this also means that it does not promote a self-similar crack propagation [80], which can be disadvantageous when looking for a stable crack growth.

#### 5. Conclusions

Adhesion science has evolved since the early years until the present sophisticated methodologies for manufacture, application and testing. This evolution promoted the diversification for a wide range of applications in broader fields for adhesive bonding with structural responsibilities. The importance of support tools to help in joint design is vital. Fracture mechanics are commonly accepted tools to characterize and help design adhesive joints. If adhesive joint fracture in mode I is well documented and there are even standards to govern its application, for mode II and mixed-mode (I+II) there are no standards and there is a lack in the fracture mechanics characterization. Furthermore, mixed-mode (I+II) is the most common loading for structures at service. There are advantages and disadvantages for each mixed-mode test reviewed in this paper, which should be taken into account when choosing the best test to perform. Analyzing both the advantages and disadvantages represents an opportunity to improve the knowledge for mixed-mode loading fracture mechanics of adhesive joints and develop a test methodology that allows to obtain good results for the energy release rate, overcoming some of the existing drawbacks. Measuring the crack length growth during the test is a difficult task and neglects the FPZ effect. The use of an equivalent crack length based on the complicance of the spciemen, including the FPZ and root rotation effects, avoids the need of crack measurement and represents a better estimate of the actual toughness of the adhesive.

#### Acknowledgements

The authors would like to thank the "Fundação Luso-Americana para o Desenvolvimento" (FLAD) for the support through project 314/06, 2007 and Instituto de Engenharia Mecânica (IDMEC).

#### References

- [1] L.F.M. da Silva, A. Öschner, R.D.e. Adams, Handbook of Adhesion Technology, 2011.
- [2] J.A. Harris, R.A. Adams, International Journal of Adhesion and Adhesives, 4 (1984) 65-78.

- [3] M.F.S.F. De Moura, J.P.M. Gonçalves, J.A.G. Chousal, R.D.S.G. Campilho, International Journal of Adhesion and Adhesives, 28 (2008) 419-426.
- [4] R.D. Adams, J.A. Harris, International Journal of Adhesion and Adhesives, 7 (1987) 69-80.
- [5] X. Zhao, R.D. Adams, L.F.M. da Silva, Journal of Adhesion Science and Technology, 25 (2011) 819-836.
- [6] A.D. Crocombe, International Journal of Adhesion and Adhesives, 9 (1989) 145-153.
- [7] X. Zhao, R.D. Adams, L.F.M. da Silva, Journal of Adhesion Science and Technology, 25 (2011) 837-856.
- [8] Z. Chen, R.D. Adams, L.M. Silva, International Journal of Fracture, 167 (2011) 221-234.
- [9] L.F.M. da Silva, A.G. Magalhães, Juntas Adesivas Estruturais, Publindústria, 2007.
- [10] D.A. Dillard, Fracture Mechanics of Adhesive Bonds, in: R.D. Adams (Ed.) Adhesive Bonding Science, Technology and Applications, CRC PressWoodhead Publishing, 2005.
- [11] A.A. Griffith, Philosophical Transactions of the Royal Society, A221 (1921) 163 198.
- [12] D. Broek, Elementary Engineering Fracture Mechanics, 4th rev. edn, M. Nijhoff;, Distributors for the U.S. and Canada, Kluwer Academic, Dordrecht; Boston Hingham, Mass., U.S.A., 1986.
- [13] A.J. Kinloch, Adhesion and Adhesives: Science and Technology, Chapman & Hall, London, 1986.
- [14] M.D. Banea, L.F.M. da Silva, Proceedings of the Institution of Mechanical Engineers, Part L: Journal of Materials Design and Applications, 223 (2009) 1-18.
- [15] L.F.M. Da Silva, R.D.S.G. Campilho, Advances In Numerical Modeling Of Adhesive Joints, SPRINGER-VERLAG BERLIN AND HEIDELBERG GMBH & CO. KG, 2012.
- [16] M.F.S.F. de Moura, J.A.G. Chousal, International Journal of Mechanical Sciences, 48 (2006) 493-503.
- [17] M. Alfano, F. Furgiuele, A. Leonardi, C. Maletta, G.H. Paulino, International Journal of Fracture, 157 (2009) 193-204.
- [18] B.R.K. Blackman, H. Hadavinia, A.J. Kinloch, J.G. Williams, International Journal of Fracture, 119 (2003) 25-46.
- [19] K.Y. Volokh, in, 2004, pp. 845-856.
- [20] J.P.M. GonÇAlves, M.F.S.F. De Moura, A.G. MagalhÃEs, P.M.S.T. De Castro, Fatigue & Fracture of Engineering Materials & Structures, 26 (2003) 479-486.
- [21] L.F.M. Da Silva, A. Öschner, Modeling of Adhesively Bonded Joints, Springer, Heidelberg, 2008.
- [22] L.F.M. da Silva, F.A.C.R.G. de Magalhães, F.J.P. Chaves, M.F.S.F. de Moura, The Journal of Adhesion, 86 (2010) 891-905.

- [23] E.J. Ripling, S. Mostovoy, H.T. Corten, The Journal of Adhesion, 3 (1971) 107-123.
- [24] G. Fernlund, M. Papini, D. McCammond, J.K. Spelt, Composites Science and Technology, 51 (1994) 587-600.
- [25] D. Bigwood, A. Crocombe, International Journal of Adhesion and Adhesives, 9 (1989) 229-242.
- [26] G. Fernlund, H. Lanting, J.K. Spelt, Journal of Composites Technology and Research 17 (1995) 3 17-330.
- [27] J.M.Q. Oliveira, M.F.S.F. de Moura, M.A.L. Silva, J.J.L. Morais, Composites Science and Technology, 67 (2007) 1764-1771.
- [28] A.B. De Morais, A.B. Pereira, in: 11th Japanese-European Symposium on Composite Materials, Porto, Portugal, 2008.
- [29] L.F.M. da Silva, D.A. Dillard, B. Blackman, R.D.e. Adams, Testing Adhesive Joints, Best Practices, Wiley, Weinheim, 2012.
- [30] ASTM D3433 99, in: Annual book of ASTM standards, West Conshohocken, ASTM 15.06, 2012, pp. 225-231.
- [31] ISO 25217:2009, in, ISO, 2009, pp. 24.
- [32] M.F. Kanninen, C.H. Popelar, Advanced Fracture Mechanics, Oxford University Press, Oxford, 1985.
- [33] R.D.S.G. Campilho, in: Departamento de Engenharia Mecânica, Faculdade de Engenharia da Universidade do Porto, 2009.
- [34] Y. Wang, J.G. Williams, Composites Science and Technology, 43 (1992) 251-256.
- [35] G. Fernlund, J.K. Spelt, Composites Science and Technology, 50 (1994) 441-449.
- [36] Z. Suo, G. Bao, B. Fan, Journal of the Mechanics and Physics of Solids, 40 (1992) 1-16.
- [37] Z. Chen, R.D. Adams, L.F.M. da Silva, International Journal of Adhesion and Adhesives, 31 (2011) 48-55.
- [38] M.D. Banea, L.F.M. da Silva, R.D.S.G. Campilho, The Journal of Adhesion, 88 (2012) 534-551.
- [39] B.F. Sørensen, T.K. Jacobsen, Engineering Fracture Mechanics, 70 (2003) 1841-1858.
- [40] J.L. Högberg, B.F. Sørensen, U. Stigh, International Journal of Solids and Structures, 44 (2007) 8335-8354.
- [41] B.R.K. Blackman, Fracture Tests, in: L.F.M. da Silva, A. Öschner, R.D. Adams (Eds.) Handbook of Adhesion Technology, Springer, Heidelberg, 2011.
- [42] D. Moore, A. Pavan, J.G. Williams, Fracture Mechanics Testing Methods for Polymers, Adhesives and Composites, Elsevier, Amsterdam, London, 2001.

- [43] L.F.M. da Silva, V.H.C. Esteves, F.J.P. Chaves, Materialwissenschaft und Werkstofftechnik, 42 (2011) 460-470.
- [44] A.J. Brunner, B.R.K. Blackman, P. Davies, Engineering Fracture Mechanics, 75 (2008) 2779-2794
- [45] B.R.K. Blackman, A.J. Brunner, J.G. Williams, Engineering Fracture Mechanics, 73 (2006) 2443-2455.
- [46] M.F.S.F. de Moura, A.B. de Morais, Engineering Fracture Mechanics, 75 (2008) 2584-2596.
- [47] B.R.K. Blackman, A.J. Kinloch, M. Paraschi, Engineering Fracture Mechanics, 72 (2005) 877-897.
- [48] S. Hashemi, A.J. Kinloch, J.G. Williams, Proceedings of the Royal Society of London. A. Mathematical and Physical Sciences, 427 (1990) 173-199.
- [49] M.F.S.F. De Moura, N. Dourado, J.J.L. Morais, F.A.M. Pereira, Fatigue & Fracture of Engineering Materials & Structures, 34 (2011) 149-158.
- [50] A. Szekrényes, J. Uj, Composites Science and Technology, 64 (2004) 2393-2406.
- [51] M.Q. Oliveira Jorge, F.S.F. de Moura Marcelo, J.L. Morais José, in: Holzforschung, 2009, pp. 597.
- [52] S. Park, D. Dillard, International Journal of Fracture, 148 (2007) 261-271.
- [53] F. Xiao, C.Y. Hui, E.J. Kramer, Journal of Materials Science, 28 (1993) 5620-5629.
- [54] L. Tong, Q. Luo, Analysis of Cracked Lap Shear (CLS) Joints, in: L. da Silva, A. Öchsner (Eds.) Modeling of Adhesively Bonded Joints, Springer Berlin Heidelberg, 2008, pp. 25-51.
- [55] J.H. Crews, J.R. Reeder, in, NASA TECHNICAL MEMORANDUM 100662, 1988.
- [56] J.R. Reeder, J.H. Crews, AIAA Journal, 28 (1990) 1270-1276.
- [57] ASTM D6671 / D6671M 06, in: Annual book of ASTM standards, West Conshohocken, ASTM 15.03, 2012.
- [58] S. Gunawardana, in: College of Aerospace Engineering, Wichita State University, 2005.
- [59] M.F. Kanninen, International Journal of Fracture, 9 (1973) 83-92.
- [60] A.B. de Morais, A.B. Pereira, Composites Science and Technology, 66 (2006) 1889-1895.
- [61] A.B. Pereira, A.B. de Morais, Composites Science and Technology, 66 (2006) 1896-1902.
- [62] C. Creton, E. Kramer, C. Hui, H. Brown, Macromolecules, 25 (1992) 3075-3088.
- [63] J.G. Williams, International Journal of Fracture, 36 (1988) 101-119.
- [64] F. Ducept, D. Gamby, P. Davies, Composites Science and Technology, 59 (1999) 609-619.

- [65] J.W. Hutchinson, Z. Suo, Mixed Mode Cracking in Layered Materials, in: W.H. John, Y.W. Theodore (Eds.) Advances in Applied Mechanics, Elsevier, 1991, pp. 63-191.
- [66] A. Agrawal, A. Karlsson, International Journal of Fracture, 141 (2006) 75-98.
- [67] B. Chen, D. Dillard, J. Dillard, R. Clark, Jr., International Journal of Fracture, 114 (2002) 167-190.
- [68] S. Bennati, M. Colleluori, D. Corigliano, P.S. Valvo, Composites Science and Technology, 69 (2009) 1735-1745.
- [69] S.H. Yoon, C.S. Hong, International Journal of Fracture, 43 (1990) R3-R9.
- [70] D. Xie, A.M. Waas, K.W. Shahwan, J.A. Schroeder, R.G. Boeman, Engineering Fracture Mechanics, 72 (2005) 2487-2504.
- [71] A. Ameli, M. Papini, J.A. Schroeder, J.K. Spelt, Engineering Fracture Mechanics, 77 (2010) 521-534.
- [72] F.J.P. Chaves, M.F.S.F. de Moura, L.F.M. Da Silva, A. Dillard David, in, 2013.
- [73] M.F.S.F. de Moura, R.D.S.G. Campilho, J.P.M. Gonçalves, Composites Science and Technology, 68 (2008) 2224-2230.
- [74] M.F.S.F. de Moura, M.A.L. Silva, A.B. de Morais, J.J.L. Morais, Engineering Fracture Mechanics, 73 (2006) 978-993.
- [75] F.J.P. Chaves, L.F.M. Da Silva, M.F.S.F. de Moura, A. Dillard David, J.O. Fonseca, in, UP Universidade do Porto, 2013.
- [76] F.J.P. Chaves, F.S.F. De Moura Marcelo, L.F.M. Da Silva, A. Dillard David, in, 2013.
- [77] K. Singh Hitendra, A. Chakraborty, E. Frazier Charles, A. Dillard David, in: Holzforschung, 2010, pp. 353.
- [78] D.A. Dillard, H.K. Singh, S. Park, D. Ohanehi, M.A. McGaw, in: SEM Annual Conference & Exposition on Experimental and Applied Mechanics, Society for Experimental Mechanics, Inc., St. Louis, 2006.
- [79] E. Nicoli, A. Dillard David, E. Frazier Charles, A. Zink-Sharp, in, 2012, pp. 623.
- [80] F.J.P. Chaves, M.F.S.F. de Moura, L.F.M. da Silva, D.A. Dillard, International Journal of Solids and Structures, 48 (2011) 1572-1578.
- [81] F.J.P. Chaves, M.F.S.F. De Moura, L.F.M. Da Silva, A. Dillard David, in Press, 2013.

PAPER 2

# FRACTURE TOUGHNESS UNDER MIXED MODE LOADINGS

## Fracture toughness of a structural adhesive under mixed

## mode loadings

Lucas F. M. da Silva<sup>1</sup>, V. H. C. Esteves<sup>1</sup>, F. J. P. Chaves<sup>2</sup>

<sup>1</sup>Departamento de Engenharia Mecânica, Faculdade de Engenharia da Universidade do Porto, Rua Dr.

Roberto Frias, 4200-465 Porto, Portugal

<sup>2</sup>Instituto de Engenharia Mecânica (IDMEC), Rua Dr. Roberto Frias, 4200-465 Porto, Portugal

#### **Abstract**

This aim of this research was to determine the fracture toughness of steel/adhesive/steel joints under mixed mode loadings. A structural and ductile epoxy adhesive was selected in this research. The experimental tests, i.e. Asymmetric Tapered Double Cantilever Beam (ATDCB), Single Leg Bending (SLB) and Asymmetric Double Cantilever Beam (ADCB), were realized to assess the fracture toughness in mixed mode. Experimental tests in pure mode I and II were also realized to complete the fracture envelope. In order to obtain the mode I critical energy release rates,  $G_{\rm Ic}$ , the standard Double Cantilever Beam test was used, whilst the critical strain energy release rate in mode II,  $G_{\rm IIc}$ , was evaluated with the End Notched Flexure test. For various mixed mode tests, the critical strain energy release rate values were partitioned into mode I and mode II components. One of the main conclusions of the present work is that the introduction of a small amount of mode II loading (shear) in the joint results in a decrease of the total fracture energy,  $G_{\rm T} = G_{\rm I} + G_{\rm II}$ , when compared to the pure mode I fracture energy.

### **Keywords**

Ductile adhesive; Double Cantilever Beam (DCB); End Notched Flexure (ENF); Asymmetric Tapered Double Cantilever Beam (ATDCB); Single Leg Bending (SLB); Asymmetric Double Cantilever Beam (ADCB).

#### 1 Introduction

An increase use of adhesively bonded joints in industrial applications has renewed the interest of mixed mode fracture research in adhesive joints. The work developed in this paper is in the field of fracture mechanics applied to structural adhesive bonded joints. In the fracture mechanics approach, an energy parameter,  $G_{c}$ - energy per unit area needed to produce failure, (fracture toughness) is used as the failure criterion. In particular, in this work a fracture characterization of adhesively bonded joints is realized when they are submitted to mixed mode loadings (I + II). Since simultaneous combination of normal and shear stresses are the most common situations found in the more diverse applications of bonded joints, the scientific community and the industries who depend of this new joining technology feel the need to have at their disposal tools and prediction methods of the strength of bonded joints subjected to this type of loadings. To overcome the lack of adequate failure criterion in mixed mode loading, the fracture envelopes arise as indispensible tools for design engineers. Fracture envelopes are graphics where strain energy release rates, G, for pure modes I and II are plotted on abscissas and ordinate axes respectively, while the mixed mode fracture energy is extended to all the area that corresponds to the graphic's quadrant.

The classical fracture mechanics approach and the more recent damage mechanics are increasingly being used to design adhesive joints [1]. The most important material

parameter in those cases is the fracture toughness. The literature has many values for the toughness in mode I, some for mode II but very little for mixed loading which is the way in which real joints are loaded. There are several tests described in the literature for testing adhesives in mixed mode conditions. Table 1 gives a summary of the main tests. The mode mixity is defined by the following equation

$$\psi = \tan^{-1} \sqrt{\frac{G_{II}}{G_{I}}}$$
 (1)

Table 1. Test methods to measure the fracture toughness of adhesives in mixed mode conditions and corresponding mode mixity.

Test Method	Schematic Representation	Mode Mixity, ψ(°)
Asymmetric Double Cantilever Beam (ADCB)		≈ 0 − 34°
Single Leg Bending (SLB)	<b>*</b>	≈ 41°
Crack Lap Shear (CLS)	<b>←</b>	≈ 49°
Asymmetric Tapered Double Cantilever Beam (ATDCB)		≈ 27°
Mixed Mode Bending (MMB)		$\psi = f(c)$

The Asymmetric Double Cantilever Beam (ADCB) test is similar to the Double Cantilever Beam (DCB) test for mode I but the beams are made with different materials or different thicknesses to have mode II in addition to mode I. The asymmetry of the beams gives a constant mixity defined by the relation between the thicknesses of the two adherends. This test has been used by several researchers [2-5] although there is some reserve about its applicability due to the little amount of mode II.

The Asymmetric Tapered Double Cantilever Beam (ATDCB) test is a relatively recent test proposed by Park and Dillard [6] which consists in a hybrid configuration where one of the substrates is tapered. The mode mixity varies with the crack length but it is in the range of 25 to 30°.

Another test for mixed mode loading is the Single Leg Bending (SLB) test proposed by Yoon and Hong [7] and that can be viewed as a modified End Notch Flexure (ENF) test. This test is quite straightforward and has been used by many researchers [5, 8] with good results.

The SLB, ADCB and ATDCB require different specimen geometry for each mode mixity ( $G_{\rm I}/G_{\rm II}$ ). However, the ideal is to have a unique specimen geometry that can be used for any mode mixity. The most common method that allows to vary the mode mixity with a single geometry is the mixed mode bending (MMB) which is an adaptation of the standard ASTM D 6671 for composite materials initially proposed by Reeder and Crews [9]. This procedure has been successfully applied to adhesive joints by several authors [4]. The MMB test combines an ENF test with a DCB test. This test is currently being developed by the authors and was not used in the present study.

The three tests described above (SLB, ADCB and ATDCB) were used to determine the failure envelope of a structural adhesive. In addition, the mode I and mode II toughness

was also determined using the DCB and ENF tests respectively to have more points in the  $G_I$  vs.  $G_{II}$  diagram.

## 2 Experimental Details

#### Materials

A ductile epoxy adhesive (2015 from Huntsman) was selected. This is a two part paste resin that cures at 40°C in 16 h. Table 2 shows the shear properties of the adhesive used in this work. The properties were determined using the thick adherend shear test [10]. The heat treated steel DIN 40CrMnMo7 was used for the substrates. It is a high strength steel with a yield strength of 900 MPa that is sufficient to keep the material in the elastic range.

Table 2. Adhesive shear properties using the thick adherend shear test method ISO 11003-2 [10].

	2015
Shear modulus	487 ± 77
G (MPa)	
Shear yield strength	$17.9 \pm 1.80$
$\tau_{ya}$ (MPa)	17.9 = 1.00
Shear strength	$17.9 \pm 1.80$
$\tau_{r}$ (MPa)	
Shear failure strain	$43.9 \pm 3.40$
$\gamma_{\rm f}$ (%)	15.7 = 5.40

## **Specimens Geometry**

The geometry used for the ENF test (Figure 1) is the one used for the DCB test (Figure 2) where the adherend thickness h is 6.35 mm. The length between the supports 2L was 270 mm and the initial crack length was 50 mm.

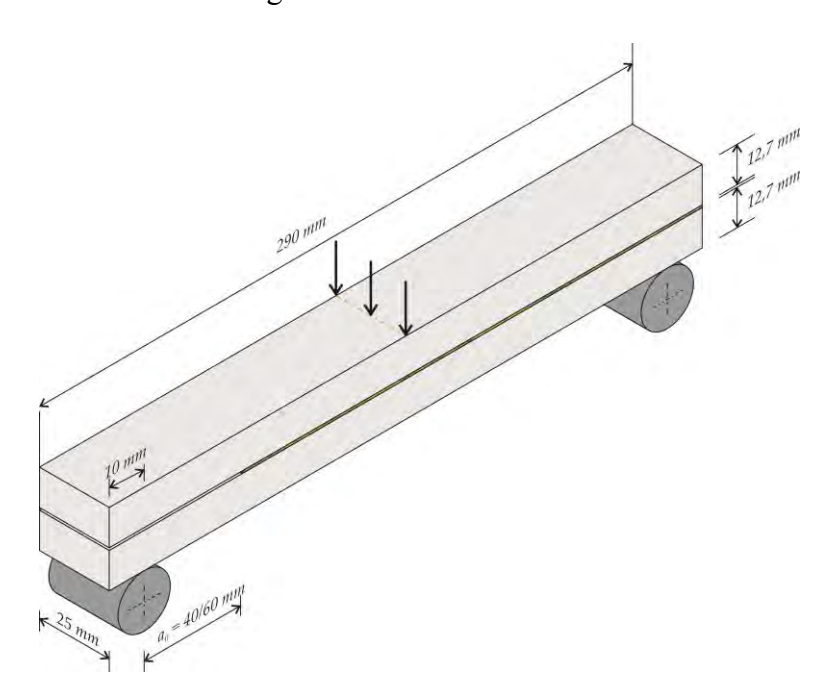


Figure 1 Geometry of the end notched flexure (ENF) test specimen.

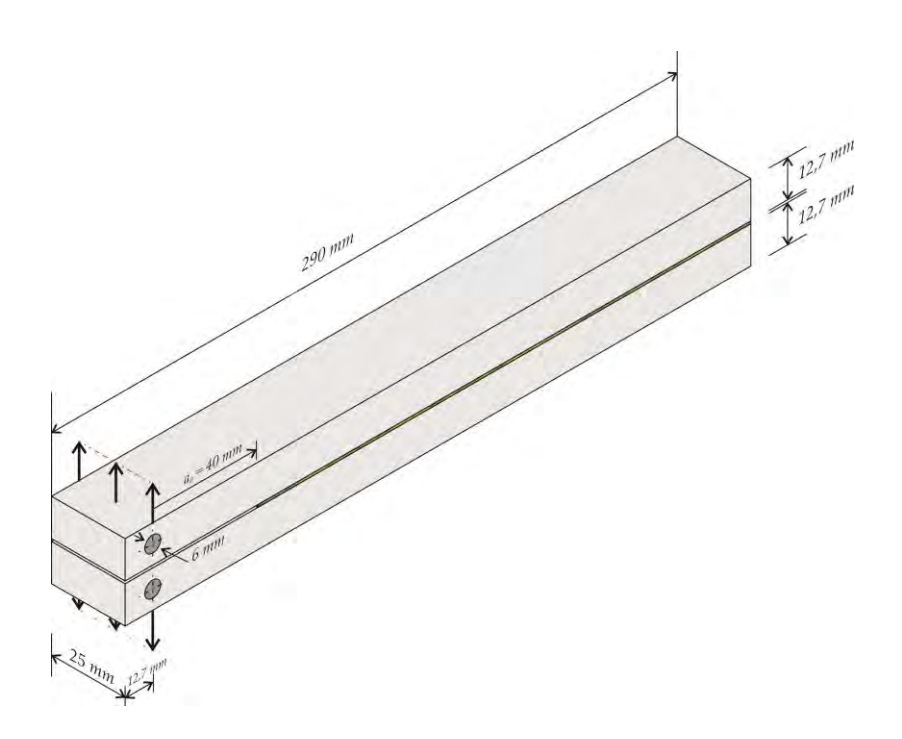


Figure 2 Geometry of the Double Cantilever beam (DCB) test specimen.

• • • •

The geometry of the ATDCB, SLB and ADCB tests are given in Figure 3, Figure 4 and Figure 5, respectively. The bondline thickness was in all cases 0.2 mm.

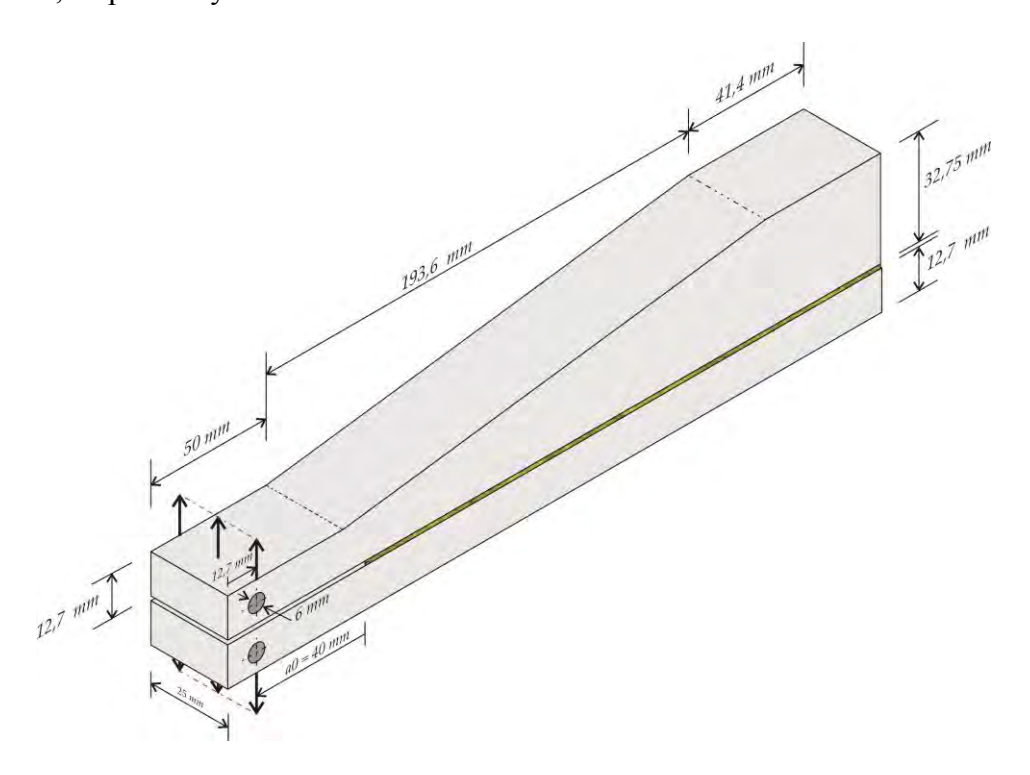


Figure 3 Geometry of the Asymmetric Tapered Double Cantilever Beam (ATDCB) test specimen.

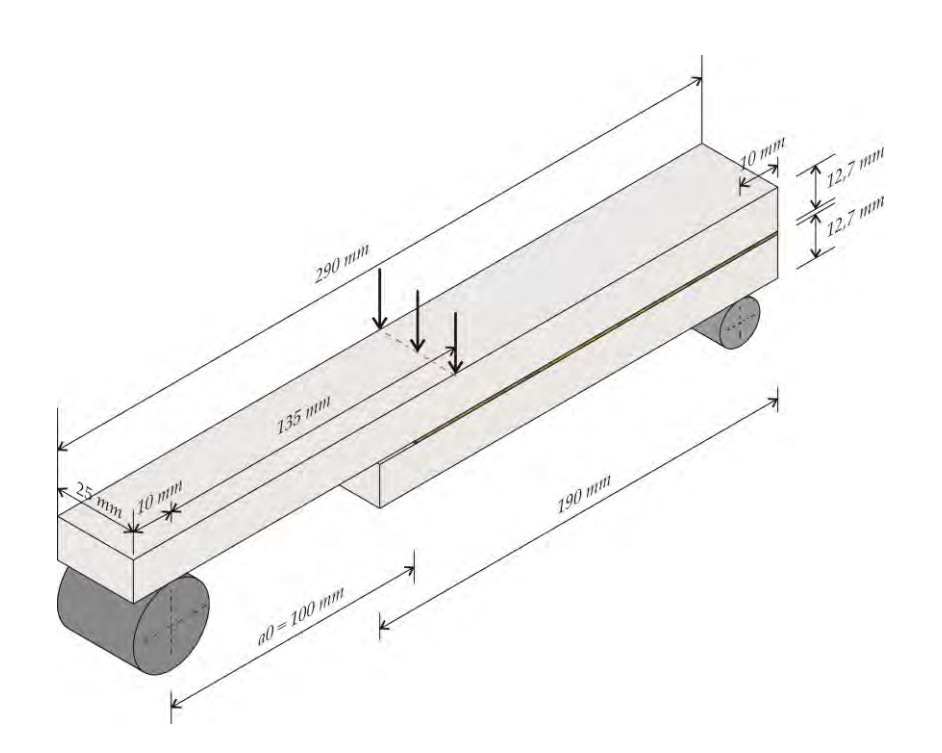


Figure 4 Geometry of the Single Leg Bending (SLB) test specimen.

290 mm

12.7 mm

25 mm

12.7 mm

Figure 5 Geometry of the Asymmetric Double Cantilever Beam (ADCB) test specimen.

### **Specimen Manufacture**

The joint surfaces were grit blasted with corundum (600 µm particles) under a pressure of 6 bar and degreased with acetone prior to the application of the adhesive. The ductile epoxy 2015 was mixed with a nozzle and applied directly on the surfaces. Spacers were inserted between the adherends before the application of the adhesive in order to control the bondline thickness. These spacers were removed after the adhesive was cured. A sharp pre-crack in the adhesive layer mid-thickness was assured using a razor blade and a gentle tap. To guarantee the correct precrack position at the adhesive layer middle plane, a simple set with a razor blade glued in between two feeler gauges was introduced in the gap between the upper and lower adherends to promote the precrack.

This set was done with a 0.1 mm thickness razor blade glued in between two feeler gauges with half the bond line thickness minus 0.05 mm to account for the razor blade thickness. A jig with spacers for the correct alignment of the adherends was used and is shown in Figure 6.





Figure 6 End notched flexure specimen fabrication (shims for bondline thickness control at the top and assembled specimens in a jig at the bottom).

### **Testing**

The specimens were tested in laboratory conditions ( $\sim 25^{\circ}\text{C}$  and  $\sim 50\%$  relative humidity) using a universal testing machine, under a constant crosshead rate of 0.25 mm/min. The load-displacement (P- $\delta$ ) curve was registered during the test. Pictures were recorded during the specimens testing with 5 s intervals using a 10 MPixel digital camera. This procedure allows measuring the crack length during its growth and afterwards collecting the P- $\delta$ -a parameters. This was performed correlating the time

elapsed since the beginning of each test between the P- $\delta$  curve and each picture (the testing time of each P- $\delta$  curve point is obtained accurately with the absolute displacement and the established loading rate). The specimens were marked with a white paint and a ruler to facilitate the crack length (a) reading. Five specimens were tested for each configuration. The general set-up is shown in Figure 7. Figure 8 shows the set-up for the specimens with an opening mode (DCB, ADCB and ATDCB), Figure 9 shows that set-up for the ENF test and Figure 10 shows the set-up for the SLB.

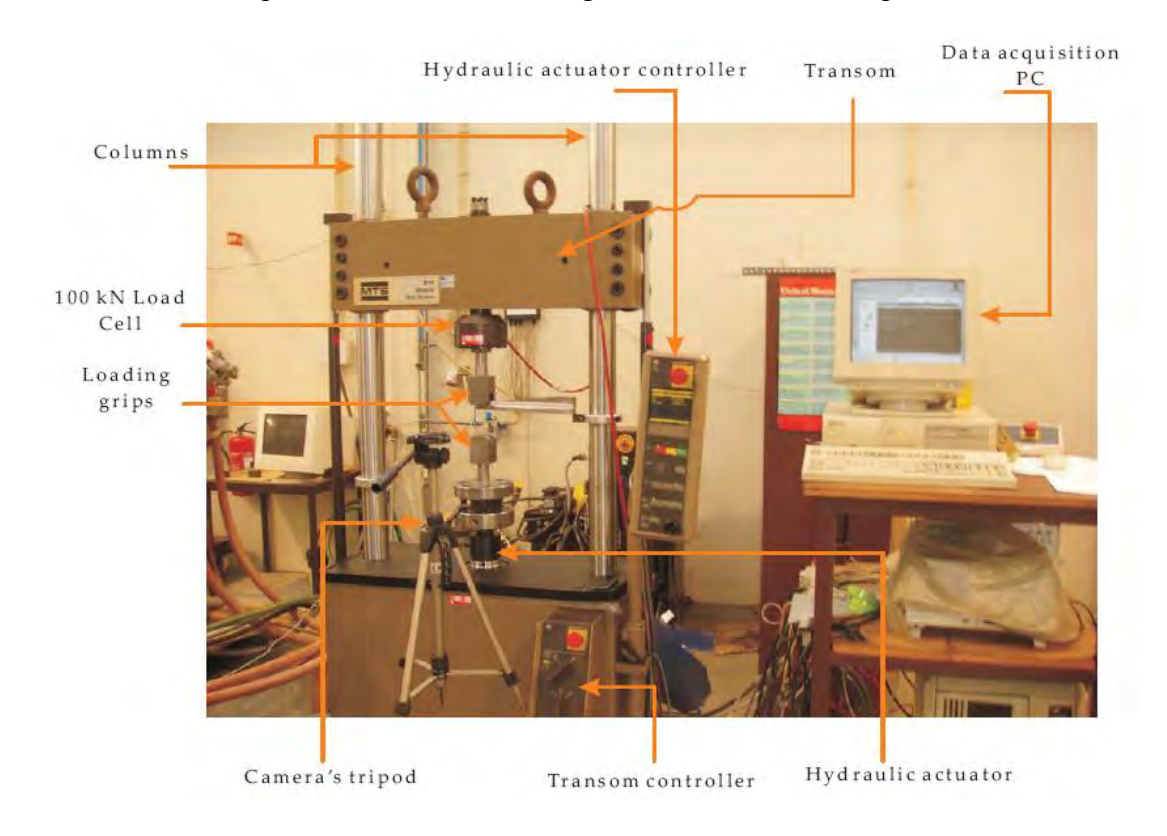


Figure 7 Complete testing setup for the different testing methods.



Figure 8 Experimental set-up of the tests in opening mode (DCB, ADCB and ATDCB).

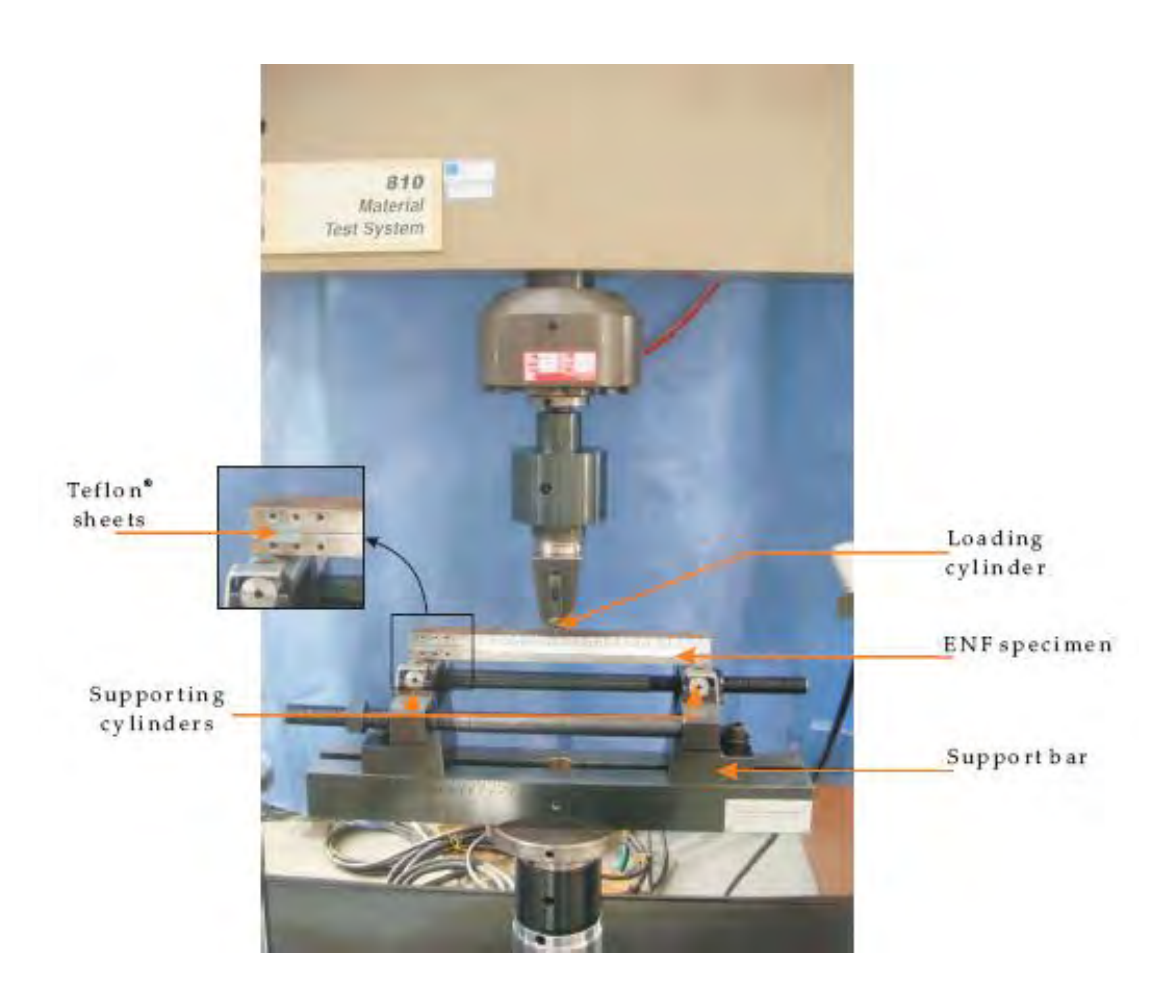


Figure 9 Experimental set-up of the ENF test.

It was verified in a previous study [11-12] that friction effects in the ENF test are mainly concentrated at the region of the pre-crack above the support. Consequently, two sheets of Teflon with a thin pellicle of lubricator between them were included in the pre-crack region in order to minimize friction effects.

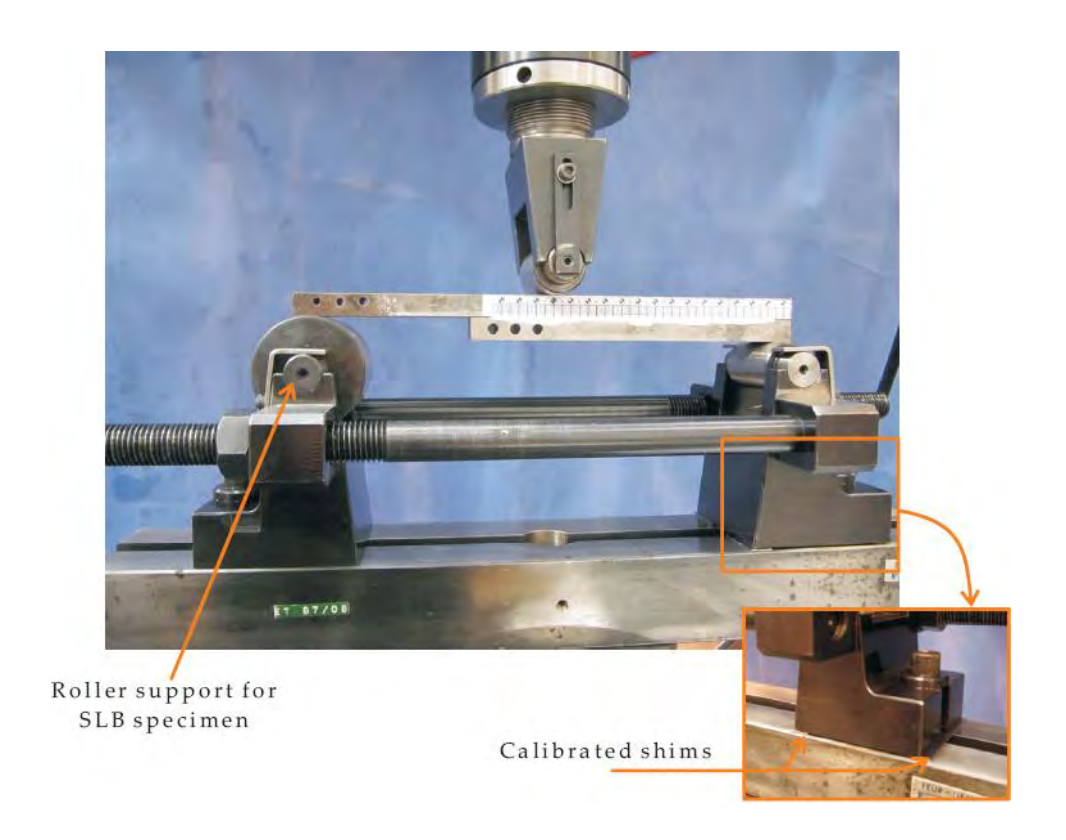


Figure 10 Experimental set-up of the SLB test.

### **Data Analysis**

### DCB Test

The critical fracture energy in pure mode I,  $G_{Ic}$ , was calculated using the beam theory and the Compliance-Based Beam Method (CBBM).

According to the beam theory and the Irwin-Kies equation  $G_{Ic}$  is given by [13]

$$G_{\rm lc} = \frac{6P^2}{b^2h^3} \left( \frac{2a^2}{E} + \frac{h^2}{5G} \right) \tag{2}$$

where P represents the load, b the specimen width, a the crack length, E the adherend Young's modulus and G the adherend shear modulus.

The CBBM was recently developed by de Moura et al. [14] and is based on the crack equivalent concept, depending only on the specimen's compliance during the test.  $G_{Ic}$  can be obtained by the following expression:

$$G_{Ic} = \frac{6P^2}{b^2h} \left( \frac{2a_{eq}^2}{h^2 E_f} + \frac{1}{5G} \right)$$
 (3)

where  $a_{eq}$  is an equivalent crack length obtained from the experimental compliance and accounting for the fracture process zone (FPZ) at the crack tip and  $E_f$  is a corrected flexural modulus to account for all phenomena affecting the P- $\delta$  curve, such as stress concentrations at the crack tip and stiffness variability between specimens. This method does not require crack length monitoring during its growth.

### **ENF** Test

The experimental measurement of the crack length is very laborious because the two substrates are against each other and make the identification of the crack tip very difficult. Also, at the crack tip the fracture process zone (FPZ) where damage of the material occurs by plasticisation and micro-crackling absorbs part of the energy. Therefore, an equivalent crack length ( $a_e$ ) that takes into account of the FPZ should be used. To overcome these two problems (crack monitoring and FPZ), de Moura and Morais [15] proposed a method that does not require the crack length measurement and that takes into account the FPZ that they called the compliance based beam method

(CBBM). Using the beam theory and accounting for the shear effects, the following equation is obtained

$$G_{\rm II} = \frac{9P^2}{16b^2 E_f h^3} \left[ \frac{C_{\rm corr}}{C_{0\rm corr}} a_0^3 + \frac{2}{3} \left( \frac{C_{\rm corr}}{C_{0\rm corr}} - 1 \right) L^3 \right]^{\frac{2}{3}}$$
 (4)

The definition of  $C_{\text{corr}}$ ,  $C_{0\text{corr}}$ ,  $a_0$  and L can be found in [15]. As for the CBBM in the DCB test, this method does not require crack length monitoring during its growth which was observed to be very difficult to perform with accuracy in the ENF test.

### **SLB Test**

 $G_{\rm I}$  and  $G_{\rm II}$  were calculated according to Equations (5) and (6) respectively which were proposed by Szekrenyes and Uj [16] based on the beam theory:

$$G_{\rm I} = \frac{12P^2a^2}{16b^2h^3E} \left[ 1 + 0.55 \left(\frac{h}{a}\right) + 0.31 \left(\frac{h}{a}\right)^2 + 0.32 \left(\frac{h}{a}\right) \left(\frac{E}{G_s}\right)^{1/2} + 0.1 \left(\frac{h}{a}\right)^2 \left(\frac{E}{G_s}\right) \right]$$
(5)

$$G_{II} = \frac{9P^2a^2}{16b^2h^3E} \left[ 1 + 00.218 \left( \frac{h}{a} \right) \left( \frac{E}{G_s} \right)^{1/2} + 0.048 \left( \frac{h}{a} \right)^2 \left( \frac{E}{G_s} \right) \right]$$
 (6)

The mode I and mode II are related by  $G_{\rm I}/G_{\rm II}=4/3$ . The load and the crack length are required for the determination of  $G_{\rm I}$  and  $G_{\rm II}$ .

### **ADCB Test**

The equation of the total strain energy release rate proposed by Creton et al. [17] based on the model of a beam on elastic foundation [18] was used:

$$G_{\rm T} = \frac{3\delta^2 E_1 E_2 h_1^3 h_2^3}{8a^4} \left[ \frac{E_1 h_1^3 C_2^2 + E_2 h_2^3 C_1^2}{\left(E_1 h_1^3 C_2^3 + E_2 h_2^3 C_1^3\right)^2} \right]$$
(7)

where  $\delta$  is the opening displacement, the subscripts 1 and 2 refer to the two adherends of the ADCB specimen,  $C_1 = 1 + 0.64(h_1/a)$  and  $C_2 = 1 + 0.64(h_2/a)$ .

The determination of  $G_{\rm I}$  and  $G_{\rm II}$  was done using the following system of equation

$$\begin{cases} \psi = \tan^{-1} \sqrt{\frac{G_{II}}{G_{I}}} \\ G_{T} = G_{I} + G_{II} \end{cases}$$
(8)

The mixity  $\psi$  corresponding to the geometry used in the resent work  $(h_2/h_1 = 0.72)$  was found to be of  $6^{\circ}$  by a finite element analysis.

### **ATDCB Test**

According to Park and Dillard [6], the total strain energy release rate is given by that corresponding to a DCB and that corresponding to a TDCB divided by two:

$$G_{\rm T} = \frac{1}{2} \left( G_{\rm Const} + G_{\rm Taper} \right) = \frac{1}{2} \left[ \frac{4P^2 \left( 3a^2 + h^2 \right)}{Eb^2 h^3} + \frac{4P^2}{Eb^2} m \right]$$
 (9)

where m is a geometric factor defined by

$$m = \frac{3a^2}{h^3} + \frac{1}{h} = \text{constant}. \tag{10}$$

The determination of  $G_{\rm I}$  and  $G_{\rm II}$  was done using the system of equation given in (8). The mode mixity  $\psi$  was calculated with a finite element analysis and was found to vary between 24° and 30°. An average value of 27° was used.

# 3 Results

### **DCB Test**

All the specimens failed cohesively in the adhesive, as shown in Figure 11.



Figure 11 Example of failure surfaces obtained with the DCB test.

A representative experimental P- $\delta$  curve of the DCB test is presented in Figure 12. The curve is practically linear up to failure (maximum load in the P- $\delta$  curve). A typical R-curve is shown in Figure 13 using the two data reductions schemes (beam theory and CBBM). R-curves are used to identify the fracture energy from the plateau corresponding to the self-similar crack propagation. A plateau appears after an initial peak probably corresponding to some blunt effect due to the radius of curvature of the blade for crack initiation.

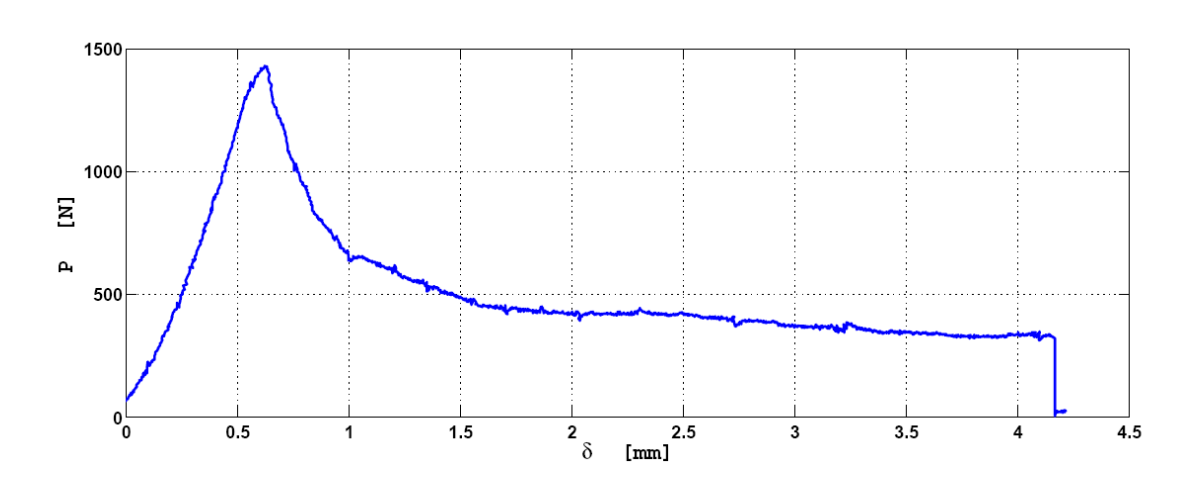


Figure 12 Representative experimental P- $\delta$  curve of the DCB test.

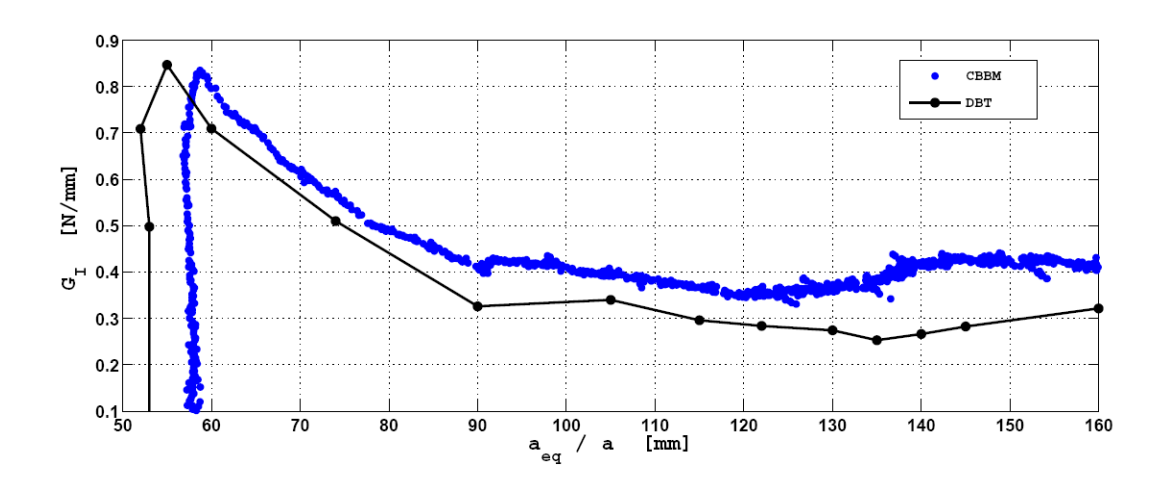


Figure 13 Typical experimental *R*-curve obtained for the DCB test using the beam theory and the CBBM.

Table 3 gives the average value and the scatter of  $G_{Ic}$  obtained with the DCB test using the CBBM. A value of 0.44 N/mm was obtained.

Table 3 Fracture toughness obtained with all the testing methods (average and standard deviation).

Test type	$G_{\rm Ic}$ (N/mm)	$G_{\rm IIc}$ (N/mm)
DCB <sup>+</sup>	$0.44 \pm 0.05$	_
ENF	_	2.1±0.21
SLB*	$0.34 \pm 0.06$	$0.32 \pm 0.06$
ADCB*	$0.41 \pm 0.04$	$0.004 \pm 0.0005$
ATDCB*	$0.32 \pm 0.04$	$0.07 \pm 0.006$

<sup>+</sup> Value corresponding to CBBM

### **ENF** Test

All the specimens failed cohesively in the adhesive, as shown in Figure 14.

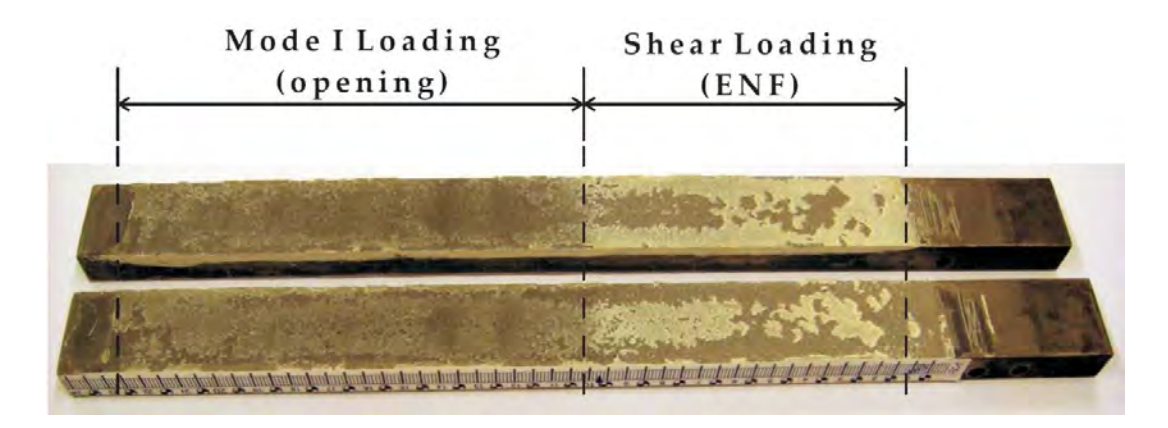


Figure 14 Example of failure surfaces obtained with the ENF test.

A representative experimental P– $\delta$  curve of the ENF is presented in Figure 15. In this case, the curve is non-linear corresponding to the adhesive plastic deformation that is more evident when mode II loading is applied. An experimental R-curve obtained using the CBBM is shown in Figure 16. A plateau is clearly seen indicating stable crack propagation. An average value of 2.1 N/mm was obtained for  $G_{\text{IIc}}$  (Table 3).

<sup>\*</sup> For these tests, the values indicated correspond to  $G_{\rm I}$  and  $G_{\rm II}$  and not  $G_{\rm Ic}$  and  $G_{\rm IIc}$ .

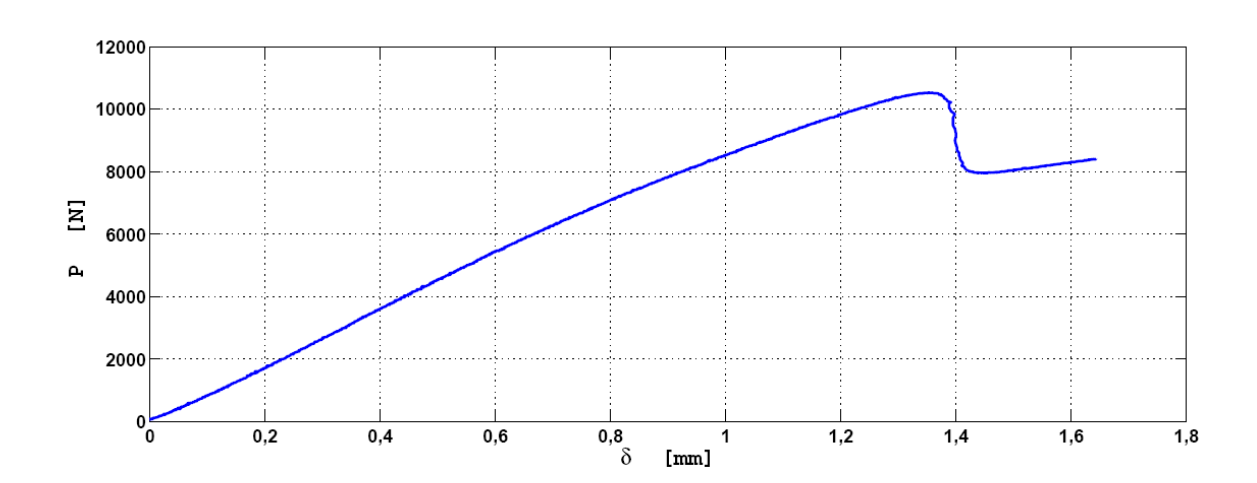


Figure 15 Representative experimental P- $\delta$  curve of the ENF test.

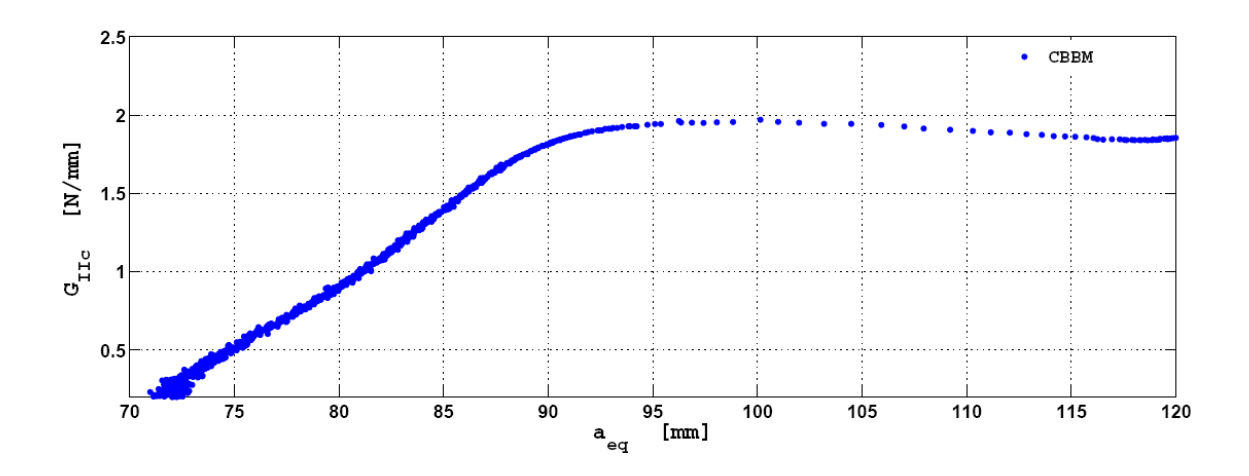


Figure 16 Typical experimental *R*-curve obtained for the ENF test using CBBM.

### **SLB Test**

All the specimens failed cohesively in the adhesive, as shown in Figure 17.



Figure 17 Example of failure surfaces obtained with the SLB test.

A representative experimental P– $\delta$  curve of the ENF is presented in Figure 18. An experimental R-curve obtained using the beam theory is shown in Figure 19. Three curves are presented corresponding to  $G_{\rm I}$ ,  $G_{\rm II}$  and  $G_{\rm T}$ . There is a slight slope in the region of the plateau which can be due to the effect of the loading roller that affects the fracture process zone ahead of the crack tip. An average value of 0.34 N/mm was obtained for  $G_{\rm I}$  and 0.32 N/mm for  $G_{\rm II}$  (Table 3).

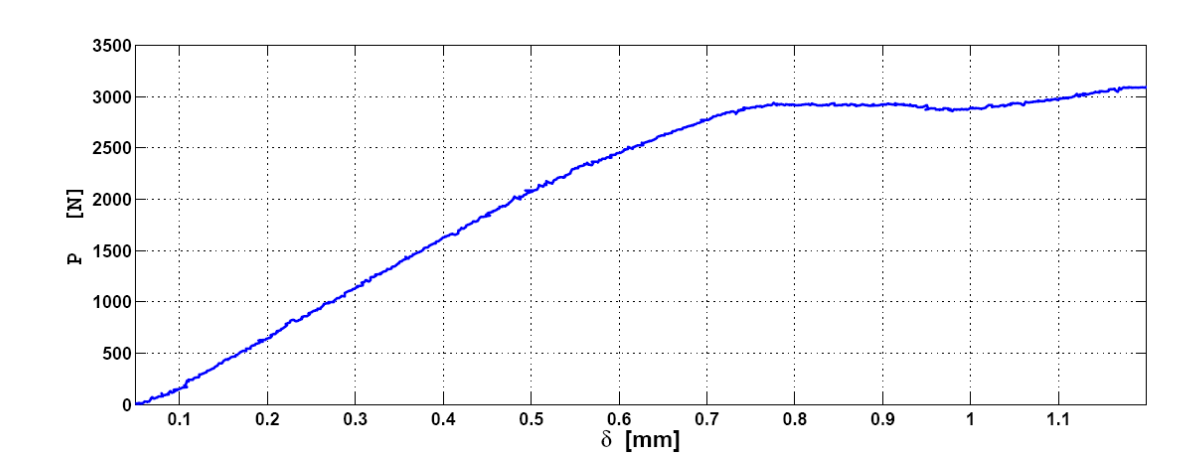


Figure 18 Representative experimental P– $\delta$  curve of the SLB test.

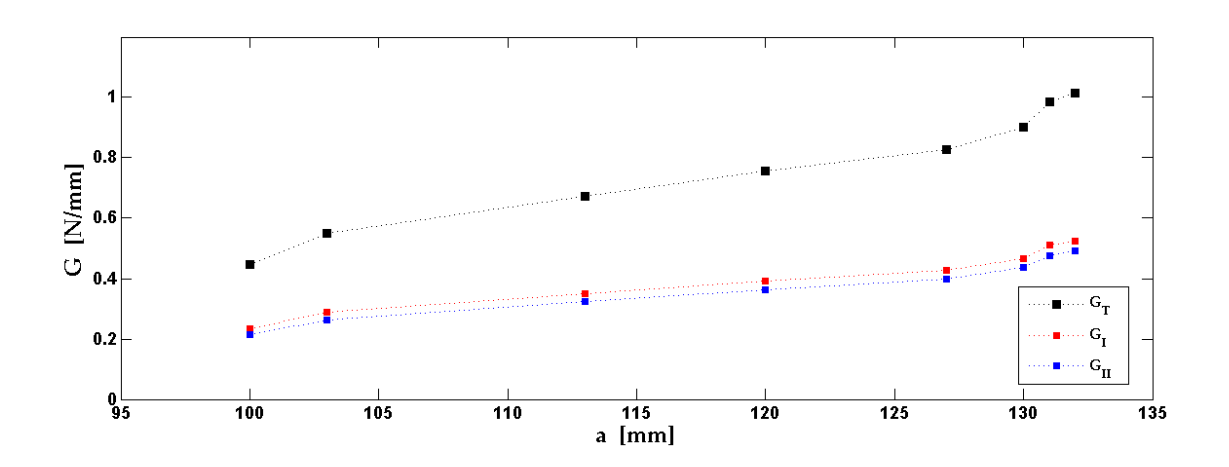


Figure 19 Typical experimental *R*-curve obtained for the SLB test using the beam theory.

### **ADCB Test**

All the specimens failed at the interface (Figure 20) although a very thin layer of adhesive could be seen on the surface.



Figure 20 Example of failure surfaces obtained with the ADCB test.

A representative experimental P– $\delta$  curve of the ADCB is presented in Figure 21. The curve is very similar to that obtained for the DCB specimen (Figure 12) although with a lower maximum load due to the addition of mode II. An experimental R-curve obtained using the beam theory is shown in Figure 22. An average value of 0.41 N/mm was obtained for  $G_{\rm I}$  and 0.004 N/mm for  $G_{\rm II}$  (Table 3).

1000 800 Ω 400 200 0 0.5 1 1.5 2 2.5 3 3.5 4 4.5 5

Figure 21 Representative experimental P– $\delta$  curve of the ADCB test.

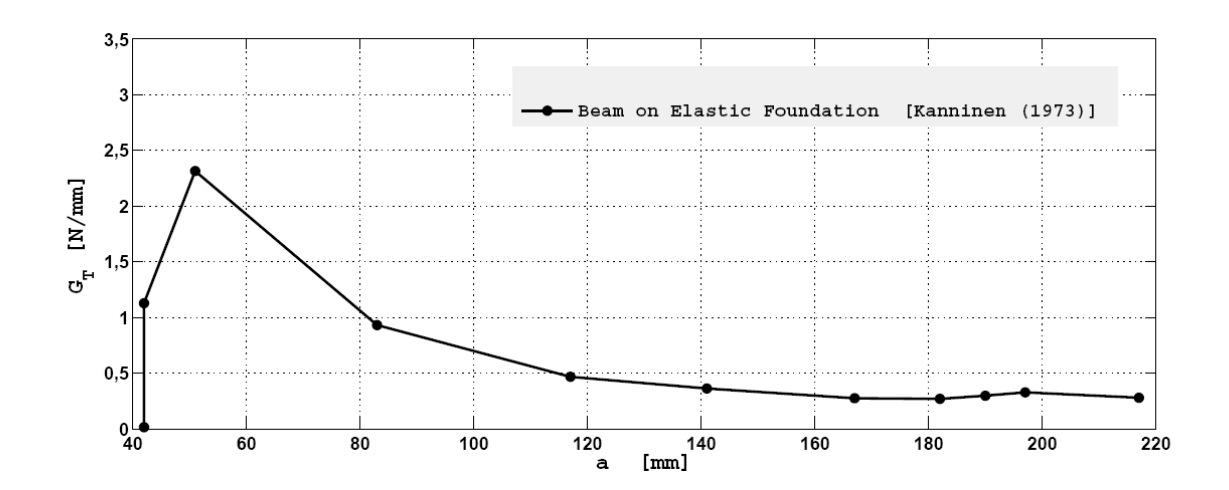


Figure 22 Typical experimental *R*-curve obtained for the ADCB test using the beam theory.

# **ATDCB Test**

As with the ADCB specimens, the ATDCB specimens failed at the interface (Figure 23) although a very thin layer of adhesive could be seen on the surface.

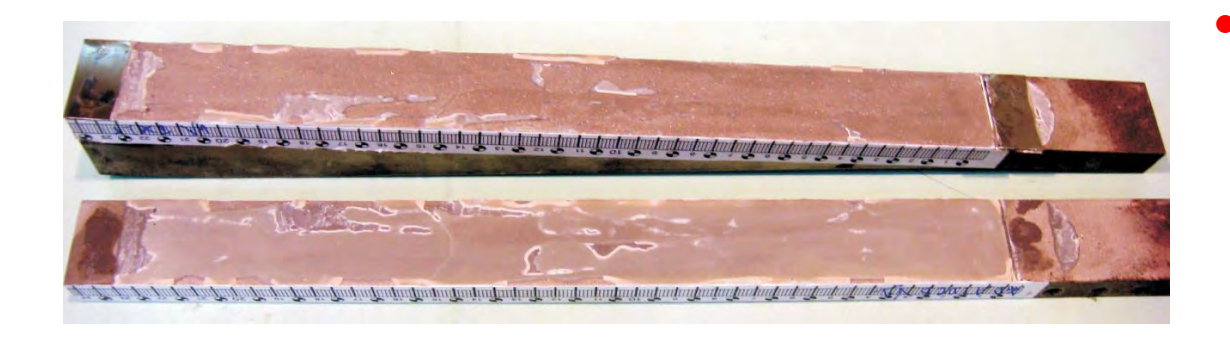


Figure 23 Example of failure surfaces obtained with the ATDCB test.

A representative experimental P– $\delta$  curve of the ATDCB is presented in Figure 24. An experimental R-curve obtained using the beam theory is shown in Figure 25. An average value of 0.32 N/mm was obtained for  $G_{\rm I}$  and 0.07 N/mm for  $G_{\rm II}$  (Table 3).

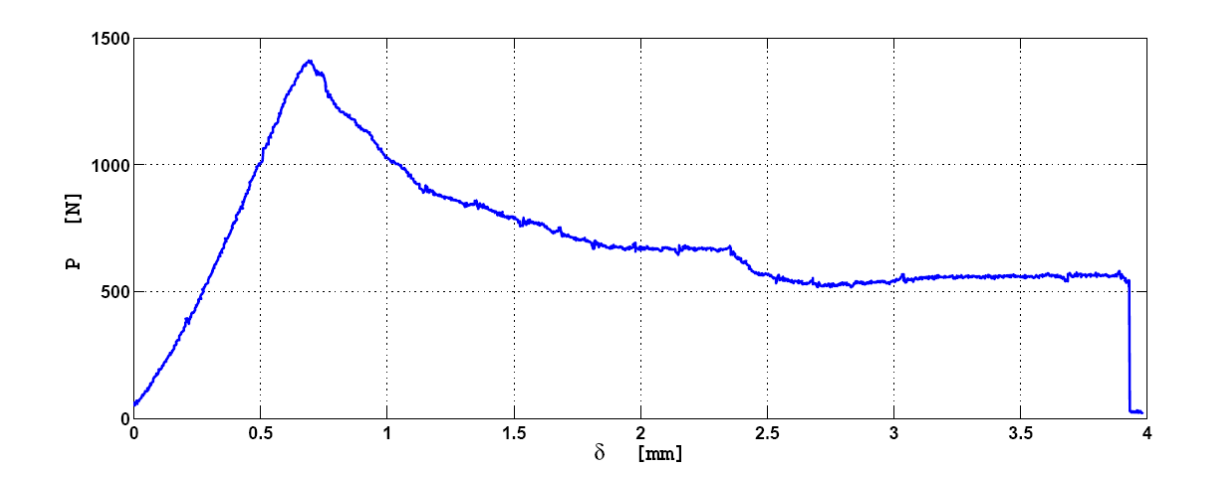


Figure 24 Representative experimental P– $\delta$  curve of the ATDCB test.

Figure 25 Typical experimental *R*-curve obtained for the ATDCB test using the beam theory.

### Failure Envelope

The results presented above and summarised in Table 3 are represented in a diagram  $G_{\rm I}$  vs.  $G_{\rm II}$  in Figure 26. The points corresponding to the SLB, ADCB and ATDCB tests are below the linear criterion, especially the ADCB and the ATDCB. It is as if the introduction of a small amount of mode II loading (shear) in the joint results in a decrease of the total fracture energy,  $G_{\rm T} = G_{\rm I} + G_{\rm II}$ , when compared to the pure mode I fracture energy. However, note that the SLB, ADCB and ATDCB fracture toughnesses were computed from the beam theory (without taking into account the FPZ), contrarily to the values for the toughness in mode I and mode II, which were computed with the CBBM. The CBBM tends to give higher values than the beam theory. Also, it is important to remember that the ADCB and ATDCB tests had a failure mode (interfacial) different from those of the DCB, ENF and SLB (cohesive in the middle of the adhesive). Since it is known that the properties of the interface are weaker than those of the adhesive, the results obtained make sense.

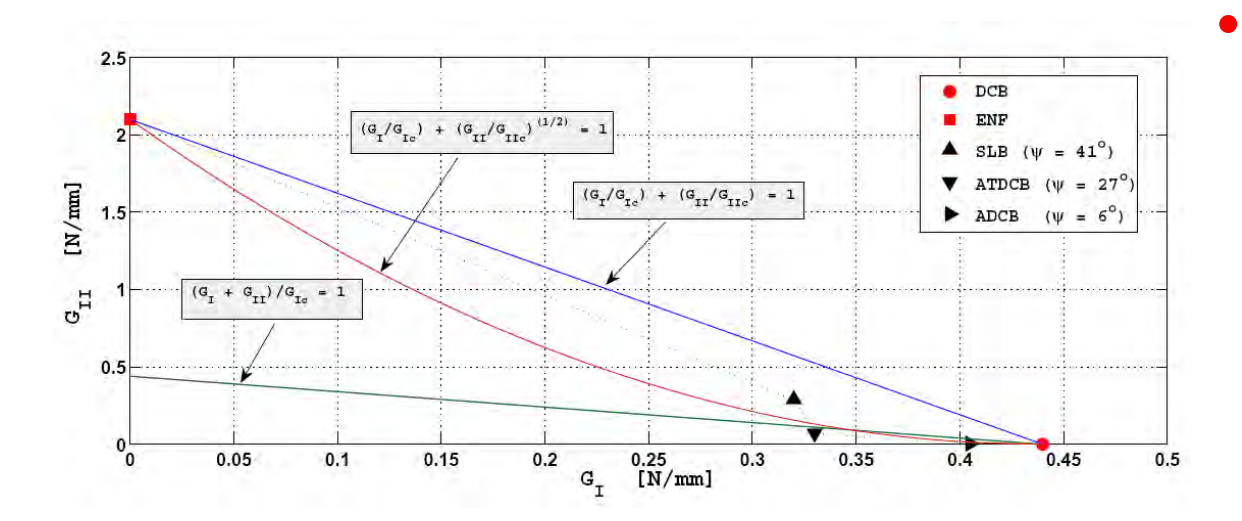


Figure 26 Failure envelope for the adhesive 2015.

### 4 Conclusions

The fracture toughness in mixed mode loading of a structural epoxy adhesive were determined using the SLB, ADCB and ATDCB tests. In addition pure mode I (DCB) and mode II (ENF) tests were carried out to complete the failure envelope. The following conclusions can be drawn:

- 1. A plateau in the *R*-curves was obtained for all tests indicating that a stable crack propagation took place giving an good estimate of the fracture toughness.
- 2. The DCB, ENF and SLB tests gave a cohesive failure and the ADCB and ATDCB tests gave an interfacial failure.
- 3. The relation between  $G_{\text{IIc}}$  and  $G_{\text{Ic}}$  is approximately 5.
- 4. The SLB test is in accordance with the linear failure criterion.
- 5. The points corresponding to the ADCB and ATDCB tests are well below the linear failure criterion because they had an interfacial failure.
- 6. The introduction of a small amount of mode II loading (shear) in the joint results in a decrease of the total fracture energy,  $G_T = G_I + G_{II}$ , when compared to the pure mode I fracture energy.

7. Determining the failure envelope with bonded joints is a difficult task because the values of the fracture toughness are influenced by the crack path and might not give the true adhesive properties.

# References

- [1] L. F. M. da Silva, A. Öchsner (Eds), Modeling of adhesively bonded joints, Springer, Heidelberg, 2008.
- [2] F. Xiao, C. Y. Hui, E. J. Kramer, *J. Mater. Sci.***1993**, *28*, 5620.
- [3] B. Chen, D. A. Dillard, J. G. Dillard, R. L. Clark, *Int. J. Fracture* **2002**, *114*, 167.
- [4] F. Ducept, D. Gamby, P. Davies, Compos. Sci. Technol. 1999, 59, 609.
- [5] D. A. Dillard, H. K. Singh, D. J. Pohlit, J. M. Starbuck, J. Adhes. Sci. Technol.2009, 23, 1515.
- [6] S. Park, D. A. Dillard, Int. J. Fracture 2007, 148, 261.
- [7] S. H. Yoon, C. S. Hong, *Int. J. Fracture* **1990**, *43*, R3.
- [8] A. Szekrenyes, J. Uj, Compos. Sci. Technol. 2004, 64, 2393.
- [9] J. R. Reeder, J. H. Crews, AIAA Journal 1990, 28, 1270.
- [10] E. A. S. Marques, L. F. M. da Silva, *J. Adhesion* **2008**, *84*, 917.
- [11] M. A. L. Silva, M. F. S. F. de Moura, J. J. L. Morais, *Compos. Part A Appl. S.*2006, 37, 1334.
- [12] L. F. M. da Silva, F. A. C. R. G. de Magalhães, F. J. P. Chaves, M. F. S. F. de Moura, J. Adhesion 2010, 86, 889.
- [13] M. F. Kanninen, C. H. Popelar, Advanced Fracture Mechanics, Oxford University Press, Oxford, 1985.

- [14] M. F. S. F. de Moura, R. D. S. G. Campilho, J. P. M. Gonçalves, *Compos. Sci. Technol.* 2008, 68, 2224.
- [15] M. F. S. F. de Moura, A. B. de Morais, Eng. Fract. Mech. 2008, 75, 2584.
- [16] A. Szekrenyes, J. Uj, Int. J. Damage Mech. 2007, 16, 5.
- [17] C. Creton, E. J. Kramer, C. Y. Hui, H. R. Brown, *Macromolecules* 1992, 25, 3075.
- [18] M. F. Kanninen, Int. J. Fracture 1973, 9, 83.

PAPER 3

# FRACTURE TOUGHNESS AS A FUNCTION OF THE ADHESIVE THICKNESS

# Mode II fracture toughness of a brittle and a ductile adhesive as a function of the adhesive thickness

Lucas F. M. da Silva<sup>1</sup>, F. A. C. R. G. de Magalhães<sup>1</sup>, F. J. P. Chaves<sup>2</sup>, M. F. S. F. de Moura<sup>1</sup>

<sup>1</sup>Departamento de Engenharia Mecânica, Faculdade de Engenharia da Universidade do Porto, Rua Dr.

Roberto Frias, 4200-465 Porto, Portugal

<sup>2</sup>Instituto de Engenharia Mecânica (IDMEC), Rua Dr. Roberto Frias, 4200-465 Porto, Portugal

### **Abstract**

The main goal of this study was to evaluate the effect of the thickness and type of adhesive on the mode II toughness of an adhesive joint. Two different adhesives were used, Araldite AV138/HV998 which is brittle and Araldite 2015 which is ductile. The end notched flexure (ENF) test was used to determine the mode II fracture toughness because it is commonly known to be the easiest and widely used to characterize mode II fracture. The ENF test consists of a three-point bending test on a notched specimen which induces a shear crack propagation through the bondline. The main conclusion is that the energy release rate for AV138 does not vary with the adhesive thickness whereas for Araldite 2015, the fracture toughness in mode II increases with the adhesive thickness. This can be explained by the adhesive plasticity at the end of the crack tip.

# Keywords

Epoxy; Brittle adhesive; Ductile adhesive; End notched flexure test; Mode II fracture toughness; adhesive thickness.

### Introduction

Adhesively bonded joints were initially designed using a continuum mechanics approach. The maximum principal stress was proposed for very brittle materials whose failure mode is normal to the direction of maximum principal stress [1-2]. However, because of the singularity of stresses at the re-entrant corners of joints, the stresses depend on the mesh size used and how close to the singular points the stresses are taken. Therefore, care must be taken when using this criterion. When ductile adhesives are used, criteria based on maximum stress are not appropriate because such joints can still carry large loads after adhesive yielding. For ductile adhesives, Adams and Harris [2] used maximum principal strain as the failure criterion for predicting joint strength. Hart-Smith [3] proposed that the maximum adhesive shear strain might be used as a failure criterion when plastic deformation of the adhesive occurred. da Silva et al. [4] implemented this criterion into a software package. Other analyses go beyond that of Hart-Smith, by taking into consideration both shear and peel contributions to plasticity, such as that of Adams and Mallick [5]. More recently, da Silva et al. [6-7] have shown for single lap joints that the maximum shear strain criterion is very accurate for ductile adhesives.

Continuum mechanics assumes that the structure and its material are continuous. Defects or two materials with re-entrant corners obviously violate such an assumption. Consequently, continuum mechanics gives no solution at these singular points because of the stress or strain singularities. Cracks are the most common defects in structures, for which the method of fracture mechanics has been developed. In linear elastic fracture mechanics (LEFM), it is well accepted that stresses calculated by using continuum mechanics are singular (infinite) at the crack tip. Although LEFM is mainly

used for dealing with sharp cracks, angular wedged notches are also of practical importance. The use of a generalized stress-intensity factor, analogous to the stress-intensity factor in classical LEFM, to predict fracture initiation for bonded joints at the interface corners has been investigated [8-10]. Damage mechanics has been used to model the progressive damage and failure of a pre-defined crack path [11-14]. The damage is confined to a zero volume line or a surface and the procedure is often referred to as a cohesive zone model (CZM). A CZM simulates the fracture process, extending the concept of continuum mechanics by including a zone of discontinuity modelled by cohesive zones, thus using both local strength and energy parameters to characterize the debonding process. This allows the approach to be of much more general utility than conventional fracture mechanics.

In order to apply a fracture mechanics or damage mechanics approach, it is necessary to have the fracture toughness of the material. The fracture toughness varies with the type of loading, i.e., mode I, II, III and mixed. Most of the data available in the literature is for the fracture toughness in mode I using the double cantilever beam. However, adhesive joints are also loaded in mode II and under mixed mode. For the determination of the toughness in mode II there are various test methods available (Figure 1): the end notched flexure (ENF) test, the end loaded split (ELS) test and the four-point notched flexure (4ENF) test. The ELS test presents large displacements and is sensitive to the clamping device. The 4ENF is more sophisticated but has problems of friction due to the loading mode in the pre-crack region. The easier and probably most common testing method for mode II is the ENF test. The ENF test consists of a three-point bending test on a pre-cracked specimen causing a shear mode loading in the adhesive.

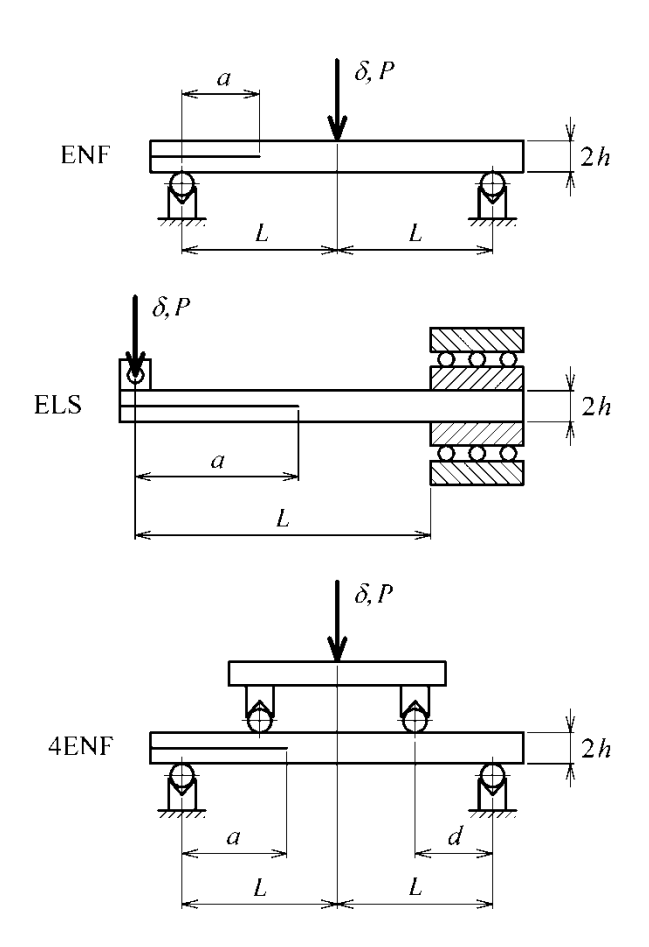


Figure 1 Schematic representation of the end notched flexure (ENF) test, end loaded split (ELS) test and four-point notched flexure (4ENF) test methods.

It is known that the adhesive toughness varies with the adhesive thickness, especially with ductile adhesives because of the constraining effects of the adherends. The thickness of the adhesive layer contributes for the joint behaviour. Thus, it should be taken into account and thoroughly studied. Boscom et al. [15-16] found that fracture energy is maximized when the adhesive layer thickness equals the one of the fracture process zone (FPZ) ahead of the crack tip. Kinloch and Shaw [17] showed that the FPZ played an important role in enhancing  $G_{\rm Ic}$  of the adhesive joint. Daghyani et al. [18-19] found a transition in the fracture process from a cohesive to an interfacial adhesive failure for thin layers. Lee et al. [20] found that as bond thickness decreases, the fracture energy either decreases monotonically, or increases, peaks, and then decreases rapidly.

Most of the results in the literature concerning the effect of the adhesive thickness is for mode I, but little is available concerning mode II, which should be the main loading mode in adhesive joints.

The main objective of the present study was to measure the mode II fracture toughness of two types of adhesive (brittle and ductile) using the ENF test as a function of the adhesive thickness.

# **Experimental details**

### 1.1 Materials

Two adhesives were selected, a very stiff and brittle epoxy (AV138/HV998 from Huntsman, Salt Lake City, UT) used in aerospace applications, and a more flexible and ductile epoxy adhesive (2015 from Huntsman). Table 1 shows the shear properties of the adhesives used in this work. The properties were determined using the thick adherend shear test [21].

The heat treated steel DIN 40CrMnMo7 was used for the substrates. It is a high strength steel with a yield strength of 900 MPa that is sufficient to keep the material in the elastic range.

Table 1 Adhesive shear properties using the thick adherend shear test method ISO 11003-2 [21].

	AV138M / HV998	2015
Shear modulus G (MPa)	1559 ± 11	487 ± 77
Shear yield strength $\tau_{ya}$ (MPa)	$25.0 \pm 0.55$	$17.9 \pm 1.80$
Shear strength $\tau_r$ (MPa)	$30.2 \pm 0.40$	$17.9 \pm 1.80$
Shear failure strain $\gamma_f$ (%)	$5.50 \pm 0.44$	$43.9 \pm 3.40$

### 1.2 Specimen geometry

The specimen geometry is represented in Figure 2. The geometry used for the ENF test is the one used for the double cantilever beam test where the adherend thickness h is 6.35 mm. The length between the supports 2L was 270 mm and the initial crack length was 50 mm. Three adhesive thicknesses were studied for each adhesive: 0.2, 0.5 and 1 mm.

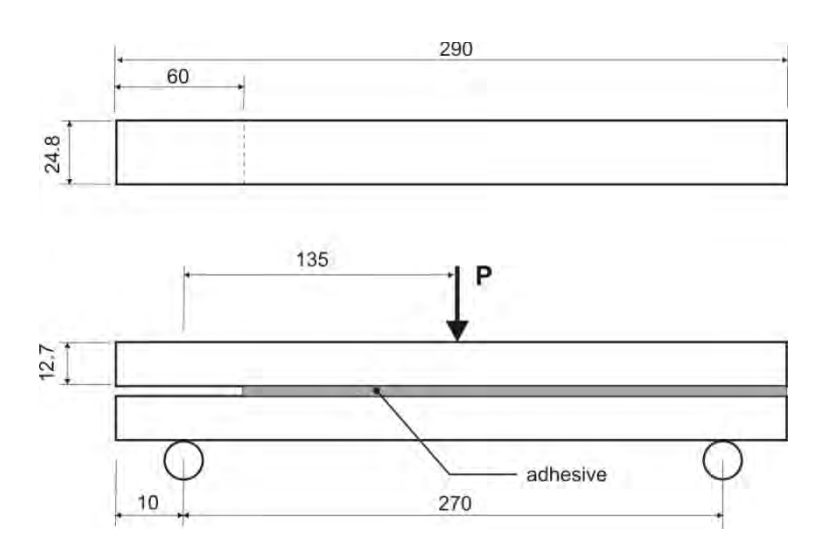


Figure 2 Geometry of the end notched flexure (ENF) test specimen (dimensions in mm).

### 1.3 Specimen manufacture

The joint surfaces were grit blasted with corundum (600 µm particles) under a pressure of 6 bar and degreased with acetone prior to the application of the adhesive. The resin and hardener of the brittle epoxy AV138/HV998 were mixed manually and applied with a spatula on the substrates. The ductile epoxy 2015 was mixed with a nozzle and applied directly on the surfaces. Spacers were inserted between the adherends before the application of the adhesive in order to control the bondline thickness. These spacers were removed after the adhesive was cured. Joints with AV138/HV998 were cured for

16h at 45°C and those with 2015 were cured for 6h at 45°C. A sharp pre-crack in the adhesive layer mid-thickness was assured using a razor blade and a gentle tap. To guarantee the correct precrack position at the adhesive layer middle plane, a simple set with a razorblade glued in between two feeler gauges was introduced in the gap between the upper and lower adherends to promote the precrack. This set was done with a 0.1 mm thickness razorblade glued in between two feeler gauges with half the bond line thickness minus 0.05 mm to account for the razorblade thickness. A jig with spacers for the correct alignment of the adherends was used and is shown in Figure 3. It was verified in a previous study [22] that friction effects in the ENF test are mainly concentrated at the region of the pre-crack above the support. Consequently, two sheets of Teflon with a thin pellicle of lubricator between them were included in the pre-crack region in order to minimize friction effects.



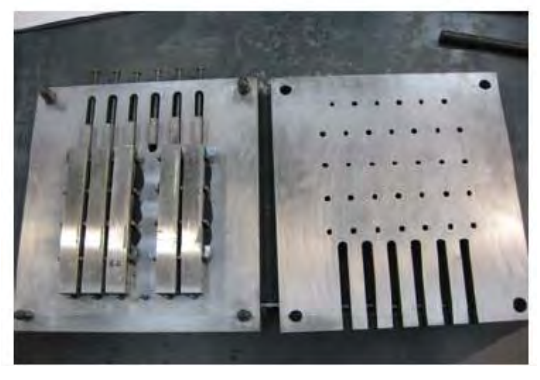


Figure 3 End notched flexure specimen fabrication (shims for bondline thickness control at the top and assembled specimens in a jig at the bottom).

# 1.4 Testing

The ENF specimens were tested in laboratory conditions ( $\sim 25^{\circ}\text{C}$  and  $\sim 50\%$  relative humidity) using a universal testing machine, under a constant crosshead rate of 0.25 mm/min. The load–displacement (P– $\delta$ ) curve was registered during the test. Despite the difficult identification of the crack tip in mode II testing, pictures were recorded during the specimens testing with 5 s intervals using a 10 MPixel digital camera. This procedure allows measuring the crack length during its growth and afterwards collecting the P– $\delta$ –a parameters. This was performed correlating the time elapsed since the beginning of each test between the P– $\delta$  curve and each picture (the testing time of each P– $\delta$  curve point is obtained accurately with the absolute displacement and the established loading rate). The specimens were marked with a white paint and a ruler to facilitate the crack length (a) reading. Three specimens were tested for each configuration.

### 1.5 Data analysis

According to linear elastic fracture mechanics [23],

$$G_{\rm c} = \frac{P_{\rm c}^2}{2b} \frac{dC}{da} \tag{1}$$

where C is the compliance defined by  $C = \delta/P$ ,  $P_c$  is the load for crack growth and b is the joint width. According to the beam theory and using Equation (1),

$$G_{\text{IIc}} = \frac{9P_{\text{c}}^2 a^2}{16h^2 F h^3}$$
 (2)

where  $G_{\text{IIc}}$  is the toughness in mode II. The toughness in mode II can also be determined by finding the partial derivative of the compliance with crack length using an analytical

equation (usually a cubic polynomial) that fits the experimental data of the compliance versus the crack length. However, in any case, the experimental measurement of the crack length is very laborious because the two substrates are against each other and make the identification of the crack tip very difficult. Also, at the crack tip the fracture process zone (FPZ) where damage of the material occurs by plasticisation and microcrackling absorbs part of the energy. Therefore, an equivalent crack length (*a*<sub>e</sub>) that takes into account of the FPZ should be used. To overcome these two problems (crack monitoring and FPZ), de Moura and Morais [24] proposed a method that does not require the crack length measurement and that takes into account the FPZ that they called the compliance based beam method (CBBM). Using the beam theory and accounting for the shear effects, the following equation is obtained

$$C = \frac{3a^3 + 2L^3}{12EI} + \frac{3L}{10Gbh} \tag{3}$$

In this equation the crack length does not include the effects of energy dissipation at the FPZ and the moduli E and G refer only to the adherends. However, it is expected that the compliance of the adhesive and its thickness, can influence the global compliance of the specimen. Consequently, an equivalent flexural modulus can be estimated considering the initial compliance  $C_0$  and the initial crack length  $a_0$ 

$$E_{\rm f} = \frac{3a_0^3 + 2L^3}{12I} \left( C_0 - \frac{3L}{10Gbh} \right)^{-1} \tag{4}$$

On the other hand, the effect of the FPZ on the compliance can be included through an equivalent crack length  $(a_e)$ , which is the sum of the real crack (a) with the correction  $(\Delta a_{\rm FPZ})$  induced by the presence of the FPZ

$$C = \frac{3(a + \Delta a_{\text{FPZ}})^3 + 2L^3}{12E_{\text{f}}I} + \frac{3L}{10Gbh}$$
 (5)

Combining Equations (5) and (4) the equivalent crack length can be obtained as a function of the current measured compliance

$$a_{\rm e} = a + \Delta a_{\rm FPZ} = \left[ \frac{C_{\rm corr}}{C_{0_{\rm corr}}} a_0^3 + \frac{2}{3} \left( \frac{C_{\rm corr}}{C_{0_{\rm corr}}} - 1 \right) L^3 \right]^{\frac{1}{3}}$$
 (6)

where  $C_{\text{corr}}$  and  $C_{0\text{corr}}$  are given by

$$C_{\text{corr}} = C - \frac{3L}{10Gbh}; \quad C_{0\text{corr}} = C_0 - \frac{3L}{10Gbh}$$

Substituting the value of  $a_e$  in Equation (2),

$$G_{\rm II} = \frac{9P^2}{16b^2 E_f h^3} \left[ \frac{C_{\rm corr}}{C_{0\rm corr}} a_0^3 + \frac{2}{3} \left( \frac{C_{\rm corr}}{C_{0\rm corr}} - 1 \right) L^3 \right]^{\frac{2}{3}}$$
 (7)

This method does not require crack length monitoring during its growth which was observed to be very difficult to perform with accuracy in the ENF test. Moreover, it provides an *R*-curve as a function of the equivalent crack length thus allowing a clear identification of the fracture energy from its plateau.

# Results

### 1.6 Brittle adhesive (AV138)

All the specimens failed cohesively in the adhesive, as shown in Figure 4.

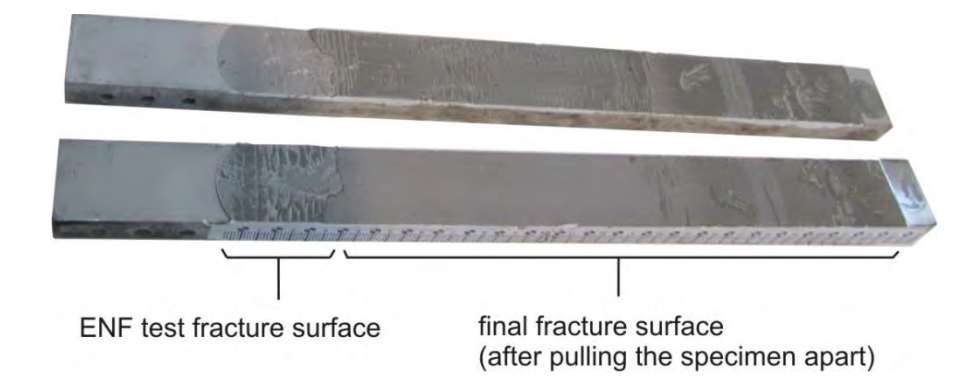


Figure 4 Failure surfaces of end notched flexure (ENF) specimens with the brittle adhesive AV138.

Representative experimental P– $\delta$  curves of the ENF specimens for each adhesive thickness are presented in Figure 5. The curves are linear to failure which is in accordance with the brittle nature of the adhesive. The crack propagation occurred suddenly after the maximum load. An experimental R-curve obtained for an adhesive thickness of 0.5 mm is shown in Figure 6. R-curves are used to identify the fracture energy from the plateau corresponding to the self-similar crack propagation. A plateau barely appears because the adhesive is brittle and leads to an unstable crack propagation. Figure 7 shows the values of  $G_{\text{IIc}}$  as a function of the adhesive thickness. The brittle adhesive AV138 is not sensitive to the adhesive thickness and gives an approximately constant value of 5 N/mm. The fracture toughness was determined using the compliance based beam method (CBBM) because it was not possible to monitor the crack during its growth due to the sudden and unstable crack propagation.

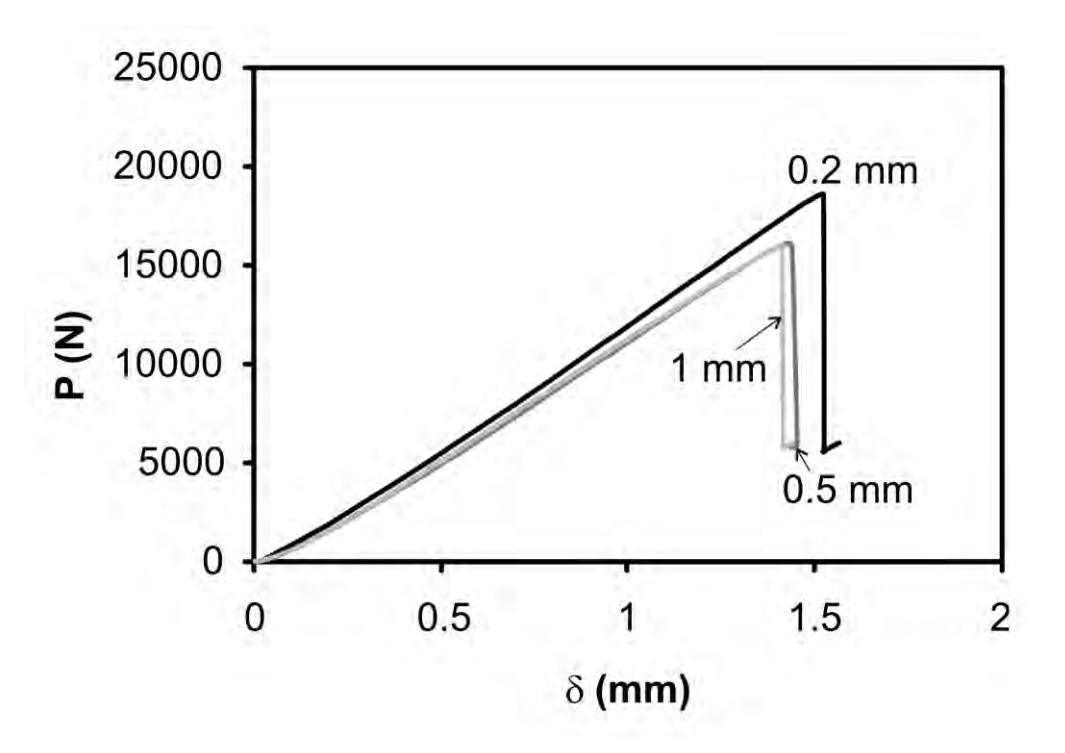


Figure 5 Representative experimental P– $\delta$  curves of the ENF specimens with the brittle adhesive AV138 as a function of the adhesive thickness.

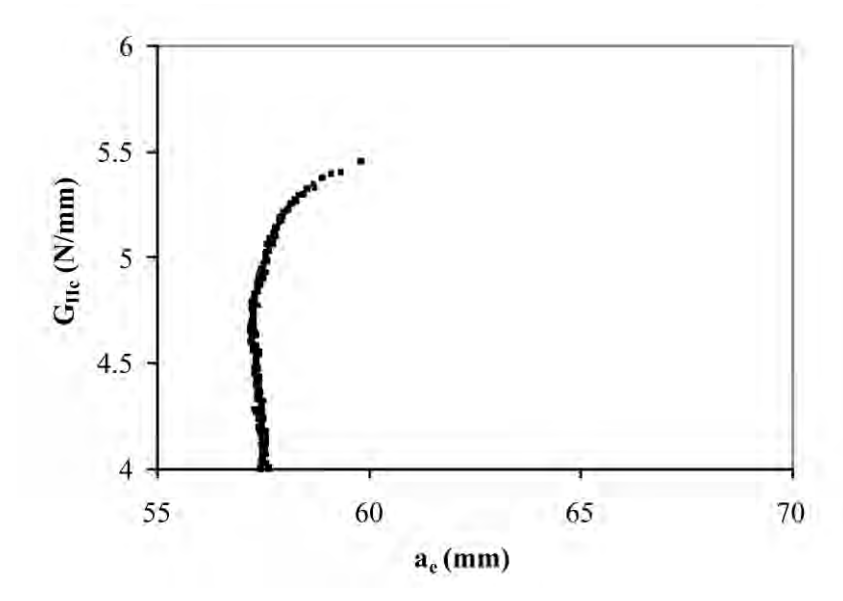


Figure 6 Typical experimental *R*-curve obtained for the brittle adhesive AV138 for a thickness of 0.5 mm.

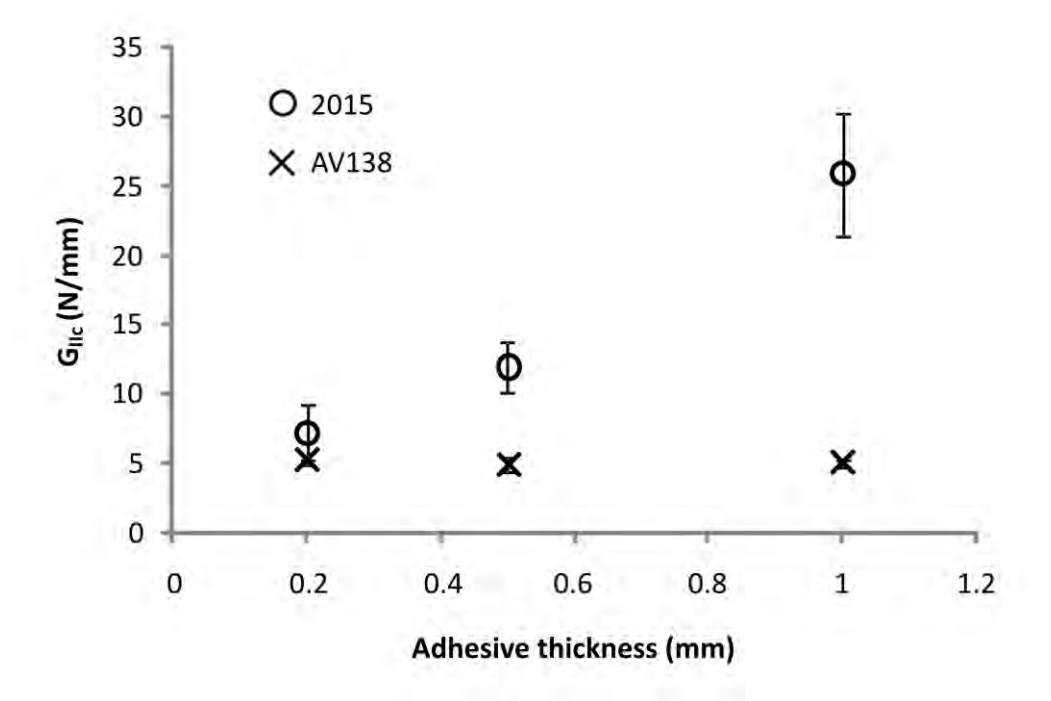


Figure 7 Mode II fracture toughness ( $G_{IIc}$ ) as a function of the adhesive thickness for a ductile adhesive (2015) and a brittle adhesive (AV138).

### 1.7 Ductile adhesive (2015)

All the specimens failed cohesively in the adhesive, as shown in Figure 8.

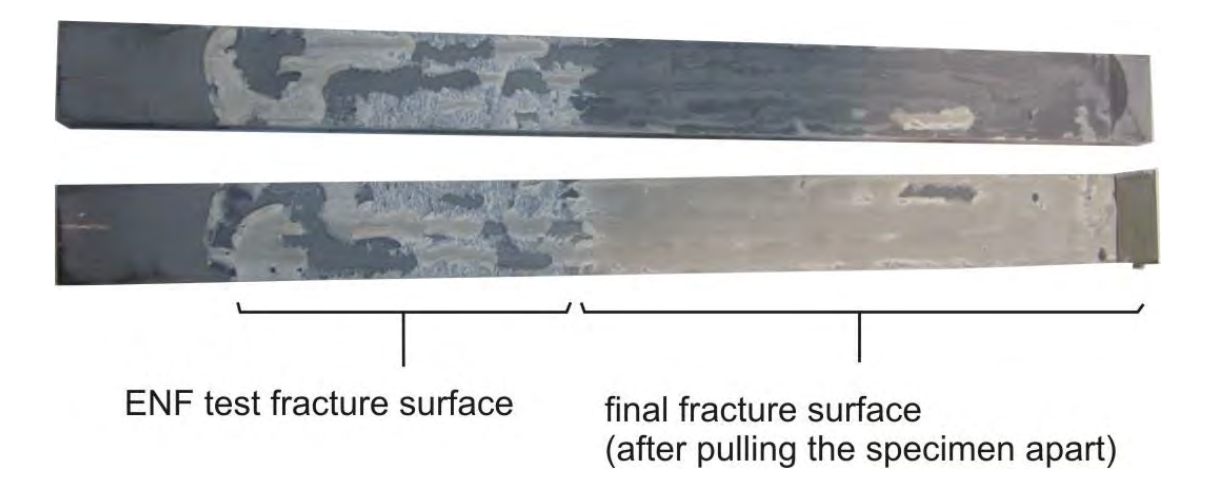


Figure 8 Failure surfaces of ENF specimens with the ductile adhesive 2015.

Representative experimental P– $\delta$  curves of the ENF specimens for each adhesive thickness are presented in Figure 9. In this case, the curves are non-linear corresponding to the adhesive plastic deformation. An experimental R-curve obtained for an adhesive thickness of 0.5 mm is shown in Figure 10. A plateau is clearly seen indicating stable crack propagation. Figure 7 shows the values of  $G_{\rm IIc}$  as a function of the adhesive thickness. The fracture toughness in mode II increases with the adhesive thickness. The values presented in Figure 7 were obtained using the CBBM method. However, in the case of the 2015 adhesive, it was possible to measure the crack length and determine the fracture toughness using the beam theory. Table 2 shows that the beam theory underestimates the  $G_{\rm IIc}$ , especially for large bondline thicknesses (0.5 and 1 mm).

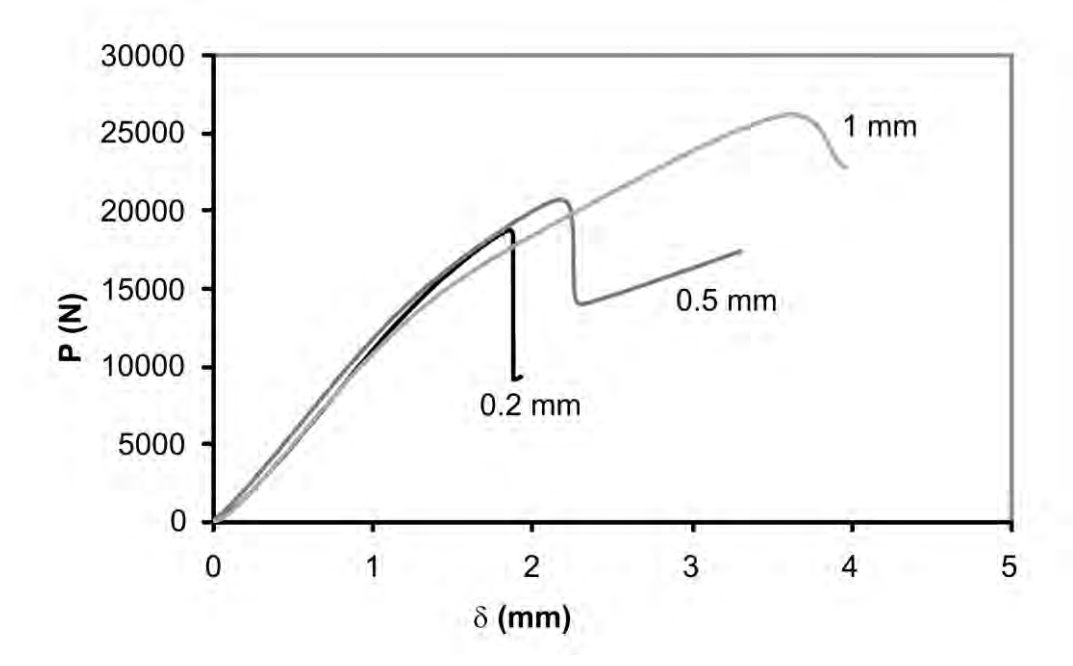


Figure 9 Representative experimental P- $\delta$  curves of the ENF specimens with the ductile adhesive 2015 as a function of the adhesive thickness.

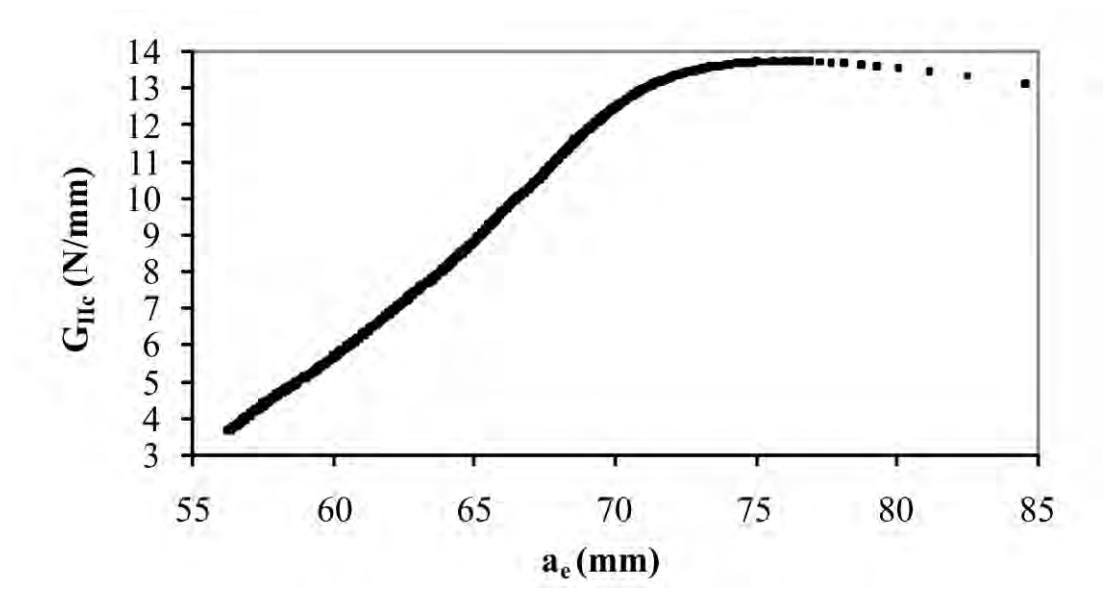


Figure 10 Typical experimental *R*-curve obtained for the ductile adhesive 2015 for a thickness of 0.5 mm.

Table 2 Fracture toughness in mode II ( $G_{IIc}$ ) determined using the beam theory and the CBBM method for the ductile adhesive 2015 (only one specimen used for each adhesive thickness).

Adhesive thickness (mm)	Beam theory $G_{\text{IIc}}$ (N/mm)	CBBM $G_{\text{IIc}}$ (N/mm)
0.5	11.3	13.2
1	21.2	32.4

# **Discussion**

In adhesive bonding it is important to understand that the adhesive layer applied in between the two bonded bodies is usually thin (of the order 0.05 to 0.2 mm for aeronautical industry and up to 1 mm or more for the civil industry), thus it behaves differently compared to the adhesive as a bulk material. If it is true that thicker adhesive layers result in bad joint properties, when the adhesive layer becomes thinner than the surface roughness it is difficult for the adhesive to promote the connection between the two surfaces because there are points where the two adherends come into contact. The ability to absorb energy, characterizing ductile or brittle adhesive plays also an important role when evaluating the bondline thickness effect. The explanation for the results presented above is probably linked with the FPZ size. Although no measurements of the FPZ were performed in this work, it is known that in the case of a brittle adhesive, the FPZ is negligible and probably the adherends do not interfere with the strain energy release rate measured. However, in the case of the ductile adhesive 2015, the results give the idea that the fracture toughness measured is influenced by the adhesive thickness, since this parameter influences decisively the natural FPZ development, as shown schematically in Figure 11.

• • • •

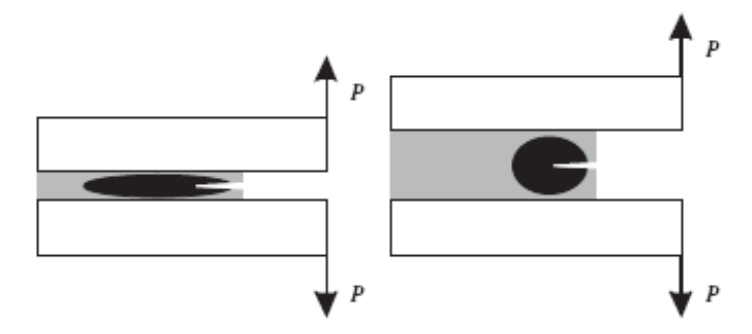


Figure 11 Fracture process zone (FPZ) as a function of the adhesive bondline thickness.

The value of  $G_{\text{IIc}}$  used for modelling purposes to design an adhesive joint should be that measured in a fracture mechanics joint with the same adhesive thickness. This aspect is often not taken into account and may lead to erroneous results.

The strain energy release rate measured here in mode II can be compared with that measured in mode I by the same authors in another paper [25]. The fracture toughness in mode I was measured using the double cantilever beam method under a test speed similar to that used in the present analysis and under the same ambient conditions. The adhesive thickness that was used is 0.5 mm. The values are presented in Table 3 along with the mode II values and the relation  $G_{\text{IIc}}/G_{\text{Ie}}$ . It is common in the literature to assume a relation of 2 for  $G_{\text{IIc}}/G_{\text{Ie}}$  when the value of  $G_{\text{IIc}}$  is unknown [24, 26]. However, the results presented here show that the relation can be much higher. Therefore, it is important to test not only in mode I but also in mode II for the true adhesive properties. Another study [27] has shown a relation of approximately 10 for  $G_{\text{IIc}}/G_{\text{Ic}}$  for adhesive toughness to be used for simulation purposes should use properties determined in conditions similar to those found in the real structure.

Table 3 Comparison of the fracture toughness in mode I ( $G_{Ic}$ ) and mode II ( $G_{IIc}$ ) for an adhesive thickness of 0.5 mm (average values).

Adhesive	$G_{\rm Ic}$ (N/mm) [24]	$G_{\rm IIc}$ (N/mm) (present study)	$G_{ m IIc}$ / $G_{ m Ic}$
Brittle (AV138)	0.346	4.91	14.2
Ductile (2015)	0.526	11.9	22.6

## **Conclusions**

The fracture toughness in mode II ( $G_{IIc}$ ) was measured using the ENF test for a brittle adhesive (AV138) and a ductile adhesive (2015) using three adhesive thicknesses (0.2, 0.5 and 1 mm). The following conclusions can be drawn:

- 1. The critical strain energy release rate ( $G_{IIc}$ ) for the brittle adhesive AV138 does not vary with the adhesive thickness and is approximately 5 N/mm.
- 2. The critical strain energy release rate ( $G_{IIc}$ ) for the ductile adhesive (2015) increases with the adhesive thickness, varying from 7.15 N/mm for 0.2 mm to 25.8 N/mm for 1 mm.
- 3. The different behaviour between the two types of adhesives can be explained by the fracture process zone (FPZ) ahead of the crack tip. In the case of the brittle adhesive, that FPZ is negligible contrarily to the case of the ductile adhesive which interferes with the adherends.
- 4. The relation  $G_{IIc}/G_{Ic}$  for the adhesives studied here is of at least one order of magnitude.

# References

- [1] Adams, R. D., Peppiatt, N. A., J. Strain Anal. 9, 185-196 (1974).
- [2] Adams, R. D., Harris, J. A., Int. J. Adhes. Adhes. 4, 65-78 (1984).
- [3] Hart-Smith, L. J., NASA Contract Report, NASA CR-112236 (1973).
- [4] da Silva, L. F. M., Lima, R. F. T., Teixeira, R. M. S., J. Adhesion 85, 889-918(2009).
- [5] Adams, R. D., Mallick, V., J. Adhesion 38, 199-217 (1992).
- [6] da Silva, L. F. M., das Neves, P. J. C., Adams, R. D., Spelt, J. K., Int. J. Adhes. Adhes. 29, 319-330 (2009).
- [7] da Silva, L. F. M., das Neves, P. J. C., Adams, R. D., Wang, A., Spelt J. K., *Int. J. Adhesion Adhesives* **29**, 331-341 (2009).
- [8] Xu, J.-Q., Liu, Y.-H., Wang, X.-G., Engineering Fracture Mechanics **63** (6), 775-790 (1999).
- [9] Groth, H. L., Int. J. Adhes. Adhes. 8, 107-113 (1988).
- [10] Gleich, D. M., Van Tooren, M. J. L., Beukers, A., J. Adhesion Sci. Technol. 15 (9), 1091-1101 (2001).
- [11] Duan, K., Hu, X., Mai, Y.-W., J. Adhesion Sci. Technol. 18(1), 39-54 (2004).
- [12] Needleman, A., J. Applied Mechanics **54**, 525-531 (1987).
- [13] Ungsuwarungsri, T., Knauss, W. G., *Int. J. Fracture* **35**, 221-241 (1987).
- [14] Tvergaard, V., Hutchinson, J. W., J. Mechanics and Physics of Solids 40, 1377-1397 (1992).
- [15] Bascom, W. D., Cottington, R. L., Jones, R. L., Peyser, P., J. Appl. Polym. Sci. 19, 2545–2562 (1975).
- [16] Bascom, W. D., Cottington, R. L., J. Adhesion 7, 333–346 (1976).
- [17] Kinloch, A. J., Shaw, S. J., *J. Adhesion* **12**, 59–77 (1981).

- [18] Daghyani, H. R., Ye, L., Mai, Y. W., J. Adhesion 53, 149–162 (1995).
- [19] Daghyani, H. R., Ye, L., Mai, Y. W., J. Adhesion 53, 163–172 (1995).
- [20] Lee, D., Ikeda, T., Miyazaki, N., Choi, N., J. Engineering Materials and Technology 126, 14-18 (2004).
- [21] Marques, E. A. S, da Silva, L. F. M., J. Adhesion 84, 917–936 (2008).
- [22] Silva, M.A.L., de Moura, M.F.S.F., Morais J.J.L., Composites: Part A 37, 1334–1344 (2006).
- [23] Irwin, G. R., Appl. Mater. Res. 3, 65-81(1963)
- [24] de Moura, M. F. S. F., de Morais, A. B., Eng. Fract. Mech. 75, 2584–2596 (2008).
- [25] da Silva, L. F. M., Carbas, R. J. C., Critchlow, G. W., Figueiredo, M. A. V., Brown, K., Int. J. Adhes. Adhes. 29: 621–632, 2009.
- [26] da Silva, L. F. M., Rodrigues, T. N. S. S., Figueiredo, M. A. V., de Moura, M. F.
   S. F., Chousal, J. A. G., J. Adhesion 82: 1091–1115, 2006.
  - [27] Campilho, R. D. S. G., de Moura, M. F. S. F., Ramantani, D. A., Morais, J. J. L., Domingues, J. J. M. S., *Int. J. Adhes. Adhes.* 29, 678–686 (200

PAPER 4

NUMERICAL ANALYSIS OF THE DAL TEST

# Numerical analysis of the dual actuator load test applied to fracture characterization of bonded joints

Filipe J.P.Chaves<sup>1</sup>, M.F.S.F. de Moura<sup>2</sup>, L.F.M. da Silva<sup>2</sup>, D. A. Dillard<sup>3</sup>

<sup>1</sup>IDMEC- Pólo FEUP, Faculdade de Engenharia da Universidade do Porto, Rua Dr. Roberto Frias, 4200-465 Porto, Portugal

<sup>2</sup>DEMec,Faculdade de Engenharia da Universidade do Porto, Rua Dr. Roberto Frias, 4200-465 Porto, Portugal

<sup>3</sup>Engineering Science and Mechanics Department, Virginia Tech, Blacksburg, VA 24061

#### **Abstract**

The dual actuator load test was numerically analysed in order to assess its adequacy for fracture characterization of bonded joints under different mixed-mode loading conditions. This test enables asymmetric loading of double cantilever beam specimens, thus providing a large range of mixed-mode combinations. A new data reduction scheme based on specimen compliance, beam theory and crack equivalent concept was proposed to overcome several difficulties inherent to the test. The method assumes that the dual actuator test can be viewed as a combination of the double cantilever beam and end loaded split tests, which are used for pure modes I and II fracture characterization, respectively. A numerical analysis including a cohesive mixed-mode damage model was performed considering different mixed-mode loading conditions to evaluate the test performance. Some conclusions were drawn about the advantages and drawbacks of the test.

**Keywords**: Bonded joints, Fracture characterization, Mixed-mode loading.

## 1. Introduction

Structural applications of adhesively bonded joints are increasing rapidly for a wide range of engineering structures and devices. As a consequence the development of design criteria based on fracture mechanics concepts has become increasingly important since the strength-based criteria are not adequate in the presence of singularities [1-3]. In this context, fracture characterization of adhesive bonded joints acquire special relevancy. Pure mode I fracture characterization is usually performed by means of the

double cantilever beam (DCB) specimen. This test is simple to execute and the fracture toughness,  $G_{\rm Ic}$  can be mathematically defined according to beam theory [4] or several improved approaches as compared in [5]. In mode II, the end notched flexure (ENF) and the end loaded split (ELS) are frequently used [2, 6-8] due to their simplicity and ability to provide pure mode II loading at the crack tip.

However, it should be noted that bonded joints in service are usually subjected to mixed-mode conditions due to geometric and loading complexities. In fact, due to their geometric characteristics (two adherends separated by a thin adhesive layer) the crack is frequently forced to grow in pre-defined planes even when the structure is under general non aligned loading, which induce mixed-mode loading conditions. Consequently, the fracture characterization of bonded joints under mixed-mode loading is a fundamental task. There are some simple tests proposed in the literature concerning this subject, as is the case of the asymmetric double cantilever beam (ADCB), the single leg bending (SLB) and the cracked lap shear (CLS). Nevertheless, these tests are limited in which concerns the variation of the mode-mixity [9], which means that different tests are necessary to cover the fracture envelope in the  $G_{\rm I}$ - $G_{\rm II}$  space. Alternatively, the mixed mode bending (MMB) test, initially proposed by Reeder and Crews [10] for interlaminar fracture characterization of composite materials, can be used. This test consists of a combination of the DCB and ENF tests and provides a simple alteration of the mode mixity by changing the lever length of the loading arm. In addition, the load applied to the specimens can be separated into mode I and mode II components by means of a mode partitioning method based on the beam theory [11]. Although the MMB test was also used in the context of composite and steel bonded joints by Ducept et al. [12] and Liu et al. [13] respectively, it requires a special test apparatus with significant dimensions, especially when testing stiff adherends. Furthermore, the MMB test does not cover the complete variation in mode mixity from mode I to mode II. Sørensen et al. [14] proposed the DCB specimen loaded with uneven bending moments at the two free beams. By varying the ratio between the two applied moments, the full mode mixity range from pure mode I to pure mode II can be generated for the same specimen geometry. Högberg and Stigh [15] proposed the mixed mode double cantilever beam specimen based on the geometry of a semi-infinite symmetric DCB specimen. The specimen is loaded by a pair of self-balancing forces whose orientation can vary to alter the mode mixity. The resulting loading combines the basic loading cases of DCB, ELS and CLS tests. An alternative solution is the dual actuator load

(DAL) [16, 17], which can be viewed as a DCB test subjected to non -symmetric loading. Effectively, the test consists of two independent hydraulic actuators operating the arms of a standard DCB specimen clamped at the other extremity. This test allows easy variation of the mode mixity by applying different displacement rates to the specimen arms by means of the two independent hydraulic actuators.

The objective of this work is to perform a detailed numerical analysis on the DAL test. Cohesive zone modeling is used to simulate damage initiation and growth for several different combinations of mode-mixity. A new data reduction scheme based on specimen compliance, beam theory and crack equivalent concept is proposed in order to overcome some difficulties inherent to the test. In addition some aspects related to non self-similar crack growth, fracture process zone development and dependency of the mode mixity as a function of crack length are discussed.

#### 2. Dual actuator load test

The DAL test is based on a DCB specimen loaded asymmetrically by means of two independent hydraulic actuators (Figure 1). The specimen is clamped at the bonded end and loaded at the debonded end by means of the independent hydraulic actuators that are attached to the specimen arms. Each hydraulic actuator pivots in order to allow some rotation to accommodate the small vertical displacements of each beam due to foreshortening. Each actuator is equipped with a load cell and a linear variable displacement transducer (LVDT), with the purpose of registering the two load-displacement curves during the test. Different combinations of applied displacement rates provide different levels of mode mixities, thus allowing an easy definition of the fracture envelope in the  $G_1$  versus  $G_{II}$  space.

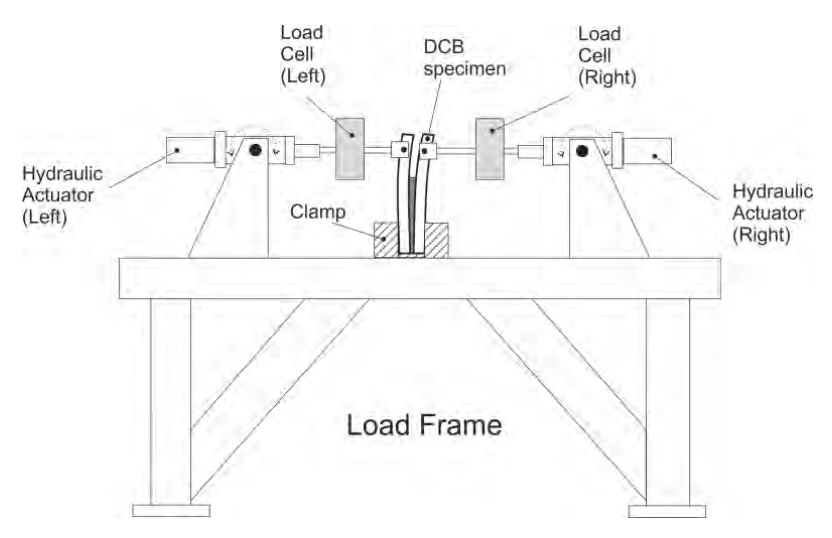


Figure 1. DAL frame [17].

## 3. Compliance based beam method

The classical data reduction schemes based on compliance calibration and beam theories require crack length monitoring during its growth. This can be considered an important limitation in cases where crack tip is not easily identified, which is the case of mode II predominant loading cases, since the crack tends to close during propagation. On the other hand, when the fracture process zone (FPZ) ahead of the crack tip is nonnegligible (as is the case of adhesives with some ductility) the energy dissipation in the FPZ must be taken into account, which does not happen when the crack length is used as a fracture parameter.

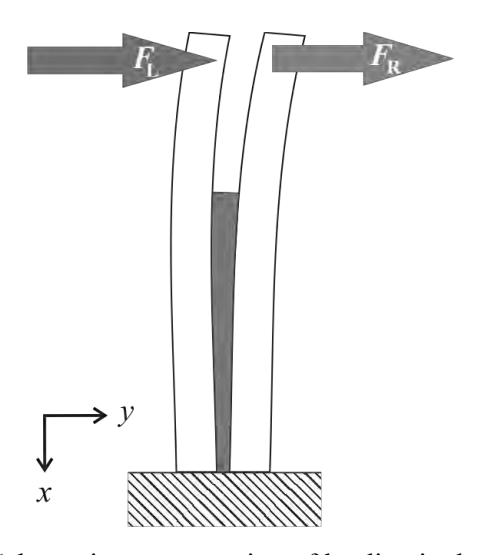


Figure 2. Schematic representation of loading in the DAL test.

In order to overcome these drawbacks, an alternative data reduction scheme based on specimen compliance, beam theory and crack equivalent concept is proposed. Using Timoshenko beam theory, the strain energy of the specimen (Figure 2) due to bending and including shear effects is

$$U = \int_0^a \frac{M_R^2}{2EI_R} dx + \int_0^a \frac{M_L^2}{2EI_L} dx + \int_a^L \frac{M_T^2}{2EI_T} dx + \int_a^L \frac{M_T^2}{2EI_T} dx + \int_a^a \int_{-h/2}^{h/2} \frac{\tau_R^2}{2G} B \, dy dx + \int_0^a \int_{-h/2}^{h/2} \frac{\tau_L^2}{2G} B \, dy dx + \int_a^L \int_{-h}^h \frac{\tau_T^2}{2G} B \, dy dx$$
 (1)

where M is the bending moment, the subscripts R and L stand for right and left adherends and T refers to the total bonded beam (of thickness 2h), E and G are the longitudinal and shear modulus, respectively, B is the specimen and bond width and I is the second moment of area of the indicated section. For the particular case of adherends with same thickness, considered in this analysis,  $I_T = 8I_R = 8I_L$ . The shear stresses induced by bending are given by

$$\tau = \frac{3}{2} \frac{V}{Bh} \left( 1 - \frac{y^2}{c^2} \right) \tag{2}$$

The parameters c and V represent, respectively, the beam half-thickness and the transverse load, on each arm for  $0 \le x \le a$ , and on total bonded beam for  $a \le x \le L$ .

From Castigliano's theorem ( $\delta = \partial U/\partial P$ , where P is the applied load and  $\delta$  the resulting displacement at the same point) the displacements of the specimen arms can be written as

$$\delta_{L} = \frac{\left(7a^{3} + L^{3}\right)F_{L}}{2Bh^{3}E} + \frac{(L^{3} - a^{3})F_{R}}{2Bh^{3}E} + \frac{3L\left[(F_{L} + F_{R}) + a(F_{L} - F_{R})\right]}{5BhG}$$

$$\delta_{R} = \frac{\left(7a^{3} + L^{3}\right)F_{R}}{2Bh^{3}E} + \frac{(L^{3} - a^{3})F_{L}}{2Bh^{3}E} + \frac{3L\left[(F_{L} + F_{R}) + a(F_{R} - F_{L})\right]}{5BhG}$$
(3)

The DAL test can be viewed as a combination of the DCB and ELS tests (Figure 3). Effectively, the DAL test consists of a mixture of opening and shear loading provided by the respective pure mode tests. Thus, the load applied to the specimen can be separated into mode I and mode II components, and beam theory can be used to find a simple data reduction scheme.

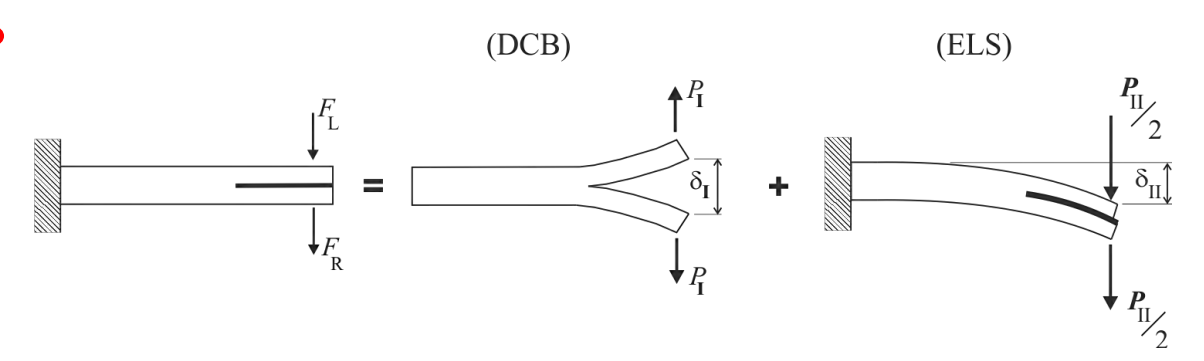


Figure 3. Schematic representation of loading in the DAL test.

From Figure 3 the following relations can be written

$$P_{\rm I} = \frac{F_{\rm R} - F_{\rm L}}{2}$$

$$P_{\rm II} = F_{\rm R} + F_{\rm L} \tag{4}$$

being  $P_{\rm I}$  and  $P_{\rm II}$  the mode I and mode II load components, respectively. The displacements become

$$\delta_{I} = \delta_{R} - \delta_{L}$$

$$\delta_{II} = \frac{\delta_{R} + \delta_{L}}{2}$$
(5)

Combining equations (3-5), the pure mode compliances become

$$C_{\rm I} = \frac{\delta_{\rm I}}{P_{\rm I}} = \frac{8a^3}{Bh^3E} + \frac{12a}{5BhG} \tag{6}$$

$$C_{II} = \frac{\delta_{II}}{P_{II}} = \frac{3a^3 + L^3}{2Bh^3E} + \frac{3L}{5BhG}$$
 (7)

It should be noted that these equations agree with the ones obtained for the DCB [2] and ELS [18] tests, respectively. This means that simple equations can be applied to DAL test after performing the partition of modes.

During the test, there are several aspects not accounted for in equations (6) and (7) that can influence the specimen behaviour. Effectively, issues like stress concentrations, root rotation effects, the presence of the adhesive, load frame flexibility, and the existence of a non-negligible fracture process zone ahead of crack tip during propagation are not included in these equations. To overcome these drawbacks, equivalent crack lengths can

be calculated from the current compliances  $C_{\rm I}$  and  $C_{\rm II}$ , which are easily obtained from the loads and displacements of the specimen arms continuously registered during the test. In mode I the equivalent crack length  $(a_{\rm eI})$  is obtained from the cubic equation (6) that can be written in the following way

$$\alpha a_{\rm el}^3 + \beta a_{\rm el} + \gamma = 0 \tag{8}$$

where

$$\alpha = \frac{8}{Bh^3E}; \quad \beta = \frac{12}{5BhG}; \quad \gamma = -C_1 \tag{9}$$

Using Matlab® software and only keeping the real solution, one obtains

$$a_{\rm el} = \frac{1}{6\alpha} A - \frac{2\beta}{A} \tag{10}$$

where

$$A = \left( \left( -108\gamma + 12\sqrt{3\left(\frac{4\beta^3 + 27\gamma^2\alpha}{\alpha}\right)} \right) \alpha^2 \right)^{\frac{1}{3}}$$
 (11)

In mode II the equivalent crack length ( $a_{eII}$ ) can be straightforwardly obtained from equation (7)

$$a_{\text{eII}} = \left[ \left( C_{\text{II}} - \frac{3L}{5BhG} \right) \frac{2Bh^3E}{3} - \frac{L^3}{3} \right]^{1/3}$$
 (12)

The strain energy release rate components can be determined using the Irwin-Kies equation

$$G = \frac{P^2}{2B} \frac{dC}{da} \tag{13}$$

For mode I, the combination of equations (6) and (13) leads to

$$G_{\rm I} = \frac{6P_{\rm I}^2}{B^2 h} \left( \frac{2a_{\rm eI}^2}{h^2 E} + \frac{1}{5G} \right) \tag{14}$$

The strain energy release rate in mode II is obtained from equations (7) and (13)

$$G_{\rm II} = \frac{9P_{\rm II}^2 a_{\rm eII}^2}{4B^2 h^3 E} \tag{15}$$

Equations (14) and (15) provide the *R*-curves in each mode during mixed-mode loading. The method only requires the data given in the load-displacement curves of the two specimen arms registered during the experimental test. The compliance-based beam method (CBBM) does not require crack length monitoring during propagation and

accounts for the FPZ effects, since it is based on current specimen compliance which is influenced by the presence of the FPZ. This method is similar to one of the methods analysed by Tamuzs et al. [19]. These authors used four ways to estimate the energy release rate in a DCB specimen and verified that the best method is based on substitution of crack length by its relationship with experimentally measured compliance.

## 4. Numerical analysis

Numerical analysis including a cohesive damage model was carried out to verify the performance of the test and the adequacy of the proposed data reduction scheme. The specimen geometry and mechanical properties utilized in the simulations are presented in Figure 4 and Table 1, respectively.

Elastic properties (Steel)		Cohesive properties (Adhesive)			
E (GPa)	G (MPa)	$\sigma_{u,I}(MPa)$	$\sigma_{\mathrm{u,II}}\left(\mathrm{MPa}\right)$	G <sub>Ic</sub> (N/mm)	$G_{\rm IIc}$ (N/mm)
210	80.77	23	23	0.6	1.2

Table 1. Elastic and cohesive properties.

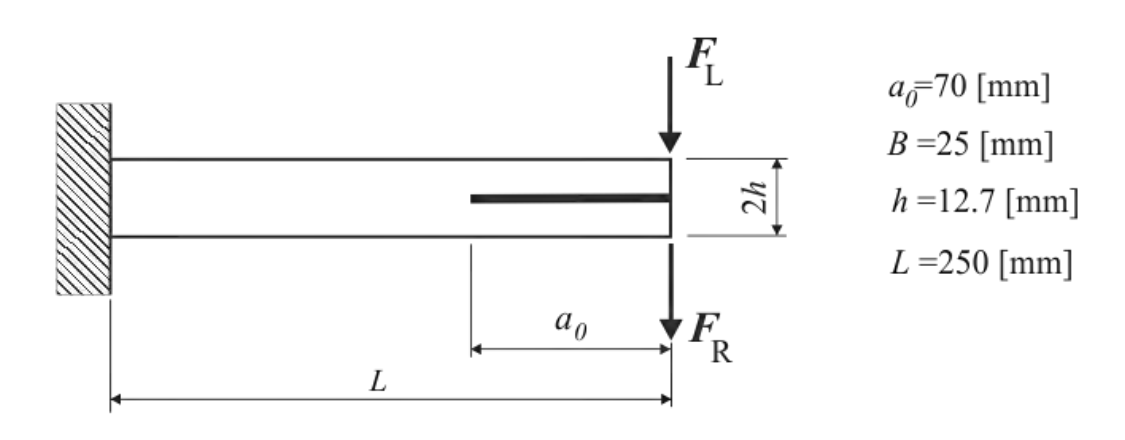


Figure 4. Specimen geometry used in the simulations of the DAL test.

The specimen was modelled with 7680 plane strain 8-node quadrilateral elements and 480 6-node interface elements with null thickness placed at the mid-plane of the bonded specimen. Plane strain conditions with reduced integration were assumed owing to considered specimen width (25 mm). A mixed-mode cohesive damage model was

incorporated in the numerical analysis. The cohesive zone model establishes a relationship between stresses and relative displacements. A linear softening relationship between stresses and relative displacements (Figure 5) is assumed to simulate a gradual material degradation during the loading process. In the initial linear region stresses are obtained from the product between the interfacial stiffness and relative displacements. The interfacial stiffness is chosen as being the highest value (usually  $10^6$ - $10^7$  N/mm<sup>3</sup>) that does not induce numerical instabilities [2]. Once the local strength ( $\sigma_{u,i}$ ) is attained the initial interface stiffness is gradually reduced leading to a linear decrease of stresses. In pure mode model, the ultimate relative displacement  $\delta_{u,i}$  is defined equating the area circumscribed by the triangle to  $G_{ic}$ . Mixed-mode damage model is an extension of pure mode model. In this case, a quadratic stress criterion is utilized to simulate damage initiation

$$\left(\frac{\sigma_{\rm I}}{\sigma_{\rm u,I}}\right)^2 + \left(\frac{\sigma_{\rm II}}{\sigma_{\rm u,II}}\right)^2 = 1 \tag{16}$$

and the linear energetic criterion

$$\left(\frac{G_{\rm I}}{G_{\rm Ic}}\right) + \left(\frac{G_{\rm II}}{G_{\rm IIc}}\right) = 1$$
(17)

to deal with damage growth. In the pure mode law, the parameters  $\delta_{0,i}$  and  $\delta_{u,i}$  (Figure 5) identify the relative displacements corresponding to damage initiation and final failure, respectively. The parameters  $\sigma_i$  and  $\sigma_{u,i}$  (i=I, II) represent the stresses and local strengths in each mode, respectively. The mixed-mode softening law (identified by the subscript m in Figure 5) is an extension of the pure mode law and is based on a combination of the two modes. The area under the triangle  $0-\sigma_{um,i}-\delta_{um,i}$  of Figure 5 represents the energy released in each mode, while the area of the  $0-\sigma_{u,i}-\delta_{u,i}$  triangle corresponds to the respective critical fracture energy. When equation (17) is satisfied damage propagation occurs and stresses are completely released, with the exception of normal compressive ones. The model is detailed in de Morais et al. [20].

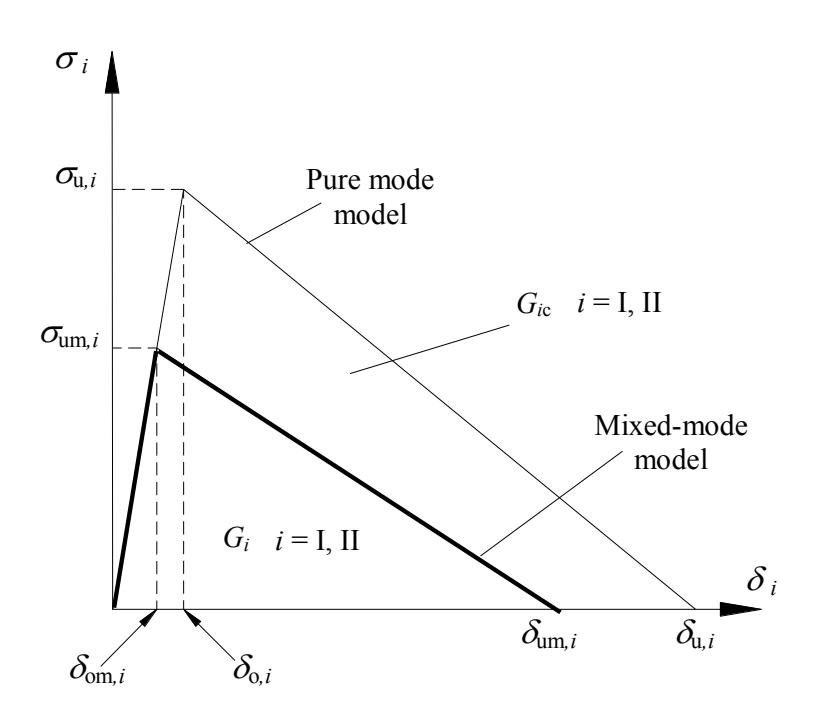


Figure 5. The linear softening law for pure and mixed-mode cohesive damage model.

#### 5. Results and discussion

In order to verify if the proposed data reduction scheme behaves well in reproducing the inputted fracture energies, two particular cases corresponding to pure mode loading were simulated. Defining a displacement ratio of  $\lambda = \delta_L/\delta_R$ , pure mode I is achieved if  $\lambda = -1$  while pure mode II takes place when  $\lambda = 1$  (Figures 2 and 3). Figure 6 presents the normalized R-curves obtained in the two cases applying the proposed method to the data given by the load-displacement curves. It can be seen that self-similar crack growth takes place and that the curves plateau near unity, thus demonstrating that the inputted values of fracture energy in the cohesive model are well reproduced when applying the proposed data reduction scheme.

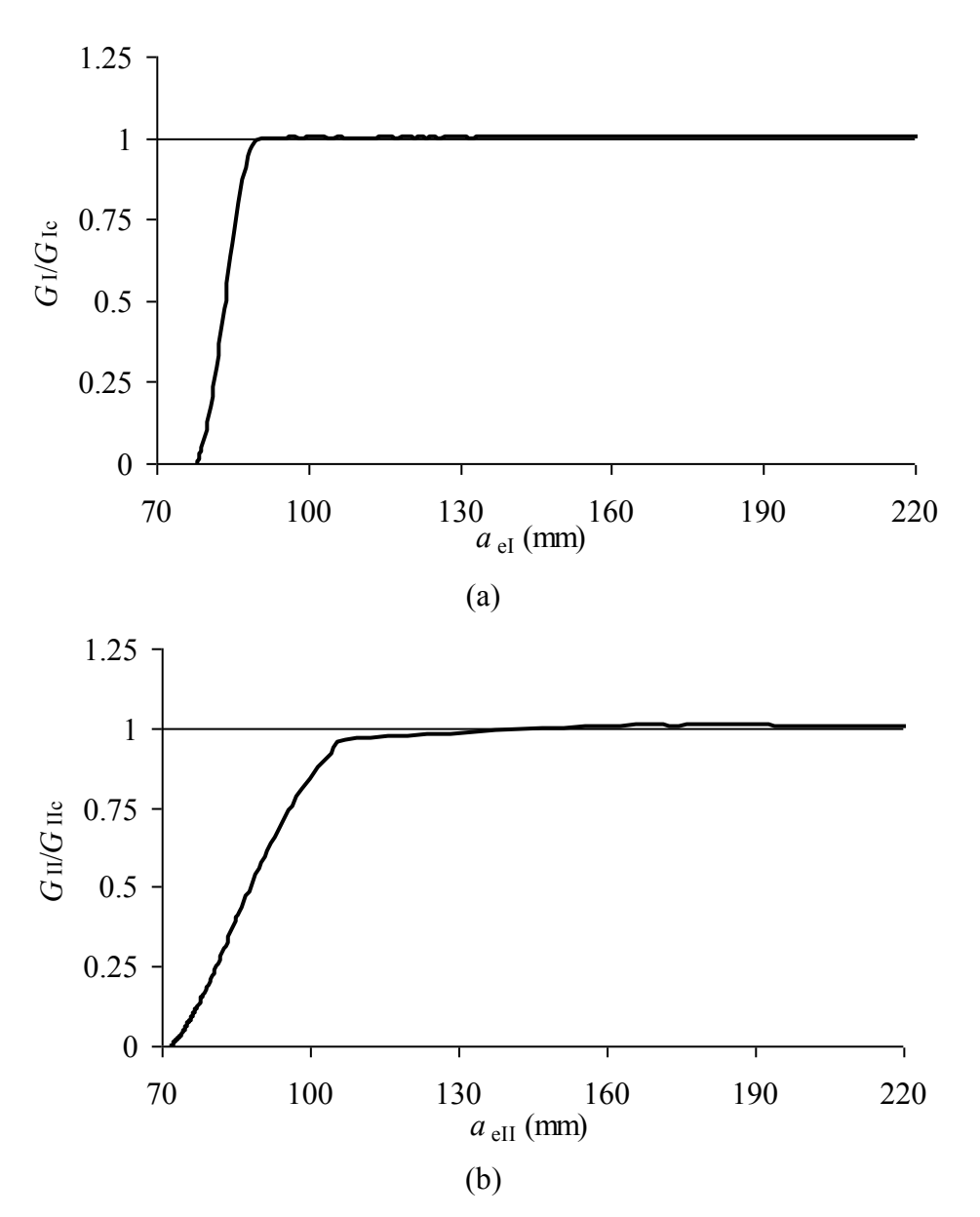


Figure 6. Normalized *R*-curves for the pure modes loading: a) Mode I; b) Mode II.

For mixed-mode conditions, several combinations of loading displacements were analysed. Six different cases were considered in the range  $-0.9 \le \lambda \le -0.1$ , while nine combinations were analysed for  $0.1 \le \lambda \le 0.9$ . In the former case the mode I loading clearly predominate, while in the latter a large range of mode mixities is covered. One of the characteristics of this test is the variation of mode-mixity as the crack grows. For example, for  $\lambda = 0.7$ , the *R*-curves vary as a function of crack length, as shown in Figure 7. Crack initiation occurs nearby the peak of the mode I *R*-curve. However, during propagation it is clearly seen that the ratio between the two modes varies.

0.5 0.4  $G_1$  (N/mm) 0.3 0.2 0.1 0 100 150 200 75 125 175 225  $a_{\rm el}$  (mm) (a) 1.2 1  $G_{II}(N/mm)$ 0.8 0.6 0.4 0.2 0 100 150 75 125 175 200 225  $a_{\rm el}$  (mm) (b)

Figure 7. *R*-curves for  $\lambda = 0.7$  (both curves were plotted as function of  $a_{\rm el}$  for better comparison).

Figure 8 plots the evolution of  $G_{\text{II}}/G_{\text{T}}$  during propagation, where  $G_{\text{T}} = G_{\text{I}} + G_{\text{II}}$ . It can be observed that the proportion of mode II component increases as the crack propagates, being sensibly constant close to the end of the test.

0.75 0.75 0.25 0.25 70 95 120 145 170 195 220  $a_{el}$  (mm)

Figure 8. Evolution of mode mixity during propagation for  $\lambda = 0.7$ .

The FPZ length corresponds to the extent ahead of crack tip where inelastic processes take place. Numerically, the FPZ length is simulated by the cohesive zone length which is easily accessed by subtracting, along the crack path, the coordinate of the first integration point behaving in the initial cohesive linear region (Figure 5) and the one corresponding to current crack length. Since the fracture energy under mode II is higher than in mode I ( $G_{\text{IIc}}$ =2 $G_{\text{Ic}}$ ), the FPZ length ( $I_{\text{FPZ}}$ ) varies during crack growth as a consequence of the mode-mixity variation, (Figure 9). The  $I_{\text{FPZ}}$  is approximately constant near to the end of the test, which is in agreement with the approximately constant mode-mixity observed in Figure 8 in the same zone. Therefore, the condition of self-similar crack growth is not satisfied, especially for the combinations whose values of  $\lambda$  cover a large range of mode-mixities.

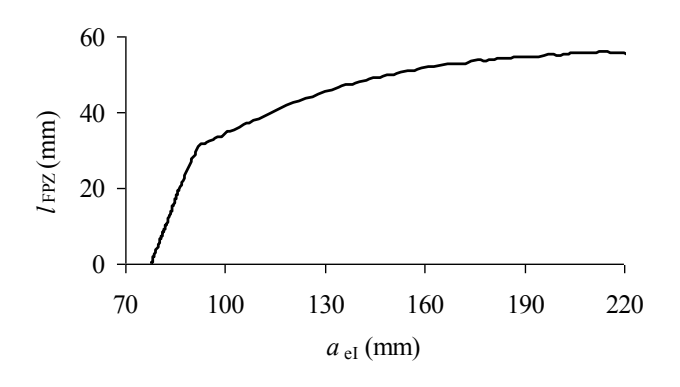


Figure 9. Evolution of the length of FPZ during crack growth.

To verify the adequacy of the test for obtaining the fracture envelope, the  $G_{\rm I}$  versus  $G_{\rm II}$  strain energies during loading were plotted in Figures 10 and 11 for negative and

positive values of  $\lambda$ , respectively. These plots include the initial loading in the elastic regime and, more importantly, the range of the mode mix ratio  $(G_I/G_{II})$  during propagation until the crack approaches the clamping region. When this happens, the mode ratio alters due to compressive effects induced in the vicinity of the clamping region. Since this phenomenon is a spurious effect, the curves were cut at the beginning of the inflexion caused by the referred effects. The line corresponding to the linear energetic criterion inputted in the cohesive damage model is also included in these figures. As already indicated, the combinations corresponding to  $-0.9 \le \lambda \le -0.1$  provide mode I predominant loading conditions (Figure 10). In fact, the combinations  $-0.9 \le \lambda \le -0.7$ , are nearly pure mode I loading conditions. The other cases  $-0.5 \le \lambda \le -0.1$ , present some range of mode-mixity, which increases with the  $\lambda$  value.

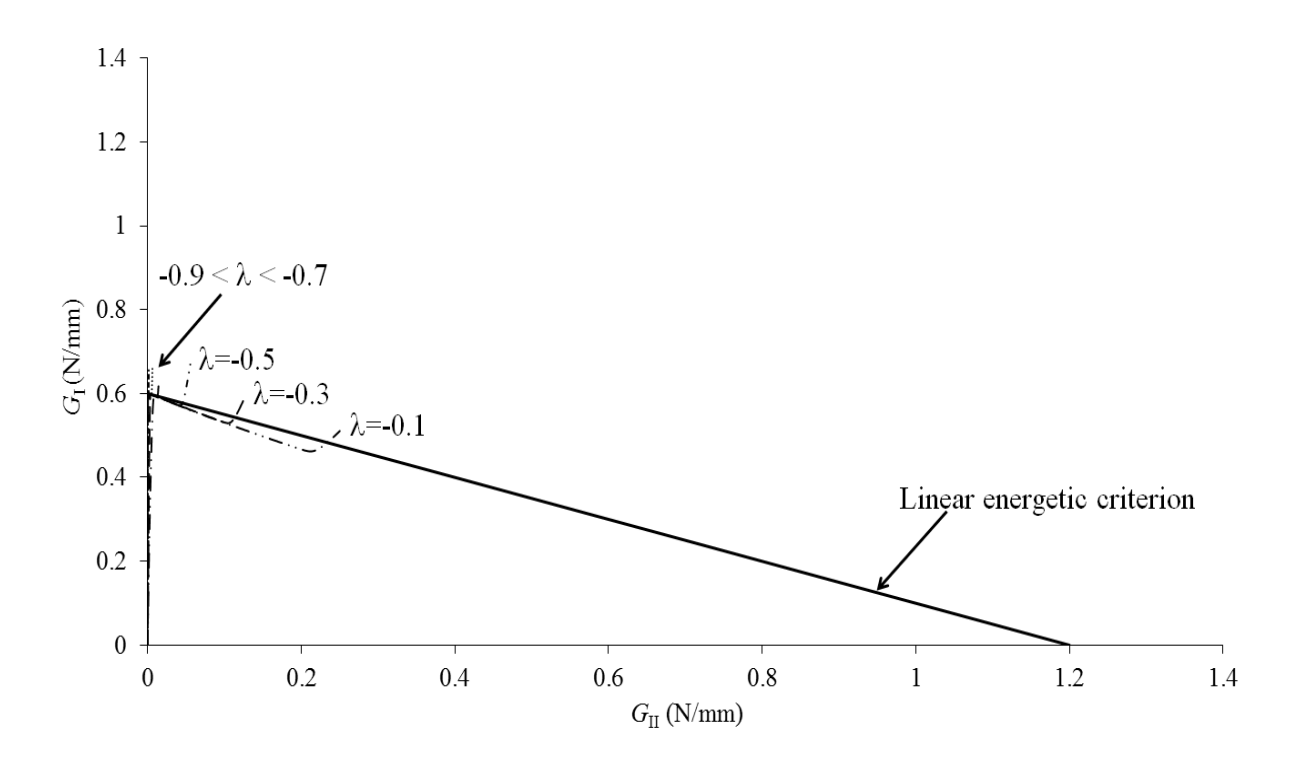


Figure 10. Plot of the  $G_{\rm I}$  versus  $G_{\rm II}$  strain energy components for  $-0.9 \le \lambda \le -0.1$ .

The combinations using the positive values of  $\lambda$  induce quite a large range of mode mixities during crack propagation, practically covering the entire fracture envelope in the  $G_{\rm I}$  versus  $G_{\rm II}$  space.

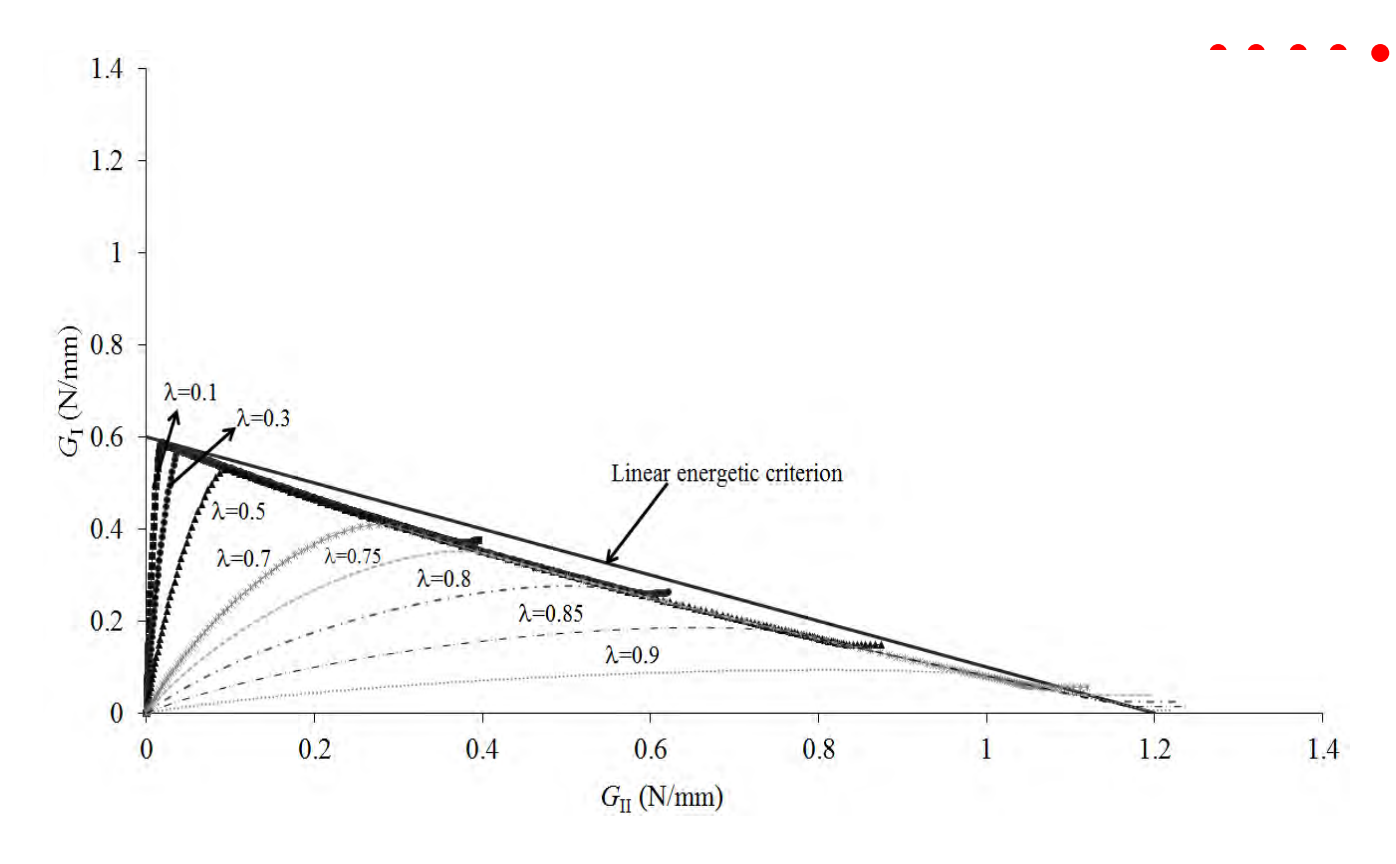


Figure 11. Plot of the  $G_{\rm I}$  versus  $G_{\rm II}$  strain energies for  $0.1 \le \lambda \le 0.9$ .

From Figure 11 it can be seen that the nine combinations analyzed for the interval  $0.1 \le \lambda \le 0.9$  provide, in the region corresponding to crack growth, an excellent reproduction of the inputted linear criterion in the vicinity of pure modes, presenting a slight difference where mixed-mode loading prevail. This difference can be explained by the non self-similar crack growth, which is more pronounced in these cases. Finally, it should be noted that practically the entire fracture envelope can be obtained using only two combinations ( $\lambda = 0.1$  and  $\lambda = 0.75$ ), which can be viewed as an important advantage of the DAL test (Figure 12).

1.4 1.2 1 8.0 V mm) 8.0 O 1 (N/mm) Linear energetic criterion 0.4  $\lambda = 0.75$ 0.2 0 0.2 0.4 0.6 0.8 1 1.2 1.4  $G_{\rm II}$  (N/mm)

Figure 12. Plot of the  $G_{\rm I}$  versus  $G_{\rm II}$  strain energies for  $\lambda=0.1$  and  $\lambda=0.75$ .

### 6. Model validation

To validate the proposed data reduction scheme, the R-curve obtained for the total strain energy release rate ( $G_T = G_I + G_{II}$ ) was compared with the one resulting from the compliance calibration method (CCM). This method is easy to apply numerically, since the crack length can be straightforwardly monitored. Using the Irwin-Kies relation (equation (13))  $G_T$  becomes

Table 1.

$$G_{\rm T} = \frac{F_{\rm R}^2}{2B} \frac{dC_{\rm R}}{da} + \frac{F_{\rm L}^2}{2B} \frac{dC_{\rm L}}{da}$$
 (18)

Polynomials of third degree were fit to the  $C_L$ =f(a) and  $C_R$ =f(a) curves to perform the differentiation. The curves  $G_T$ =f( $a_e$ ) obtained by the CCM and the CBBM are plotted in Figure 13 for the range of  $a_e$  corresponding to crack growth without influence of discussed spurious effects. Although the CCM is a function of a, the  $a_e$  was used to provide better comparison between the two methods. It can be concluded that both methods provide consistent results. Additionally, the agreement increases as the conditions of self-similar crack propagation (constant FPZ length – Figure 9) become more evident.

• • • •

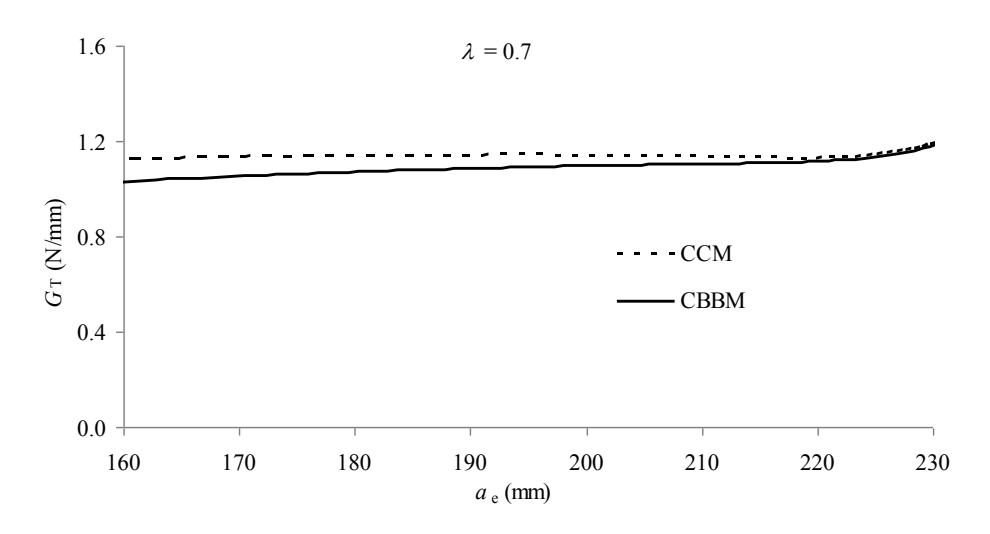


Figure 13. Plot of the  $G_T$ =f( $a_e$ ) curves obtained by CCM and CBBM for  $\lambda = 0.7$ .

#### 7. Conclusions

The objective of this work was to numerically study the adequacy of the dual actuator load test to characterize the fracture behaviour of bonded joints under different mixedmode loading conditions. A cohesive zone model was used to simulate damage initiation and growth under different combinations of mode-mixity. Additionally, a new data reduction scheme based on specimen compliance, beam theory and crack equivalent concept was proposed to overcome some problems intrinsic to the test. The model provides a simple mode partitioning method and does not require crack length monitoring during the test, which can lead to incorrect estimation of fracture energy due to measurements errors. Furthermore, since the current compliance is used to estimate the equivalent crack length, the method is able to account indirectly for the presence of a non-negligible fracture process zone. This aspect is fundamental, namely in the fracture characterization of adhesives with some ductility. The method was firstly applied to the pure mode loading cases and excellent agreement was achieved with the fracture values inputted in the cohesive model. Under mixed-mode loading it was verified that in some cases the mixed-mode ratio alters significantly during crack propagation, thus leading to non self-similar crack growth. The positive values of the displacement ratio ( $\lambda$ ) covered almost all the fracture envelope, although the negative values only provide the mode I predominant loading cases. Considering the cases of positive  $\lambda$ , it was verified that good agreement with the inputted linear energetic

criterion was obtained in the vicinity of pure mode loading. A slight difference relative to the inputted linear energetic criterion was observed in the central region of the  $G_{\rm I}$  versus  $G_{\rm II}$  plot, corresponding to mixed-mode loading. This difference was attributed to the non self-similar crack propagation conditions that are more pronounced in these cases. Finally, it was observed that only two combinations of the displacement ratio are sufficient to cover almost all the adhesive fracture envelope, which constitutes an important advantage of the dual actuator load test when used with fixed displacement rates.

The proposed data reduction scheme was compared to the compliance calibration method for the total energy release rate during propagation. It was observed that both methods delivers consistent results namely when the conditions of self-similar crack growth prevail.

#### **Acknowledgements**

The authors would like to thank the "Fundação Luso-Americana para o Desenvolvimento" (FLAD) for the support through project 314/06, 2007 and *Instituto de Engenharia Mecânica* (IDMEC).

## References

- [1] R.D. Adams, The Journal of Adhesion, 30 (1989) 219-242.
- [2] M.F.S.F. de Moura, R.D.S.G. Campilho, J.P.M. Gonçalves, Composites Science and Technology, 68 (2008) 2224-2230.
- [3] L.F.M. Da Silva, A. Öschner, Modeling of Adhesively Bonded Joints, Springer, Heidelberg, 2008.
- [4] ASTM D3433 99, in: Annual book of ASTM standards, West Conshohocken, ASTM 15.06, 2012, pp. 225-231.
- [5] B. Blackman, J.P. Dear, A.J. Kinloch, S. Osiyemi, Journal of Materials Science Letters, 10 (1991) 253-256.
- [6] B.R.K. Blackman, A.J. Kinloch, M. Paraschi, Engineering Fracture Mechanics, 72 (2005) 877-897.
- [7] K. Leffler, K.S. Alfredsson, U. Stigh, International Journal of Solids and Structures, 44 (2007) 530-545.
- [8] L.F.M. da Silva, F.A.C.R.G. de Magalhães, F.J.P. Chaves, M.F.S.F. de Moura, The Journal of Adhesion, 86 (2010) 891-905.

- . . . .
- [9] D.A. Dillard, H.K. Singh, D.J. Pohlit, J.M. Starbuck, Journal of Adhesion Science and Technology, 23 (2009) 1515-1530.
- [10] J.R. Reeder, J.H. Crews, AIAA Journal, 28 (1990) 1270-1276.
- [11] J.H. Crews, J.R. Reeder, in, NASA TECHNICAL MEMORANDUM 100662, 1988.
- [12] F. Ducept, P. Davies, D. Gamby, International Journal of Adhesion and Adhesives, 20 (2000) 233-244.
- [13] Z. Liu, G. R.B., G.M. Newaz, in: Proceedings of the American Society of Composites, Fifteenth Technical Conference, College Station, Texas, USA, September, 2000.
- [14] B. Sørensen, K. Jørgensen, T. Jacobsen, R. Østergaard, International Journal of Fracture, 141 (2006) 163-176.
- [15] J.L. Hogberg, U. Stigh, Engineering Fracture Mechanics, 73 (2006) 2541-2556.
- [16] D.A. Dillard, H.K. Singh, S. Park, D. Ohanehi, M.A. McGaw, in: SEM Annual Conference & Exposition on Experimental and Applied Mechanics, Society for Experimental Mechanics, Inc., St. Louis, 2006.
- [17] K. Singh Hitendra, A. Chakraborty, E. Frazier Charles, A. Dillard David, in: Holzforschung, 2010, pp. 353.
- [18] M.A.L. Silva, J.J.L. Morais, M.F.S.F. de Moura, J.L. Lousada, Engineering Fracture Mechanics, 74 (2007) 2133-2147.
- [19] V. Tamuzs, S. Tarasovs, U. Vilks, Composites Science and Technology, 63 (2003) 1423-1431.
- [20] A.B. de Morais, M.F. de Moura, J.P.M. Gonçalves, P.P. Camanho, Mechanics of Materials, 35 (2003) 641-652.

PAPER 5

# FRACTURE CHARACTERIZATION OF BONDED JOINTS USING THE DAL (EXPERIMENTAL)

Fracture characterization of bonded joints using the Dual Actuator Load apparatus

Filipe J.P. Chaves <sup>1</sup>, M.F.S.F. de Moura <sup>2</sup>, L.F.M. da Silva <sup>2</sup>, D.A. Dillard <sup>3</sup>

<sup>1</sup> IDMEC – Pólo FEUP, Faculdade de Engenharia da Universidade do Porto, Rua Dr. Roberto Frias, 4200-465 Porto, Portugal

<sup>2</sup> DEMec, Faculdade de Engenharia da Universidade do Porto, Rua Dr. Roberto Frias, 4200-465 Porto, Portugal

<sup>3</sup> Engineering Science and Mechanics Department, Virginia Tech, Blacksburg, VA 24061, United States

**Abstract** 

Mixed-mode I+II fracture characterization tests of steel- bonded joints were carried out with the Dual Actuator Load (DAL) apparatus using a previously developed data reduction scheme in order to obtain the fracture envelop. This test consists on an independent loading of the specimen arms of a clamped double cantilever beam which allows an easy variation of the I+II mode mixity in fracture characterization altering the applied displacement rates. Difficulties inherent to crack monitoring during its propagation and imperfections of initial crack manufacture are well managed with the proposed method. Three different cases corresponding to different mode mixities were tested. The experimental results revealed that the linear energetic criterion performs well in describing the fracture envelop of these bonded joints.

Keywords: Bonded joints, Fracture characterization, Mixed-mode loading, DAL test

1. Introduction

Adhesively bonded joints are being applied to a wide range of devices and engineering structures. Consequently, the development of design failure criteria based on fracture mechanics concepts has become increasingly important since the strength-based criteria are not adequate in the presence of singularities [1-4]. In this context, fracture characterization of adhesive bonded joints acquire special relevancy. Pure mode I

fracture characterization is usually performed by means of the double cantilever beam (DCB) specimen [5]. This test is simple to execute and the fracture toughness,  $G_{\rm Ic}$  can be mathematically defined according to the beam theory (described in ASTM D 3433-99) or several improved approaches, as compared in [4]. In mode II, the end notched flexure (ENF) and the end loaded split (ELS) are frequently used [2, 5-7] due to their simplicity and ability to provide pure mode II loading at the crack tip.

Due to the geometric characteristics of adhesively bonded joints (two adherends separated by a thin adhesive layer), the crack is frequently forced to grow in pre-defined planes which induce mixed-mode loading conditions. Consequently, the fracture characterization of bonded joints under mixed-mode loading is essential. There are some simple tests proposed in the literature concerning this subject, as is the case of the asymmetric double cantilever beam (ADCB), the single leg bending (SLB) and the cracked lap shear (CLS) previously studied by da Silva et al. [8]. Nevertheless, these tests are limited in which concerns the variation of the mode-mixity [9], which means that different tests are necessary to cover the fracture envelope in the  $G_{I}$ - $G_{II}$  space. Alternatively, the mixed mode bending (MMB) test, initially proposed by Reeder and Crews [10] for interlaminar fracture characterization of composite materials, can be used. This test consists of a combination of the DCB and ENF tests and provides a simple alteration of the mode mixity by changing the lever length of the loading arm. In addition, the load applied to the specimens can be separated into mode I and mode II components by means of a mode partitioning method based on the beam theory [11]. Although the MMB test was also used in the context of composite and steel bonded joints by Ducept et al.[12] and Liu et al.[13] respectively, it requires a special test apparatus with significant dimensions, especially when testing stiff adherends. An alternative solution is the dual actuator load (DAL)[14, 15], which can be viewed as a DCB test subjected to non-symmetric loading. Effectively, the test consists of two independent hydraulic actuators operating the arms of a standard DCB specimen clamped at the other extremity. This test allows easy variation of the mode-mixity by applying different displacement rates to the specimen arms by means of the two independent hydraulic actuators. A data reduction scheme based on crack equivalent concept was developed in a previous study [16] to obtain the fracture energy of adhesively bonded joints using the DAL test. Crack growth measurement is not an easy task and can be inaccurate because it neglects the effect of the fracture process zone

ahead of the crack tip. The data reduction scheme proposed in [16] is able to take it into account and does not require crack length monitoring in the course of the test. The model was validated numerically in the previous study [16] using finite element analysis and the Calibration Compliance Method (CCM).

In the present study, the data reduction technique developed in [16] is used to treat experimental results of DAL tests obtained with high grade steel specimens bonded with an epoxy adhesive. Three different combinations of mixed-mode in the  $G_{\rm I}$ - $G_{\rm II}$  space were tested. The R-curves resulting from the compliance based data reduction scheme allowed to define the strain energy components which were used to define the fracture envelop. The linear energetic criterion proved to be a good representation of the found trend.

## 2. Experimental details

## 2.1. Specimens preparation

DAL specimens were manufactured with high grade steel (Table 1). The surface preparation consisted in sandblasting and cleaning with acetone.

Elastic properties (Steel)		Hardness	Code	
E (GPa)	G (MPa)	(HB)	DIN	
210	80.77	270-350	40 CrMnMo 7	

Table 1. Steel specimen properties.

An epoxy adhesive – Araldite<sup>®</sup> AV138M with HB998 hardener (Huntsman) – was used to bond the substrates. The adhesive was characterized in previous studies [7, 17] and the stress-strain curves can be seen in Figure 1.

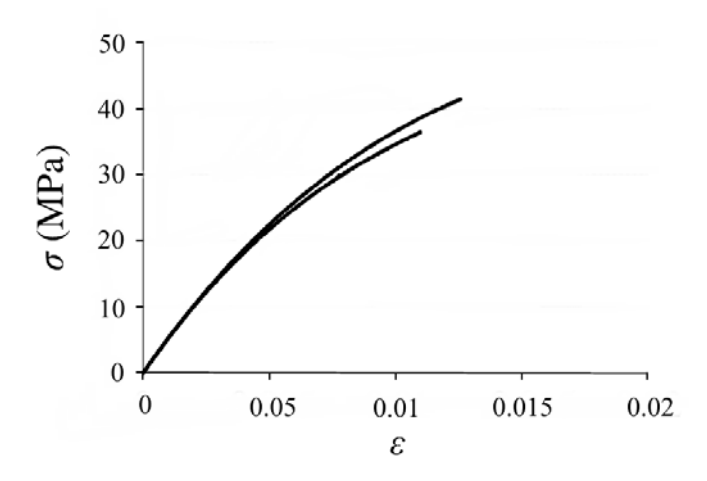


Figure 1.  $\sigma$ – $\varepsilon$  curves of the Araldite<sup>®</sup> AV138.

A mould with pins was used to guarantee alignment of the lower and upper beams (Figure 2a and 2b). A pre-crack was made using a razor blade within the spacers used to obtain a constant bondline thickness of 1 mm. After adhesive application on the substrates, the joints were cured in a hot press at a constant pressure of 2 MPa and temperature of 40°C for 16 hours (Figure 2c). After curing the remaining adhesive that overflows was carefully removed.

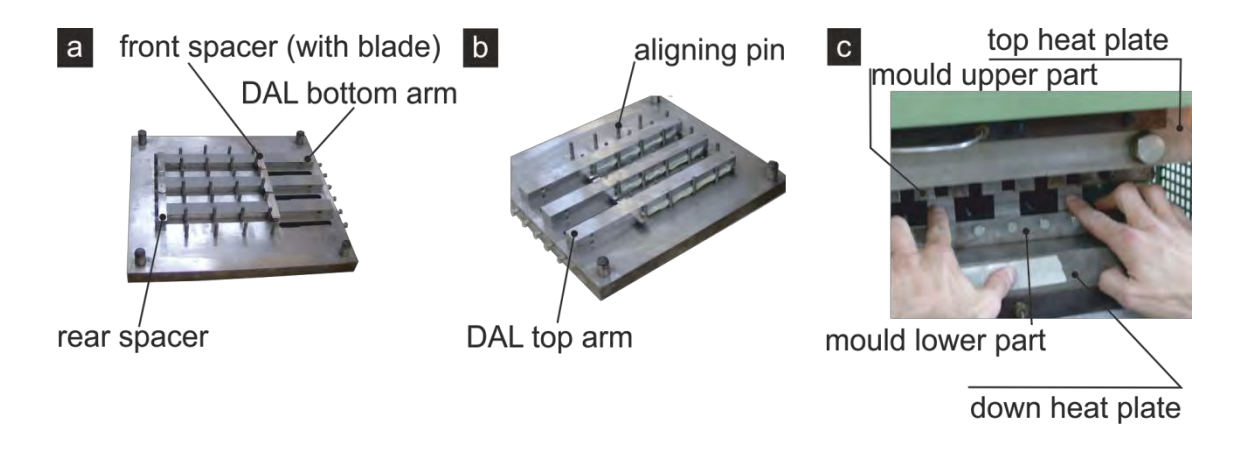


Figure 2. Specimens manufacture using a mould and heated plates press.

The specimen geometry is in accordance with the ASTM D3433-99, as shown in Figure 3.

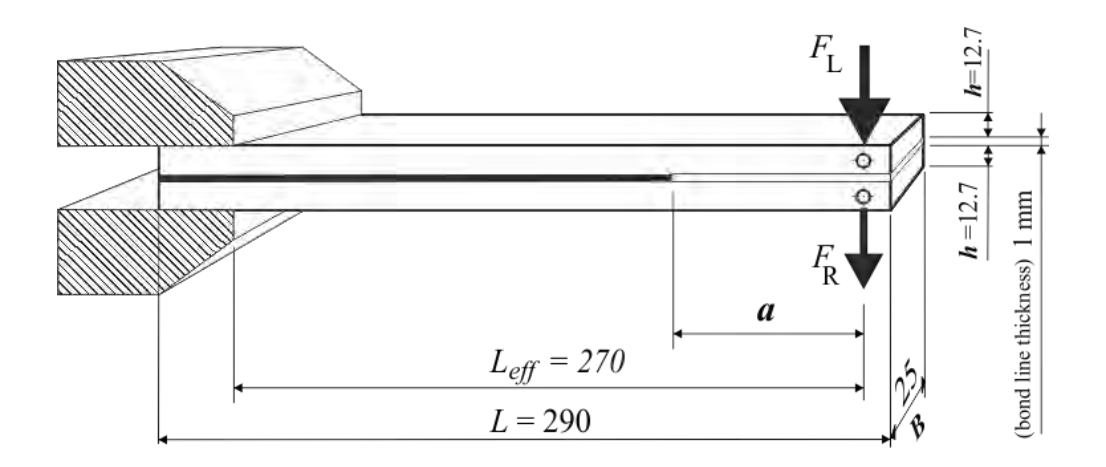


Figure 3. Specimen geometry (dimensions are in mm).

## 2.2. Testing procedure

The DAL test is based on a DCB specimen loaded asymmetrically by means of two independent hydraulic actuators (Figure 4). The specimen bonded end is clamped (20 to 25 mm) and loaded at the debonded end by means of two independent hydraulic actuators that are attached to the specimen arms with pins (Figure 5 left). Each hydraulic actuator pivots in order to allow some rotation to accommodate the small vertical displacements of each beam due to foreshortening. Each actuator is equipped with a load cell and a linear variable displacement transducer (LVDT), with the purpose of registering the two load—displacement curves during the test. Different combinations of applied displacement rates provide different levels of mode mixities, thus allowing an easy definition of the fracture envelop in the  $G_{\rm I}$  versus  $G_{\rm II}$  space.

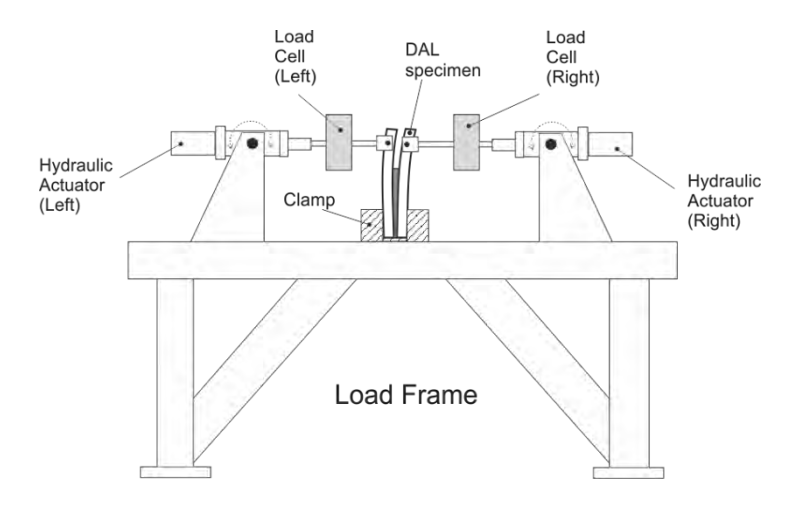


Figure 4. DAL frame.

A digital level ensures the horizontal alignment of each actuator arm, as well as the specimen perpendicularity (Figure 5 left). Forces and displacements are registered to be subsequently used in the data reduction scheme which is based on specimen compliance.

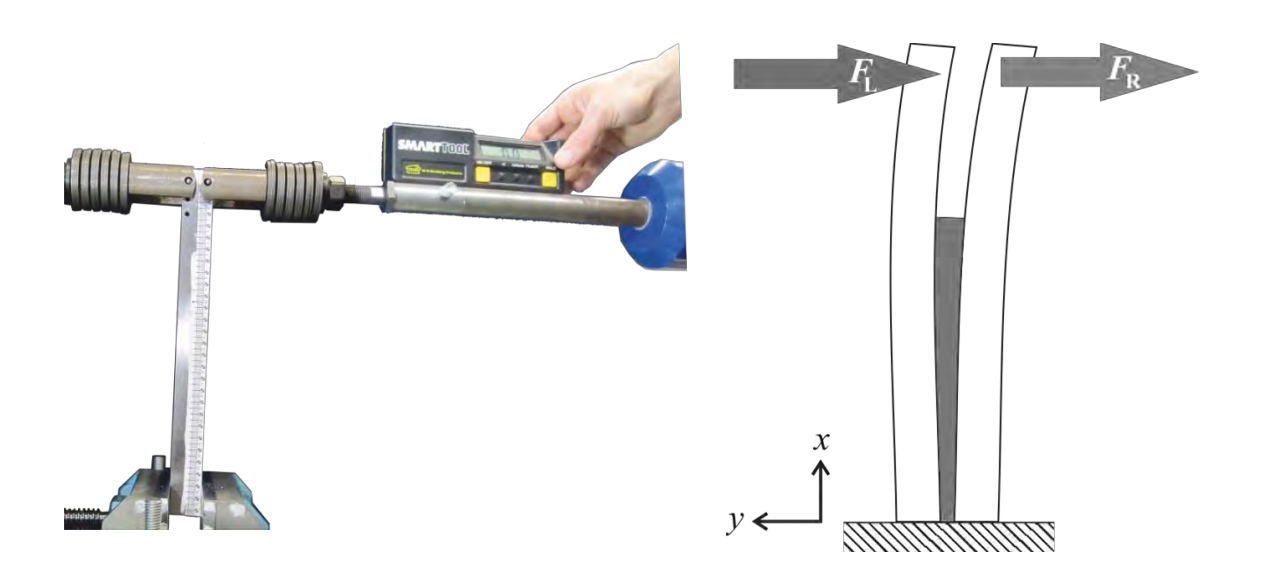


Figure 5. Specimen fixture to the DAL frame assuring the left actuator arm levelling (left) and a schematic representation of loading in the DAL test (right).

Three specimens were testes under different mixed-mode I+II loading conditions. The rate displacement ratio  $\lambda$  is defined by

$$\lambda = \delta_{\rm L}/\delta_{\rm R} \tag{1}$$

where  $\delta_L$  is the displacement rate of the left arm and  $\delta_R$  the displacement rate of the right arm. Pure mode I is achieved if  $\lambda = -1$  while pure mode II takes place when  $\lambda = 1$ . Since the selected adhesive was already characterized under pure modes in previous studies[7, 17], it was decided to test three different combinations:  $\lambda = -0.25$  which corresponds to a predominant mode I loading case,  $\lambda = 0.75$  for mixed mode with similar participation of both modes and  $\lambda = 0.9$  for a predominant mode II loading situation.

#### 2.3. Data reduction scheme

The data reduction scheme developed in [16] is based on beam theory, specimen compliance and crack equivalent concept. The DAL test can be viewed as being a combination of the DCB and ELS tests for pure modes fracture characterization (Figure 6).

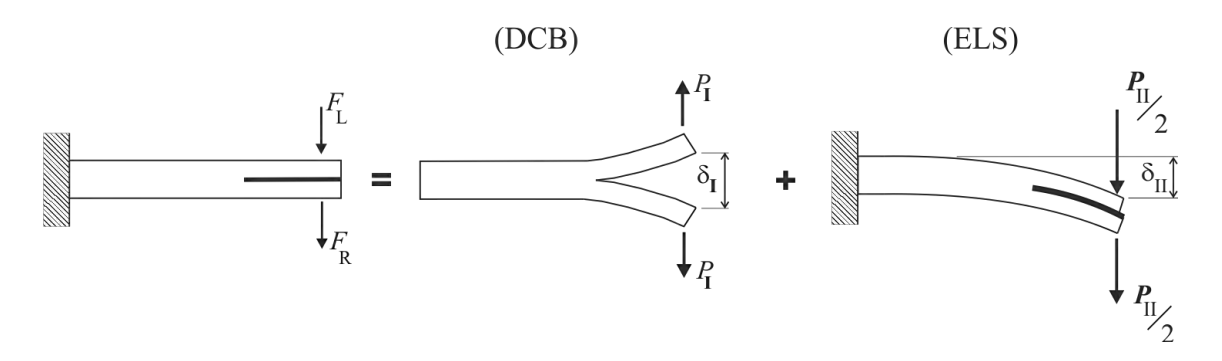


Figure 6. Schematic representation of loading in the DAL test.

Considering the schematic representation of load equilibrium of Figure 6 the load displacement data  $F_L$  -  $\delta_L$  and  $F_R$  -  $\delta_R$  can be converted in a combination of  $P_I$  -  $\delta_I$  and  $P_{II}$  -  $\delta_{II}$  through the following relations

$$P_{\rm I} = \frac{F_{\rm R} - F_{\rm L}}{2} \tag{2}$$

$$P_{\rm II} = F_{\rm R} + F_{\rm L}$$

$$\delta_{\rm I} = \delta_{\rm R} - \delta_{\rm L}$$

$$\delta_{\rm II} = \frac{\delta_{\rm R} + \delta_{\rm L}}{2} \tag{3}$$

thus providing a simple mode partitioning method to be used in the proposed data reduction scheme [16]. The compliances corresponding to each mode can be obtained by means of the Timoshenko beam theory

$$C_{\rm I} = \frac{\delta_{\rm I}}{P_{\rm I}} = \frac{8a^3}{Bh^3E} + \frac{12a}{5BhG} \tag{4}$$

$$C_{II} = \frac{\delta_{II}}{P_{II}} = \frac{3a^3 + L^3}{2Bh^3E} + \frac{3L}{5BhG}$$
 (5)

where B is the specimen width (Figure 3), h is the height for each specimen harm (Figure 3), E and G are the Young's and the shear modulus of the adherends, respectively. Since the monitoring of crack length during its propagation is a difficult

task, namely in cases where mode II loading predominate, an equivalent crack length procedure is adopted solving previous equations (4 and 5) to find a [16]. Using the Irwin-Kies equation applied to each mode

$$G = \frac{P^2}{2B} \frac{dC}{da} \tag{6}$$

the R-curves for mode I ( $G_{\rm I}$ =f( $a_{\rm eI}$ )) and mode II ( $G_{\rm II}$ =f( $a_{\rm eII}$ )) can be obtained

$$G_{\rm I} = \frac{6P_{\rm I}^2}{B^2h} \left( \frac{2a_{\rm eI}^2}{h^2E} + \frac{1}{5G} \right) \tag{7}$$

$$G_{\rm II} = \frac{9P_{\rm II}^2 a_{\rm eII}^2}{4B^2 h^3 E} \tag{8}$$

where  $a_{\rm el}$  and  $a_{\rm ell}$  are the equivalent crack lengths issuing from equations (4 and 5). Another advantage of this method is that is included indirectly the effect of the Fracture Process Zone (FPZ) since its presence influences the specimen compliance which is used to get the strain energy release rates.

### 3. Results

#### 3.1.Load-displacement curves

The DAL test provides two load-displacements curves corresponding to the left actuator  $(F_L-\delta_L)$  and to the right actuator one  $(F_R-\delta_R)$ . Figure 7 presents load-displacement curves of the  $\lambda=-0.25$  case. The right actuator has positive displacement values in agreement with the displacement rate imposed of 1 mm/min and the left actuator has negative values reflecting the imposed displacement rate of -0.25 mm/min. The right actuator shows a maximum load close to 1100 N and quite similar, thus reflecting a predominant mode I loading. The maximum displacements ( $\delta_F \cong 3.64$  mm and  $\delta_L \cong -0.9$  mm) comply with the considered displacement rate ratio.

Figure 8 shows the load-displacement curves for the  $\lambda = 0.75$  situation. Both load-displacement curves have a positive displacement in agreement with their positive displacement ratio of 1 mm/min for the right actuator and 0.75 mm/min for the left actuator.

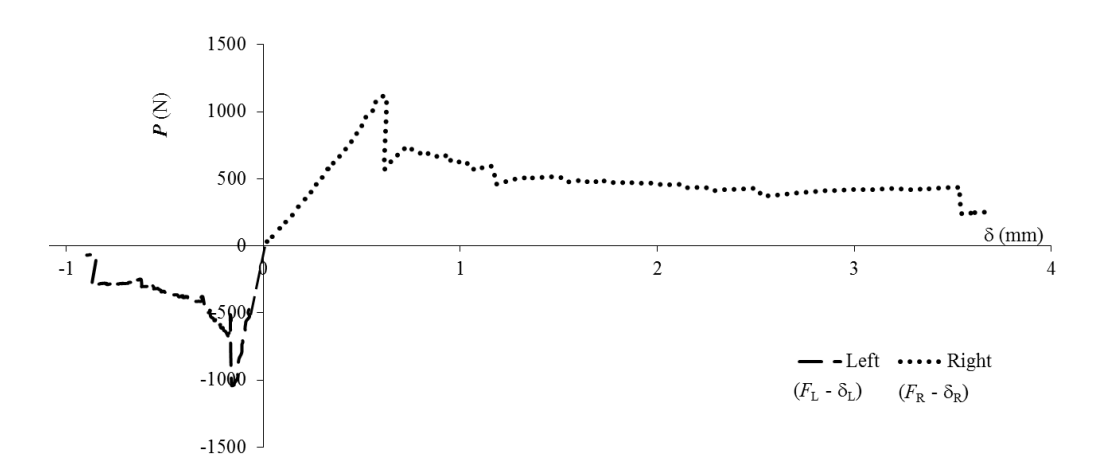


Figure 7. Load displacement curve for  $\lambda = -0.25$ .

The maximum displacement for the right actuator is 15.1 mm and the maximum value for the left actuator is 11.2 mm. Computing Equation 1 with these values, the displacement rate ratio value ( $\lambda = 0.742$ ) is slightly lower than the chosen value. The right actuator shows positive values for the whole loading while the left actuator shows very small values up to 6 mm of applied displacement, becoming monotonically increasing and negative after this point which corresponds to damage onset. It can be concluded that when debonding occurs, the stress release in the arm of the DCB specimen loaded with the lower displacement give rise to the cited negative loading value, which means that the loading device is pulling the arm.

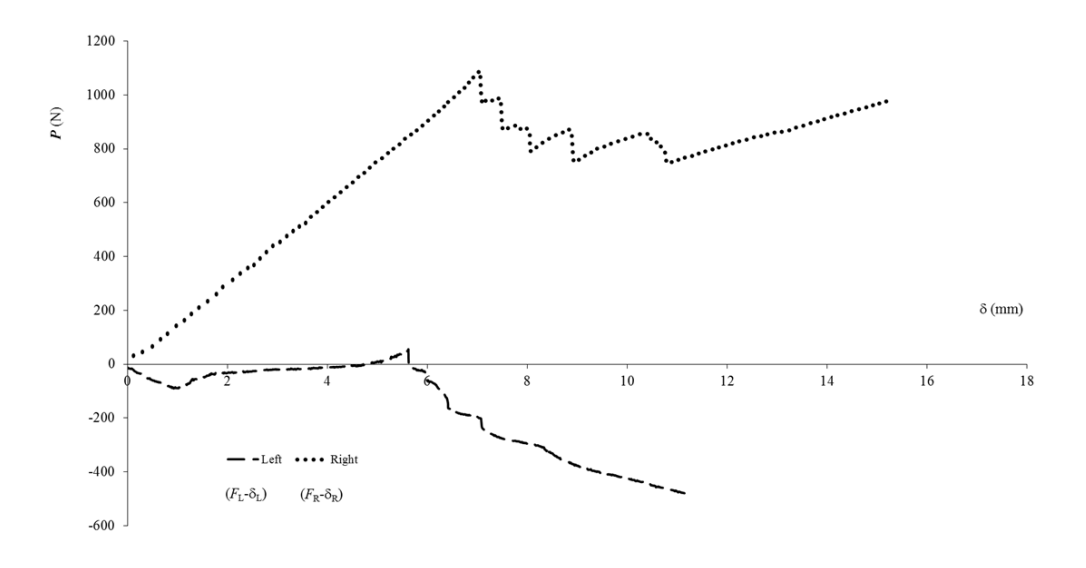


Figure 8. Load displacement curves for  $\lambda = 0.75$ .

Figure 9 shows the load-displacements curves considering the displacement rate ratio  $\lambda$  = 0.9 which is representative of a situation of predominant mode II loading. The maximum displacement value for the right actuator displacement is 12.6 mm and that for the left actuator is 11.6 mm. Computing Equation 1 with these values, a displacement ratio of 0.9 is obtained. The right actuator registers positive load values with a maximum of 1200 N. The left actuator registers a residual load over the first 4 mm of displacement and then shows positive values near 200 N at 8 mm of displacement. From this point, failure occurs and negative load values arise for the same reasons given above in the case of  $\lambda$  = -0.75.

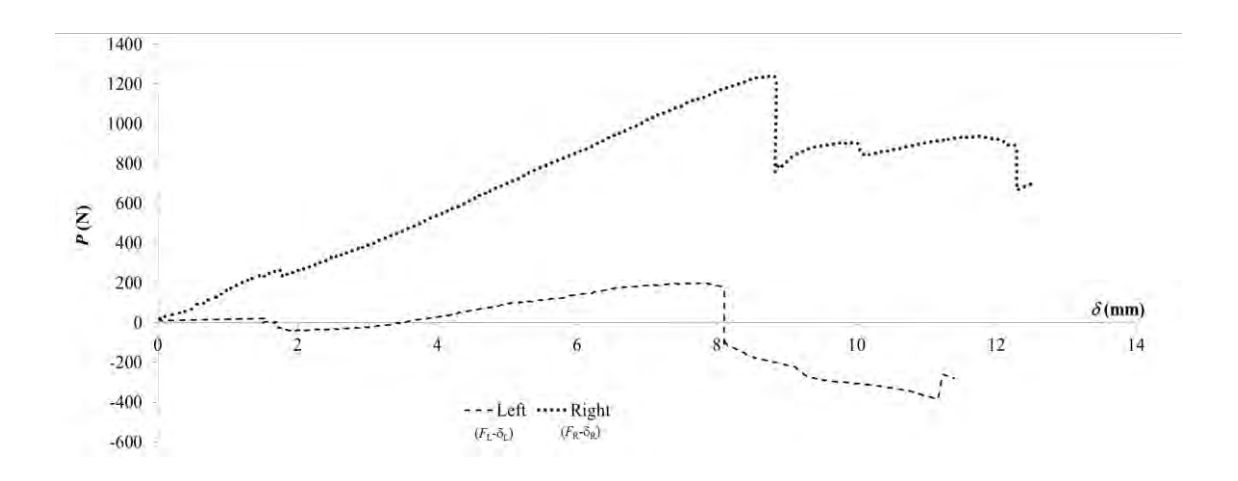


Figure 9. Load displacement curve for  $\lambda = 0.9$ .

#### 3.2. Resistance curves (*R*-curves)

The *R*-curves of the several analysed cases can be easily obtained through the presented data reduction scheme (equations (7) and (8)). The *R*-curves for  $\lambda = -0.25$  loading case are presented in Figure 10. As expected the presence of mode II is negligible relative to mode I component which reveals an approximately constant plateau. In fact, the value of  $G_I$  decreases abruptly from 0.5 N/mm to 0.3 N/mm at crack starting advance. This is in agreement with the sudden decrease of load verified in the respective load-displacement curve (Figure 7). This peak value can be attributed to crack bluntness that artificially increases the fracture energy at crack starting advance which, in fact, is a spurious value. The steady state value of 0.3 N/mm is the one representative of fracture energy under this loading situation. This can be viewed as an important advantage of the

proposed method which, giving rise to *R*-curves permits to overcome the described problem and to determine accurate fracture values.

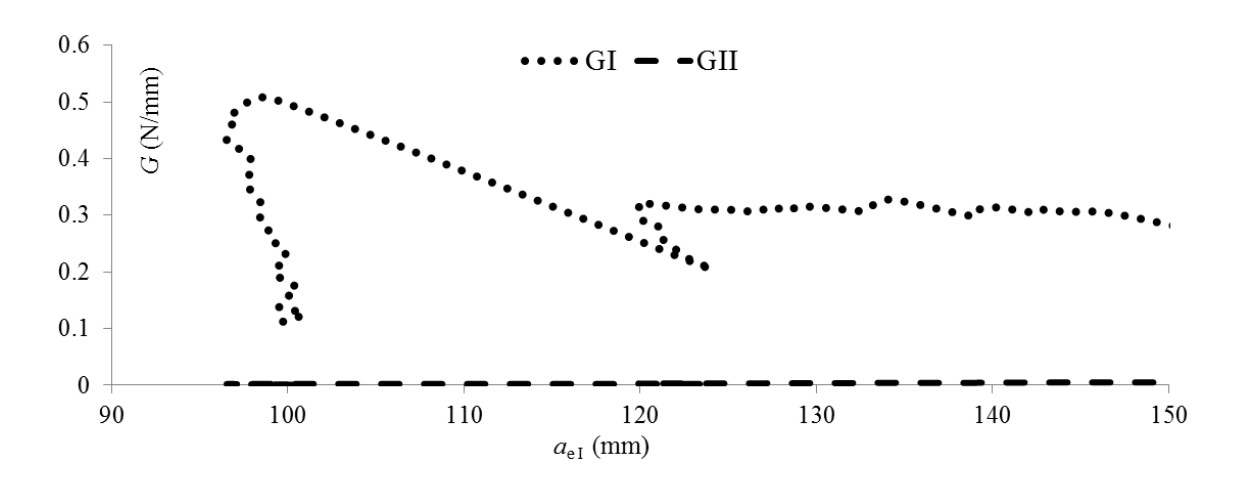


Figure 10. . *R*-curves for  $\lambda = -0.25$  loading case.

Figure 11 reports to the  $\lambda = 0.75$  displacement rate ratio. Clearly a more stable situation takes place which is in agreement with the behaviour of the corresponding load-displacement curve shown in Figure 8. Effectively, the post-peak region of both load-displacement curves reveals a more stable load evolution which reflects also on the respective *R*-curves. These plateau regions observed in both *R*-curves are a symptom of self-similar crack growth for a given extent. It should also be noted that the strain energy component in mode I is lower than the one of mode II but not negligible, which means that  $\lambda = 0.75$  leads to a mixed-mode loading with a mode ratio  $(G_{\rm II}/G_{\rm I})$  approximately equal to 2.5.

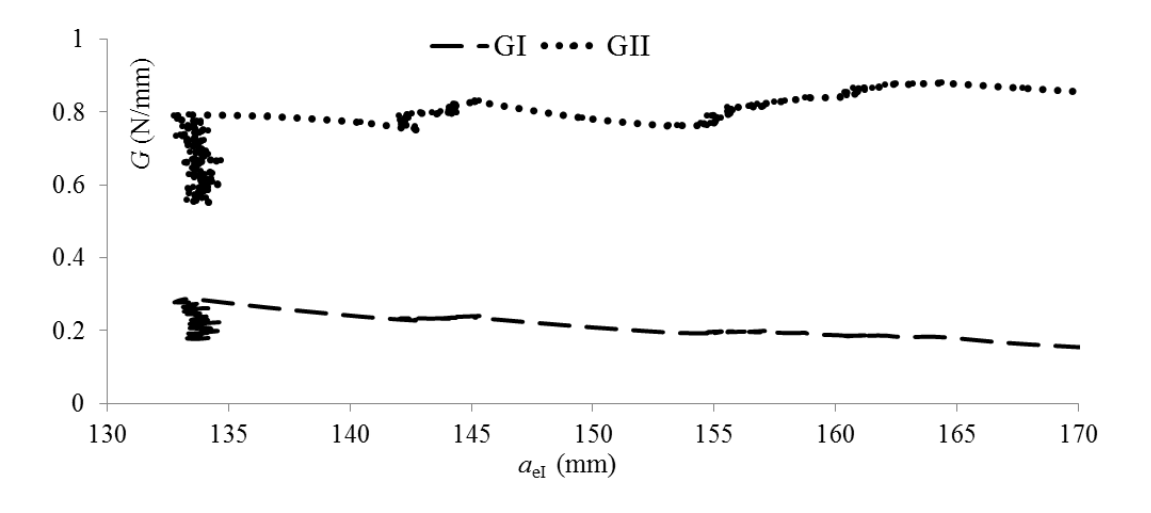


Figure 11. R-curves for  $\lambda = 0.75$  loading case.

• • • •

The R-curves of the  $\lambda = 0.9$  displacement rate ratio are plotted in Figure 12. As it can be seen, unstable crack growth occurs at crack initiation which is also in agreement with the behaviour reported in Figure 9 (sudden drop load after the peak). A clearly predominant mode II loading is present (mixed-mode ratio approximately equal to 7 at crack starting advance), thus revealing that the proposed setup is able to deal with different mixed-mode loading cases.

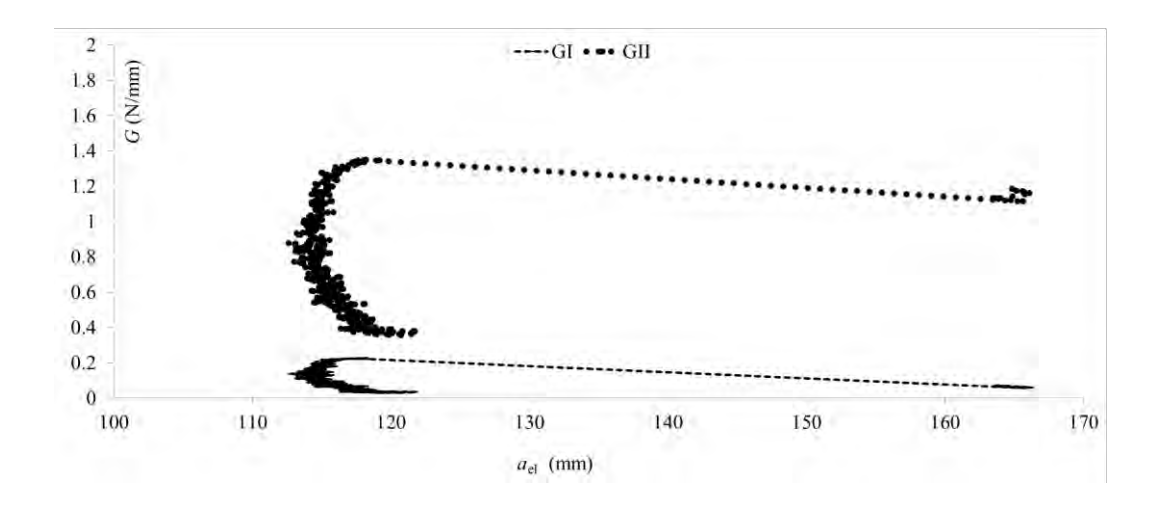


Figure 12. *R*-curves for  $\lambda = 0.9$  loading case.

# 3.3. Fracture envelopes

The previously values of fracture energy release rate in mode I and mode II (R-curves), can be used to outline a fracture envelop allowing the definition of a fracture criterion. Figure 13 presents the fracture envelop using normalized values of fracture energy ( $G_{\rm I}/G_{\rm T}$  versus  $G_{\rm II}/G_{\rm T}$ ). This representation allows a better visualization of the modemixity of each performed test. In addition, the representation of the linear energetic criterion

$$\frac{G_{\rm I}}{G_{\rm Ic}} + \frac{G_{\rm II}}{G_{\rm IIc}} = 1\tag{9}$$

is also included. The values of  $G_{Ic}$  and  $G_{IIc}$  used for plotting the linear criterion are those obtained in previous studies [7, 17] and are shown in Table 2.

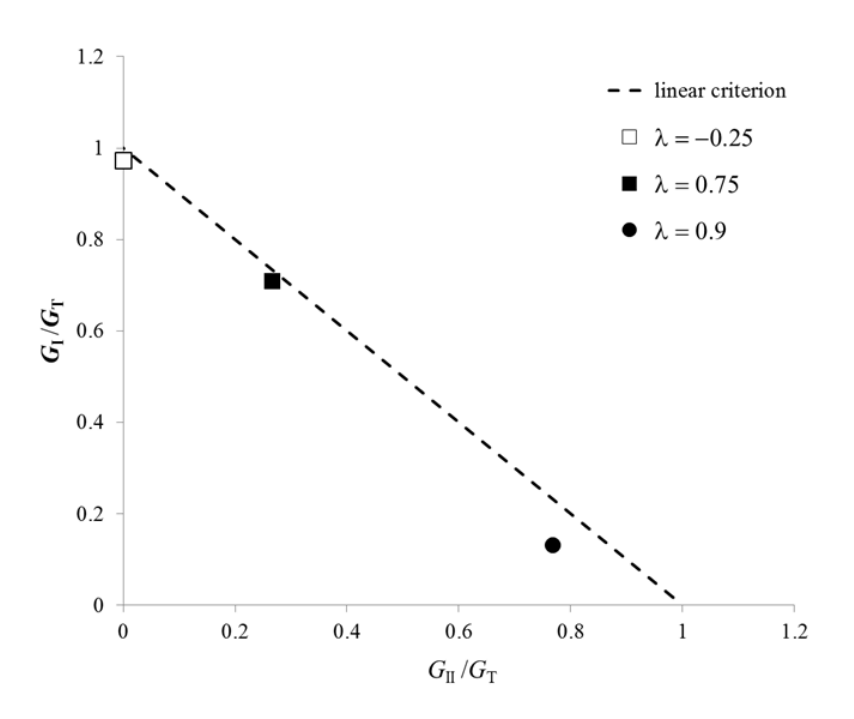


Figure 13. Envelop composition for Araldite<sup>®</sup> AV138 with 1.0 mm bondline thickness tested at a displacement ratio of  $\lambda = 1.0$  mm.

It can be observed that both,  $\lambda$  = -0.25 and  $\lambda$  = 0.75, fit well the linear criterion but a small difference is found for the  $\lambda$  = 0.9, which corresponds to a predominant mode II loading case. In a previous work [18] involving mixed-mode I+II fracture characterization of wood bonded joints using the Mixed-Mode Bending test (MMB) a similar behaviour was observed. In fact, it was verified that the linear energetic criterion performs well with the exception of the pure mode II fracture toughness. This circumstance was explained by unavoidable shear sliding effects in the pure mode II fracture tests (ENF) that contribute to increase spuriously the measured fracture energy. In fact, the presence of a small quantity of mode I loading opens slightly the crack and avoids the interaction of crack surfaces, thus contributing to diminish the toughness relatively to pure mode II fracture characterization tests.

Table 2. Critical energy release rate values for pure mode I and II for adhesive Araldite® AV138M with bondline thickness of 1 mm [7, 17].

Fracture energies	G <sub>Ic</sub> (N/mm)	G <sub>IIc</sub> (N/mm)
Araldite® AV138M	0.36	4.7

• • • •

#### 4. Conclusions

Fracture characterization tests for I+II mixed-mode loading considering the DAL test were performed on steel-epoxy bonded joints. The test is based on independent loading of the DCB specimen arms by means of two independent hydraulic actuators. Although a special device is required the test presents the advantage of an easy variation of the mode-mixity by applying different displacement rates to the specimen arms. Three different mixed-mode combinations were considered in order to cover predominant mode I, mixed-mode with non-negligible presence of both modes and a predominant mode II case. A data reduction scheme based on specimen compliance beam theory and crack equivalent concept previously developed [16] was applied to the experimental results in the present study. The data reduction technique provides the R-curves which allow defining the strain energy release rate components for each situation. This aspect is particularly important since the spurious effects of crack blunting can be easily overcome using the strain energy release rate values at the plateau that rises after the initial popup of the R-curves. In addition it does not require crack length monitoring during its propagation and accounts for the presence of the FPZ which can be remarkable especially in fracture characterization of ductile adhesives.

# Acknowledgments

The authors thank the "Fundação Luso-Americana para o Desenvolvimento" (FLAD) for the support through project 314/06, 2007 and Instituto de Engenharia Mecânica (IDMEC).

#### References

- [1] R.D. Adams, The Journal of Adhesion, 30 (1989) 219-242.
- [2] M.F.S.F. de Moura, R.D.S.G. Campilho, J.P.M. Gonçalves, International Journal of Solids and Structures, 46 (2009) 1589-1595.
- [3] X. Zhao, R.D. Adams, L.F.M. da Silva, Journal of Adhesion Science and Technology, 25 (2011) 819-836.

- [4] L.F.M. Da Silva, A. Öschner, Modeling of Adhesively Bonded Joints, Springer, Heidelberg, 2008.
- [5] L.F.M. da Silva, D.A. Dillard, B. Blackman, R.D.e. Adams, Testing Adhesive Joints, Best Practices, Wiley, Weinheim, 2012.
- [6] K. Leffler, K.S. Alfredsson, U. Stigh, International Journal of Solids and Structures, 44 (2007) 530-545.
- [7] L.F.M. da Silva, F.A.C.R.G. de Magalhães, F.J.P. Chaves, M.F.S.F. de Moura, The Journal of Adhesion, 86 (2010) 891-905.
- [8] L.F.M. da Silva, V.H.C. Esteves, F.J.P. Chaves, Materialwissenschaft und Werkstofftechnik, 42 (2011) 460-470.
- [9] D.A. Dillard, H.K. Singh, D.J. Pohlit, J.M. Starbuck, Journal of Adhesion Science and Technology, 23 (2009) 1515-1530.
- [10] J.R. Reeder, J.H. Crews, AIAA Journal, 28 (1990) 1270-1276.
- [11] J.H. Crews, J.R. Reeder, in, NASA TECHNICAL MEMORANDUM 100662, 1988.
- [12] F. Ducept, P. Davies, D. Gamby, International Journal of Adhesion and Adhesives, 20 (2000) 233-244.
- [13] Z. Liu, G. R.B., G.M. Newaz, in: Proceedings of the American Society of Composites, Fifteenth Technical Conference, College Station, Texas, USA, September, 2000.
- [14] D.A. Dillard, H.K. Singh, S. Park, D. Ohanehi, M.A. McGaw, in: SEM Annual Conference & Exposition on Experimental and Applied Mechanics, Society for Experimental Mechanics, Inc., St. Louis, 2006.
- [15] K. Singh Hitendra, A. Chakraborty, E. Frazier Charles, A. Dillard David, in: Holzforschung, 2010, pp. 353.
- [16] F.J.P. Chaves, M.F.S.F. de Moura, L.F.M. da Silva, D.A. Dillard, International Journal of Solids and Structures, 48 (2011) 1572-1578.
- [17] L.F.M. da Silva, R.J.C. Carbas, G.W. Critchlow, M.A.V. Figueiredo, K. Brown, International Journal of Adhesion and Adhesives, 29 (2009) 621-632.
- [18] M.F.S.F. de Moura, J.M.Q. Oliveira, J.J.L. Morais, N. Dourado, Construction and Building Materials, 25 (2011) 1956-1962.

PAPER 6

NUMERICAL VALIDATION FOR MIXED-MODE I+II CHARACTERIZATION OF BONDED JOINTS

# Numerical validation of a crack equivalent method for mixed-mode I+II fracture characterization of bonded joints

Filipe J.P. Chaves<sup>1</sup>, M.F.S.F. de Moura<sup>2</sup>, L.F.M. da Silva<sup>2</sup>, D.A. Dillard<sup>3</sup>

<sup>1</sup>IDMEC- Pólo FEUP, Faculdade de Engenharia da Universidade do Porto, Rua Dr. Roberto Frias, 4200-465 Porto, Portugal

## Abstract

The present work is dedicated to development of a crack equivalent data reduction scheme applied to the load jig previously developed by Fernlund and Spelt in order to characterize fracture of bonded joints under mixed-mode I+II loading. The jig allows for easy alteration of the mode-mixity and permits covering the full range of mixed-mode I+II combinations. A data reduction scheme based on specimen compliance, beam theory and crack equivalent concept is proposed to overcome several difficulties inherent to the test analysis. The method assumes that the performed test can be viewed as a combination of the double cantilever beam and asymmetrically loaded end-notched flexure tests, which provide modes I and II fracture characterization, respectively. A numerical analysis including a cohesive mixed-mode I+II damage model was performed considering different mixed-mode loading conditions to validate the proposed data reduction scheme. Issues regarding self-similar crack growth and fracture process zone development are discussed. It was verified that the considered in-plane mix mode fracture criterion is well captured using the proposed data reduction scheme.

**Keywords**: Bonded joints, fracture characterization, mixed-mode I+II loading, in-plane mode mixity, analysis method, CBBM, compliance-based beam method.

#### 1. Introduction

Bonded joints are being increasingly applied in structures involving risk, as is the case of the aeronautical, automotive, and civil infrastructure industries. The classical strength

<sup>&</sup>lt;sup>2</sup> DEMec,Faculdade de Engenharia da Universidade do Porto, Rua Dr. Roberto Frias, 4200-465 Porto, Portugal

<sup>&</sup>lt;sup>3</sup> Engineering Science and Mechanics Department, Virginia Tech, Blacksburg, VA 24061

prediction based on stress or strain analysis may not be adequate in the presence of singularities which occur frequently in bonded joints. As a result, the development of sophisticated design criteria including progressive damage analysis is of fundamental importance. In this context cohesive zone modelling that combine stress-based criteria to simulate damage initiation and fracture mechanics criteria to deal with damage growth acquires special relevancy [1-5]. Fracture mechanics-based criteria require prior characterization of the joint under mixed-mode loading, since bonded joints in real applications often experience such situations. In fact, a crack or debond within an adhesive bond is usually obliged to propagate in a pre-defined plane (thin adhesive layer), independent of the general loading, which induces mixed-mode loading conditions. Consequently, the development of expedited procedures to perform mixed-mode I+II fracture characterization of bonded joints becomes a fundamental issue.

Several tests proposed in the literature can be applied to fracture characterization of bonded joints under mixed-mode I+II loading. Some of these are limited in the range of possible variation of mode mixity, which means that a complete description of the fracture envelope under mixed-mode I+II loading is not possible in such a configuration. This is the case of the asymmetric double cantilever beam (ADCB), the single leg bending (SLB) and the cracked lap shear (CLS) [6]. Nevertheless, there are alternatives that overcome this drawback. This is the case of the mixed-mode bending (MMB) test [7], which can be viewed as a combination of the double cantilever beam (DCB) and end-notched flexure (ENF) tests frequently used for fracture characterization under pure mode I and II loading, respectively. This test allows a large range of mode mixities and an easy alteration of the mode mixity by changing the lever length of the loading arm. However, a special apparatus with considerable dimensions is required, especially for fracture characterization of bonded joints with stiff adherends [8], [9]. Sørensen et al.[10] proposed the DCB specimen loaded by bending moments at the two free beams by means of a special device specially conceived. The mode mixity of the applied loading can be varied altering the ratio between the two applied moments. Högberg and Stigh [11] proposed the mixed mode double cantilever beam specimen based on the geometry of a semi-infinite symmetric DCB specimen. The specimen is loaded by a pair of self-balancing forces whose orientation can vary to alter the mode mixity. Singh et al., [12], have proposed the dual actuator load (DAL) method, which can be viewed as a DCB test subjected to non-symmetric loading. Two independent hydraulic actuators load the arms of a standard DCB specimen clamped at the other

extremity. This test allows easy variation of the mode mixity by applying different displacement rates or loads to the specimen arms by means of the two independent hydraulic actuators. Fernlund and Spelt [13] proposed a special jig which allows mixed-mode fracture testing of adhesive joints and composite laminates over the entire range of mode mix using a standard DCB specimen. The authors used elementary beam theory as a data reduction scheme, which requires monitoring the crack extension during propagation. This task is not easy to be accomplished with the required accuracy, especially in cases when mode II loading predominates, which does not occur in mode I predominant tests, where crack tip is opened, thus facilitating the identification of its tip.

The objective of this work is to propose a simple and expedited data reduction scheme for the test developed by Fernlund and Spelt [13]. The method is based on specimen compliance, beam theory and crack equivalent concept and is proposed to overcome some difficulties inherent to the test analysis, namely crack length monitoring during its growth. The model is validated numerically by means of a detailed numerical analysis using cohesive mixed-mode I+II zone modeling. The numerical model is used to simulate damage initiation and growth for several different combinations of modemixity and the results treated through the proposed data reduction scheme. Some aspects related to self-similar crack growth and fracture process zone development are discussed. The resulting fracture envelope is compared with the input mixed-mode I+II fracture criterion.

# 2. Loading jig

The loading jig developed by Fernlund and Spelt [13] consists primarily of two rigid beams linked to each other, to the specimen, and to a base plate (Figure 1).

Different jig geometries can be achieved by altering the four distances,  $s_1$  -  $s_4$ , thereby varying the mode-mixity of the induced loading. Changing the above referred distances leads to different loads,  $F_1$  and  $F_2$ , applied to the upper and lower adherends, respectively, of the tested specimens (Figure 2). The jig also permits the realization of pure mode tests, namely the Double Cantilever Beam (DCB) for mode I and the End-Notched Flexure (ENF) for mode II, thus being versatile in the context of fracture characterization.

• • • •

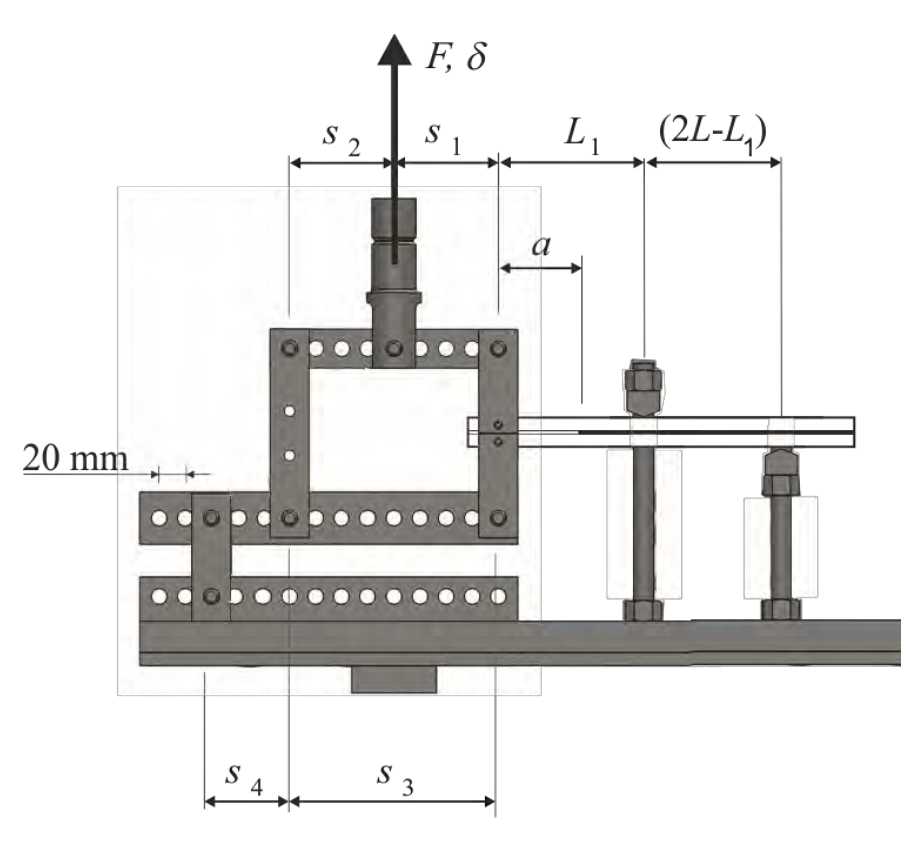


Figure 1. Load jig.

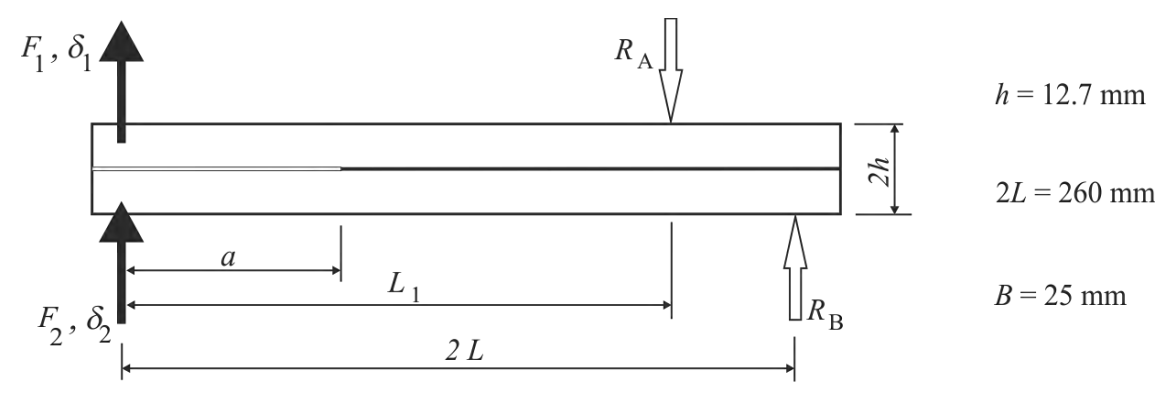


Figure 2. Schematic representation of specimen loading and dimensions (*B* is the specimen width).

# 3. Compliance based beam method

The classical data reduction schemes based on compliance calibration and beam theories are based on crack length monitoring during its propagation. However, there are two limitations related to this aspect. In fact, this task is not easy to be accomplished with the required accuracy namely in cases where mode II loading predominate, since

the crack faces remain in contact during its propagation. The second limitation is related to the energy dissipation at the fracture process zone (FPZ) ahead of the crack tip, which can be non-negligible as is the case of adhesives with some inelastic behaviour. The consideration of the clear crack length (not including the influence of the FPZ size), as a fracture parameter in beam theory equations does not allow accounting for this energy. An alternative procedure based on an equivalent crack concept can be used with remarkable advantages. The proposed method is based on Timoshenko beam theory and uses the current specimen compliance to estimate an equivalent crack during the test. Using the Timoshenko beam theory, the strain energy of the specimen (Figure 2) due to bending and including shear effects is

$$U = \int_{0}^{a} \frac{M_{1}^{2}}{2EI_{1}} dx + \int_{0}^{a} \frac{M_{2}^{2}}{2EI_{2}} dx + \int_{a}^{L_{1}} \frac{M_{T_{(a \to L_{1})}}^{2}}{2EI_{T}} dx + \int_{L_{1}}^{2L} \frac{M_{T_{(L_{1} \to 2L)}}^{2}}{2EI_{T}} dx + \int_{L_{1}}^{a} \frac{M_{T_{(L_{1} \to 2L)}}^{2}}{2EI_{T}} dx + \int_{a}^{a} \int_{-h/2}^{h/2} \frac{\tau_{1}^{2}}{2G} B \, dy dx + \int_{0}^{a} \int_{-h/2}^{h/2} \frac{\tau_{2}^{2}}{2G} B \, dy dx + \int_{a}^{L_{1}} \int_{-h}^{h} \frac{\tau_{T_{(a \to L_{1})}}^{2}}{2G} B \, dy dx + \int_{L_{1}}^{L_{1}} \int_{-h}^{h} \frac{\tau_{T_{(L_{1} \to 2L)}}^{2}}{2G} B \, dy dx$$
 (1)

where M is the bending moment, the subscripts 1 and 2 stand for upper and lower adherends and T refers to the total bonded beam (of thickness 2h), E and G are the longitudinal and shear modulus, respectively, B is the specimen and bond width and I is the second moment of area of the indicated section. For adherends with the same thickness, as considered in this analysis,  $I_T = 8I_1 = 8I_2$ . The shear stresses induced by transverse loading of beams are given by

$$\tau = \frac{3}{2} \frac{V}{Bh} \left( 1 - \frac{y^2}{c^2} \right) \tag{2}$$

The parameters c and V represent, respectively, the beam half-thickness and the transverse load, on each arm for  $0 \le x \le a$ , and on total bonded beam for  $a \le x \le 2L$ .

Using the Castigliano's theorem ( $\delta = \partial U/\partial P$ , where P is the applied load and  $\delta$  the resulting displacement at the same point) the displacements of the specimen arms at the loaded extremities can be written as

$$\delta_{1} = \frac{\partial U}{\partial F_{1}} = \frac{4 \left[ a^{3} F_{1} + \frac{(F_{1} + F_{2}) \left(2LL_{1}^{2} - a^{3}\right)}{8} \right]}{Bh^{3} E} + \frac{3 \left[ 2aF_{1} + (F_{1} + F_{2}) \left(L_{1} - a + \frac{L_{1}^{2}}{2L - L_{1}}\right) \right]}{5BhG}$$

$$\delta_{1} = \frac{\partial U}{\partial F_{1}} = \frac{4\left[a^{3}F_{1} + \frac{(F_{1} + F_{2})\left(2LL_{1}^{2} - a^{3}\right)}{8}\right]}{Bh^{3}E} + \frac{3\left[2aF_{1} + (F_{1} + F_{2})\left(L_{1} - a + \frac{L_{1}^{2}}{2L - L_{1}}\right)\right]}{5BhG}$$

$$\delta_{2} = \frac{\partial U}{\partial F_{2}} = \frac{4\left[a^{3}F_{2} + \frac{(F_{1} + F_{2})\left(2LL_{1}^{2} - a^{3}\right)}{8}\right]}{Bh^{3}E} + \frac{3\left[2aF_{2} + (F_{1} + F_{2})\left(L_{1} - a + \frac{L_{1}^{2}}{2L - L_{1}}\right)\right]}{5BhG}$$
(3)

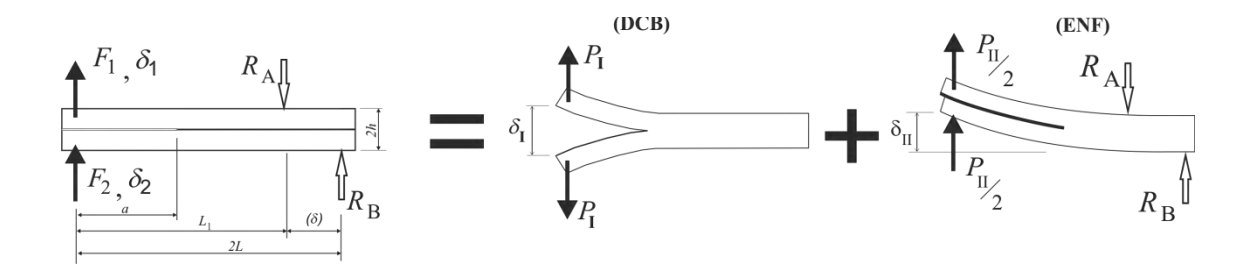


Figure 3. Spelt jig loading scheme.

The present test induces a combination of opening and shear loading applied to the specimen that can be partitioned in order to get the components corresponding to mode I and mode II solicitations. The mode I component is induced by an opening loading and mode II will result from longitudinal sliding at the crack tip. Consequently, the partitioning method complies with those objectives (Figure 3). The mode I loading reflects the Double Cantilever Beam (DCB) specimen and the mode II can be viewed as the End-Notched Flexure (ENF) loaded asymmetrically – it should be remembered that the ENF is a three-point bending test loaded at the mid-span. From Figure 3 the following relations can be obtained

$$F_{1} = P_{I} + \frac{P_{II}}{2}; \quad F_{2} = -P_{I} + \frac{P_{II}}{2}$$

$$\delta_{1} = \frac{\delta_{I}}{2} + \delta_{II}; \quad \delta_{2} = -\frac{\delta_{I}}{2} + \delta_{II}$$

$$(4)$$

The corresponding pure modes (I and II) loading and displacement components become

$$P_{\rm I} = \frac{F_{\rm I} - F_{\rm 2}}{2}; \quad \delta_{\rm I} = \delta_{\rm I} - \delta_{\rm 2}$$

$$P_{\rm II} = F_1 + F_2; \quad \delta_{\rm II} = \frac{\delta_1 + \delta_2}{2}$$
 (5)

Combining equations (3 and 5), the pure mode compliances can be obtained

$$C_{\rm I} = \frac{\delta_{\rm I}}{P_{\rm I}} = \frac{8a^3}{Bh^3E} + \frac{12a}{5BhG} \tag{6}$$

$$C_{II} = \frac{\delta_{II}}{P_{II}} = \frac{3a^3 + 2LL_1^2}{2Bh^3E} + \frac{6LL_1}{5BhG(2L - L_1)}$$
(7)

As expected, equation (6) is equal to that obtained for a DCB [14] and equation (7) is compatible with results for an ENF specimen [15] when  $L_1$ =L, i.e., where the specimen is loaded at its mid-span. This achievement is quite interesting, as it allows the use of simple equations to obtain the strain energy components.

One of the critical issues intrinsic to the generality of the fracture tests is the difficulty of monitoring the crack length during its propagation. This task is especially challenging to accomplish with the required accuracy when mode II loading predominates, since the crack tends to grow with its faces in contact, making crack tip identification difficult. Additionally, there are several aspects not included in equations (6) and (7) that can influence specimen behaviour. Effectively, issues like stress concentrations and root rotation effects at the crack tip, the presence of the adhesive layer and the eventual existence of a non-negligible fracture process zone ahead of crack tip during propagation are not included in these beam theory equations, although they influence the specimen compliance. In order to overcome the referred inaccuracies, an equivalent crack length procedure is used. The procedure is based on the estimation of the equivalent crack lengths using equations (6) and (7), from the current compliances  $C_{\rm I}$  and  $C_{\rm II}$ , which are easily obtained from the loads and displacements of the specimen arms continuously registered during the test. The achievement of the equivalent crack length in mode I  $(a_{el})$  requires the solution of a cubic equation (6) that can be written in the following way

 $\alpha a_{el}^3 + \beta a_{el} + \gamma = 0 \tag{8}$ 

where

$$\alpha = \frac{8}{Bh^3E}; \quad \beta = \frac{12}{5BhG}; \quad \gamma = -C_1 \tag{9}$$

Using Matlab® software and only keeping the real solution, one obtains

$$a_{\rm el} = \frac{1}{6\alpha} A - \frac{2\beta}{A} \tag{10}$$

where

$$A = \left( \left( -108\gamma + 12\sqrt{3\left(\frac{4\beta^3 + 27\gamma^2\alpha}{\alpha}\right)} \right) \alpha^2 \right)^{\frac{1}{3}}$$
 (11)

In mode II the equivalent crack length  $(a_{ell})$  can be directly obtained from equation (7)

$$a_{\text{eII}} = \left[ \left( C_{\text{II}} - \frac{6LL_{1}}{5BhG(2L - L_{1})} \right) \frac{2Bh^{3}E}{3} - \frac{2LL_{1}^{2}}{3} \right]^{1/3}$$
 (12)

The components of the strain energy release rate can be determined by means of the Irwin-Kies equation

$$G = \frac{P^2}{2B} \frac{dC}{da} \tag{13}$$

For mode I, the combination of equations (6) and (13) leads to

$$G_{\rm I} = \frac{6P_{\rm I}^2}{B^2 h} \left( \frac{2a_{\rm el}^2}{h^2 E} + \frac{1}{5G} \right) \tag{14}$$

. . . .

The strain energy release rate in mode II is obtained from equations (7) and (13)

$$G_{\rm II} = \frac{9P_{\rm II}^2 a_{\rm eII}^2}{4B^2 h^3 E} \tag{15}$$

Equations (14) and (15) represent the evolution of the strain energy release rates components during the test (R-curves), thus providing the identification of the modemixity as well as the total fracture energy of the test. The proposed method only requires recording the load F (Figure 1) and displacement components applied to each arm of the specimen ( $\delta_1$ ,  $\delta_2$ ) during the test (Figure 2). The load components ( $F_1$  and  $F_2$ ) can be straightforwardly obtained from the load applied by the machine (F) and static equilibrium of each loading arm (Figure 1)

$$F_1 = F \frac{s_2}{s_3}$$
;  $F_2 = F \frac{s_1 s_4}{s_3 (s_3 + s_4)}$  (16)

The displacements applied to the specimen arms ( $\delta_1$  and  $\delta_2$ ) must be monitored during the test using two LVDTs. These devices could be attached to the base plate and maintained in contact with the vertical links attached to the specimen arms extremities in order to measure their displacements. Following this procedure the load frame compliance will not influence the specimen measured compliance. Since the method is essentially based on the compliance of the specimen arms it is named compliance-based beam method (CBBM). Following the proposed procedure it is not necessary to perform crack length monitoring during propagation. Additionally, the energy dissipated at nonnegligible FPZ is accounted for since the current specimen compliances are influenced by the presence of the FPZ.

## 4. Numerical analysis

In order to verify the performance of the proposed method as well as the ability of the jig to provide a rigorous characterization of the fracture envelope under mixed-mode I+II of bonded joints, a numerical analysis including cohesive zone modelling was performed. The specimen geometry and mechanical properties used in the simulations are presented in Figure 2 and Table 1, respectively.

Table 1. Elastic and cohesive properties [5].

Elastic properties		Cohesive properties					
(Steel)		(Adhesive)					
E	G	$\sigma_{\! ext{u,I}}$	$\sigma_{ m u,II}$	$G_{ m Ic}$	$G_{ m IIc}$	$\delta_{2,\mathrm{I}}$	$\delta_{2, ext{II}}$
(GPa)	(GPa)	(MPa)	(MPa)	(N/mm)	(N/mm)	(mm)	(mm)
210	80.77	23	23	0.6	1.2	0.0187	0.2062

Figure 4 presents the considered mesh and corresponding boundary conditions.

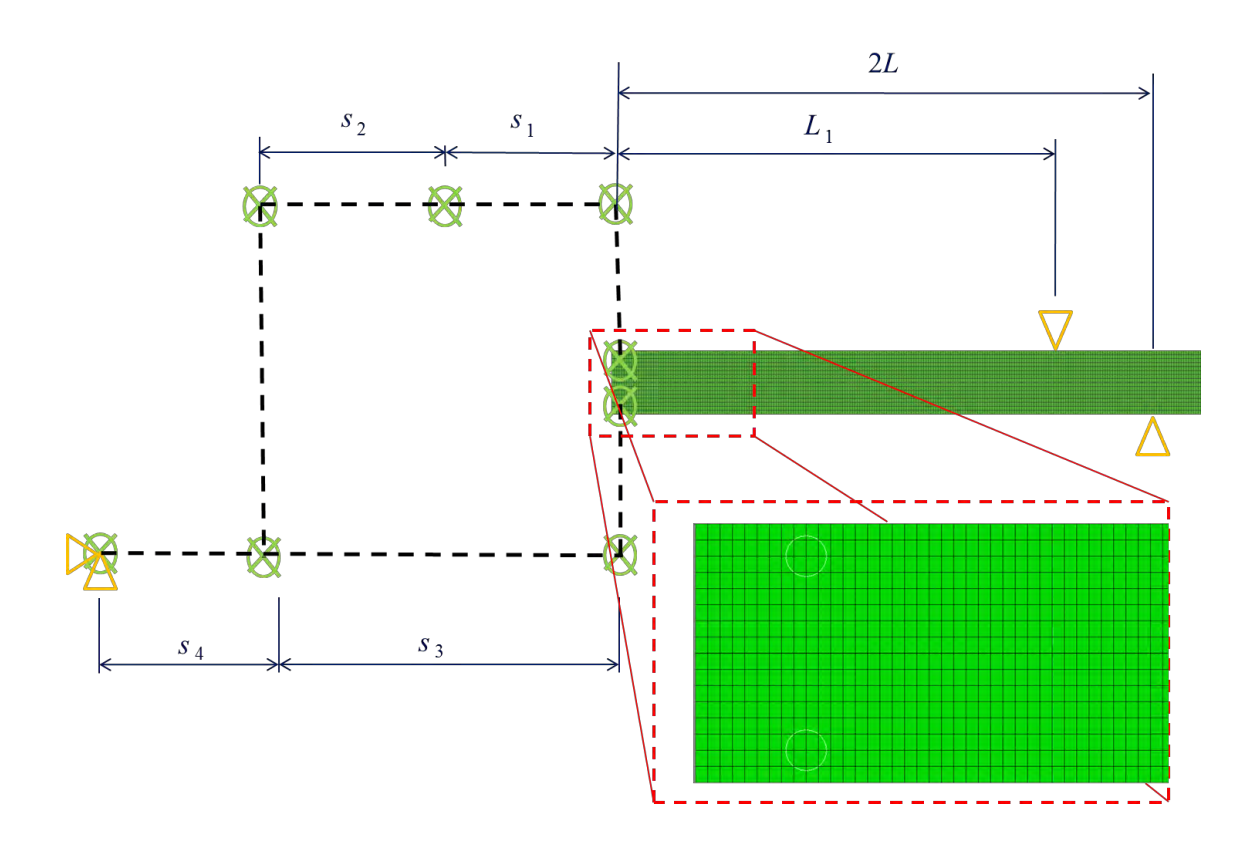


Figure 4. Mesh and the boundary conditions used in the numerical analysis.

The loading device was simulated by a combination of rigid beams and links (Figure 4) that reproduce the experimental setup. The specimen was modelled with 3600 plane strain 8-node quadrilateral elements and 280 6-node interface elements with null thickness placed at the mid-plane of the bonded specimen. The interface elements include a cohesive zone mixed-mode I+II damage model to simulate damage onset and propagation within the adhesive. The cohesive zone model establishes a relationship

between stresses and relative displacements between specimen arms [16, 17]. The behaviour of the adhesive is integrated in the cohesive damage law considered. A trapezoidal cohesive damage model was considered in the numerical analysis (Figure 5). The trapezoidal laws are particularly adequate for adhesives with ductile behaviour [16-18]. In the pure mode model, the slope of the initial linear part is dictated by the interface stiffness, which is obtained by the ratio between the relevant adhesive elastic modulus (E in mode I and G in mode II) and its thickness. Once the local strength ( $\sigma_{u,i}$ ) is obtained, a plateau zone takes place to simulate adhesive plastic behaviour. The third linear softening part between stresses and relative displacements is assumed to simulate a gradual material degradation during the loading process. In the pure mode model, the ultimate relative displacement  $\delta_{u,i}$  is defined by equating the area circumscribed by the trapezoid to  $G_{ic}$  (i=I, II). Mixed-mode I+II damage model is an extension of pure mode model. In this case, a quadratic stress criterion is utilized to identify damage initiation

$$\left(\frac{\sigma_{\rm I}}{\sigma_{\rm u,I}}\right)^2 + \left(\frac{\sigma_{\rm II}}{\sigma_{\rm u,II}}\right)^2 = 1 \tag{17}$$

The linear energetic criterion

$$\left(\frac{G_{\rm I}}{G_{\rm lc}}\right) + \left(\frac{G_{\rm II}}{G_{\rm llc}}\right) = 1$$
(18)

and the quadratic one

$$\left(\frac{G_{\rm I}}{G_{\rm Ic}}\right)^2 + \left(\frac{G_{\rm II}}{G_{\rm IIc}}\right)^2 = 1\tag{19}$$

were used to simulate damage propagation. The area under the trapezoid  $0-\sigma_{\text{um},i}-\delta_{2\text{m},i}-\delta_{2\text{m},i}$  of Figure 5 represents the energy released in each mode, while the area of the  $0-\sigma_{\text{u},i}-\delta_{2,i}-\delta_{\text{u},i}$  trapezoid corresponds to the respective critical fracture energy. When equations (18) or (19) are satisfied damage propagation occurs and stresses are completely released, with the exception of normal compressive ones. The model is detailed in de Moura et al. [17].

• • • •

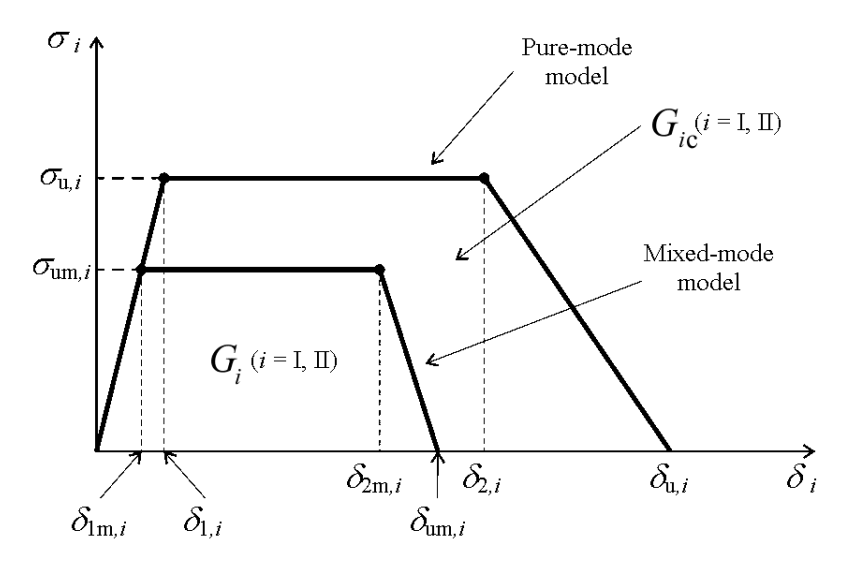


Figure 5. The trapezoidal softening law for pure and mixed-mode cohesive damage model.

#### 5. Results and discussion

In order to validate the proposed data reduction scheme when applied to the Spelt device seven scenarios were considered in the  $G_{\rm I}$ - $G_{\rm II}$  space, including the pure mode cases. The mode mixity between different scenarios was changed by altering the distances  $s_1$ - $s_4$  (Figure 1).

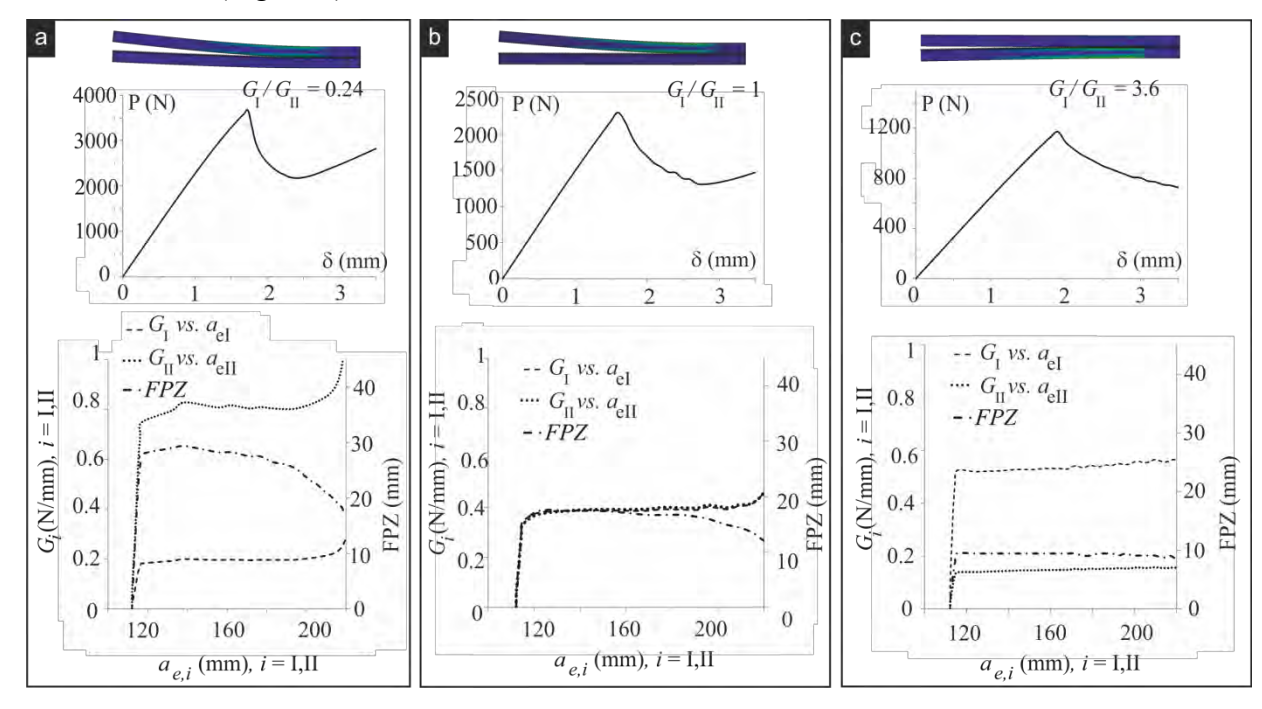


Figure 6. Deformed shapes, load-displacement curves and *R*-curves for three mixed-mode loadings.

Figure 6 represents the deformed shape and the corresponding load-displacement and Rcurves for three different cases representing predominantly mode I ( $G_I/G_{II}=3.6$ ) and mode II  $(G_I/G_{II}=0.24)$  and a balanced mixed-mode loading  $(G_I/G_{II}=1)$ . The R-curves were obtained by means of equations (14) and (15), i.e., only requiring the data issuing from the load-displacement curve. It can be verified that the R-curves for each energy component present a clear plateau defining the corresponding value of energy during propagation. The existence of these plateaus is an indication that self-similar crack growth with a constant size FPZ ahead of crack tip is fulfilled during mixed-mode I+II crack propagation, which is essential to perform adequate fracture characterization for each mode-mixity. In order to confirm this statement, the evolution of the FPZ length is also presented in the R-curves graphs. The FPZ length corresponds to the extent ahead of crack tip where inelastic processes take place. Numerically, the FPZ length is simulated by the cohesive zone length, which is easily accessed by subtracting, along the crack path, the coordinate of the last integration point behaving in the initial branch of the cohesive law (Figure 5) and the one corresponding to current crack length. In other words, the FPZ length is constituted by the points undergoing softening, i.e., the points behaving in the second and third branches of the cohesive law. It should be noted that in all cases, there exists a quite stable plateau. In the cases  $G_I/G_{II}=0.24$  and  $G_I/G_{II}=1$ the referred plateau is followed by a decrease of FPZ length, which reflects the spurious compressive effect of the loading  $R_A$  (see Figure 2) when crack tip approaches to this point, thus leading to an artificial increase of the energy components. This means that a determined distance (depending on the material being characterized) between the precrack length and the loading point A (distance  $L_1$ -a in Figure 2) must be guaranteed to avoid false estimations of fracture energy.

In order to validate the proposed CBBM the classical compliance calibration method (CCM) was also applied to the numerical results. This method is easy to apply numerically, since the crack length can be straightforwardly monitored, which does not happen experimentally. Using the Irwin-Kies relation (equation (13))  $G_T$  becomes

$$G_{\rm T} = \frac{F_1^2}{2B} \frac{dC_1}{da} + \frac{F_2^2}{2B} \frac{dC_2}{da}$$
 (20)

Polynomials of third degree were fit to the  $C_1$ =f(a) and  $C_2$ =f(a) curves to perform the differentiation. The curves  $G_T$ =f( $a_e$ ) obtained by the CCM and the CBBM are plotted in

Figure 7, considering the three representative cases of mode-mix, for the range of  $a_e$  corresponding to crack growth without influence of discussed spurious effects. Although the CCM is a function of a, the  $a_e$  was used to provide better comparison between the two methods. It can be concluded that both methods provide results that are in close agreement, thus validating the proposed CBBM.

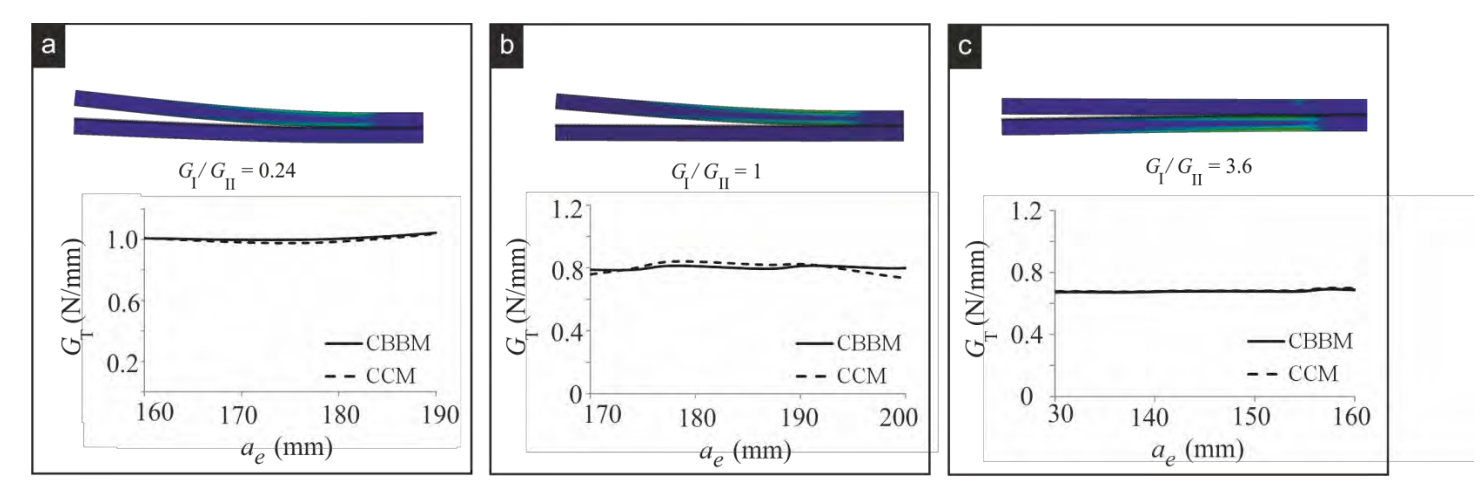


Figure 7. Plot of the  $G_T$  = f( $a_e$ ) curves obtained by the CCM and the CBBM for  $G_I/G_{II}$ =0.24;1 and 3.6.

The R-curves were also obtained for the remaining mixed-mode combinations. The main goal was to verify whether the linear energetic criterion (equation (18)) considered in the numerical simulations is well reproduced when applying the proposed data reduction scheme to the numerical results, i.e., the applied load P and the resultant displacements of each arm,  $\delta_1$  and  $\delta_2$ . With this aim, the values issuing from the plateau of the R-curves are plotted in a graph of the  $G_I$ - $G_{II}$  space (Figure 8) and compared to the straight line representing the linear energetic criterion (equation (18)). A similar procedure was followed using the quadratic energetic criterion (equation (19)) and considering the same seven scenarios (Table 2). The good agreement obtained for both criteria demonstrates that the proposed model can be applied with success as a straightforward data reduction scheme for the present mixed-mode I+II fracture characterization test.

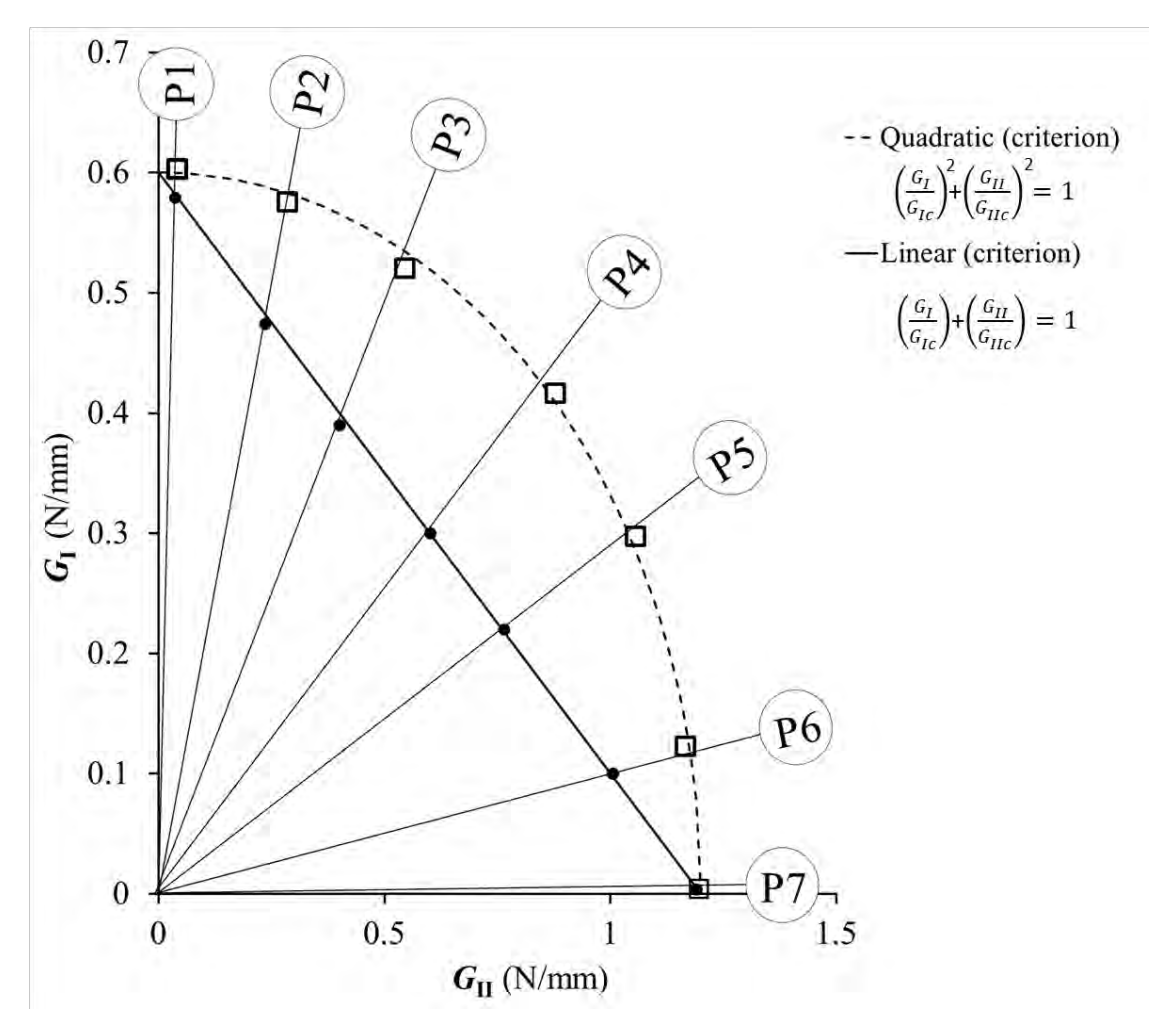


Figure 8. Fracture envelope for the seven scenarios analyzed considering the linear (●) and quadratic (□) criteria.

Table 2. Different scenarios used for the fracture envelope calculation.

	Jig arrangement						
Scenarios	$s_1$ (mm)	$s_2$ (mm)	$s_3$ (mm)	<i>s</i> <sub>4</sub> (mm)			
P1	100	40	140	-60			
P2	120	40	160	-120			
Р3	40	120	160	40			
P4	60	80	140	60			
P5	60	80	140	120			
P6	40	40	80	100			
<b>P7</b>	100	40	140	80			

#### 7. Conclusions

The objective of this work is to propose a suitable data reduction scheme applied to the test developed by Fernlund and Spelt [13] in order to characterize fracture of bonded joints under different mixed-mode I+II loading conditions. The method is based on specimen compliance, beam theory and crack equivalent concept. It provides a simple mode partitioning method and does not require crack length monitoring during the test, which is advantageous since measurements errors can originate incorrect estimation of fracture energy. Additionally, the presence of an eventual non-negligible fracture process zone is indirectly accounted for, since the current compliance is used to estimate the equivalent crack length. This aspect is fundamental, namely in the fracture characterization of adhesives with some ductility.

In order to validate the procedure a numerical analysis considering cohesive mixed-mode I+II damage model was performed. Several different scenarios covering all the mixed-mode range were considered. It was verified that R-curves present a steady plateau in conformity with a constant fracture process zone length, thus revealing the conditions of self-similar crack propagation which are fundamental to a rigorous fracture characterization. The proposed data reduction scheme was compared with the compliance calibration method for the total energy release rate during propagation and excellent agreement was observed. Finally, the values of the energy components issuing from the plateau of the R-curves were plotted in a  $G_I$ - $G_{II}$  space for all the scenarios analysed. It was observed that both the linear and quadratic energetic fracture criteria considered in the numerical analysis were correctly reproduced by the numerical results using the proposed data reduction scheme.

It should be noted that the validity of the present model is intrinsically associated to the limits of applicability of the Timoshenko beam theory. For pronounced non-linear problems it is expectable that beam theory equations do not propitiate accurate results.

# Acknowledgements

The authors would like to thank the "Fundação Luso-Americana para o Desenvolvimento" (FLAD) for the support through project 314/06, 2007 and *Instituto de Engenharia Mecânica* (IDMEC).

#### References

- [1] Q.D. Yang, M.D. Thouless, International Journal of Fracture, 110 (2001) 175-187.
- [2] B.R.K. Blackman, H. Hadavinia, A.J. Kinloch, J.G. Williams, International Journal of Fracture, 119 (2003) 25-46.
- [3] T. Andersson, U. Stigh, International Journal of Solids and Structures, 41 (2004) 413-434.
- [4] M.F.S.F. de Moura, J.A.G. Chousal, International Journal of Mechanical Sciences, 48 (2006) 493-503.
- [5] R.D.S.G. Campilho, M.F.S.F.d. Moura, D.A. Ramantani, J.P.M. Gonçalves, Ciência & Tecnologia dos Materiais, 20 (2008) 81-86.
- [6] D.A. Dillard, H.K. Singh, D.J. Pohlit, J.M. Starbuck, Journal of Adhesion Science and Technology, 23 (2009) 1515-1530.
- [7] J.R. Reeder, J.H. Crews, AIAA Journal, 28 (1990) 1270-1276.
- [8] F. Ducept, P. Davies, D. Gamby, International Journal of Adhesion and Adhesives, 20 (2000) 233-244.
- [9] Z. Liu, G. R.B., G.M. Newaz, in: Proceedings of the American Society of Composites, Fifteenth Technical Conference, College Station, Texas, USA, September, 2000.
- [10] B. Sørensen, K. Jørgensen, T. Jacobsen, R. Østergaard, International Journal of Fracture, 141 (2006) 163-176.
- [11] J.L. Hogberg, U. Stigh, Engineering Fracture Mechanics, 73 (2006) 2541-2556.
- [12] K. Singh Hitendra, A. Chakraborty, E. Frazier Charles, A. Dillard David, in: Holzforschung, 2010, pp. 353.
- [13] G. Fernlund, J.K. Spelt, Composites Science and Technology, 50 (1994) 441-449.
- [14] M.F.S.F. de Moura, R.D.S.G. Campilho, J.P.M. Gonçalves, Composites Science and Technology, 68 (2008) 2224-2230.
- [15] M.F.S.F. de Moura, M.A.L. Silva, A.B. de Morais, J.J.L. Morais, Engineering Fracture Mechanics, 73 (2006) 978-993.
- [16] M. Alfano, F. Furgiuele, L. Pagnotta, G.H. Paulino, Journal of Testing and Evaluation, 39 (2010) 1-8.
- [17] M.F.S.F. de Moura, R.D.S.G. Campilho, J.P.M. Gonçalves, International Journal of Solids and Structures, 46 (2009) 1589-1595.
- [18] G. Alfano, Composites Science and Technology, 66 (2006) 723-730.

PAPER 7

APPARATUS AND METHOD PATENT

# Apparatus and method for characterization of bonded joints mixedmode I+II fracture

Filipe J.P. Chaves<sup>1</sup>, L.F.M. da Silva<sup>2</sup>, M.F.S.F. de Moura<sup>2</sup>, David A. Dillard<sup>3</sup>, J.O. Fonseca<sup>4</sup>

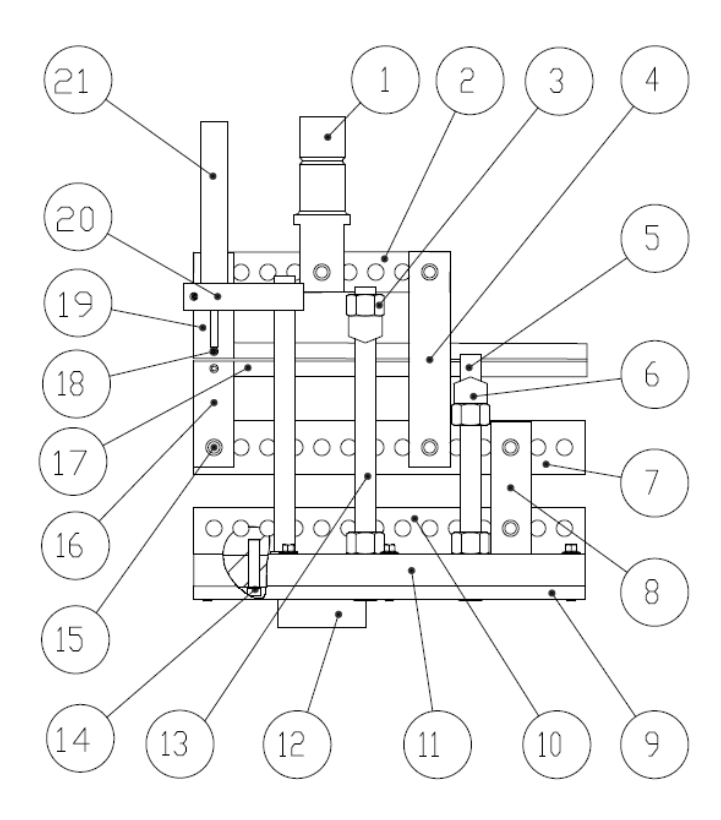
<sup>1</sup> IDMEC- Pólo FEUP, Faculdade de Engenharia da Universidade do Porto, Rua Dr. Roberto Frias, 4200-465 Porto, Portugal

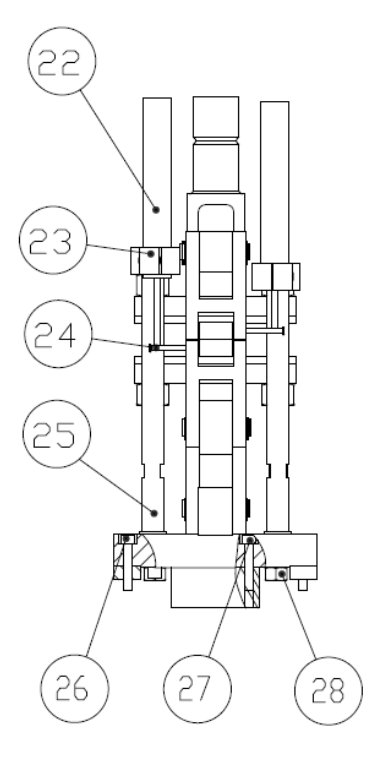
<sup>2</sup> DEMec,Faculdade de Engenharia da Universidade do Porto, Rua Dr. Roberto Frias, 4200-465 Porto, Portugal

<sup>3</sup> Engineering Science and Mechanics Department, Virginia Tech, Blacksburg, VA 24061

#### Abstract

The present invention relates to an apparatus for measuring the toughness of adhesive joints in various fracture modes from mode I (opening) to mode II (shear) relying exclusively on the load-displacement curve obtained from an universal testing machine and the displacement information from two linear variable differential transformer – LVDT - connected to the specimen beams. This apparatus is an evolution from the jig presented by Spelt [1] and its operation is different from those existing on the market, mostly because it does not use the crack length measurement, instead it uses the displacement obtained from the LVDTs. It presents also another great advantage when compared to the existing solutions that places the specimen in the opposite side of the loading jig, because this invention place the specimen inside its structure, thus reducing the overall dimensions and facilitating the required test operations, improving the usability. Relying exclusively on three machine outputs, the load–displacement data and the displacement data from the two LVDTs, it allows an automated data reduction scheme and, therefore, renders an easier analysis that is accurate, not depending on human observation.





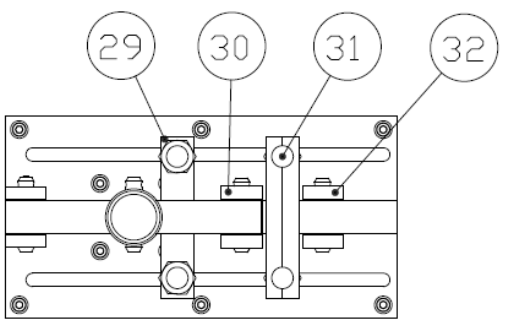


FIG. 1

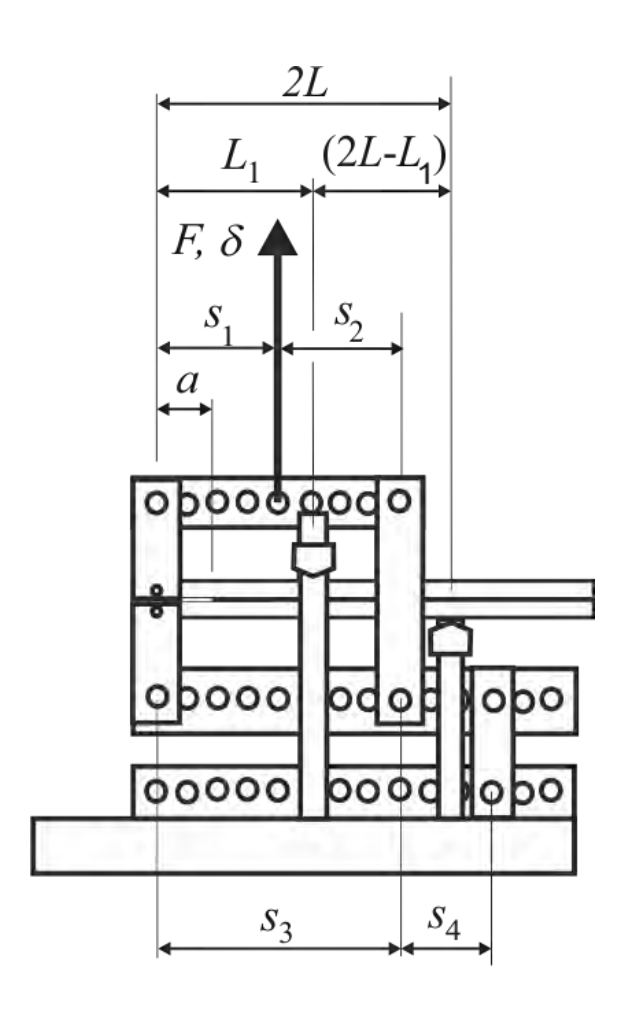
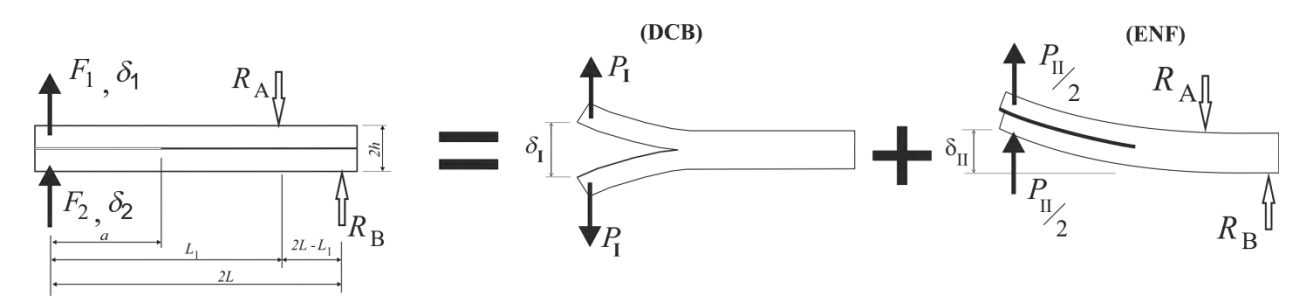


FIG. 2



$$F_1 = F \frac{s_2}{s_3}$$
 ;  $F_2 = F \frac{s_1 s_4}{s_3 (s_3 + s_4)}$ 

$$P_{\rm I} = \frac{F_1 - F_2}{2}$$

$$P_{\rm II} = F_1 + F_2$$

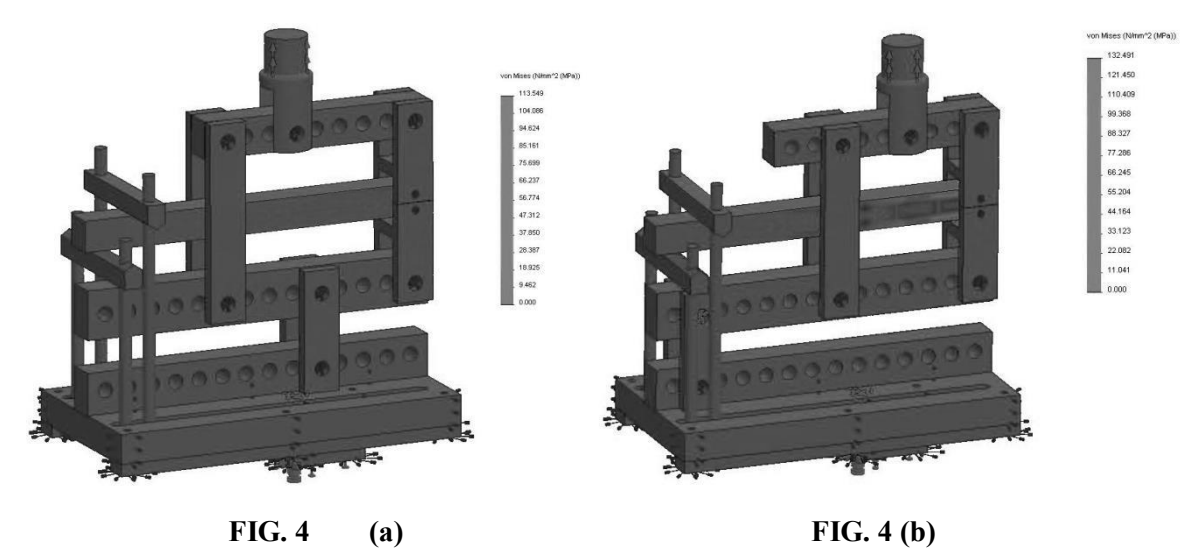
$$\delta_{\rm I} = \delta_{\rm l} - \delta_{\rm 2}$$

$$\delta_{\rm II} = \frac{\delta_1 + \delta_2}{2}$$

FIG. 3 (a) Specimen loading

Mode I loading

Mode II loading



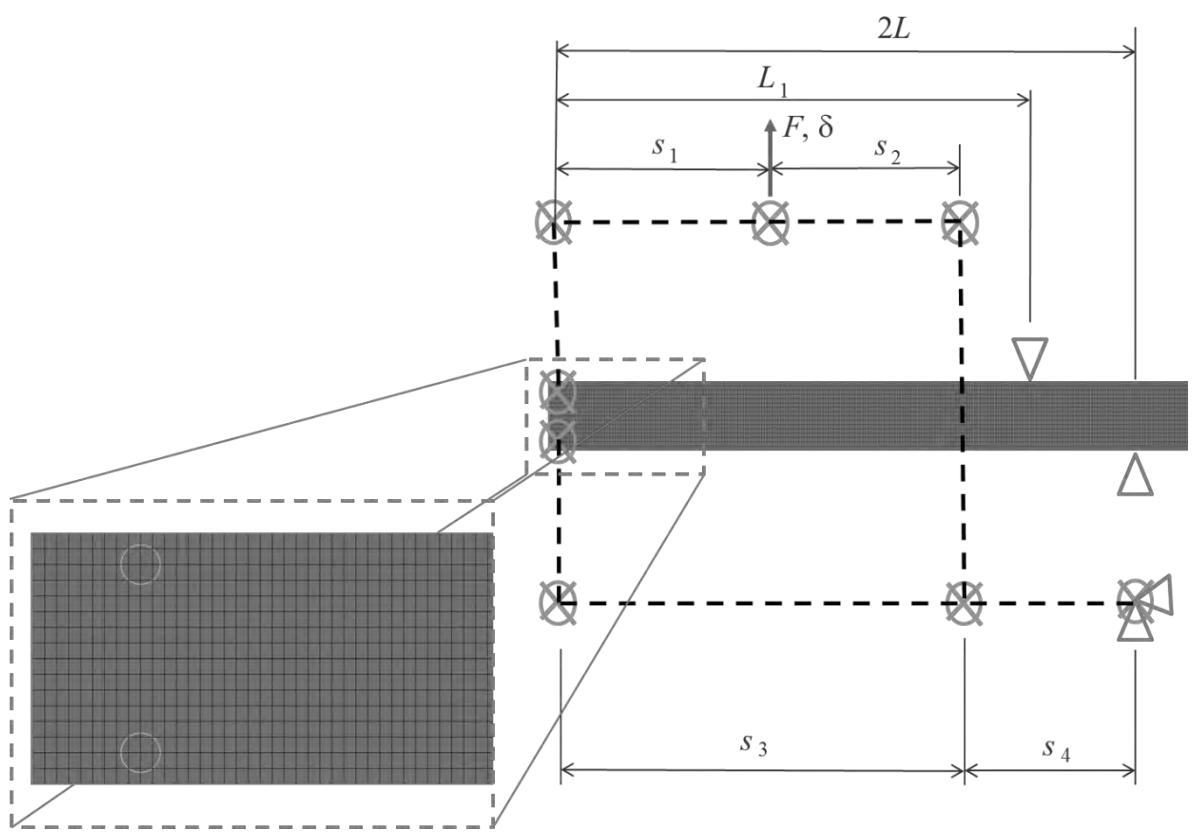
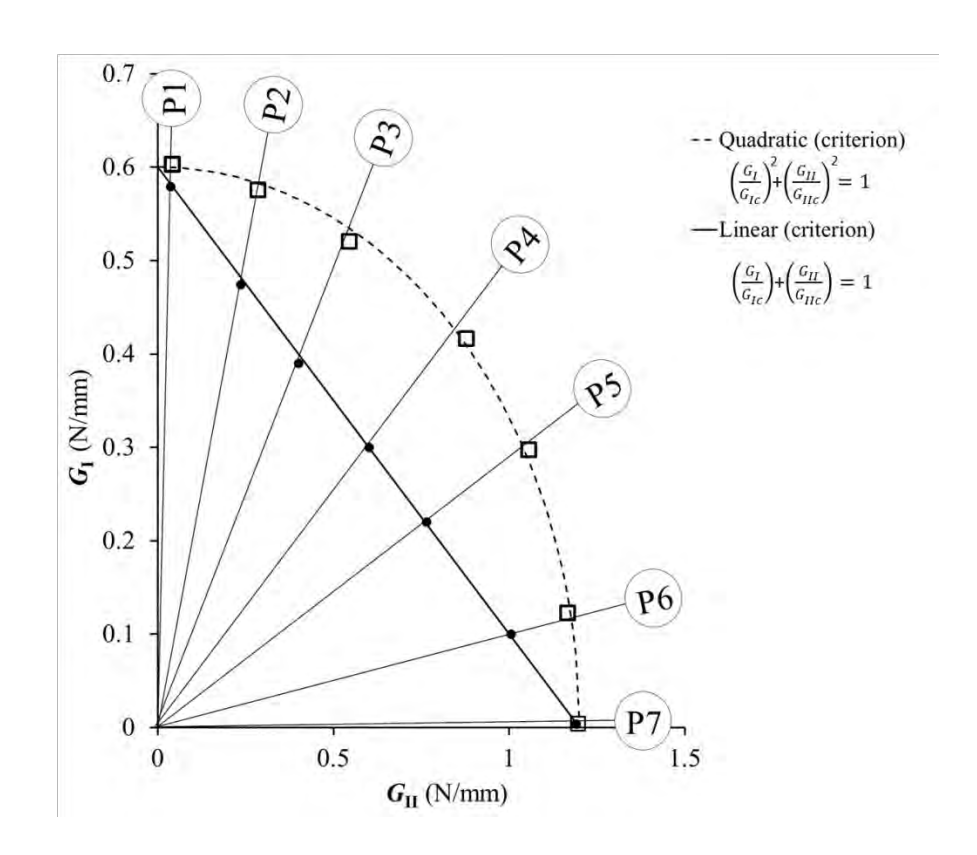
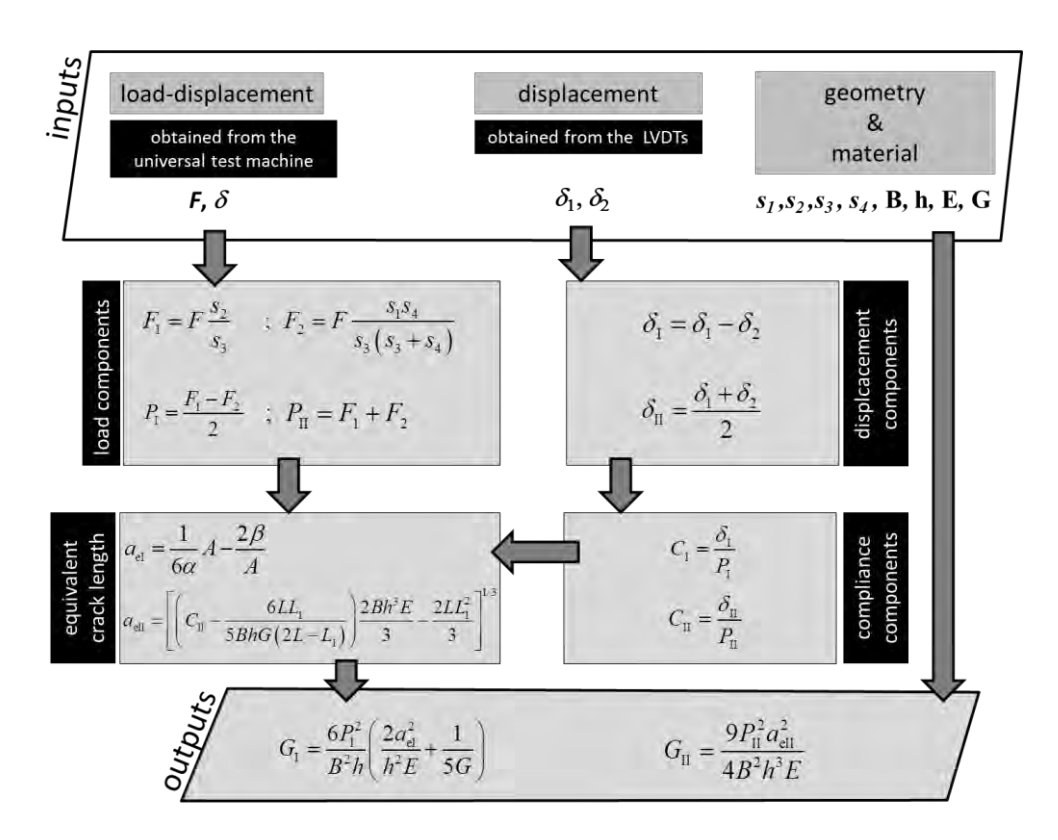


FIG. 5



Fracture envelope for the seven scenarios analyzed considering the linear  $(\bullet)$  and quadratic  $(\Box)$  criteria.

FIG. 6



**FIG.** 7

# **Background of the invention**

Adhesive bonding of structures used in aeronautic and automotive industries are an important application that optimizes the strength and weight of the overall structure. The interest in adhesive joint design is growing, and the knowledge to support the design criteria in order to forecast the joint behavior to the service loads is a major contribution. Fracture mechanics is a good methodology to characterize the adhesive joint and supported by Damage Mechanics, which defines the cohesive parameters, embodies a powerful tool for simulation and design of adhesive joints. To apply these tools, adhesive joint fracture characterization in mode I, mode II and mixed mode (I+II) must be obtained, and there are several tests proposed to achieve that goal. These tests are time consuming and dependable of the technician that performs the tests, because they all rely on visual measurements done for the crack length. Even when high speed cameras, and sophisticated image analysis software are used, such as digital image processing (DIP) as the one proposed by Richter et al. [2], the Fracture Process Zone (FPZ) and the root rotation are not taken into account. This is troublesome, because the fracture process zone effect is very important and should be considered to contemplate the contribution of the hidden damaged adhesive ahead of the visible crack tip [3].

Toughness is usually expressed in terms of the critical value for the strain release rate  $(G_c)$  which is the energy dissipated during fracture when the crack grows. It is the energy needed for a crack tip to propagate and must also take into account the fracture process zone ahead of the crack tip.

A research done for the assessment of the state of the art for these apparatus returned some results for mixed-mode fracture toughness determination of steel, aluminum and other materials with spiral-grooved specimens as described in US6588283, and a mixed mode I/II/III fracture grip interface AU2008101040 similar to the modified Arcan test [4] that is used for adhesive joint testing. Reeder and Crews have also developed a mixed mode test apparatus and method, as described in US4926694 used for delamination of composites. Spelt developed a mechanism [1] to test the mixed mode fracture (mode I + II) of adhesive joints, that requires the measurement of the crack length during propagation. Dillard et al. [5] developed a double actuator loading frame with two hydraulic actuators and two load cells to apply different displacement rates to each beam of the specimen. These apparatus and machines are able to test the specimen in almost all the envelop range for mode I and II, but there are other alternatives to obtain a limited mixed mode ratio, using different specimen geometries. This is the case of the

asymmetric double cantilever beam (ADCB), the single leg bending (SLB) and the cracked lap shear (CLS) [6].

## **Summary of the invention**

The present invention provides a test apparatus to apply simultaneously opening and shear stress in a test specimen to determine the fracture mechanics properties of the specimen (adhesive joint).

This invention also provides a test apparatus which applies mode I and mode II loads to a test specimen (adhesive joint) while measuring the displacement of each beam and applied load, allowing to measure its strength.

The presented apparatus provides a variation of the mode I/II ratio over a broad range of the fracture envelop.

Another object of the presented invention is to provide an easily calculated mode I/II ratio by simple stress analysis.

The presented invention also provides an easy set up and compact test apparatus for an easy test procedure.

This invention provides an innovative methodology for computation of the test data, allowing obtaining values for toughness characterization with little effort using the system compliance.

The apparatus provides the values for the displacements of each beam of the specimen test, avoiding measuring the crack length.

The embodiment of the presented test apparatus (FIG. 1) includes a base (11) fastened to an adaptor (12) to a universal testing machine, facing down, and upwards fastened to a beam (10) with fourteen holes that is connected by a pin to two vertical arms (8 and 32) that connects to another fourteen holes beam (7) pivoting in the middle towards another two arms (4 and 30) connected by means of another pin and at the extremity connected to a H shaped specimen grip (16) with another pin (15). The two arms (4 and 30) where the beam pivots are connected at the top to another nine hole beam (2) that is connected with another pin in the middle span to the universal testing machine load cell by means of a threaded cylinder which is the upper universal testing machine connector (1) and at the other extremity is connected to another H shaped specimen grip (18). The specimen (17) is a common DCB as specified in the ASTM D3433-99 [7], connected to the low and up H shaped specimen grip (16 and 18) with two calibrated pins (18 and 24) which are in close contact with two LVDTs supported by a fixer (20) fastened to a

vertical threaded rod (25) connected to the base with a nut and a washer. The DCB specimen is also supported at the other end by a wedge beam (6) connected to two vertical threaded rods (5 and 31) which are connected to the base with nuts and washers. Two vertical threaded rods (13 and 25) connected to the base with nuts and washers, supports another wedge beam (29) in close contact with the specimen. This two wedge beams (6 and 29) provides a fixture for the DCB specimen.

## Brief description of the drawings

- FIG. 1 is a schematic illustration of a first embodiment of the present invention;
- FIG 2 is a schematic illustration of the apparatus geometric variables, leading to different loading possibilities;
- FIG 3 (a) is a schematic illustration showing mixed mode bending specimen loading with formulae for the two loads loading the specimen upper (F1) and lower beams (F2);
- FIG 3 (b) is a schematic illustration of mode I and formulae for the mode I component of loading;
- FIG 3 (c) is a schematic illustration of mode II and formulae for the mode II component of loading;
- FIG. 4 (a) is a plot from a finite element analysis of the apparatus done with Solidworks<sup>®</sup> for a predominant mode I loading;
- FIG. 4 (b) is a plot from a finite element analysis of the apparatus done with Solidworks® for a predominant mode II loading;
- FIG. 5 is a schematic illustration for the numerical model done with ABAQUS® showing the specimen's mesh and a mesh detail;
- FIG. 6 shows the fracture envelop  $G_{\rm I} G_{\rm II}$  resulting from numerical analysis done with a model in ABAOUS<sup>®</sup> for a linear and a quadratic criterion.

### **Detailed description of the preferred embodiments**

The test apparatus shown in FIG 1 is composed by three horizontal beams with holes (2, 7 and 10), four vertical arms (4, 8, 30 and 32), a connector to the universal testing machine (1) load cell and two H shaped specimen connectors (16 and 19) loading each beam of the specimen (17), connected by pins. The vertical arms (4,8,30 and 32) and the universal testing machine connector (1) are connected to the holed horizontal beams (2, 7 and 10) with pins (15) easily interchangeable allowing to vary the relative distances between them, as shown in FIG 2 (S1, S2, S3 and S4). The holed horizontal beam at the bottom (10) is firmly connected to the apparatus base (11) with 3 fasteners (14), preventing pivoting unlike the other two holed horizontal beams (2 and 7) which can pivot by the connection pins. Both holed horizontal

beams (2 and 7) are connected to the specimen (17) by two H shaped connectors (16 and 19) transferring the load by two pins (18 and 24) which are in close contact with the LVDTs (21 and 22) sensing rods allowing to measure the displacement for each specimen (17) beam. LVDT (21) registers the specimen's upper beam displacement ( $\delta_1$ ) while LVDT (22) registers the specimen's lower beam displacement ( $\delta_2$ ). The connector to the universal testing machine (1) transfers the load of the apparatus to the load cell registering the load (F), while the other adaptor (12) facing down from the apparatus base (11) connects to the universal testing machine actuator recording the imposed displacement to the apparatus (δ). The load-displacement curve is obtained, combining these two registered values (F and  $\delta$ ). The adaptor (12) to the universal testing machine is connected to the apparatus base (11) with 4 fasteners (27). The apparatus base (11) has two lateral guides (9) providing fixture for the nuts (28) that connects the vertical threaded rods (5, 13, 25 and 31) using washers. The two vertical threaded rods (5 and 31) are connected with nuts to the wedge beam (6) that is in contact with the lower specimen's surface, supporting it. The two other vertical rods (13 and 25) are connected with nuts to the wedge beam (29) that is in abutment with the upper specimen's surface. Moving these vertical threaded rods (5, 13, 25 and 31) changes the relative distances  $L_1$  and  $2L-L_1$  as shown in FIG. 2. Moving the pins along the holes of the horizontal holed beams (2, 7 and 10) changes the relative position of the vertical arms (4 and 8) altering the  $s_2$ ,  $s_3$  and  $s_4$  dimensions of FIG. 2. Using the same pin relocation for the upper universal testing machine connector (1) along the holes of the horizontal holed beam (2) modifies the  $s_1$  and  $s_2$  dimensions shown in FIG. 2. The H shaped specimen connectors (16 and 19) can also be displaced along the horizontal holed beams (2 and 7) by moving the pins and modifying the  $s_1$ ,  $s_4$  and also the  $L_1$  and  $2L-L_1$  dimensions in FIG. 2. When the apparatus is loaded by the universal testing machine the specimen beams are loaded with the loads  $F_1$  and  $F_2$  as shown in FIG. 3 (a) showing also the equations to obtain these loads from the geometric conditions  $s_1$ ,  $s_2$ ,  $s_3$  and  $s_4$  applied through load F which were developed by Fernlund and Spelt [1]. This combination of loads together with the imprisonment given by the two wedge beams (6 and 29) from FIG. 1 promotes the mode ratio between mode I and mode II loading. FIG. 3 (b) shows the mode I loading components obtained from the loads  $F_1$  and  $F_2$  and the respective equations. FIG. 3 (c) shows the mode II loading components obtained from loads  $F_1$  and  $F_2$  and the respective equations. The displacement for mode I  $(\delta_1)$  is also shown in FIG. 3 (b) with the equation using the displacements registered with the LVDTs (21 and 22) from FIG. 1, which are also used to calculate the displacement for mode II ( $\delta_2$ ) as shown in FIG. 3 (c). The base (11) and guides (9) are made of construction steel, while the other parts, like the horizontal holed beams (2, 7 and 10), the vertical arms (4, 8, 30 and 32), the H shaped specimen connectors (16 and 19), the wedge beams (6 and 29) and both the universal testing machine connectors (1 and 12) are made of high grade steel, providing a higher strength when compared

to the tested specimen (17). Pins, fasteners, nuts, washers and the threaded rods are standard parts. The apparatus was designed with FEA to optimize the assembly stiffness for a maximum load of 20 kN as shown in FIG. 4 (a) for a predominant mode I loading and in FIG. 4 (b) for a predominant mode II loading. Each part was also optimized with FEA, in order to obtain the best performance. The specimen is a DCB with two beams bonded together with a structural adhesive, as defined by ASTM D3433 – 99 [7].

FIG. 3 (a) shows the specimen loading of each beam (upper and lower) in terms of the applied load F and the dimensions  $s_1$ ,  $s_2$ ,  $s_3$  and  $s_4$ , defined by the relative position between the upper universal testing machine connector (1), the H shaped specimen connectors (16 and 19) and the vertical arms (4, 8, 30 and 32). As shown in FIG. 3 (b) the mode I component of this loading is:

$$P_{1} = \frac{F_{1} - F_{2}}{2}$$
 (Eq.1.)

and the mode I component of the displacement is:

$$\delta_1 = \delta_1 - \delta_2 \tag{Eq.2.}$$

Toughness is usually expressed in terms of the critical value of strain release rate (G) for the test specimen when the specimen loading causes the crack growth.

The components of the strain energy release rate can be determined by means of the Irwin-Kies equation [8]:

$$G = \frac{P^2}{2R} \frac{dC}{da}$$
 (Eq.3.)

The compliance based beam (CBBM) [9] theory applied to this test, leads to:

$$G_{\rm I} = \frac{6P_{\rm I}^2}{B^2h} \left( \frac{2a_{\rm eI}^2}{h^2E} + \frac{1}{5G} \right)$$
 (Eq.4.)

where  $G_1$  is the mode I strain energy release rate,  $P_1$  is the mode I load, B is the specimen width, h is the specimen half-thickness, E is the adherend Young's modulus and G is the adherend

shear modulus. The equivalent crack length  $a_{\rm el}$  is obtained solving the mode I compliance cubic equation:

$$C_{\rm I} = \frac{\delta_{\rm I}}{P_{\rm I}} = \frac{8a^3}{Bh^3E} + \frac{12a}{5BhG}$$
 (Eq.5.)

that can be written in the following way

$$\alpha a_{\rm el}^3 + \beta a_{\rm el} + \gamma = 0 \tag{Eq.6.}$$

where

$$\alpha = \frac{8}{Bh^3E}; \quad \beta = \frac{12}{5BhG}; \quad \gamma = -C_1$$
 (Eq.7.)

Using Matlab® software and only keeping the real solution, one obtains

$$a_{\rm el} = \frac{1}{6\alpha} A - \frac{2\beta}{A}$$
 (Eq.8.)

where

$$A = \left( \left( -108\gamma + 12\sqrt{3\left(\frac{4\beta^3 + 27\gamma^2\alpha}{\alpha}\right)} \right) \alpha^2 \right)^{\frac{1}{3}}$$
 (Eq.9.)

FIG. 3(c) shows the mode II portion of the specimen loading, to be:

$$P_{II} = F_1 + F_2$$
 (Eq.10.)

and the mode II component of the displacement is:

$$\delta_{\text{II}} = \frac{\delta_1 + \delta_2}{2} \tag{Eq.11.}$$

Following the same compliance based beam theory as defined by de Moura et al. [10], the strain energy release rate for mode II is given by:

$$G_{\rm II} = \frac{9P_{\rm II}^2 a_{\rm eII}^2}{4B^2 h^3 E}$$
 (Eq.12.)

where  $P_{\text{II}}$  is the mode II load, B is the specimen width, h is the specimen half-thickness, E is the adherend Young's modulus and G is the adherend shear modulus. The equivalent crack length  $a_{\text{eII}}$  is obtained solving the mode II compliance equation:

$$C_{II} = \frac{\delta_{II}}{P_{II}} = \frac{3a^3 + 2LL_1^2}{2Bh^3E} + \frac{6LL_1}{5BhG(2L - L_1)}$$
 (Eq.13.)

and is given by:

$$a_{\text{eII}} = \left[ \left( C_{\text{II}} - \frac{6LL_1}{5BhG(2L - L_1)} \right) \frac{2Bh^3E}{3} - \frac{2LL_1^2}{3} \right]^{1/3}$$
 (Eq.14.)

Equations 1 to 14 define a data reduction scheme (FIG. 7) that is a novelty, and is proposed after numerical validation done with a model simulation using ABAQUS® software. The loading device was simulated by a combination of rigid beams and links that reproduce the experimental setup. The specimen was modeled with 3600 plane strain 8-node quadrilateral elements and 280 6-node interface elements with null thickness placed at the mid-plane of the bonded specimen as shown in FIG. 5. The interface elements include a cohesive zone mixed-mode I+II damage model to simulate damage onset and propagation within the adhesive. The cohesive zone model establishes a relationship between stresses and relative displacements between specimen arms. The behaviour of the adhesive is integrated in the cohesive damage law considered. Cohesive properties of the adhesive and the specimen's beam elastic properties are shown in Table 1. This model is based in the work of de Moura et al. [11].

Table 1. Elastic and cohesive properties.

Elastic prope	erties (Steel)	Cohesive properties (Adhesive)					
Е	G	$\sigma_{\!\!\scriptscriptstyle  m u,I}$	$\sigma_{\!\scriptscriptstyle  m u,II}$	$G_{ m Ic}$	$G_{ m IIc}$	$\delta_{2,\mathrm{I}}$	$\delta_{2, ext{II}}$
(GPa)	(GPa)	(MPa)	(MPa)	(N/mm)	(N/mm)	(mm)	(mm)
210	80.77	23	23	0.6	1.2	0.0187	0.2062

Two energetic criteria were programed in order to obtain the envelopes for:

the linear energetic criterion

$$\left(\frac{G_{\rm I}}{G_{\rm Ic}}\right) + \left(\frac{G_{\rm II}}{G_{\rm IIc}}\right) = 1 \tag{Eq.15.}$$

 $\bullet$   $\bullet$   $\bullet$ 

and the quadratic energetic criterion

$$\left(\frac{G_{\rm I}}{G_{\rm Ic}}\right)^2 + \left(\frac{G_{\rm II}}{G_{\rm IIc}}\right)^2 = 1 \tag{Eq.16.}$$

Seven scenarios were considered in the  $G_{I}$ - $G_{II}$  space, including the pure mode cases as shown in Table 2. The mode mixity between different scenarios was changed by altering the distances  $s_{I}$ - $s_{4}$  by moving the pins of the vertical arms (4,8, 30 and 32), the upper universal testing machine connector (1) and the H shaped specimen connectors (16 and 19) as shown in FIG. 2.

Table 2. Different scenarios used for the fracture envelope calculation.

	Jig arrangement					
Scenarios	<i>s</i> <sub>1</sub> (mm)	<i>s</i> <sub>2</sub> (mm)	s <sub>3</sub> (mm)	s <sub>4</sub> (mm)		
P1	100	40	140	-60		
P2	120	40	160	-120		
Р3	40	120	160	40		
P4	60	80	140	60		
P5	60	80	140	120		
P6	40	40	80	100		
P7	100	40	140	80		

FIG. 6 shows a good agreement obtained for both criteria demonstrating that the proposed model can be applied with success as a straightforward data reduction scheme (FIG. 7) for the present mixed-mode I+II fracture characterization test.

The many features and advantages of the present invention are apparent from the detail specification, and, thus, it is intended by the appended claims to cover all such features and advantages of this apparatus and method which fall within the true spirit and scope of the invention. Further, since numerous modifications and changes will readily occur to those skilled in the art based upon the disclosure herein, it is not desired to limit the invention to the exact configuration construction and operations illustrated and described. Accordingly, all suitable modifications and equivalents may be resorted to falling within the scope and the spirit of the invention.

What is claimed is:

1. An apparatus for testing a DCB specimen with two bonded beams with a structural adhesive, comprised of:

a lower connector to a universal testing machine fastened to the base;

a base having two guides and opposite ends;

a first holed horizontal beam fastened to the base;

two first vertical arms connecting the first horizontal holed beam to a second holed horizontal beam using two pins, one for the first horizontal holed beam and another for the second horizontal holed beam;

a second horizontal holed beam connected to the previous vertical arms and two second vertical arms connecting to third holed horizontal beam where it can pivots by two pins;

two second vertical arms connecting to the third holed horizontal holed beam with a pin;

a third horizontal holed beam connected to the previous vertical arms and to the upper connector to a universal testing machine by a pin;

a lower H shaped specimen connector linked to the second horizontal holed beam by a pin;

an upper H shaped specimen connector linked to the third horizontal holed beam by a pin;

four threaded rods connected to the base with nuts and washers, and holding two wedge beams for specimen fixture;

two wedge beams for specimen fixture connected to the previous four threaded rods using nuts;

two threaded rods connected to the base with nuts and washers, holding two fixtures for the LVDTs;

two LVDTs fixtures fastened to the threaded rods;

two LVDTs hold by two fixtures fastened to the threaded rods and touching two pins connecting to the specimen beams;

2 steel pins loading the specimen upper and lower beams, connecting to the H shaped specimen connectors;

7 steel pins which transfer the loads connecting the different apparatus parts;

7 fasteners;

12 nuts:

- 2. An apparatus according to claim 1, wherein the upper H shaped specimen connector at an  $s_1$  distance from load F, transfers the load to the upper specimen beam at the first end hole by a pin.
- 3. An apparatus according to claim 1, wherein the lower H shaped specimen connector at an  $s_4$  distance from the second vertical arm, transfers the load to the lower specimen beam at the first end hole by a pin.
- 4. An apparatus according to claim 1, wherein the third horizontal holed beam pivots in three pins, the first one is connected to the upper H shaped specimen connector at one end, another pivoting pin is located in between the two ends and connects to the upper universal testing machine connector, and the third one pivoting at the second vertical arms at the other end of the beam.
- 5. An apparatus according to claim 1, wherein the second horizontal holed beam pivots in three pins, the first one is connected to the lower H shaped specimen connector at one end, another pivoting pin is located in between the two ends and connects to the second vertical arms, and the third one pivoting at the third vertical arms at the other end of the beam.
- 6. An apparatus according to claim 1, wherein the wedge beams supported by threaded rods provide fixture to the test specimen.
- 7. An apparatus according to claim 1, wherein the left side LVDT is connected to the specimen's connecting pin registering the upper beam displacement.
- 8. An apparatus according to claim 1, wherein the right side LVDT is connected to the specimen's connecting pin registering the lower beam displacement.
- 9. An apparatus according to claim 1, wherein the first vertical arm is positionally adjustable along the first and second horizontal holed beam.
- 10. An apparatus according to claim 1, wherein the second vertical arm is positionally adjustable along the second and third horizontal holed beam.
- 11. An apparatus according to claim 1, wherein the lower H shaped specimen connector is positionally adjustable along the second horizontal holed beam.
- 12. An apparatus according to claim 1, wherein the upper H shaped specimen connector is positionally adjustable along the third horizontal holed beam.

- 13. An apparatus according to claim 1, wherein the upper universal test machine connector is positionally adjustable along the third horizontal holed beam.
- 14. An apparatus according to claim 1, wherein the threaded rods are positionally adjustable along the base.
- 15. A mixed-mode method for testing a DCB specimen with two bonded beams with an adhesive for the joint fracture comprising:
  - placing the specimen in between the two fixtures provided by the wedge beams;
  - connecting the superior specimen beam to the upper H shaped specimen connector by means of a pin;
  - connecting the inferior specimen beam to the lower H shaped specimen connector by means of another pin;
  - connect the H shaped specimens connectors (upper and lower) to the third and second horizontal holed beams with pins;
  - connect the third horizontal beam to the upper universal test machine connector (transferring the load to the load cell) with a pin;
  - connect the third horizontal holed beam to the second horizontal beam with two vertical arms and a pin;
  - connect the second horizontal holed beam to the second two vertical arms with a pin;
  - connect the second horizontal holed beam to the first horizontal holed beam fastened to the base with two vertical arms with a pin;
  - applying a displacement to the apparatus by moving the set-up downwards using the universal test machine actuator, will apply a load to both specimen beams related with the transferred load to the load cell by the upper universal test machine connector;
  - registering the displacement occurred at both specimen beams with the LVDTs.
- 16. A method according to claims 9 to 13, further comprising the dimensions  $s_1$ ,  $s_2$ ,  $s_3$  and  $s_4$  to vary the ratio of opening and shear stress.
- 17. A method of determining the envelop fracture toughness  $G_{\rm I}$  vs.  $G_{\rm II}$  of a bonded specimen comprising the steps of:
  - providing a DCB specimen composed of two beams bonded together with adhesive;
  - applying a mixed ratio opening and shear loading to the specimen;
  - measuring the load with the universal test machine load cell and also the machine's actuator displacement.
  - measuring the displacements of each specimen beam with two LVDTs;
  - calculating the mode I and mode II stress release rate energies  $G_{\rm I}$  and  $G_{\rm II}$  from the computation of the registered load and displacements.

18. A method for the calculation of the mode I and mode II strain energy release rates  $G_{\rm I}$  and  $G_{\rm II}$  using a spreadsheet implementing a proposed data reduction scheme.

#### References

- [1] G. Fernlund, J.K. Spelt, Composites Science and Technology, 50 (1994) 441-449.
- [2] V. Richter-Trummer, E.A. Marques, F.J.P. Chaves, J.M.R.S. Tavares, L.F.M. da Silva, P.M.S.T. de Castro, Materialwissenschaft und Werkstofftechnik, 42 (2011) 452-459.
- [3] M.F.S.F. de Moura, R.D.S.G. Campilho, J.P.M. Gonçalves, Composites Science and Technology, 68 (2008) 2224-2230.
- [4] J.Y. Cognard, P. Davies, B. Gineste, L. Sohier, Composites Science and Technology, 65 (2005) 359-368.
- [5] D.A. Dillard, H.K. Singh, S. Park, D. Ohanehi, M.A. McGaw, in: SEM Annual Conference & Exposition on Experimental and Applied Mechanics, Society for Experimental Mechanics, Inc., St. Louis, 2006.
- [6] D.A. Dillard, H.K. Singh, D.J. Pohlit, J.M. Starbuck, Journal of Adhesion Science and Technology, 23 (2009) 1515-1530.
- [7] ASTM D3433 99, in: Annual book of ASTM standards, West Conshohocken, ASTM 15.06, 2012, pp. 225-231.
- [8] G.R. Irwin, J.A. Kies, Welding Journal Research Supplement, 33 (1954) 193-198.
- [9] J.M.Q. Oliveira, M.F.S.F. de Moura, M.A.L. Silva, J.J.L. Morais, Composites Science and Technology, 67 (2007) 1764-1771.
- [10] M. de Moura, Journal of Adhesion Science and Technology, 20 (2006) 37-52.
- [11] M.F.S.F. De Moura, J.P.M. Gonçalves, J.A.G. Chousal, R.D.S.G. Campilho, International Journal of Adhesion and Adhesives, 28 (2008) 419-426.

# MIXED MODE I+II FRACTURE CHARACTERIZATION OF BONDED JOINTS (EXPERIMENTAL)

# Mixed-mode I+II fracture characterization of bonded joints using a multi mode apparatus

Filipe J.P. Chaves<sup>1</sup>, L.F.M. da Silva<sup>2</sup>, M.F.S.F. de Moura<sup>2</sup>, David A. Dillard<sup>3</sup>, J.O. Fonseca<sup>4</sup>

<sup>1</sup>IDMEC- Pólo FEUP, Faculdade de Engenharia da Universidade do Porto, Rua Dr. Roberto Frias, 4200-465 Porto, Portugal

<sup>2</sup>DEMec,Faculdade de Engenharia da Universidade do Porto, Rua Dr. Roberto Frias, 4200-465 Porto, Portugal

<sup>3</sup>Engineering Science and Mechanics Department, Virginia Tech, Blacksburg, VA 24061

#### Abstract

The present work presents the experimental test results to assess the toughness of an adhesive joint, using a previously defined crack equivalent data reduction scheme applied to a new multi-mode apparatus, inspired in a load jig previously developed by Fernlund and Spelt. The jig allows for easy alteration of the mode-mixity and permits covering the full range of mixed-mode I+II combinations. A data reduction scheme based on specimen compliance, beam theory and crack equivalent concept is used to overcome several difficulties inherent to the test analysis. The method assumes that the performed test can be viewed as a combination of the double cantilever beam and asymmetrically loaded end-notched flexure tests, which provide modes I and II fracture characterization, respectively. A numerical analysis including a cohesive mixed-mode I+II damage model was performed considering different mixed-mode loading conditions to validate the proposed data reduction scheme. Issues regarding self-similar crack growth and fracture process zone development are discussed. It was verified that the considered in-plane mix mode fracture criterion is well captured using the proposed data reduction scheme.

**Keywords**: Bonded joints, fracture characterization, mixed-mode I+II loading, compliance-based beam method.

#### 1. Introduction

Bonded joints are being increasingly applied in structures for aeronautical, automotive, and civil infrastructure industries. In the presence of singularities which occur frequently in bonded joints, the classical strength prediction based on stress or strain analysis may not be suitable. Instead, the development of sophisticated design criteria including progressive damage analysis is of fundamental importance. The characterization of the joint under mixed-mode loading is fundamental for the fracture mechanics-based criteria, since bonded joints in real applications often experience such situations. A crack or debond within an adhesive joint usually propagates in a predefined plane (thin adhesive layer), independent of the general loading, which induces mixed-mode loading conditions. Therefore, the development of expedited procedures to perform mixed-mode I+II fracture characterization of bonded joints becomes a fundamental issue.

Several tests proposed in the literature can be applied to fracture characterization of bonded joints under mixed-mode I+II loading [1]. Some of these are limited in the range of possible variation of mode mixity, which means that a complete description of the fracture envelop under mixed-mode I+II loading is not possible in such a configuration. This is the case of the asymmetric double cantilever beam (ADCB), the single leg bending (SLB) and the cracked lap shear (CLS) [2]. Nevertheless, there are alternatives that overcome this drawback. This is the case of the mixed-mode bending (MMB) test [3], which can be viewed as a combination of the double cantilever beam (DCB) and end-notched flexure (ENF) tests frequently used for fracture characterization under pure mode I and II loading, respectively. This test allows a large range of mode mixities and an easy alteration of the mode mixity by changing the lever length of the loading arm. However, a special apparatus with considerable dimensions is required, especially for fracture characterization of bonded joints with stiff adherends [4, 5]. Sørensen et al.[6] proposed the DCB specimen loaded by bending moments at the two free beams by means of a special device specially conceived. The mode mixity of the applied loading can be varied altering the ratio between the two applied moments. Högberg and Stigh [7] proposed the mixed mode double cantilever beam specimen based on the geometry of a semi-infinite symmetric DCB specimen. The specimen is loaded by a pair of selfbalancing forces whose orientation can vary to alter the mode mixity. Singh et al., [8], have proposed the dual actuator load (DAL) method, which can be viewed as a DCB test subjected to non-symmetric loading. Two independent hydraulic actuators load the

arms of a standard DCB specimen clamped at the other extremity. This test allows easy variation of the mode mixity by applying different displacement rates or loads to the specimen arms by means of the two independent hydraulic actuators [9, 10]. Fernlund and Spelt [11] proposed a special jig which allows mixed-mode fracture testing of adhesive joints and composite laminates over the entire range of mode mix using a standard DCB specimen. The authors used elementary beam theory as a data reduction scheme, which requires monitoring the crack extension during propagation. This task is not easy to be accomplished with the required accuracy, especially in cases when mode II loading predominates, which does not occur in mode I predominant tests, where crack tip is opened, thus facilitating the identification of the tip.

The objective of this work is to propose a simple and expedited test methodology for the evaluation of adhesive joints mixed-mode fracture. The method is based on specimen compliance, beam theory and crack equivalent concept and is proposed to overcome some difficulties inherent to the test analysis, namely crack length monitoring during its growth. A patent has been submitted describing in detail the apparatus and the data reduction technique to obtain the strain energy release rate in mode I and mode II. Here the technique is briefly described and results are presented for a structural epoxy adhesive. The test is validated numerically by means of a detailed numerical analysis using cohesive mixed-mode I+II zone modeling. The resulting fracture envelope is compared with the linear mixed-mode I+II fracture criterion.

#### 2. Loading jig

The proposed loading jig is a test apparatus to apply simultaneously opening and shear stress in a test specimen to determine the fracture mechanics properties of the adhesive joint. This apparatus applies mode I and mode II loads to a test specimen (adhesive joint) while measuring the displacement of each beam and applied load, allowing to measure its strength. This test provides a variation for the mode I/II ratio over a broad range of the fracture envelop.

The loading jig is fully described in Patent [12] and is an improvement inspired in the apparatus proposed by Fernlund and Spelt [11] consisting primarily of two rigid beams linked to each other, to the specimen, and to a base plate (Figure 1). Different jig geometries can be achieved by altering the four distances,  $s_1 - s_4$ , thereby varying the mode-mixity of the induced loading. Changing the above referred distances leads to

different loads,  $F_1$  and  $F_2$ , applied to the upper and lower adherends, respectively, of the tested specimens (Figure 2). Pure mode tests, namely the DCB for mode I and the ENF for mode II, are also available to perform with this apparatus, proving to be versatile in the context of fracture characterization.

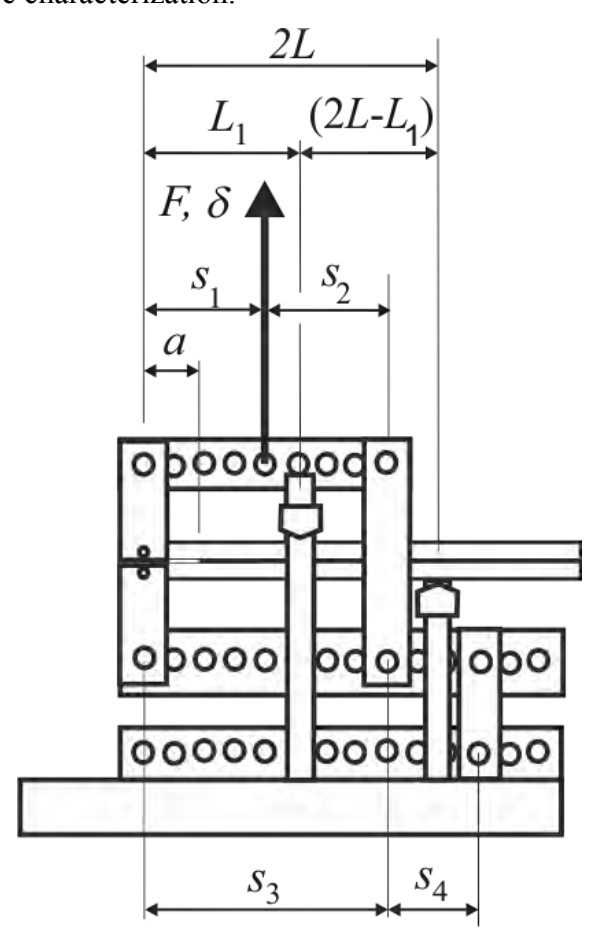


Figure 1. Load jig schematics.

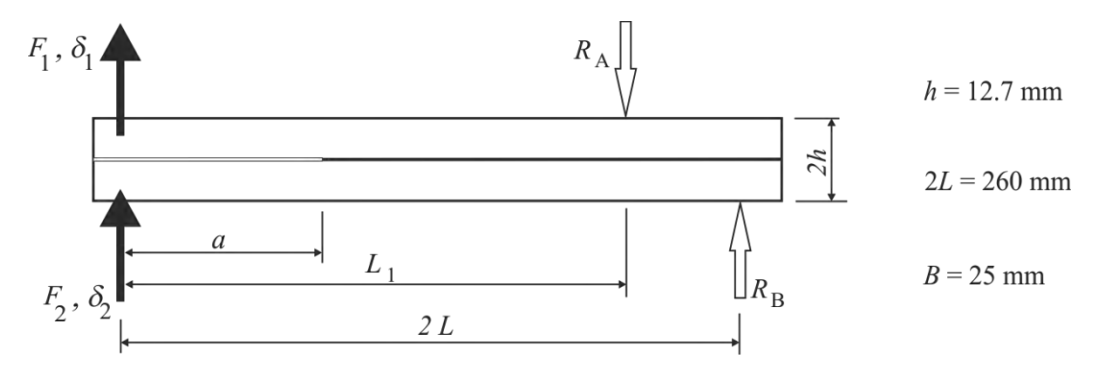


Figure 2. Schematic representation of specimen loading and dimensions (*B* is the specimen width).

• • • •

# 2.1 - Test procedure

The proposed apparatus is fixed into an universal testing machine (UTS) and two linear variable differential transformers (LVDTs) are also set up in place and connected to the UTS data acquisition system. One end of the DCB specimen is connected to the apparatus with two pins that contact with the LVDT measuring rod to measure de displacement of each beam,  $\delta_1$  and  $\delta_2$ . The specimen must be levelled adjusting the back support (wedge beam) that will define the 2L dimension.

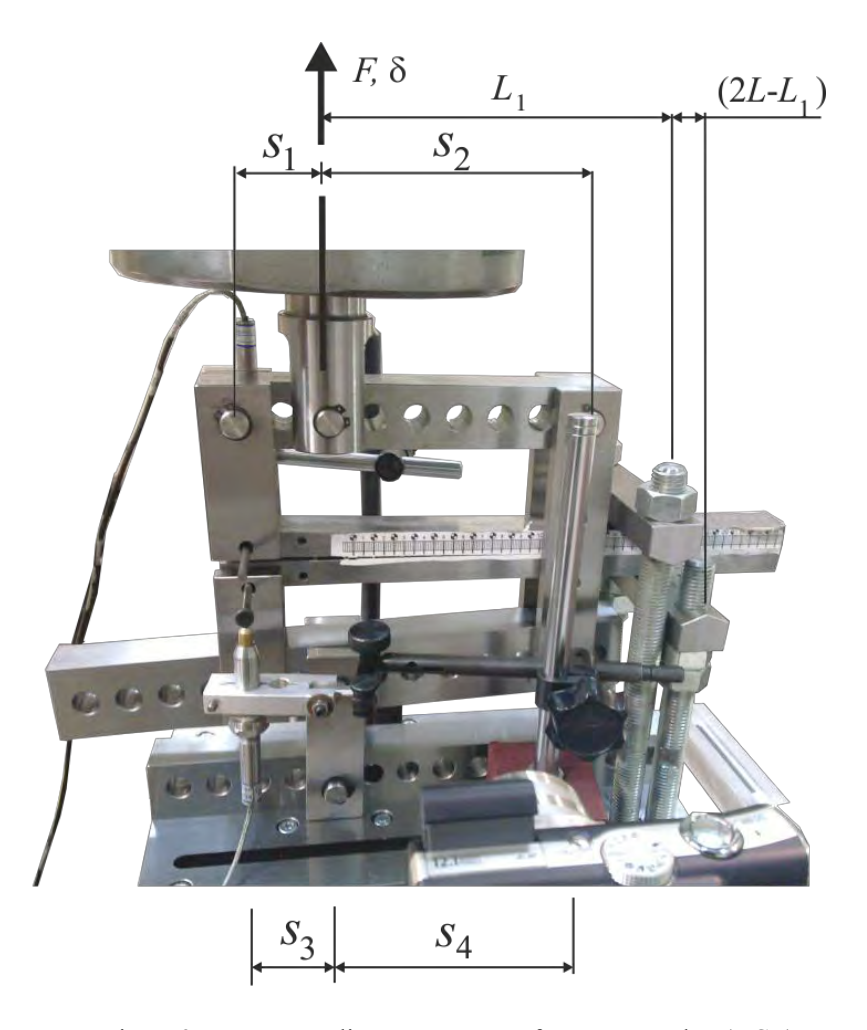


Figure 3. Loading apparatus set for a pure mode I (DCB) test.

# 2.2 Specimens

The specimens were manufactured with high grade steel (Table 1). The surface preparation consisted in sandblasting and cleaning with acetone. A mould with pins was

used to guarantee alignment of the lower and upper beams (Figure 4 b). A pre-crack was made using a razor blade within the spacers used to obtain a constant bondline thickness of 0.2 mm (Figure 4 a). After adhesive application on the substrates, the joints were cured in a hot press at a constant pressure and temperature (Figure 4 c). After curing, the remaining adhesive that overflows was carefully removed and a paper ruler was bonded to the sides of the joint for crack measurement.

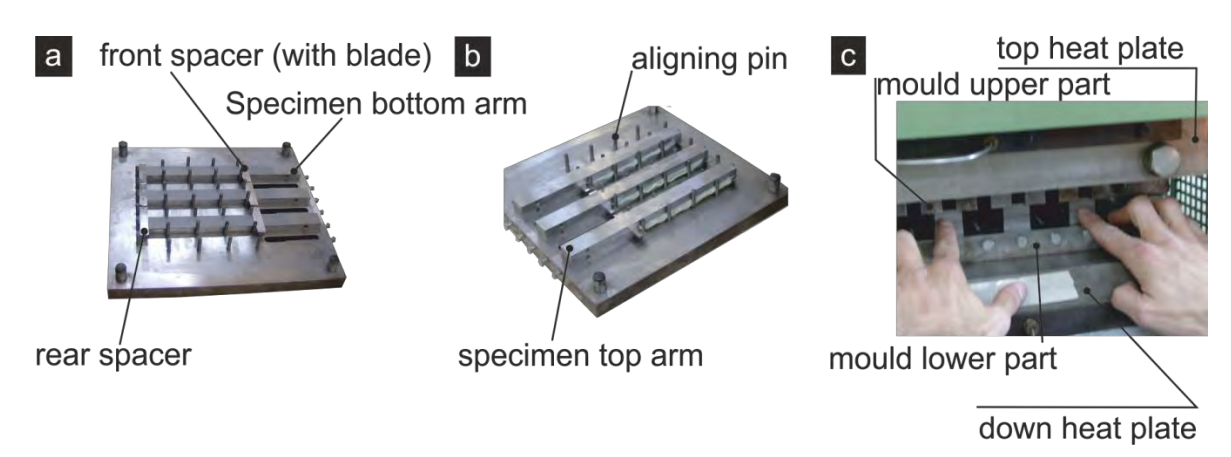


Figure 4. Specimen manufacture using a mould and heated plates press

Table 1. Steel specimen properties.

Elastic properties (Steel)		Hardness	Code
E (GPa)	G (MPa)	(HB)	DIN
210	80.77	270-350	40 CrMnMo 7

The specimen geometry is in accordance with the ASTM D3433-99 [13], as shown in Figure 2.

A ductile epoxy adhesive, Araldite<sup>®</sup> 2015 (Huntsman) was used. This adhesive was already characterized in previous studies [1, 14]. The stress-strain curve is shown in Figure 5 and critical energy release rate in mode I and mode II are given in Table 2.

30 - 25 - 20 - 15 - 10 - 5 - 0 0 0.01 0.02 0.03 0.04 0.05 0.06  $\varepsilon$ 

Figure 5.  $\sigma$ – $\varepsilon$  curves of the Araldite<sup>®</sup> 2015.

Table 2. Critical energy release rate values for pure mode I and II for each adhesive and bondline thicknesses [1, 14].

	$G_{\rm Ic}$ (N/mm)	$G_{\mathrm{IIc}}\left(\mathrm{N/mm}\right)$
Araldite® 2015	0.43	4.7

#### 2.3 - Data Reduction Scheme

The classical data reduction schemes based on compliance calibration and beam theories are based on crack length monitoring during its propagation. However, there are two limitations related to this aspect. In fact, this task is not easy to be accomplished with the required accuracy namely in cases where mode II loading predominate, since the crack faces remain in contact during its propagation. The second limitation is related to the energy dissipation at the fracture process zone (FPZ) ahead of the crack tip, which can be non-negligible as is the case of adhesives with some inelastic behaviour. The consideration of the clear crack length (not including the influence of the FPZ size), as a fracture parameter in beam theory equations does not allow accounting for this energy. An alternative procedure based on an equivalent crack concept can be used with remarkable advantages. The proposed method [15] is based on Timoshenko beam theory and uses the current specimen compliance to estimate an equivalent crack during the test. Using the Timoshenko beam theory, the strain energy of the specimen (Figure 2) due to bending and including shear effects is

$$U = \int_{0}^{a} \frac{M_{1}^{2}}{2EI_{1}} dx + \int_{0}^{a} \frac{M_{2}^{2}}{2EI_{2}} dx + \int_{a}^{L_{1}} \frac{M_{T_{(a \to L_{1})}}^{2}}{2EI_{T}} dx + \int_{L_{1}}^{2L} \frac{M_{T_{(L_{1} \to 2L)}}^{2}}{2EI_{T}} dx + \int_{L_{2}}^{a} \frac{M_{T_{(L_{1} \to 2L)}}^{2}}{2EI_{T}} dx + \int_{a}^{a} \int_{-h/2}^{h/2} \frac{\tau_{1}^{2}}{2G} B \, dy dx + \int_{0}^{a} \int_{-h/2}^{h/2} \frac{\tau_{2}^{2}}{2G} B \, dy dx + \int_{a}^{L_{1}} \int_{-h}^{h} \frac{\tau_{T_{(a \to L_{1})}}^{2}}{2G} B \, dy dx + \int_{L_{1}}^{L_{1}} \int_{-h}^{h} \frac{\tau_{T_{(L_{1} \to 2L)}}^{2}}{2G} B \, dy dx$$
 (1)

where M is the bending moment, the subscripts 1 and 2 stand for upper and lower adherends and T refers to the total bonded beam (of thickness 2h), E and G are the longitudinal and shear modulus, respectively, B is the specimen and bond width and I is the second moment of area of the indicated section. For adherends with the same thickness, as considered in this analysis,  $I_T = 8I_1 = 8I_2$ . The shear stresses induced by transverse loading of beams are given by

$$\tau = \frac{3}{2} \frac{V}{Bh} \left( 1 - \frac{y^2}{c^2} \right) \tag{2}$$

The parameters c and V represent, respectively, the beam half-thickness and the transverse load, on each arm for  $0 \le x \le a$ , and on total bonded beam for  $a \le x \le 2L$ .

Using the Castigliano's theorem ( $\delta = \partial U/\partial P$ , where P is the applied load and  $\delta$  the resulting displacement at the same point) the displacements of the specimen arms at the loaded extremities can be written as

$$\delta_{1} = \frac{\partial U}{\partial F_{1}} = \frac{4\left[a^{3}F_{1} + \frac{(F_{1} + F_{2})(2LL_{1}^{2} - a^{3})}{8}\right]}{Bh^{3}E} + \frac{3\left[2aF_{1} + (F_{1} + F_{2})\left(L_{1} - a + \frac{L_{1}^{2}}{2L - L_{1}}\right)\right]}{5BhG}$$

$$\delta_{2} = \frac{\partial U}{\partial F_{2}} = \frac{4\left[a^{3}F_{2} + \frac{(F_{1} + F_{2})(2LL_{1}^{2} - a^{3})}{8}\right]}{Bh^{3}E} + \frac{3\left[2aF_{2} + (F_{1} + F_{2})\left(L_{1} - a + \frac{L_{1}^{2}}{2L - L_{1}}\right)\right]}{5BhG}$$

$$(3)$$

The present test induces a combination of opening and shear loading applied to the specimen that can be partitioned in order to get the components corresponding to mode I and mode II solicitations. The mode I component is induced by an opening loading

and mode II will result from longitudinal sliding at the crack tip. Consequently, the partitioning method complies with those objectives (Figure 6). The mode I loading reflects the DCB specimen and the mode II can be viewed as the ENF loaded asymmetrically. It should be noted that the ENF is a three-point bending test loaded at the mid-span. From Figure 6 the following relations can be obtained

$$F_{1} = P_{I} + \frac{P_{II}}{2}; \quad F_{2} = -P_{I} + \frac{P_{II}}{2}$$

$$\delta_{1} = \frac{\delta_{I}}{2} + \delta_{II}; \quad \delta_{2} = -\frac{\delta_{I}}{2} + \delta_{II}$$
(4)

The corresponding pure modes (I and II) loading and displacement components become

$$P_{\mathrm{I}} = \frac{F_{1} - F_{2}}{2}; \quad \delta_{\mathrm{I}} = \delta_{1} - \delta_{2}$$

$$P_{\mathrm{II}} = F_{1} + F_{2}; \quad \delta_{\mathrm{II}} = \frac{\delta_{1} + \delta_{2}}{2}$$
(5)

Combining Equations (3 and 5), the pure mode compliances can be obtained

$$C_{\rm I} = \frac{\delta_{\rm I}}{P_{\rm I}} = \frac{8a^3}{Bh^3E} + \frac{12a}{5BhG} \tag{6}$$

$$C_{II} = \frac{\delta_{II}}{P_{II}} = \frac{3a^3 + 2LL_1^2}{2Bh^3E} + \frac{6LL_1}{5BhG(2L - L_1)}$$
(7)

As expected, Equation (6) is equal to that obtained for a DCB [16] and Equation (7) is compatible with results for an ENF specimen [17] when  $L_1$ =L, i.e., where the specimen is loaded at its mid-span. This achievement is quite interesting, as it allows the use of simple equations to obtain the strain energy components.

One of the critical issues intrinsic to the generality of the fracture tests is the difficulty of monitoring the crack length during its propagation. This task is especially challenging to accomplish with the required accuracy when mode II loading predominates, since the crack tends to grow with its faces in contact, making crack tip

identification difficult. Additionally, there are several aspects not included in Equations (6) and (7) that can influence the specimen behaviour. Effectively, issues like stress concentrations and root rotation effects at the crack tip, the presence of the adhesive layer and the eventual existence of a non-negligible FPZ ahead of crack tip during propagation are not included in these beam theory equations, although they influence the specimen compliance. In order to overcome the referred inaccuracies, an equivalent crack length procedure is used. The procedure is based on the estimation of the equivalent crack lengths using Equations (6) and (7), from the current compliances  $C_{\rm I}$  and  $C_{\rm II}$ , which are easily obtained from the loads and displacements of the specimen arms continuously registered during the test. The equivalent crack length in mode I ( $a_{\rm el}$ ) is defined by:

$$a_{\rm el} = \frac{1}{6\alpha} A - \frac{2\beta}{A} \tag{8}$$

where

$$A = \left( \left( -108\gamma + 12\sqrt{3\left(\frac{4\beta^3 + 27\gamma^2\alpha}{\alpha}\right)} \right) \alpha^2 \right)^{\frac{1}{3}}$$
 (9)

$$\alpha = \frac{8}{Bh^3E}; \quad \beta = \frac{12}{5BhG}; \quad \gamma = -C_1$$
 (10)

In mode II the equivalent crack length  $(a_{ell})$  can be directly obtained from equation (7)

$$a_{\text{eII}} = \left[ \left( C_{\text{II}} - \frac{6LL_{1}}{5BhG(2L - L_{1})} \right) \frac{2Bh^{3}E}{3} - \frac{2LL_{1}^{2}}{3} \right]^{1/3}$$
 (11)

The components of the strain energy release rate can be determined by means of the Irwin-Kies equation [18]:

$$G = \frac{P^2}{2R} \frac{dC}{da} \tag{12}$$

For mode I, the combination of Equations (6) and (12) leads to

$$G_{\rm I} = \frac{6P_{\rm I}^2}{B^2 h} \left( \frac{2a_{\rm el}^2}{h^2 E} + \frac{1}{5G} \right) \tag{13}$$

The strain energy release rate in mode II is obtained from Equations (7) and (12)

$$G_{\rm II} = \frac{9P_{\rm II}^2 a_{\rm eII}^2}{4R^2 h^3 E} \tag{14}$$

Equations (13) and (14) represent the evolution of the strain energy release rates components during the test (R-curves), thus providing the identification of the mode-mixity as well as the total fracture energy of the test. The proposed method only requires recording the load F and displacement components applied to each arm of the specimen ( $\delta_1$ ,  $\delta_2$ ) during the test (Figure 2). The load components ( $F_1$  and  $F_2$ ) can be straightforwardly obtained from the load applied by the machine (F) and static equilibrium of each loading arm (Figure 1):

$$F_1 = F \frac{s_2}{s_3}$$
;  $F_2 = F \frac{s_1 s_4}{s_3 (s_3 + s_4)}$  (15)

Since the method is essentially based on the compliance of the specimen arms it is named compliance-based beam method (CBBM). Following the proposed procedure, it is not necessary to perform crack length monitoring during propagation. Additionally, the energy dissipated at non-negligible FPZ is accounted for since the current specimen compliances are influenced by the presence of the FPZ.

The nominal phase angle of loading  $\psi$ , as defined by Fernlund and Spelt [11] is also an important value, helping to discriminate each loading case, and is defined by:

$$\psi = \arctan\left(\sqrt{G_{II}/G_{I}}\right); \ \psi = \arctan\left[\frac{\sqrt{3}\left(\frac{F_{1}}{F_{2}}+1\right)}{2\left(\frac{F_{1}}{F_{2}}-1\right)}\right]$$
 (16)

• • •

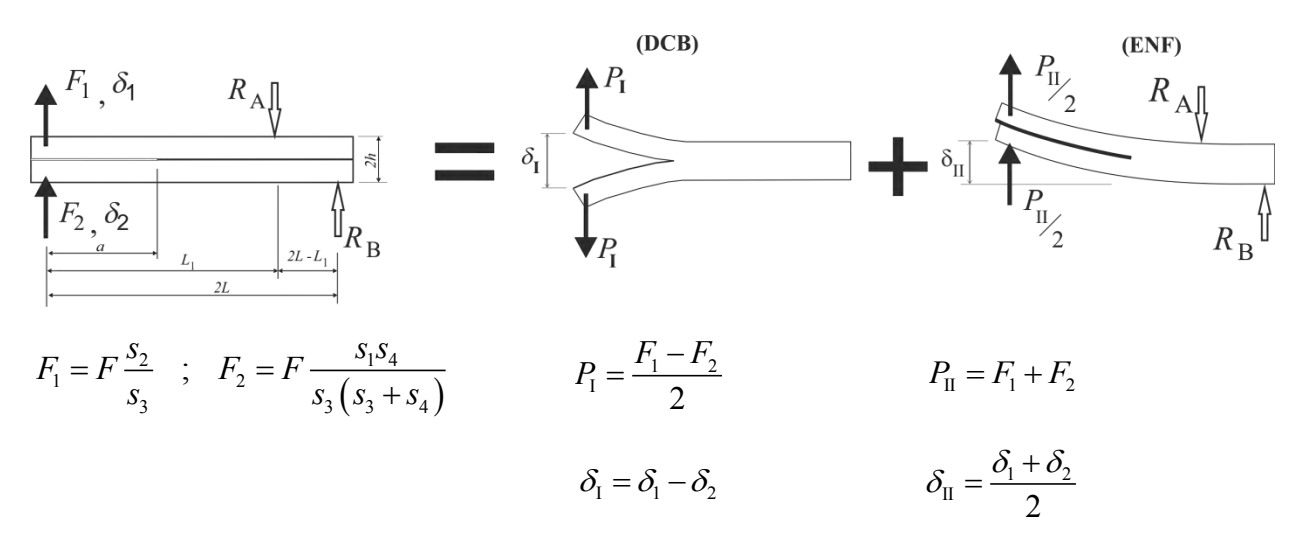


Figure 6. Spelt jig loading scheme with mode I and mode II partition.

# 3 – Experimental results

Three combinations for the  $s_1$ - $s_4$  dimensions were tested. Numerical studies [15] indicated that pure mode I (DCB test) was possible to perform, but pure mode II (ENF) could not be achieved. The dimensions to obtain the opening pure mode I were set as  $s_1$ =40 mm,  $s_2$ =120 mm,  $s_3$ =160 mm and  $s_4$ =-120 mm as shown in Figure 3.

The remaining two combinations, were set in order to obtain a predominant mode I test  $-s_1$ =60 mm,  $s_2$ =100 mm,  $s_3$ =160 mm and  $s_4$  = 80 mm - as a second set-up with  $\psi$  = 20° and the third set-up to obtain a predominant mode II test with  $\psi$  = 85° -  $s_1$ =80 mm,  $s_2$ =60 mm,  $s_3$ =140 mm and  $s_4$  = 100 mm.

The load-displacement  $(F-\delta)$  curve obtained from the universal testing machine and also the displacements  $(\delta_1 \text{ and } \delta_2)$  recorded by the LVDTs at the loading pins, for the first apparatus set up ( Figure 3 with  $s_1$ =40 mm ,  $s_2$ =120 mm ,  $s_3$ =160 mm and  $s_4$ =-120 mm) are shown in the graph of Figure 7. Using this data to calculate the energy release rate, it was possible to compute the R-curve for this loading case as shown in Figure 8. The nominal phase angle of loading  $\psi$  for this case is  $0^\circ$ .

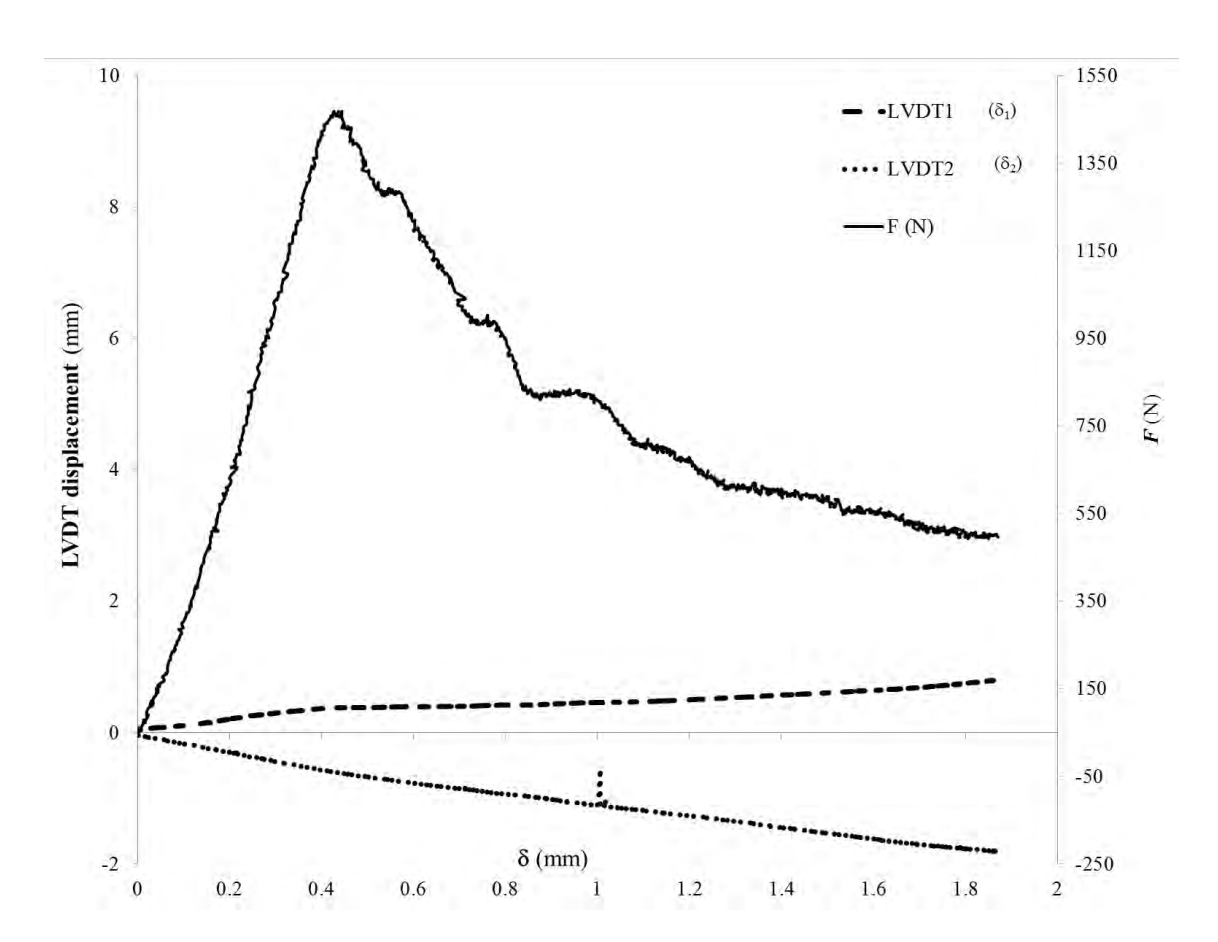


Figure 7. Load displacement and LVDTs displacement curves for pure mode I loading case ( $s_1$ =40 mm ,  $s_2$ =120 mm ,  $s_3$ =160 mm and  $s_4$ =-120 mm),  $\psi$ =0°.

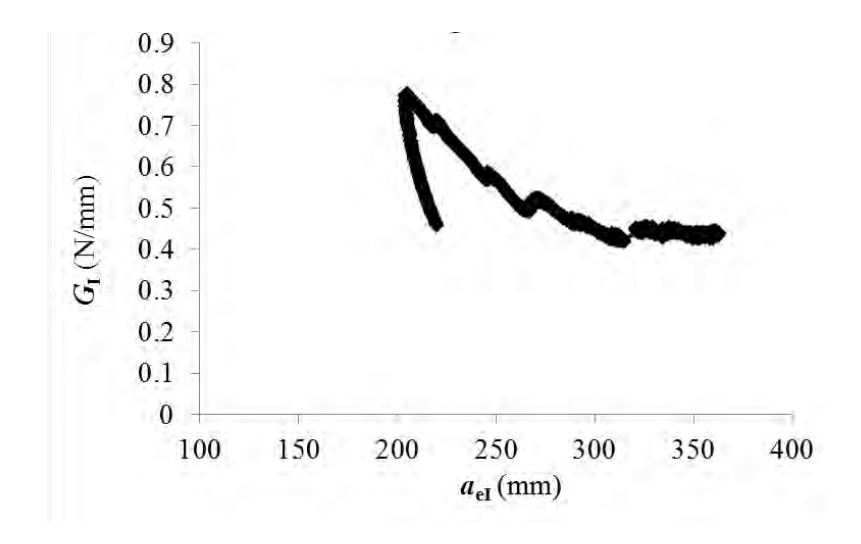


Figure 8. R-curve for the first loading case (pure mode I,  $s_1$ =40 mm ,  $s_2$  =120 mm ,  $s_3$ =160 mm and  $s_4$  = -120 mm).

The second loading case, ( $s_1$ =60 mm,  $s_2$ =100 mm,  $s_3$ =160 mm and  $s_4$  = 80 mm) load-displacement (F- $\delta$ ) and the specimen beams displacements ( $\delta_1$  and  $\delta_2$ ) recorded by the LVDTs at the loading pins, are shown in Figure 9. The nominal phase angle of loading  $\psi$  for this case is 20°.

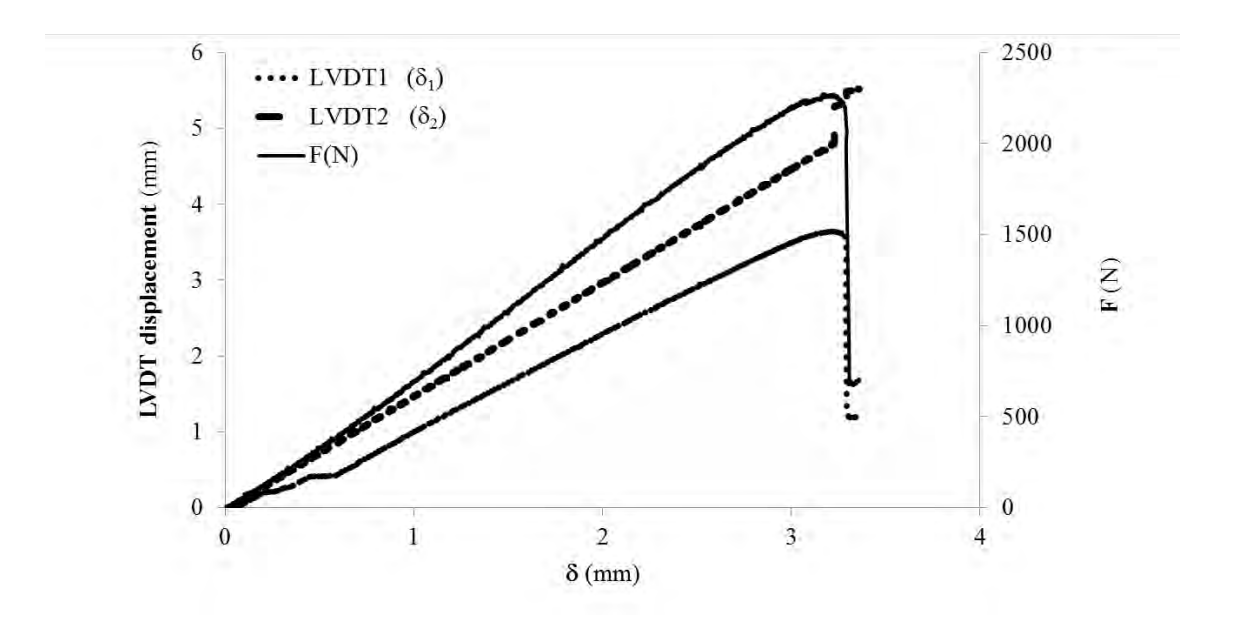


Figure 9. Load displacement and LVDTs displacement curves for the second loading case ( $s_1$ =60 mm ,  $s_2$ =100 mm ,  $s_3$ =160 mm and  $s_4$  = 80 mm),  $\psi$  = 20°.

The resulting R-curves for mode I and mode II are plotted in Figure 10.

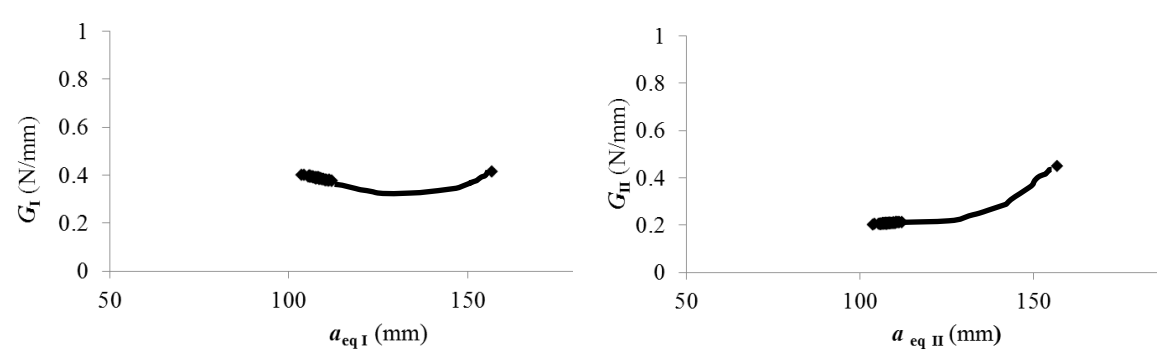


Figure 10. Mode I (left) and mode II (right) R-curves for the second loading case (s1= 60 mm, s2=100 mm, s3=160 mm and s4 = 80 mm).

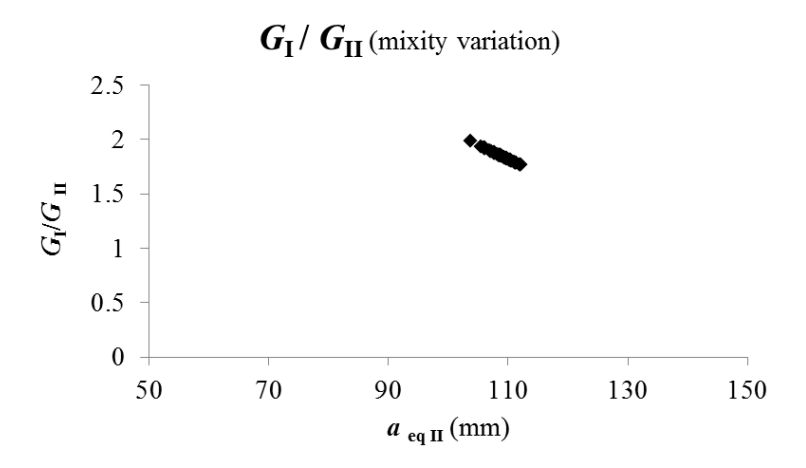


Figure 11.  $G_{\rm I}/G_{\rm II}$  ratio variation for the second loading case (s1=60 mm, s2=100 mm, s3=160 mm and s4 = 80 mm).

For the third loading case ( $s_1$ =80 mm,  $s_2$ =60mm,  $s_3$ =140 mm and  $s_4$ =100 mm), the load-displacement (F- $\delta$ ) and the displacements ( $\delta_1$  and  $\delta_2$ ) recorded by the LVDTs at the loading pins, are shown in Figure 12. The nominal phase angle of loading  $\psi$  for this case is 85°.

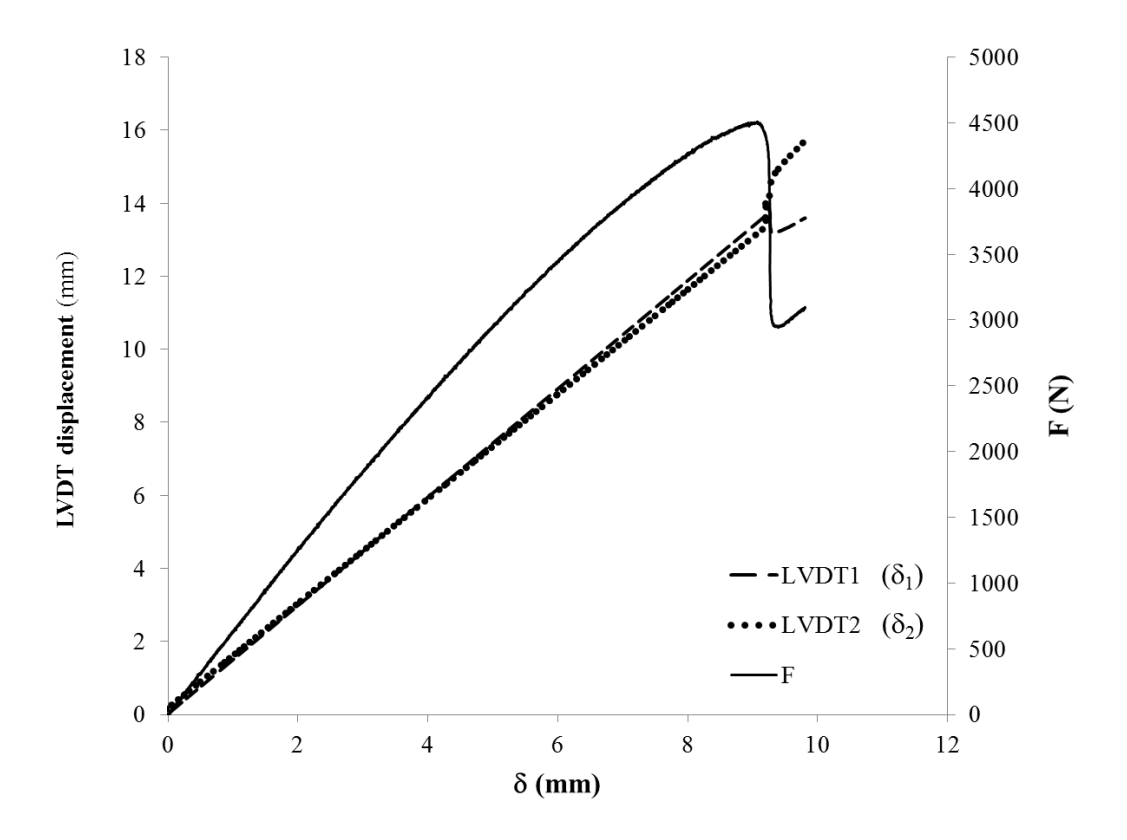


Figure 12. Load displacement and LVDTs displacement curves for the third loading case  $(s_1=80 \text{ mm}, s_2=60 \text{ mm}, s_3=140 \text{ mm} \text{ and } s_4=100 \text{ mm}), \psi=85^{\circ}.$ 

Computing this data with the proposed data reduction scheme, the resulting R-curves for mode I and mode II are plotted as shown in Figure 13.

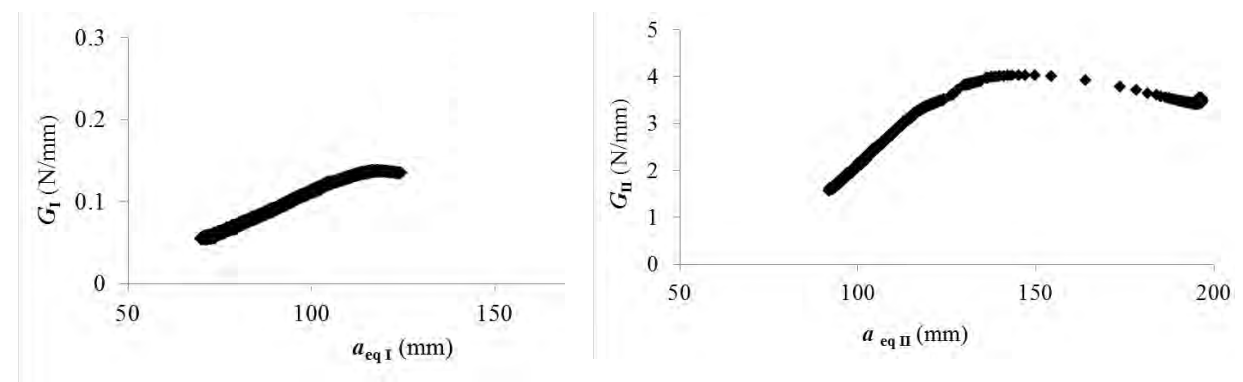


Figure 13. Mode I (left) and mode II (right) R-curves for the third loading case ( $s_1$ =80 mm,  $s_2$ =60 mm,  $s_3$ =140 mm and  $s_4$  = 100 mm).

A graph showing the development of the mode-mixity for this test is also plotted in Figure 14, to understand the effect of this ratio.

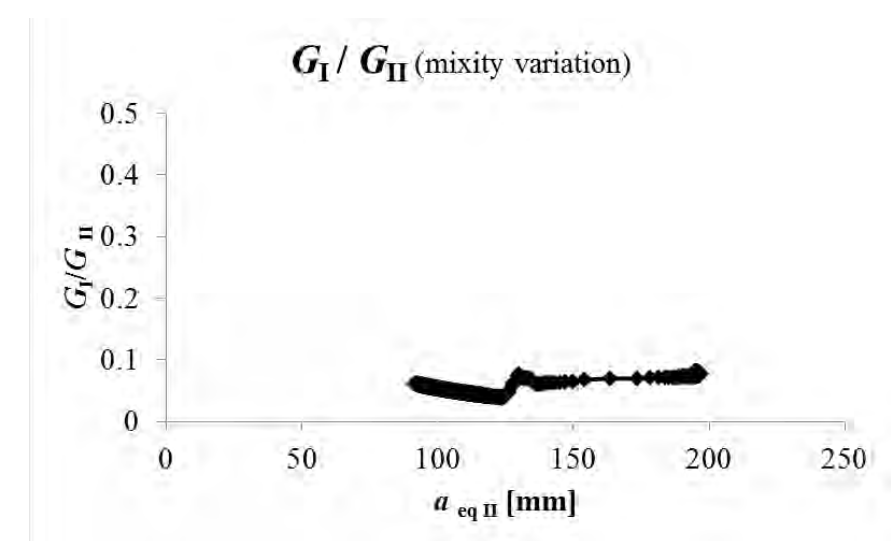


Figure 14.  $G_{\rm I}/G_{\rm II}$  ratio variation for the third loading case ( $s_1$ =80 ,  $s_2$ =60 ,  $s_3$ =140 and  $s_4$  = 100 (mm)).

Using the previous information, it is possible to obtain a fracture envelop with these three points of the energy release rate in mode I ( $G_{II}$ ) and mode II ( $G_{II}$ ) for each combination as shown in Figure 15.

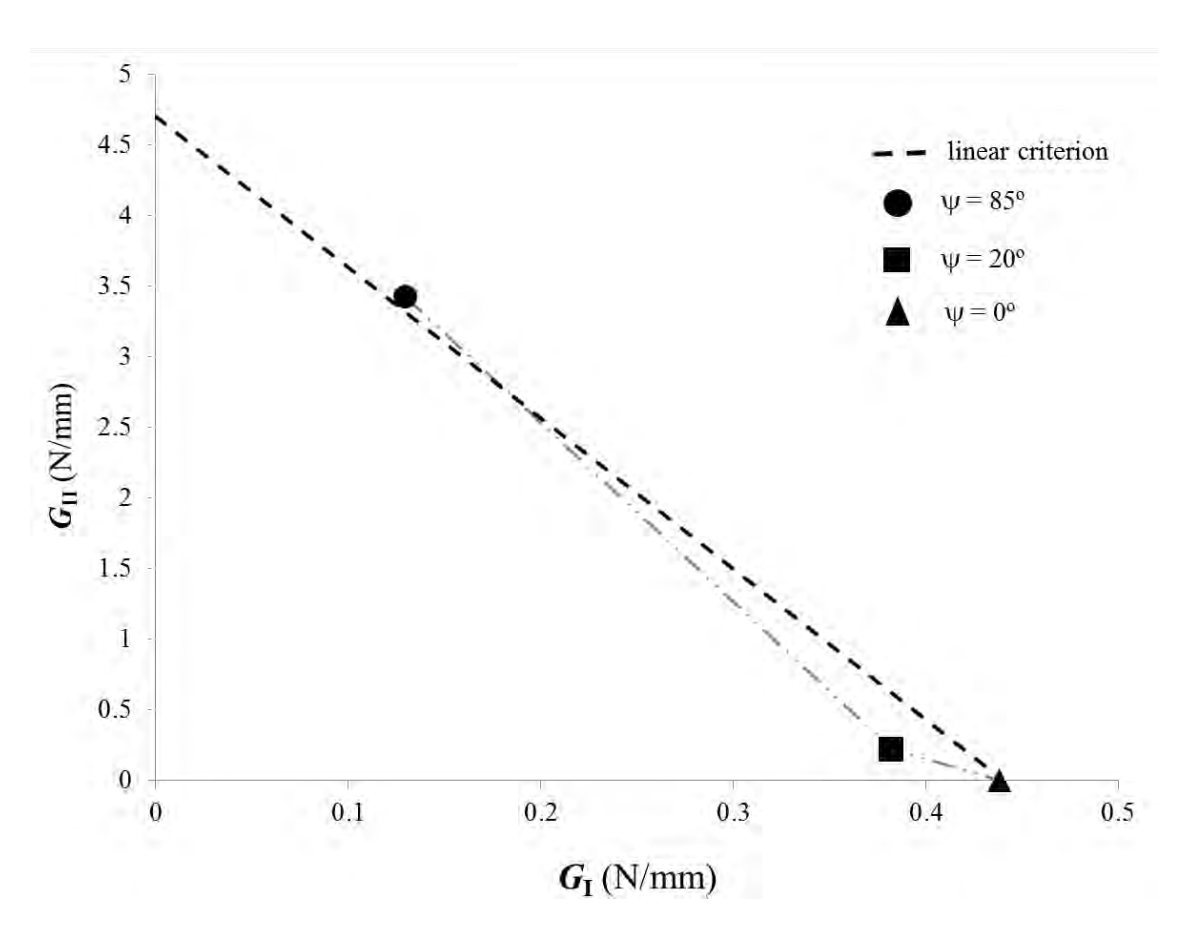


Figure 15. Fracture envelop for the three combinations ( $\psi = 85^{\circ}$ ,  $\psi = 20^{\circ}$  and  $\psi = 0^{\circ}$ ).

## 4 - Numerical modelling

In order to verify the performance of the proposed method as well as the ability of the jig to provide a rigorous characterization of the fracture envelope under mixed-mode I+II of bonded joints, a numerical analysis including cohesive zone modelling was performed. The specimen geometry and mechanical properties used in the simulations are presented in Figure 2 and Table 1, respectively. Figure 16 presents the considered mesh and corresponding boundary conditions. The loading device was simulated by a combination of rigid beams and links (Figure 16) that reproduce the experimental setup. The specimen was modelled with 3600 plane strain 8-node quadrilateral elements and 280 6-node interface elements with null thickness placed at the mid-plane of the bonded specimen. The interface elements include a cohesive zone mixed-mode I+II damage model to simulate damage onset and propagation within the adhesive. The cohesive zone model establishes a relationship between stresses and relative displacements between specimen arms [19, 20]. The behaviour of the adhesive is integrated in the cohesive damage law considered. A trapezoidal cohesive damage model was considered

in the numerical analysis (Figure 17). The trapezoidal laws are particularly adequate for adhesives with ductile behaviour [20-22]. In the pure mode model, the slope of the initial linear part is dictated by the interface stiffness, which is obtained by the ratio between the relevant adhesive elastic modulus (E in mode I and G in mode II) and its thickness. Once the local strength ( $\sigma_{u,i}$ ) is obtained, a plateau zone takes place to simulate adhesive plastic behaviour. The third linear softening part between stresses and relative displacements is assumed to simulate a gradual material degradation during the loading process. In the pure mode model, the ultimate relative displacement  $\delta_{u,i}$  is defined by equating the area circumscribed by the trapezoid to  $G_{ic}$  (i=I, II). Mixed-mode I+II damage model is an extension of pure mode model. In this case, a quadratic stress criterion is utilized to identify damage initiation

$$\left(\frac{\sigma_{\rm I}}{\sigma_{\rm u,I}}\right)^2 + \left(\frac{\sigma_{\rm II}}{\sigma_{\rm u,II}}\right)^2 = 1 \tag{18}$$

The linear energetic criterion

$$\left(\frac{G_{\rm I}}{G_{\rm Ic}}\right) + \left(\frac{G_{\rm II}}{G_{\rm IIc}}\right) = 1$$
(19)

was used to simulate damage propagation. The area under the trapezoid  $0-\sigma_{\text{um},i}-\delta_{2\text{m},i}-\delta_{2\text{m},i}$  of Figure 17 represents the energy released in each mode, while the area of the  $0-\sigma_{\text{u},i}-\delta_{2,i}-\delta_{\text{u},i}$  trapezoid corresponds to the respective critical fracture energy. When equation (19) is satisfied, damage propagation occurs and stresses are completely released, with the exception of normal compressive ones. The model is detailed in de Moura et al. [21].

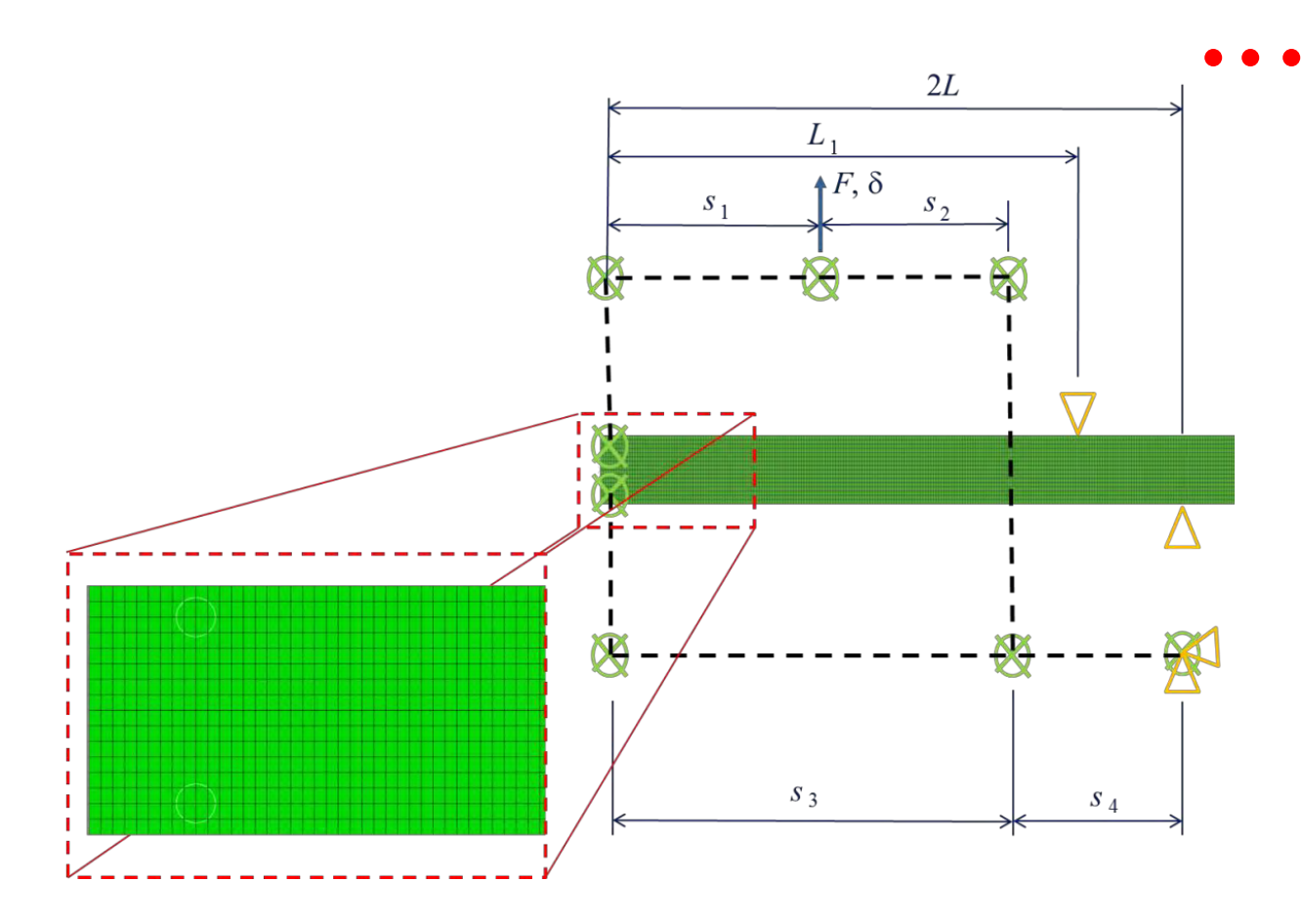


Figure 16. Numerical model mesh and boundary conditions.

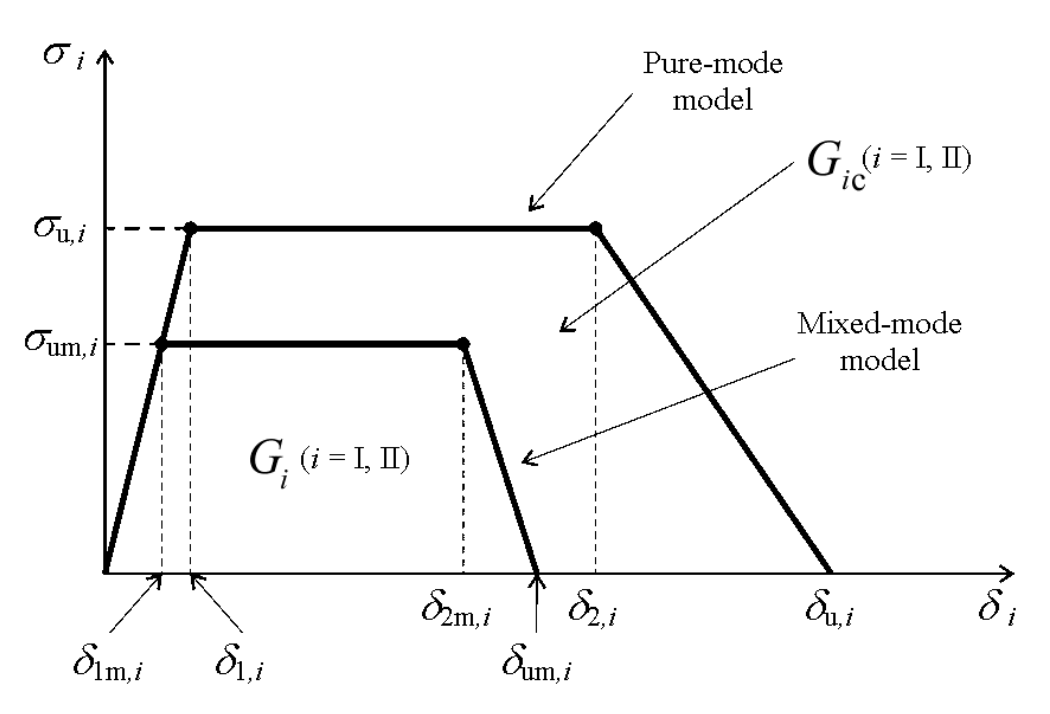


Figure 17. Trapezoidal softening law for pure and mixed-mode cohesive damage model.

The numerical and experimental load-displacement curves for each loading case are presented in Figure 19, Figure 21 and .

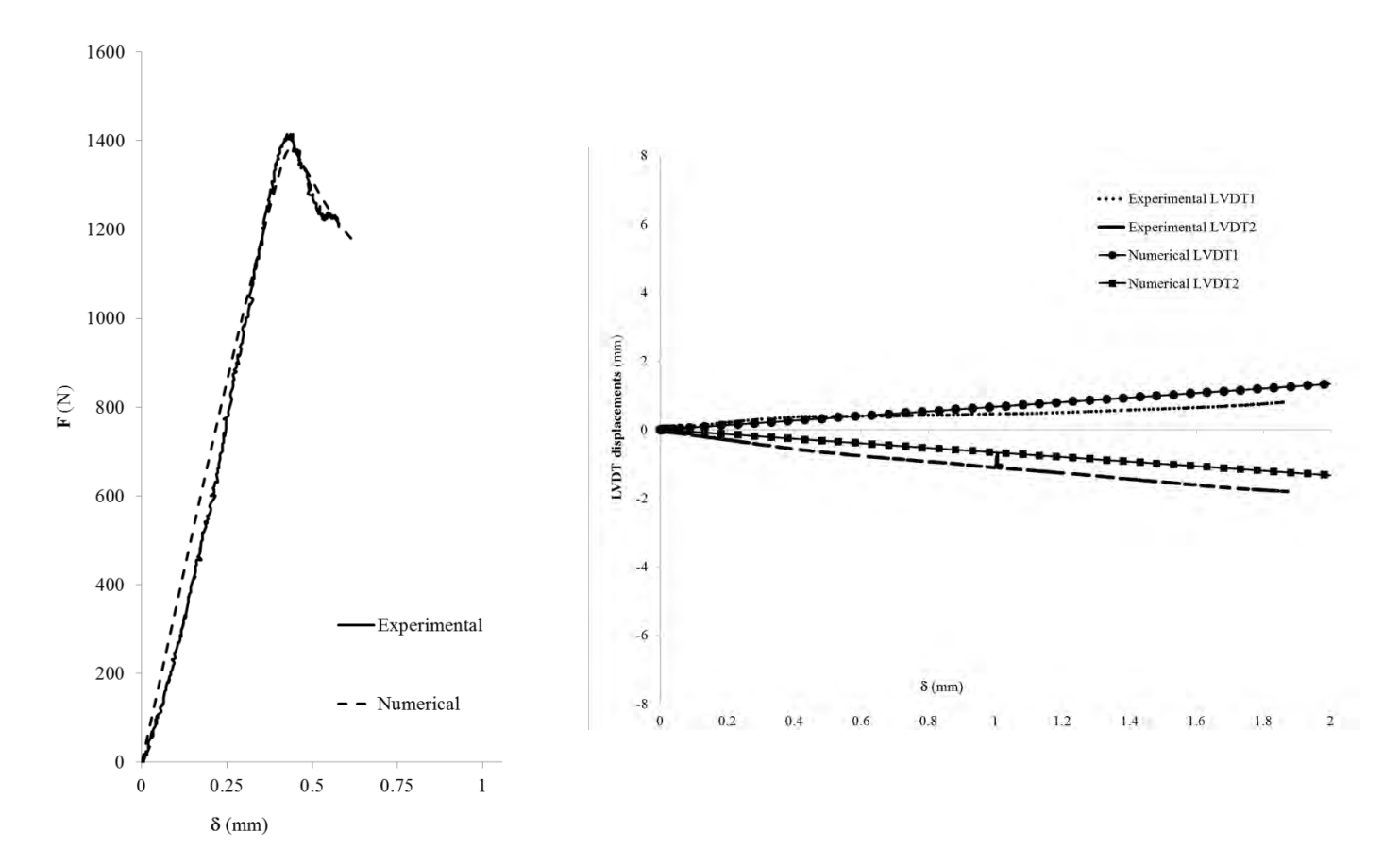


Figure 18. Experimental and numerical load-displacement curves (left) and LVDT displacement curves (right) for the first test  $\psi = 0^{\circ}$ .

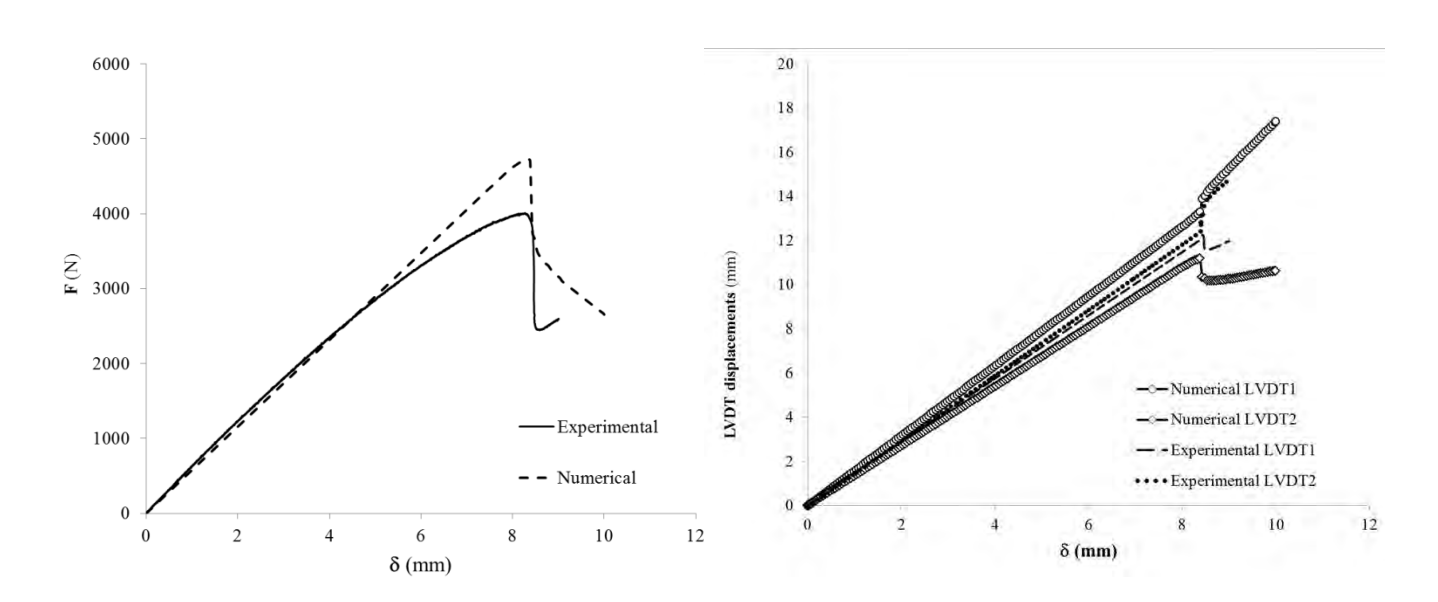


Figure 19. Experimental and numerical load-displacement curves (left) and LVDT displacement curves (right) for the second test  $\psi = 20^{\circ}$ .

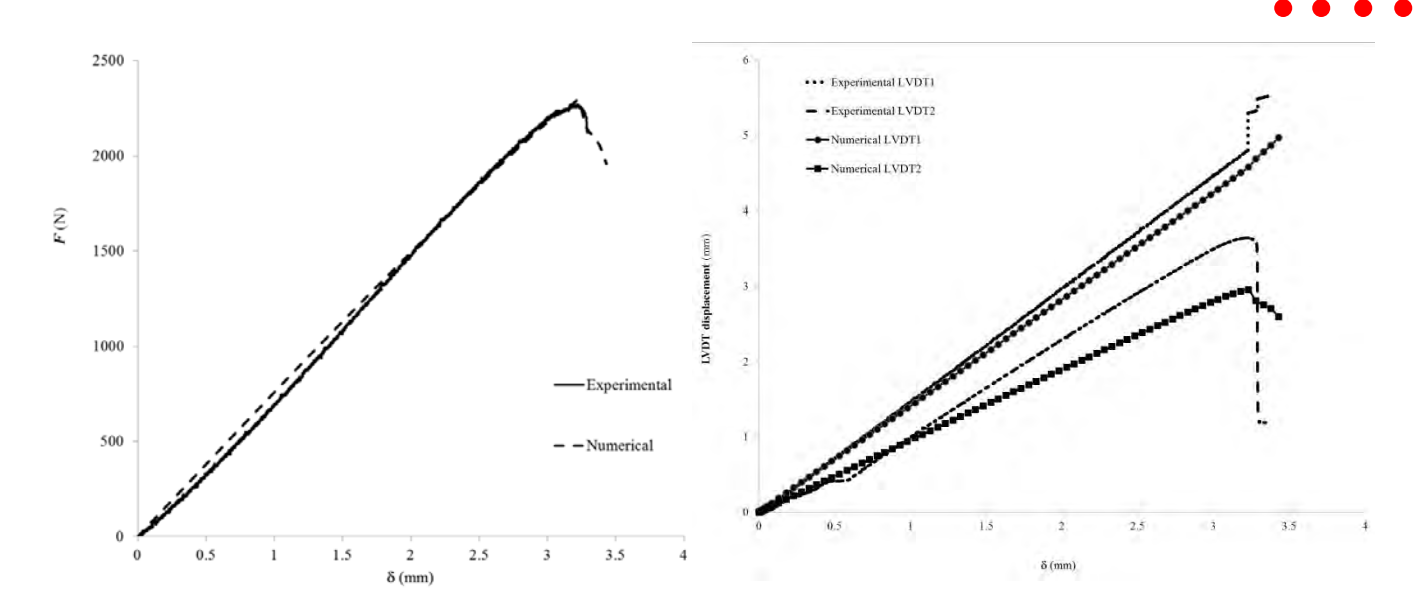


Figure 20. Experimental and numerical load-displacement curves (left) and LVDT displacement curves (right) for the third test  $\psi = 85^{\circ}$ .

#### 5 - Discussion

The presented apparatus allowed to obtain three different combinations for testing loads in mode I (opening) and mode II (shear) resulting in three different load-displacement curves. Furthermore, each test registered the displacement of the upper and lower specimen beams using a LVDT for each one. The first combination characterized by  $\psi = 0^{\circ}$ , implements a DCB test in pure mode I, and reported a good verification for the ability of this apparatus to perform fracture tests in mode I. The resulting load-displacement curve (Figure 8) is characteristic of a DCB test, and provides a good approximation to tests previously done by the authors [1] as shown in Figure 21. The computed energy release rate for this test is plotted in Figure 8 and shows a blunt effect caused by the round tip of the initial crack, and then stabilizes at a plateau near 0.438 N/mm for the mode I energy release rate,  $G_{\rm I}$ . This value is in agreement with previously works published by the authors [1] and Campilho, Moura et al. [23].

The second combination for a  $\psi$  = 20°, provided a mixed mode (I+II) test resulting a load-displacement curve in Figure 12 with a higher value for the maximum force when compared to the first combination. This test results were computed in two energy release rates for both mode I and mode II which are plotted in Figure 10Figure 8 and

shows a plateau near 0.382 N/mm for the mode I energy release rate,  $G_{\rm I}$ , on the left and another plateau near 0.22 N/mm for the mode II energy release rate,  $G_{\rm II}$ , on the right. This is in accordance with a mode I predominant test.

The mode mixity ratio  $G_I/G_{II}$ , plotted in Figure 11, has little variation showing that this test promotes a self-similar crack propagation.

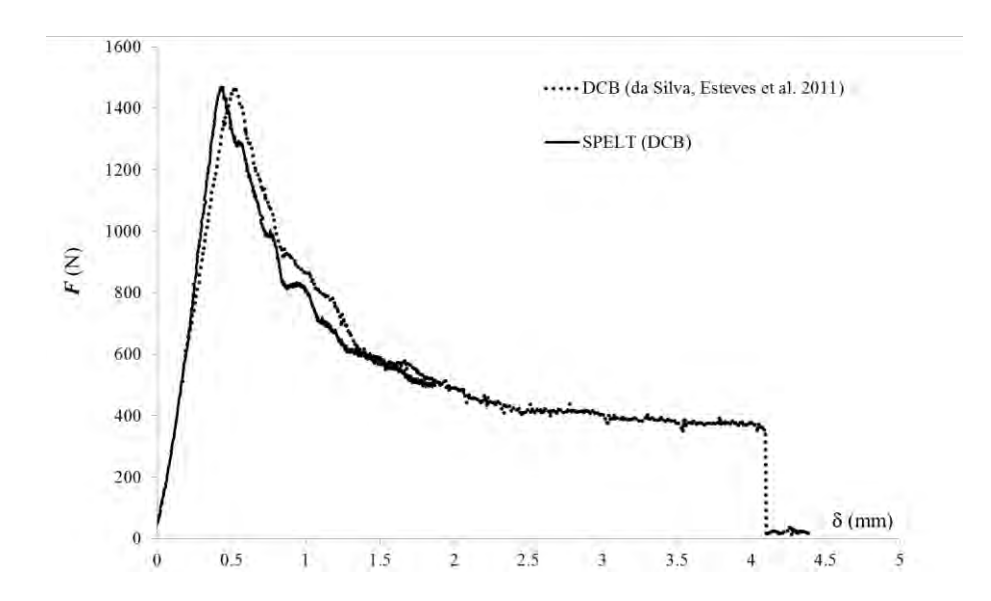


Figure 21. Comparison between the first combination test (DCB,  $\psi$ =0°) and a previously performed pure mode I DCB test by da Silva, Esteves et al. [1].

The third combination with  $\psi=85^\circ$ , provided a mixed mode (I+II) test (Figure 12) with a higher value for the maximum force when compared to the second and first combinations. Both the load-displacement data and the LVDTs displacements were computed in two energy release rates for both mode I and mode II which are plotted in Figure 13 showing a plateau near 0.13 N/mm for the mode I energy release rate,  $G_{\rm I}$ , on the left and another plateau near 3.42 N/mm for the mode II energy release rate,  $G_{\rm II}$ , on the right. The higher value for  $G_{\rm II}$  is in accordance with a mode II predominant test as expected.

. . . .

Once again, the mode mixity ratio  $G_I/G_{II}$ , plotted in Figure 14, has little variation underlining that this test promotes a self-similar crack propagation.

The values obtained for the energy release rates from the three tests were plotted in a graph in order to obtain a fracture envelop presented in Figure 15. This fracture envelop shows a correct relative positioning for each test and a moderate accordance with the linear criterion defined in equation (19).

The numerical approximation to the experimental load-displacement curves has a better agreement in the first ( $\psi$ =0°) and third ( $\psi$ =85°) combinations tested, however the second combination ( $\psi$  = 20°) is moderately close. The displacements ( $\delta$ 1) and ( $\delta$ 2) registered with LVDTs are also compared and present also a good approximation in the three cases.

### 6 - Conclusions

A test apparatus developed for mixed-mode (I+II) adhesive joint fracture mechanics characterization is presented. Three combinations for different mode mixities ( $\psi = 0^{\circ}$ ,  $\psi = 20^{\circ}$  and  $\psi = 85^{\circ}$ ) were tested and the experimental results were analysed with a novel data reduction technique [15]. The results obtained for the first combination tested ( $\psi = 0^{\circ}$ ), proved to be in close agreement with a DCB test performed for pure mode I characterization returning load-displacement values consistent with previous works [1] and confirming the same value for mode I toughness ( $G_{\rm I}$ ). The second ( $\psi = 20^{\circ}$ ) and third ( $\psi = 85^{\circ}$ ) combinations tested, allowed to perform a mixity variation that were analysed and gave consistent results within the fracture envelop for Araldite 2015. The fracture envelop plotted with the three tests presents a moderately good agreement with the linear criterion. Another interesting point resides in the self-similar crack propagation confirmed by a very low variation of the mode mixity ratios during the performed tests.

A numerical simulation of the tests with cohesive zone elements isong a linear criterion showed good agreement with the experimental results, thus validating the whole methodology.

The test method presented, avoids the crack length measurement that is a time consuming and sometimes impossible task to perform and is also a compact apparatus allowing to test the simplest geometry like a DCB specimen, simplifying the test procedure and specimen manufacture.

This could be a good tool for adhesive joint design, because it allows an easier test, improving the usability and data computation to obtain expedite results.

# Acknowledgements

The authors would like to thank the "Fundação Luso-Americana para o Desenvolvimento" (FLAD) for the support through project 314/06, 2007 and *Instituto de Engenharia Mecânica* (IDMEC).

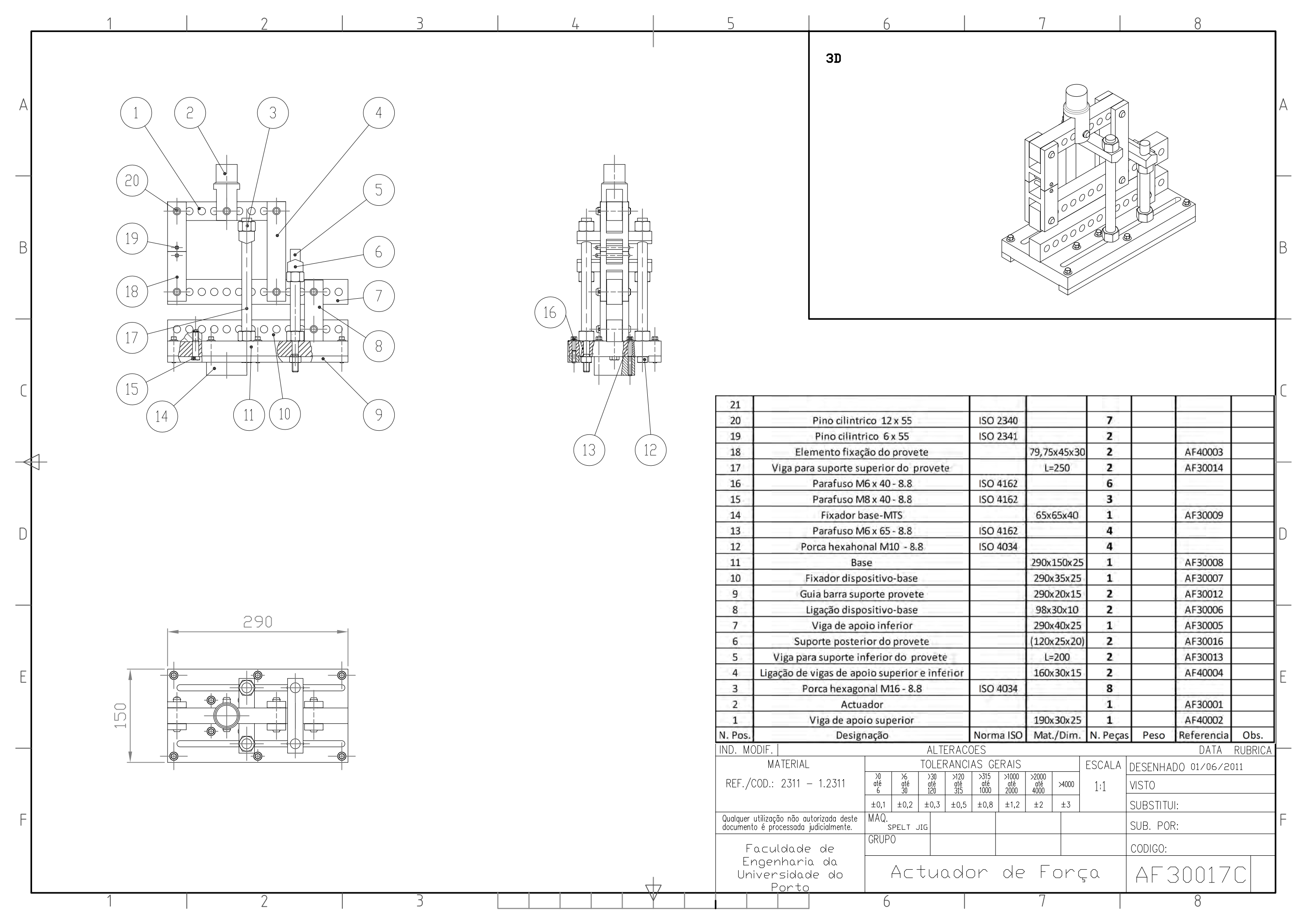
#### References

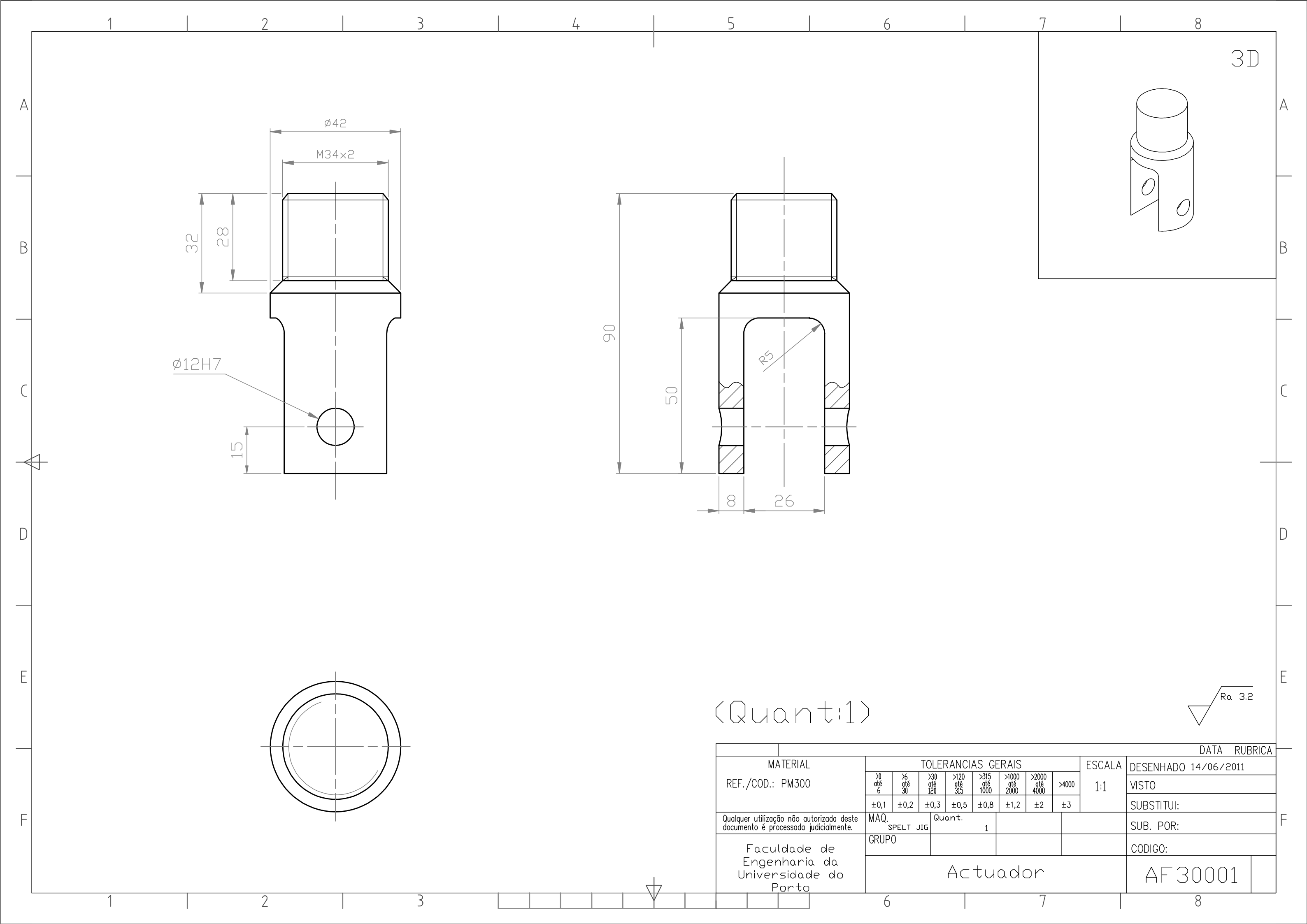
- [1] L.F.M. da Silva, V.H.C. Esteves, F.J.P. Chaves, Materialwissenschaft und Werkstofftechnik, 42 (2011) 460-470.
- [2] D.A. Dillard, H.K. Singh, D.J. Pohlit, J.M. Starbuck, Journal of Adhesion Science and Technology, 23 (2009) 1515-1530.
- [3] J.R. Reeder, J.H. Crews, AIAA Journal, 28 (1990) 1270-1276.
- [4] F. Ducept, P. Davies, D. Gamby, International Journal of Adhesion and Adhesives, 20 (2000) 233-244.
- [5] Z. Liu, G. R.B., G.M. Newaz, in: Proceedings of the American Society of Composites, Fifteenth Technical Conference, College Station, Texas, USA, September, 2000.
- [6] B. Sørensen, K. Jørgensen, T. Jacobsen, R. Østergaard, International Journal of Fracture, 141 (2006) 163-176.
- [7] J.L. Hogberg, U. Stigh, Engineering Fracture Mechanics, 73 (2006) 2541-2556.
- [8] K. Singh Hitendra, A. Chakraborty, E. Frazier Charles, A. Dillard David, in: Holzforschung, 2010, pp. 353.

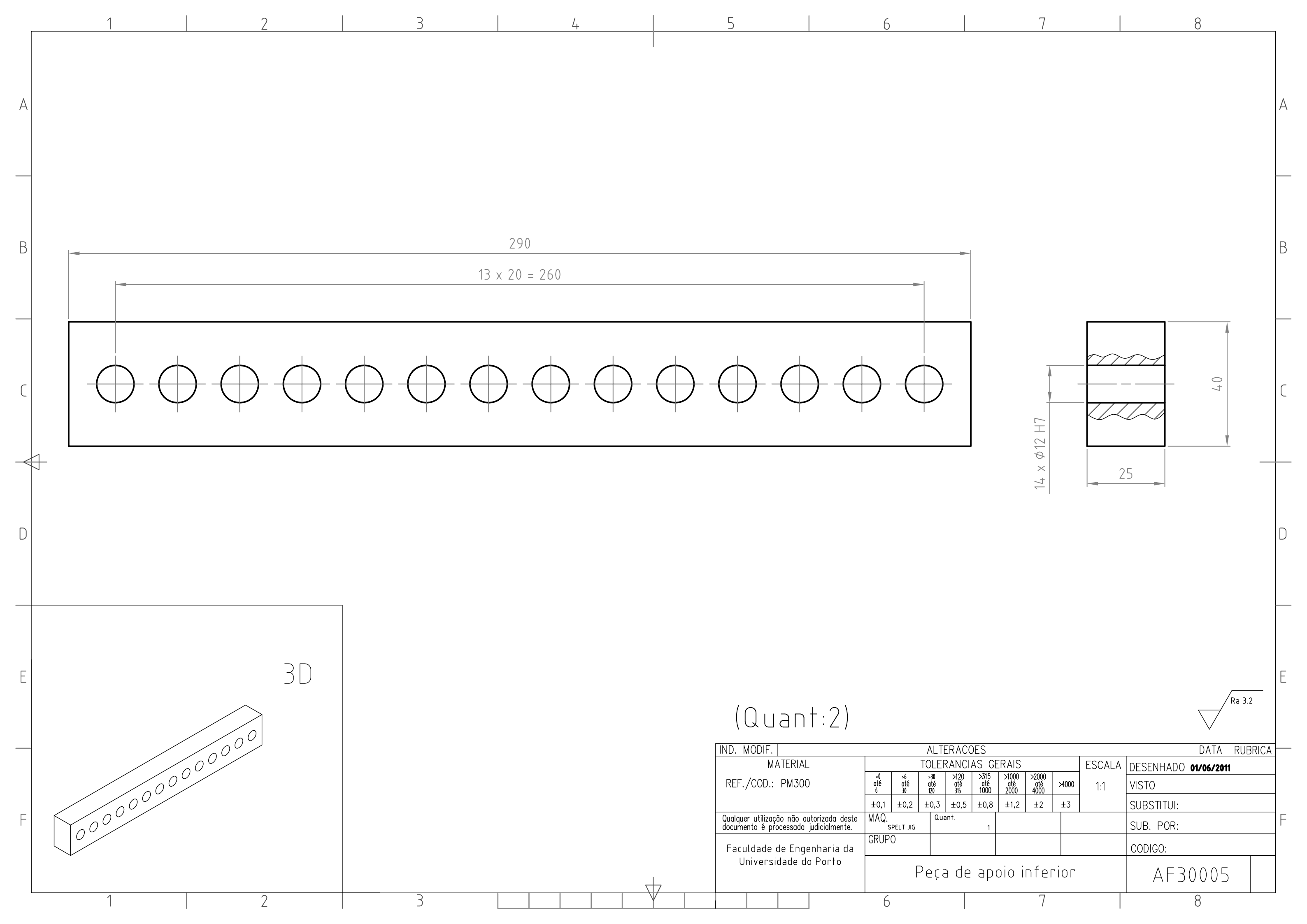
- [9] F.J.P. Chaves, M.F.S.F. de Moura, L.F.M. da Silva, D.A. Dillard, International Journal of Solids and Structures, 48 (2011) 1572-1578.
- [10] D.A. Dillard, H.K. Singh, S. Park, D. Ohanehi, M.A. McGaw, in: SEM Annual Conference & Exposition on Experimental and Applied Mechanics, Society for Experimental Mechanics, Inc., St. Louis, 2006.
- [11] G. Fernlund, J.K. Spelt, Composites Science and Technology, 50 (1994) 441-449.
- [12] F.J.P. Chaves, L.F.M. Da Silva, M.F.S.F. de Moura, A. Dillard David, J.O. Fonseca, in, UP Universidade do Porto, 2013.
- [13] ASTM D3433 99, in: Annual book of ASTM standards, West Conshohocken, ASTM 15.06, 2012, pp. 225-231.
- [14] L.F.M. da Silva, F.A.C.R.G. de Magalhães, F.J.P. Chaves, M.F.S.F. de Moura, The Journal of Adhesion, 86 (2010) 891-905.
- [15] F.J.P. Chaves, M.F.S.F. de Moura, L.F.M. Da Silva, A. Dillard David, in, 2013.
- [16] M.F.S.F. de Moura, R.D.S.G. Campilho, J.P.M. Gonçalves, Composites Science and Technology, 68 (2008) 2224-2230.
- [17] M.F.S.F. de Moura, M.A.L. Silva, A.B. de Morais, J.J.L. Morais, Engineering Fracture Mechanics, 73 (2006) 978-993.
- [18] G.R. Irwin, J.A. Kies, Welding Journal Research Supplement, 33 (1954) 193-198.
- [19] M. Alfano, F. Furgiuele, A. Leonardi, C. Maletta, G.H. Paulino, International Journal of Fracture, 157 (2009) 193-204.
- [20] M. Alfano, F. Furgiuele, L. Pagnotta, G.H. Paulino, Journal of Testing and Evaluation, 39 (2010) 1-8.
- [21] M.F.S.F. de Moura, R.D.S.G. Campilho, J.P.M. Gonçalves, International Journal of Solids and Structures, 46 (2009) 1589-1595.
- [22] G. Alfano, Composites Science and Technology, 66 (2006) 723-730.
- [23] R.D.S.G. Campilho, M.F.S.F.d. Moura, D.A. Ramantani, J.P.M. Gonçalves, Ciência & Tecnologia dos Materiais, 20 (2008) 81-86.

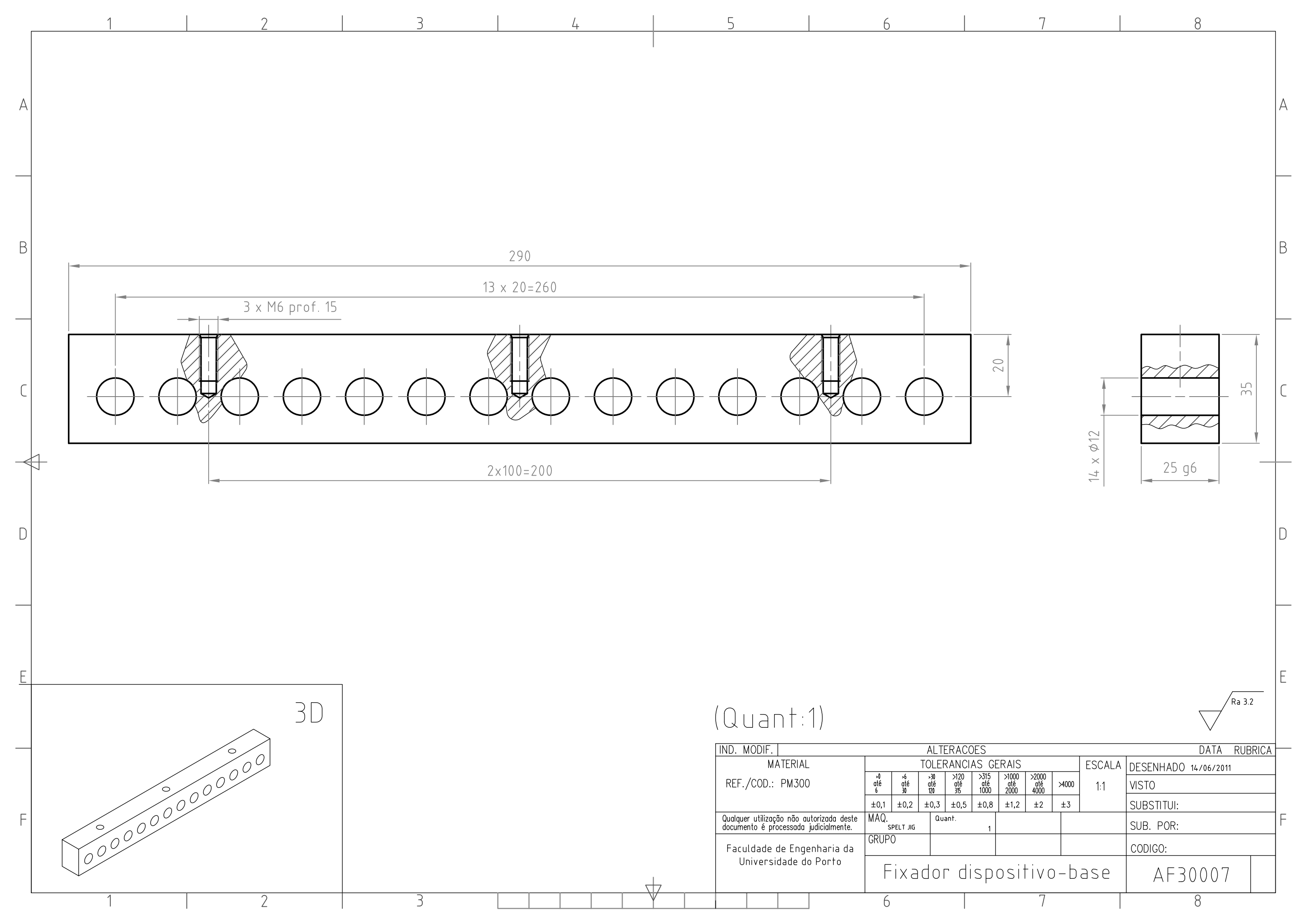
**APPENDIX** 

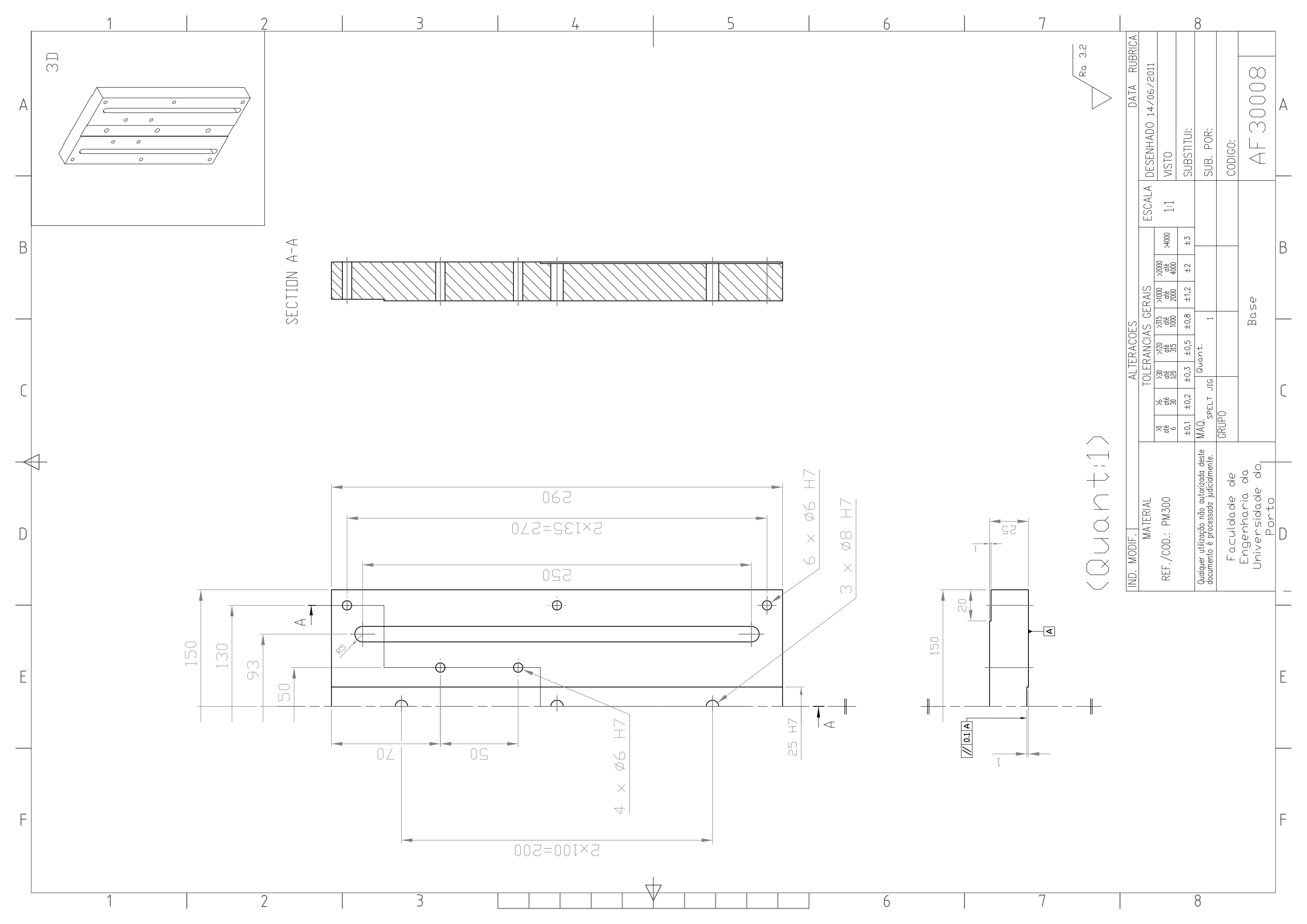
APPARATUS TECHNICAL DRAWINGS

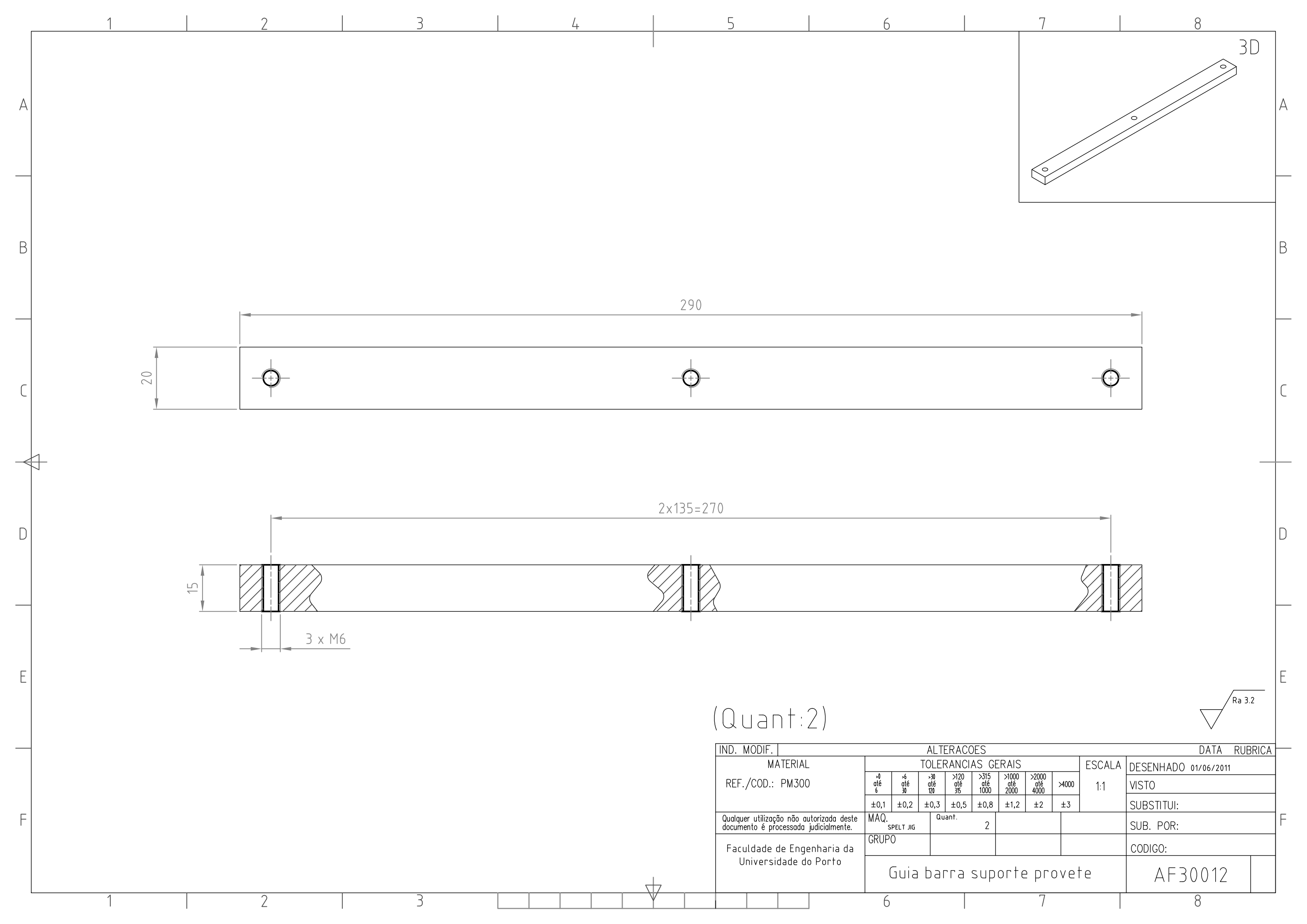


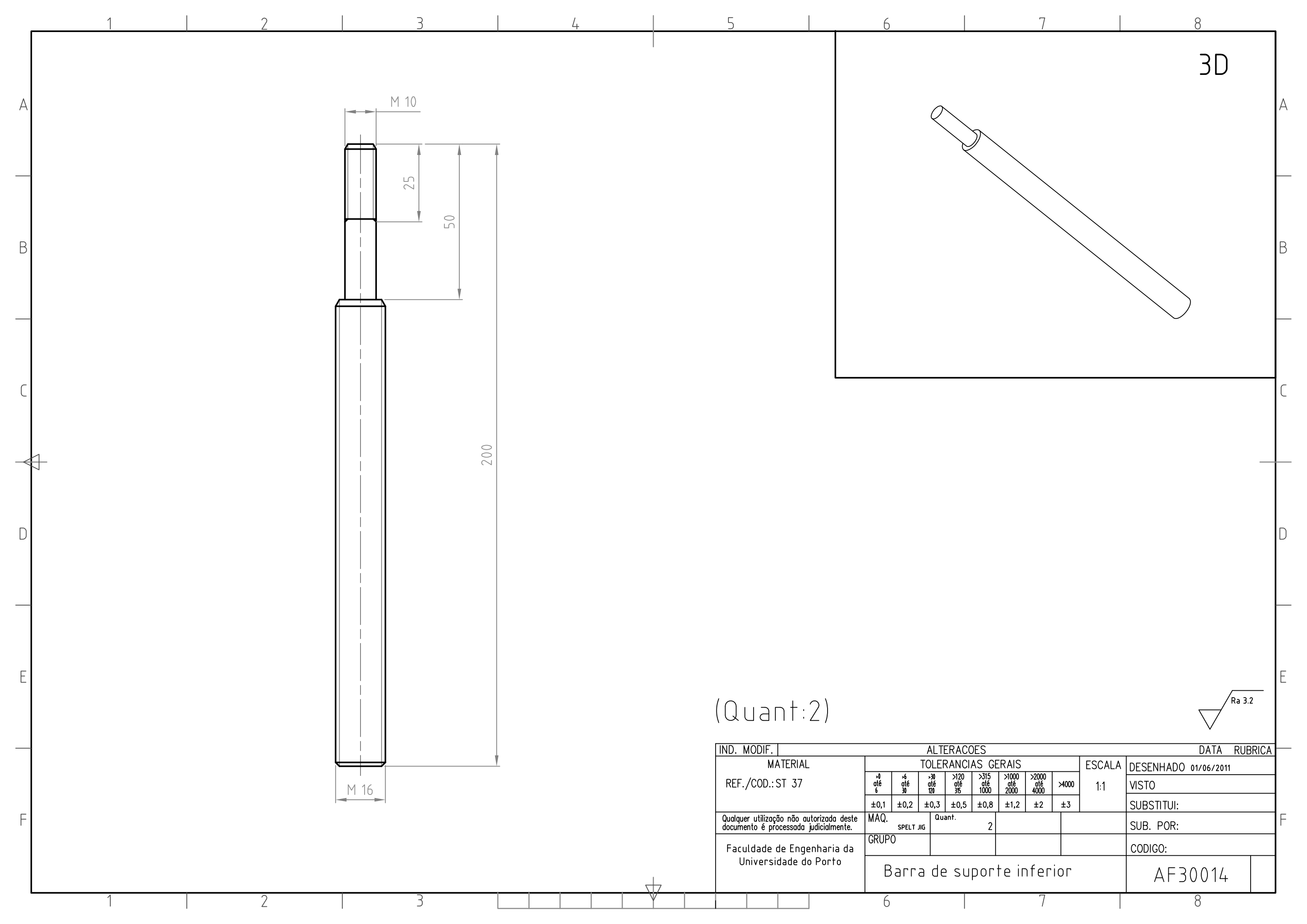


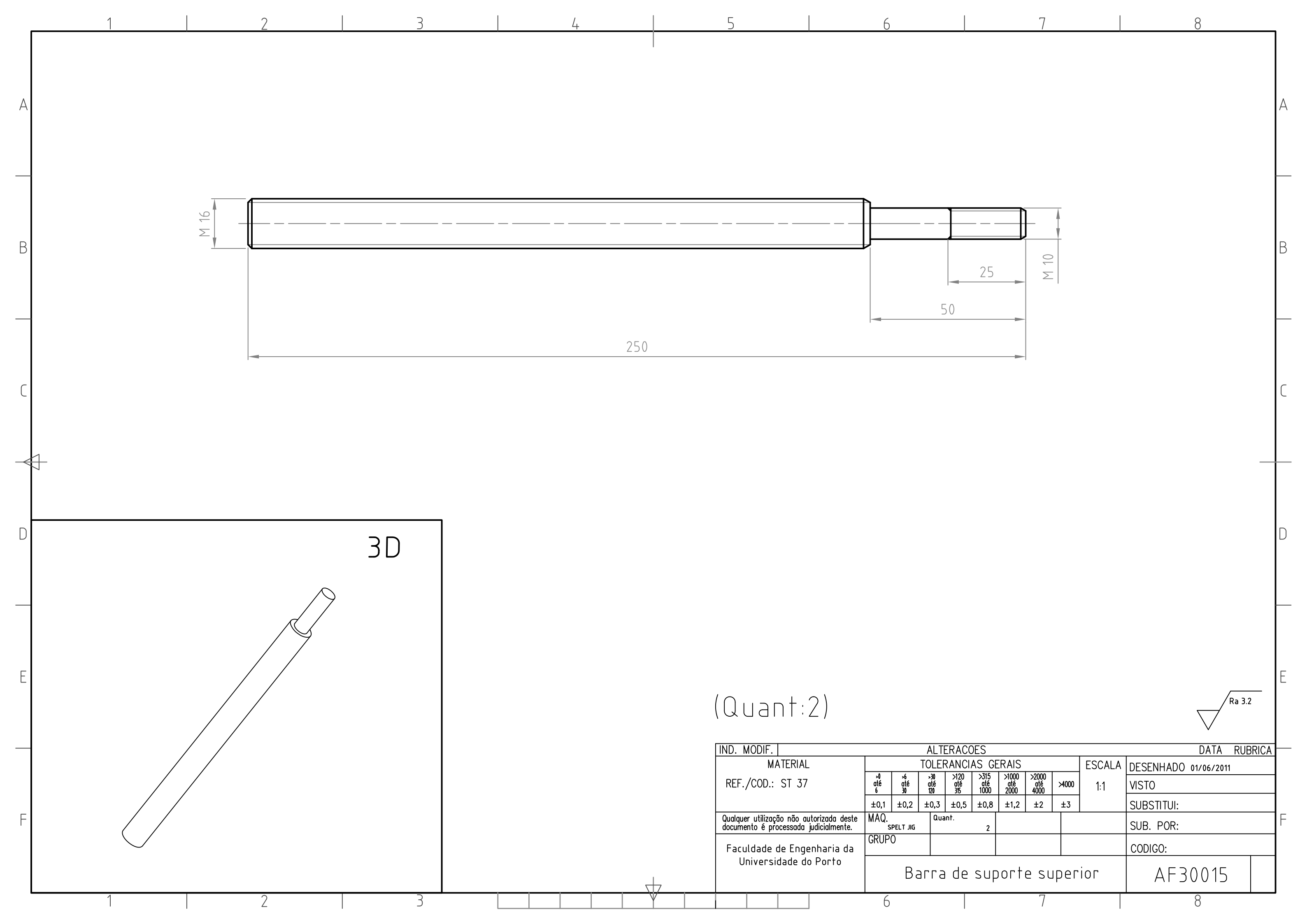


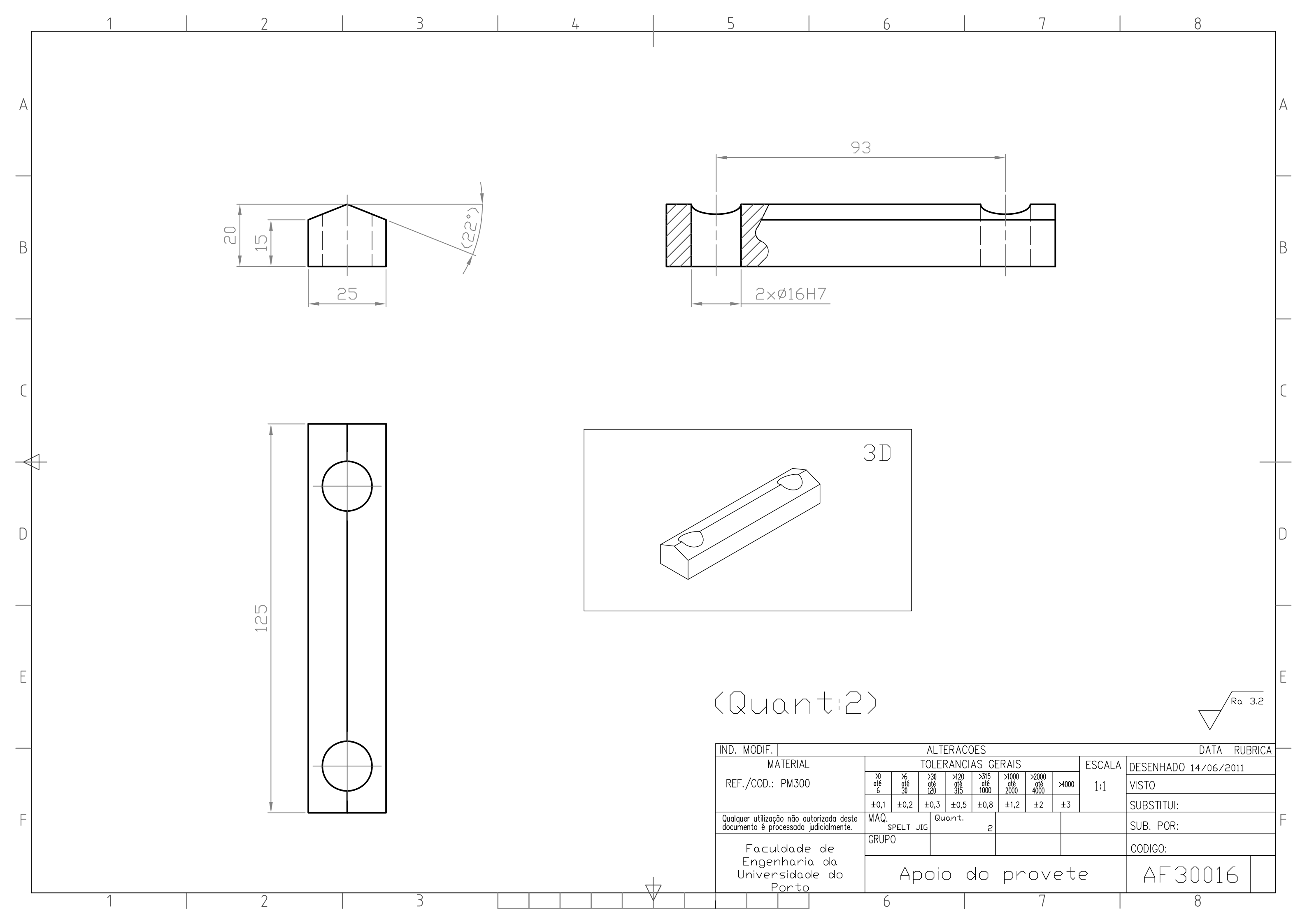


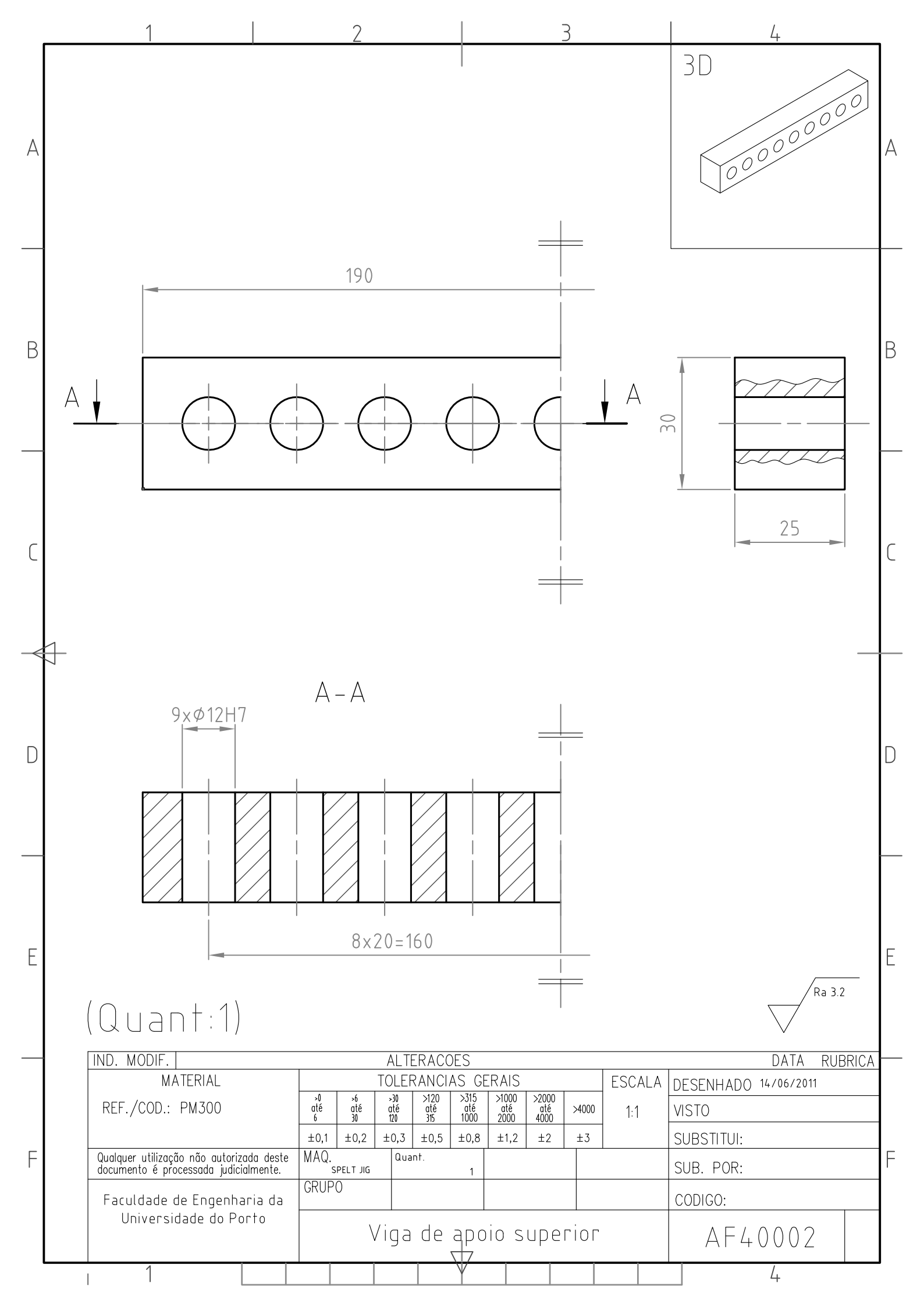


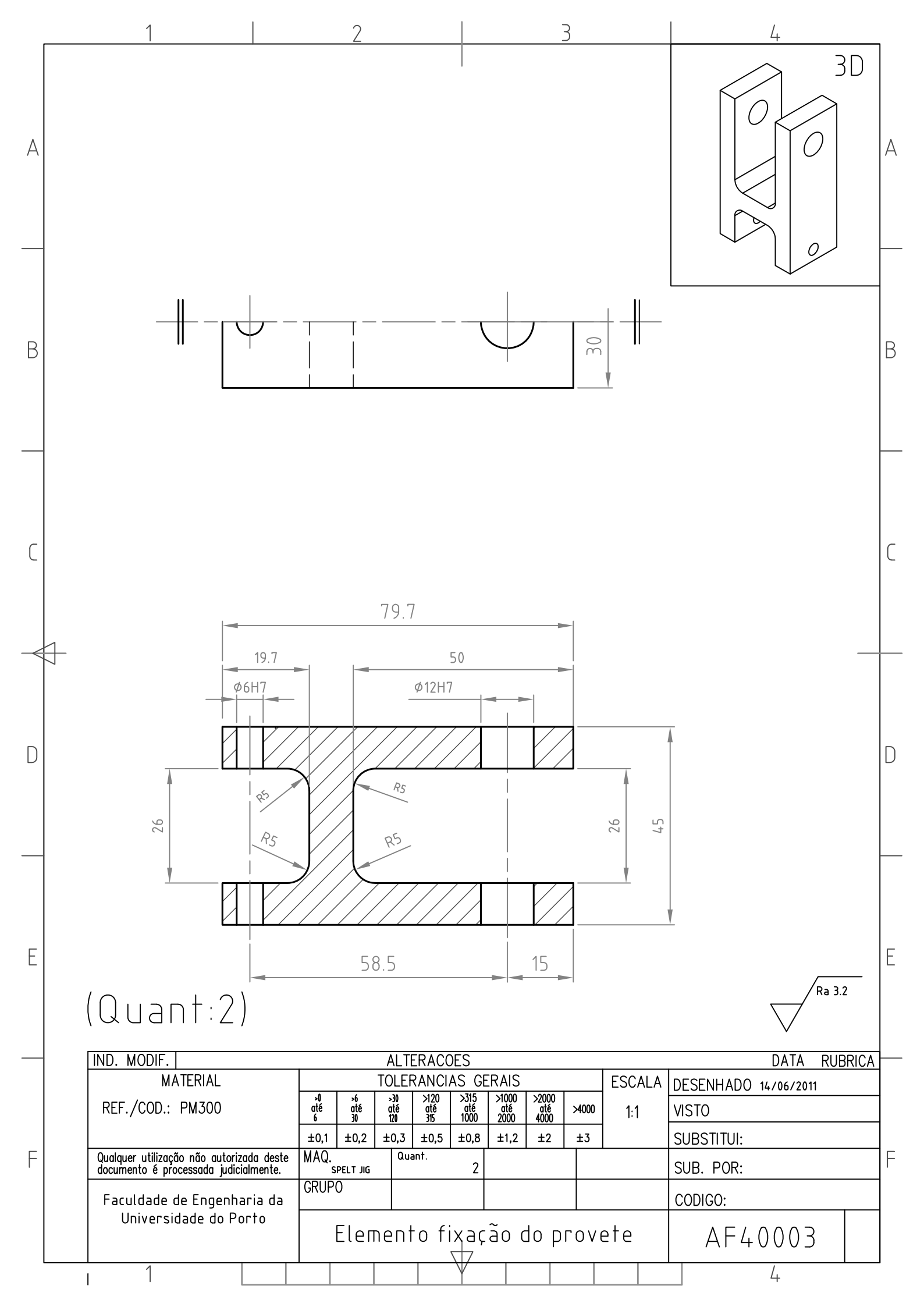


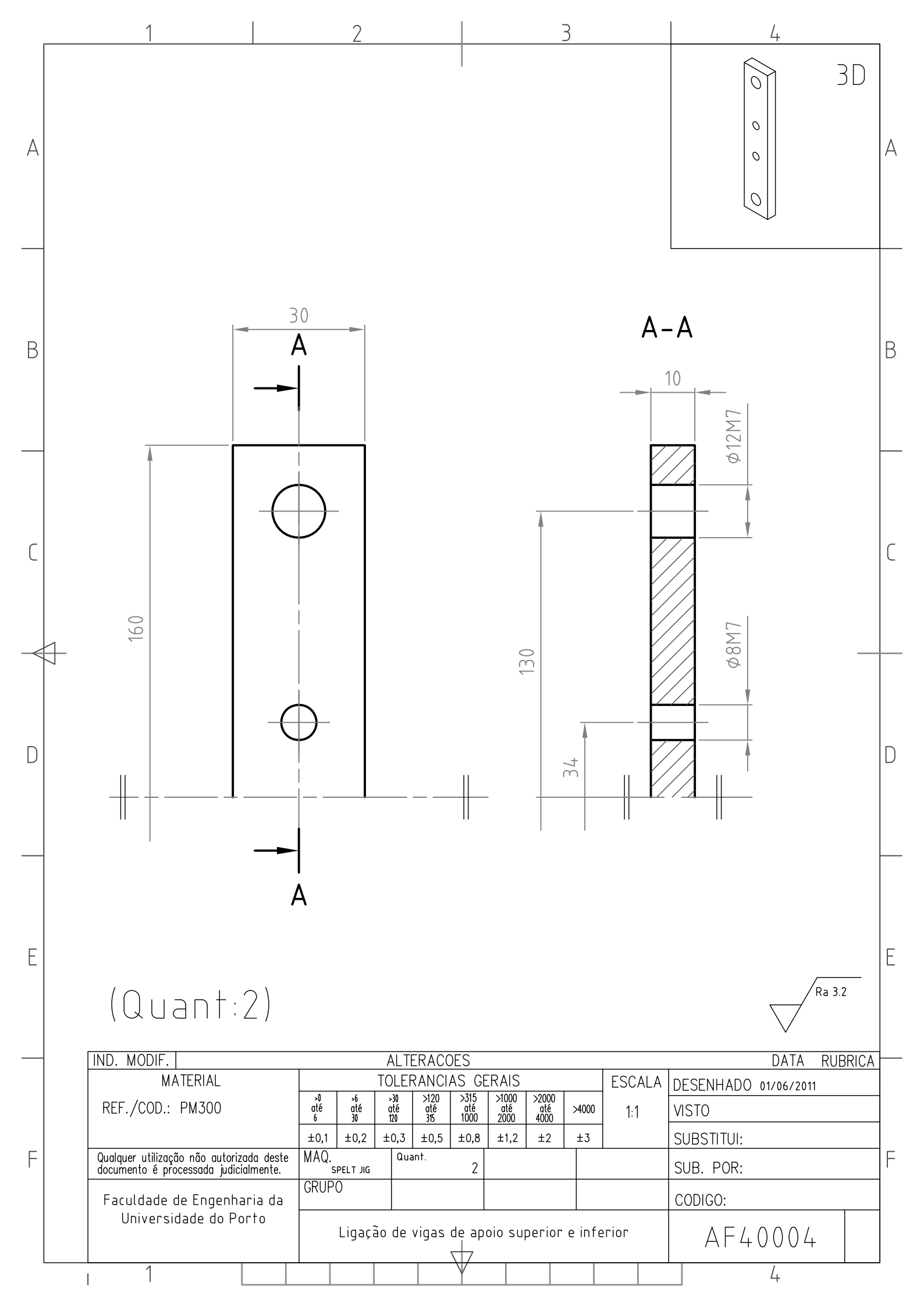


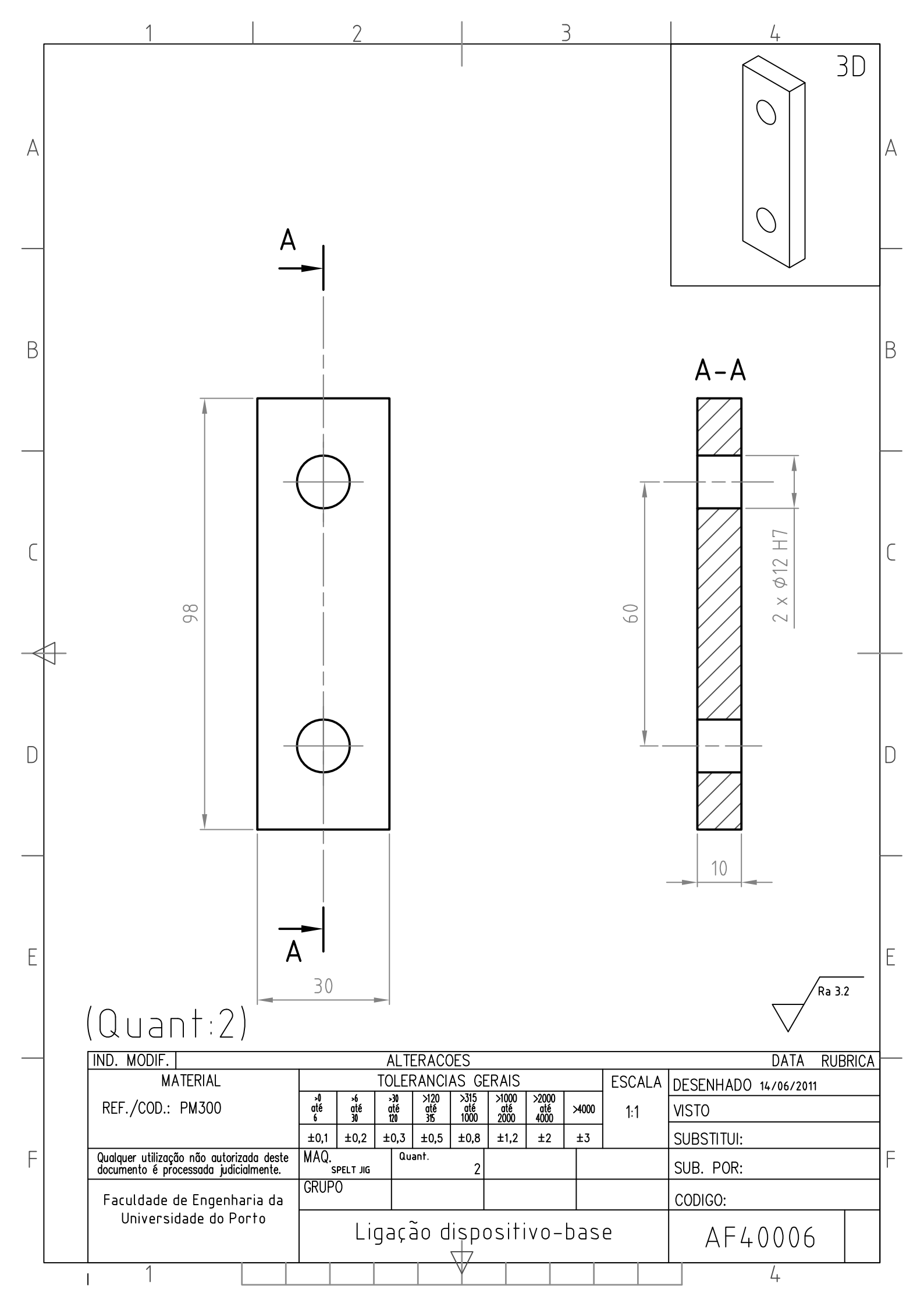


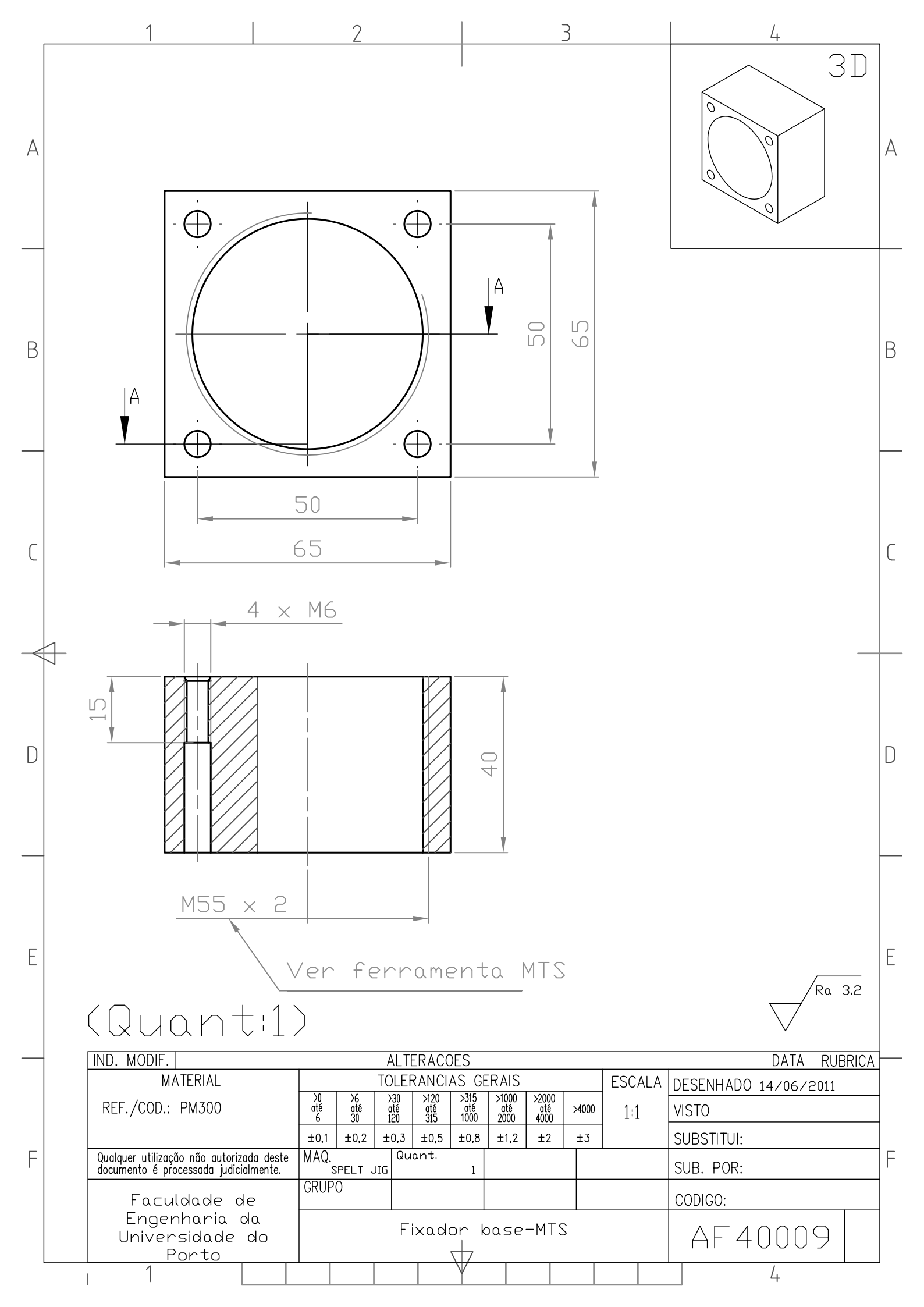














Faculdade de Engenharia da Universidade do Porto Rua Dr. Roberto Frias, s/n 4200-465, PORTO - PORTUGAL www.fe.up.pt